

University of Alberta

Development and Characterization of New Stationary Phases for
Hydrophilic Interaction Liquid Chromatography

by

Mohammed Elsayed Abdelatif Ibrahim

A thesis submitted to the Faculty of Graduate Studies and Research
in partial fulfillment of the requirements for the degree of

Doctor of Philosophy

Department of Chemistry

©Mohammed Elsayed Abdelatif Ibrahim

Spring 2014
Edmonton, Alberta

Permission is hereby granted to the University of Alberta Libraries to reproduce single copies of this thesis and to lend or sell such copies for private, scholarly or scientific research purposes only. Where the thesis is converted to, or otherwise made available in digital form, the University of Alberta will advise potential users of the thesis of these terms.

The author reserves all other publication and other rights in association with the copyright in the thesis and, except as herein before provided, neither the thesis nor any substantial portion thereof may be printed or otherwise reproduced in any material form whatsoever without the author's prior written permission.

ABSTRACT

Hydrophilic interaction liquid chromatography (HILIC) has gained high popularity among separation scientists in the last two decades due to its ability to retain polar analytes. Many new HILIC stationary phases with different selectivities have appeared in the recent literature. Such developments require tools which can classify and compare the selectivity of these HILIC columns. In this thesis, straightforward and simple selectivity plots were constructed and used to classify HILIC stationary phases into bare silica, zwitterionic, neutral and amine-based phases.

Silica monoliths show weak retention under HILIC conditions. In this thesis, the HILIC retention characteristics of silica monoliths were enhanced through surface modification with hydrophilic cationic latex nanoparticles. High efficiency ($H \sim 25\text{--}110 \mu\text{m}$) separations of carboxylic acids, amino acids and nucleotides were achieved. Due to their positive charge, the latex nanoparticles introduce anion exchange as another source of interaction. Consequently, these latex coated silica monoliths should exhibit mixed mode (HILIC/anion exchange) retention. Herein, the mixed mode retention of three different latex coated silica monoliths was studied. The AS9-SC latex coated silica monolith possessing the highest ion exchange capacity ($44.1 \mu\text{eq/column}$) separated six chaotropic and kosmotropic anions in less than 2.5 min.

Silica is chemically unstable under extreme pH conditions. On the other hand, porous graphitic carbon (PGC) has high pH stability. Being a hydrophobic

material, typically usage of PGC is restricted to reversed phase chromatography. In the presented thesis, a carbon-based HILIC stationary phase was developed as a new class of HILIC stationary phases *via* diazonium chemistry. The potential of this phase (carboxylate-PGC) as a HILIC phase was demonstrated by separation of carboxylic acids, phenols, amino acids and nucleotides. Carboxylate-PGC phase showed different selectivity than 35 columns.

The efficiency of carbon-based phases is lower than silica due to slow mass transfer kinetics. Herein, we developed a hybrid phase comprising of 5 μm core-shell silica particles coated with 50 nm anionic carbon nanoparticles. This hybrid phase exhibited the unique selectivity of carbon and the high efficiency of core-shell silica particles. Fast and high efficiency HILIC separations of carboxylates and pharmaceuticals were achieved with efficiencies up to 85,000 plates/m.

ACKNOWLEDGEMENTS

I would like to express my profound gratitude and sincere thanks to my supervisor Prof. Dr. Charles A. Lucy for his continuous guidance, infinite support and encouragement throughout the development of this work.

I would like also to convey my special thanks to my lab mate Dr. M. Farooq Wahab, for his helpful collaboration which has resulted in two complete research projects.

This work was sponsored by the Natural Sciences and Engineering Research Council of Canada (NSERC) and the University of Alberta. The financial support of NSERC, the Provost Doctoral Entrance Scholarship (University of Alberta), Queen Elizabeth II scholarship, and Thermo Fisher Scientific Corporation is highly appreciated.

Dr. Knut Irgum's (University of Umea, Sweden) generosity in sharing his raw results is gratefully acknowledged. I am highly grateful to Dr. Harald Ritchie (Thermo Fisher Scientific) for a gift of porous graphitic carbon particles. I would also like to thank Phenomenex for their gift of the core-shell silica particles. The help of Dr. Nikolai Sinkov (University of Alberta) with the construction of confidence ellipses is highly appreciated.

Special and warm thanks to my colleagues in Lucy research group, for their help and cooperation. I would like to express my deepest thanks and great appreciation to my parents and my wife for their support and encouragement.

TABLE OF CONTENTS

CHAPTER ONE: Introduction	1
1.1 Motivation and Thesis Overview	1
1.2 High Performance Liquid Chromatography (HPLC)	4
1.2.1 Chromatography Theory and Terms	5
1.2.1.1 Retention	5
1.2.1.2 Efficiency (N) and Plate Height (H)	8
1.2.1.3 Selectivity Factor (α) and Resolution (R_s)	9
1.2.1.4 Band Broadening: van Deemter Equation and Parameters	11
1.2.2 Modes of Chromatography	16
1.2.2.1 Reversed Phase Liquid Chromatography (RPLC)	16
1.2.2.1.1 Alkyl-Silica RPLC Phases	18
1.2.2.1.2 Porous Graphitic Carbon (PGC)	20
1.2.2.2 Normal Phase Liquid Chromatography (NPLC)	20
1.2.2.3 Hydrophilic Interaction Liquid Chromatography (HILIC)	21
1.2.2.4 Ion-Exchange Chromatography	22
1.3 Summary	25
1.4 References	26
CHAPTER TWO: Stationary Phases for Hydrophilic Interaction Liquid Chromatography	30
2.1 Hydrophilic Interaction Liquid Chromatography	30
2.2 Historical Aspects of HILIC Stationary Phases	32
2.3 Modes of Retention of HILIC	33
2.4 HILIC Stationary Phases	34
2.4.1 Underivatized Silica	34
2.4.1.1 Totally Porous Silica Particles	36
2.4.1.2 Superficially Porous (Core-Shell) Silica particles	42
2.4.1.3 Monolithic Silica	42
2.4.1.4 Ethylene Bridged Hybrids (BEH)	44
2.4.2 Derivatized Silica	46
2.4.2.1 Neutral Derivatized Silica	46
2.4.2.1.1 Amide Silica	46
2.4.2.1.2 Diol Silica	48
2.4.2.1.3 Cyanopropyl Silica	51
2.4.2.1.4 Cyclodextrin Based Silica	52
2.4.2.2 Zwitterionic Derivatized Silica	54
2.4.2.2.1 Sulfoalkylbetaine Silica	54
2.4.2.2.2 Obelisc R and Obelisc N Columns	55
2.4.2.3 Positively Charged Derivatized Silica	56
2.4.2.3.1 Aminopropyl	56
2.4.2.3.2 Latex Coated Silica	58

2.4.2.4 Negatively Charged Derivatized Silica	59
2.4.3 Non Silica Based Stationary Phases	61
2.4.3.1 Amino Phases	61
2.4.3.2 Sulfonated S-DVB Phases	63
2.5 Commercial HILIC Phases	63
2.5.1 Efficiency Comparison	64
2.5.2 Retention and Selectivity Comparisons	79
2.6 Summary	90
2.7 References	90
CHAPTER THREE: A Simple Graphical Representation of Selectivity in Hydrophilic Interaction Liquid Chromatography	99
3.1 Introduction	99
3.2 Experimental	101
3.2.1 Apparatus	101
3.2.2 Reagents and Materials	101
3.2.3 Chromatographic Conditions	102
3.2.4 Tested Columns and Test Probes	102
3.3 Results and Discussion	103
3.3.1 Selection of Test Pairs	104
3.3.2 Hydrophilicity vs. Ion Exchange Characteristics of HILIC Phases	108
3.3.3 Ion Exchange vs. Participation in H-bonding	114
3.3.4 HILIC-Phase Selectivity Chart	116
3.4 Conclusions	119
3.5 References	120
CHAPTER FOUR: Agglomerated Silica Monolithic Column for Hydrophilic Interaction Liquid Chromatography	123
4.1 Introduction	123
4.2 Experimental	126
4.2.1 Reagents and Materials	126
4.2.2 Apparatus	127
4.2.3 Calculations	128
4.3 Results and Discussion	128
4.3.1 Effect of %ACN in HILIC Mode	128
4.3.2 Separation of Hydrophilic Analytes on AS9-SC Coated Silica Monolith	131
4.3.2.1 Fast Separation of Naphthalene, Uracil and Cytosine	131
4.3.2.2 Separation of Benzoates	133
4.3.2.3 Separation of Nucleotides	136
4.3.2.4 Separation of Amino Acids	136
4.3.3 Electrostatic Repulsion Hydrophilic Liquid Interaction Chromatographic (ERLIC) Behavior of the Dionex AS9-SC Coated Silica Monolith.	139

4.3.4 Stability of the AS9-SC Coated Silica Monolith	141
4.4 Conclusions	141
4.5 References	143
CHAPTER FIVE: Mixed Mode HILIC/Anion-Exchange Separations on Latex Coated Silica Monoliths	146
5.1 Introduction	146
5.2 Experimental	151
5.2.1 Apparatus	151
5.2.2 Reagents and Materials	151
5.2.3 Tested Columns and Latex Coating	152
5.2.4 Measurement of the Ion Exchange Capacity	153
5.2.5 Measurement of the Water Layer Volume	153
5.3 Results and Discussion	153
5.3.1 Characterization of Latex Coated Monoliths	154
5.3.2 Fast HILIC Separations on Latex Coated Monoliths	159
5.3.3 Selectivity of Latex Coated Silica Monoliths	163
5.3.4 Influence of the Anion Nature on the Mixed Mode Retention Mode	167
5.3.4.1 Effect of Buffer Strength	167
5.3.4.2 Effect of % ACN	174
5.4 Conclusions	178
5.5 References	178
CHAPTER SIX: Carboxylate Modified Porous Graphitic Carbon – A New Class of Hydrophilic Interaction Liquid Chromatography Phases	183
6.1 Introduction	183
6.2 Experimental	186
6.2.1 Reagents	186
6.2.2 Apparatus	187
6.2.3 Method	188
6.2.3.1 Synthesis of the Stationary Phase (Carboxylate-PGC)	188
6.2.3.2 Packing of the Stationary Phase (Carboxylate-PGC)	189
6.2.3.3 Mobile Phase Preparation	189
6.2.4 Characterization of PGC Phases	190
6.3 Results and Discussion	191
6.3.1 Characterization of the Carboxylate-PGC	193
6.3.2 Approaches for Packing Carboxylate-PGC	200
6.3.3 HILIC Behavior of Unmodified and Carboxylate-PGC	201
6.3.4 HILIC Selectivity of Carboxylate-PGC	203
6.3.5 Switching Retention Mode of Carboxylate-PGC with pH	209
6.3.6. Chromatographic Separations on Carboxylate-PGC at High pH	209
6.3.7 Column Stability and Retention Time Reproducibility	214
6.4 Conclusions	217

6.5 References	217
CHAPTER SEVEN: Hybrid Carbon Nanoparticles Modified Core-Shell Silica: A High Efficiency Carbon-Based Phase for Hydrophilic Interaction Liquid Chromatography	223
7.1 Introduction	223
7.2 Experimental	227
7.2.1 Apparatus	227
7.2.2 Materials	227
7.2.3 Preparation of the Hybrid Carbon-Silica Stationary Phase	228
7.2.3.1 Synthesis of Carboxylate Modified Carbon Nanoparticles (Carboxylate-Carbon)	228
7.2.3.2 Coating of Core-Shell Silica with Latex Nanoparticles (Latex Coated Core-Shell Silica)	229
7.2.3.3 Modification of Latex Coated Core-Shell Silica with Carboxylate-Carbon (Hybrid Carbon-Silica Phase)	230
7.2.3.4 Column Packing Procedure	230
7.2.4 Characterization of the Carbon-Silica Hybrid Phase	231
7.2.5 Efficiency Calculations	231
7.3 Results and Discussion	232
7.3.1 Physical Characterization of the Hybrid Carbon-Silica Phase	233
7.3.2 HILIC Properties of the Hybrid Phase	239
7.3.3 Selectivity of the Hybrid Carbon-Silica Phase	239
7.3.4 Mixed Mode Behavior of the Hybrid Carbon-Silica Phase	245
7.3.5 Isomeric Selectivity of the Hybrid Carbon-Silica Phase	245
7.3.6 Efficiency of the Hybrid Carbon-Silica Phase	247
7.3.7 HILIC Applications of the Hybrid Carbon-Silica Phase	250
7.3.8 Reproducibility and Stability of the Hybrid Carbon-Silica Phase	252
7.4 Conclusions	255
7.5 References	256
CHAPTER EIGHT: Conclusions and Future Work	260
8.1 Conclusions	260
8.2 Future Work	262
8.2.1 Development of New Multimodal Stationary Phases	262
8.2.2 Sulfonated Porous Graphitic Carbon for HILIC	265
8.2.3 Factors Affecting the Selectivity Plot of HILIC Stationary Phases	265
8.2.4 Covalently Modified Carbon Clad Silica Phase for HILIC	267
8.3 References	268
Appendix I. Chemical Structures	271

LIST OF TABLES

2.1	Characteristics of commercial HILIC phases	38
2.2	Chemical structures of some selected silica-based HILIC phases	49
2.3	Comparison of HILIC column efficiencies	66
3.1	Characteristics of the tested stationary phases	105
4.1	Comparison of efficiencies of model analytes on the AS9-SC coated silica monolith vs. commercial HILIC columns	134
5.1	Characteristics of the studied latex nanoparticles	150
5.2	Water layer volume and ion exchange capacity of latex coated monoliths	157
6.1	Surface composition from XPS survey scans of unmodified PGC and carboxylate-PGC	198
7.1	Bulk composition analysis of the materials employed in the synthesis of the hybrid carbon-silica phase	234
7.2	Average XPS surface composition of the materials employed in the synthesis of the hybrid carbon-silica phase in atomic percentages	235

LIST OF FIGURES

1.1	Schematic of the different parts of a modern HPLC system	6
1.2	Graphical measurement of the asymmetry factor (B/A) of a non-Gaussian tailing peak	10
1.3	Schematic representation of the multipath band diffusion (A term)	13
1.4	The van Deemter plot (solid line). The A, B and C terms are represented as dashed lines	14
1.5	Chemical synthesis of derivatized silica phases	19
1.6	The different types of interactions between the analyte and the stationary phase in HILIC	23
2.1	Formation of the water rich layer on the surface of stationary phase under HILIC conditions	31
2.2	Different types of silanols on the surface of silica	37
2.3	Assembly of small silica particles into spherical aggregates	43
2.4	Schematic of Waters (Milford, MA, USA) BEH phase	47
2.5	Chemical structure of different types of cyclodextrins	53
2.6	Schematic diagram of Obelisc R and Obelisc N	57
2.7	Structure of the agglomerated latex coated silica monolith	60
2.8	Synthesis of poly(succinimide) based silica stationary phases	62
2.9	van Deemter plots of 3 μm and 5 μm TSKgel Amide-80	68
2.10	Relationship between retention and separation efficiency of different HILIC columns	69
2.11	Separation of nucleic acid bases and nucleosides on: (A) YMC-Pack NH ₂ (B) TSKgel Amide-80 (C) ZIC-HILIC and (D) Atlantis HILIC Silica columns.	72
2.12	Separation of acidic compounds on 4 different columns	73
2.13	Separations of pyrimidines (upper) and purines (lower) on silica columns	74
2.14	van Deemter plot for Cyclobond I HILIC Column	76
2.15	Separation of 2-amino-2-ethyl-1,3-propanediol and tromethamine on different amine-based HILIC columns	78
2.16	Chromatograms of eight solutes on five different HILIC columns	85
2.17	Separation of uracil, adenosine, uridine, cytosine, cytidine and guanosine on diol, cross-linked diol, polyhydroxy and Polyvinyl alcohol phase	86
2.18	Separation of uracil, adenosine, uridine, cytosine, cytidine and guanosine on amino, imidazole and triazole phase	87
2.19	Separation of nucleosides on various HILIC phases	88
2.20	Score and loading biplot of the two first components of the model	89
3.1	Hydrophilicity vs. ion exchange selectivity plot of HILIC phases	109

3.2	Ion exchange vs. H-bond formation capability selectivity plot of HILIC phases	115
3.3	The HILIC-Phase Selectivity Chart	117
4.1	Effect of %ACN on the retention of naphthalene, cytosine and phthalic acid on the AS9-SC coated silica monolith	129
4.2	Fast HILIC separation of naphthalene, uracil and cytosine on the latex coated silica monolith	132
4.3	Separation of benzoates on the latex coated silica monolith	135
4.4	HILIC separation of nucleotides on the latex coated silica monolith	137
4.5	HILIC separation of amino acids on the latex coated silica monolith	138
4.6	Effect of salt concentration on ERLIC separation of histidine and aspartic acid on the latex coated silica monolith	140
4.7	Stability of the latex coated AS9-SC coated silica monolith in HILIC mode	142
5.1	Separation of acetate, formate, bromate, nitrate, thiocyanate and iodide on Onyx bare silica monolith	156
5.2	Fast separation of acetate, formate, bromate, nitrate, thiocyanate and iodide on the latex A coated Chromolith silica monolith	160
5.3	Fast separation of acetate, formate, bromate, nitrate, thiocyanate and iodide on the latex B coated Onyx silica monolith	161
5.4	Fast separation of acetate, formate, bromate, nitrate, thiocyanate and iodide on the latex C coated Onyx silica monolith	162
5.5	Selectivity plot of latex coated silica monoliths	166
5.6	Effect of buffer strength on the retention of anions on the latex A coated Onyx silica monolith	169
5.7	Effect of buffer strength on the retention of bromate and thiocyanate on the latex A coated silica monolith	170
5.8	Effect of buffer strength on the retention of (A) iodide and (B) formate on latex coated Onyx silica monoliths	172
5.9	Effect of buffer strength on the retention of acetate, bromate, nitrate and thiocyanate on the latex B coated Onyx silica monolith	173
5.10	Effect of % ACN on the retention of anions on the latex A coated Chromolith silica monolith	175
5.11	Effect of % ACN on the retention of anions on the latex B coated Onyx silica monolith	176
5.12	Effect of % ACN on the retention of formate and iodide on the latex C coated Onyx silica monolith	177

6.1	The scheme for creating carboxylate functionality on porous graphitic carbon	192
6.2	The difference in wettability between PGC and carboxylate-PGC in deionized water	194
6.3	Scanning electron microscopy (SEM) images of both unmodified PGC (top) and carboxylate-PGC (bottom)	195
6.4	Survey XPS scans of PGC (as received) and carboxylate-PGC	197
6.5	High resolution deconvoluted XPS spectrum of oxygen 1s band	199
6.6	Retention behavior of uracil and 1-naphthoic acid on carboxylate-PGC and Hypercarb as a function of % ACN in the eluent	202
6.7	Selectivity plot of Carboxylate-PGC and PGC (Hypercarb TM) with respect to 35 commercial columns	204
6.8	Comparison of the selectivity of six aromatic carboxylic acids on nine different column chemistries and carboxylate-PGC under HILIC mode	207
6.9	Selectivity changes with pH on carboxylate-PGC for aniline, benzoic acid and toluene	210
6.10	Separation of aromatic carboxylic acids, nucleotides, phenols, and amino acids on carboxylate-PGC	212
6.11	Stability of carboxylate-PGC column under strong alkaline conditions	215
6.12	Reproducibility comparison of carboxylate-PGC under HILIC mode	216
7.1	Schematic for the preparation of the hybrid carbon-silica phase	226
7.2	Thermogravimetry curves in oxygen atmosphere of the unmodified carbon and carboxylate-carbon nanoparticles	236
7.3	Thermogravimetry curves in oxygen atmosphere of the bare core-shell silica and hybrid carbon-silica phase material	237
7.4	Effect of % ACN on the retention of benzoate and uracil on the hybrid carbon-silica phase under HILIC conditions	240
7.5	Selectivity plot of the hybrid carbon-silica phase vs. silica and polymer based- stationary phases	242
7.6	Selectivity of six aromatic acids on the hybrid carbon-silica phase vs. ten HILIC stationary phases	244
7.7	HILIC/RPLC mixed mode retention behavior of the hybrid carbon-silica phase	246
7.8	Isomeric separations on the hybrid carbon-silica phase	248
7.9	van Deemter plots for the hybrid carbon-silica and carboxylate-PGC columns.	249
7.10	HILIC separations of (A) biological acids and (B) phenols on the hybrid carbon-silica phase	251
7.11	Fast HILIC separation of pain relief pharmaceuticals on the hybrid carbon-silica	253

7.12	Reproducibility studies of the hybrid carbon-silica phase	254
8.1	The design of the proposed multimodal stationary phase along with the expected retention modes (RPLC, HILIC and Ion exchange).	264

LIST OF SYMBOLS AND ABBREVIATIONS

Symbol	Parameters
Å	Angstroms
ACN	Acetonitrile
ADP	Adenosine 5'-diphosphate
AEPD	2-amino-2-ethyl-1,3-propanediol
AMP	Adenosine 5'-monophosphate
A _s	Asymmetry
A term	Multipath band broadening term
ATP	Adenosine 5'-triphosphate
AU	Arbitrary units
BEH	Ethylene Bridged hybrid
BTEE	1,2-Bis(triethoxysilyl) ethane
B term	Longitudinal diffusion
BTMA	Benzyltrimethylammonium (ion)
C	Concentration
CD	Cyclodextrin
C _{i,S}	Concentration of the solute in the mobile phase
C _{i,M}	Concentration of the solute in the mobile phase
°C	Celsius
CMP	Cytidine monophosphoric acid
C term	Resistance to mass transfer
C ₈	Octyl

C ₁₈	Octadecyl
DDAB	Didodecyldimethylammonium bromide
DEAE	Diethylaminoethyl
d _f	The thickness of the stationary phase
d _c	the diameter of the channels in the column packing
D _M	Diffusion coefficient of solute in the mobile phase
D _S	Diffusion coefficient of solute in the stationary phase
d _p	Particle diameter
ERLIC	Electrostatic repulsion hydrophilic interaction chromatography
ESI	Electrospray ionization
ESI-MS	Electrospray ionization mass spectrometry
eV	electron volt
E ^{y-}	Eluent anion with charge y-
F	Flow rate
GMP	Guanosine monophosphate
H	Plate height
<i>h</i>	Reduced plate height
h	Hour(s)
HETP	Height equivalent to theoretical plate
HILIC	Hydrophilic interaction liquid chromatography
HPLC	High performance liquid chromatography
i.d.	Internal diameter
<i>i</i> _M	Analyte <i>i</i> in the mobile phase

i_s	Analyte i in the stationary phase
IC	Ion chromatography
k	Retention factor
κ_i	Distribution constant
k_w	Retention factor in the absence of the strong solvent
L	Column length
LC	Liquid chromatography
LC-MS	Liquid chromatography – mass spectrometry
LC-MS/MS	Liquid chromatography – tandem mass spectrometry
M	Mobile phase
mM	Millimolar
min	Minutes
mV	Millivolts
M Ω	Megaohms
N	Efficiency, Plate number
N_{corr}	Corrected efficiency
$n_{i,S}$	the number of moles of an analyte in the stationary phase
$n_{i,M}$	the number of moles of an analyte in the mobile phase
NPLC	Normal phase liquid chromatography
ODS	Octadecyl silica
ΔP	Pressure drop
Pa	Pascal
PALC	<i>Per</i> aqueous liquid chromatography

PCA	Principal component analysis
PEEK	Polyether ether ketone
PGC	Porous graphitic carbon
pH	Negative logarithm of the hydrogen ion concentration
pK _a	Negative logarithm of the acid dissociation constant
PREG	Polar retention effect on graphite
psi	Pounds per square inch
R _s	Resolution
R	An organic functional group
RP	Reversed phase
RPLC	Reversed phase liquid chromatography
RSD	Relative standard deviation
RSF	Relative sensitivity factor
S	Stationary phase
SD	Standard deviation
S-DVB	Sulfonated divinylbenzene
SEM	Scanning electron microscopy
<i>Sol</i>	Solution
SPP	Superficially porous particles
<i>T</i>	Temperature
TEA	Triethylamine
TEOS	Tetraethoxysilane
TFA	Trifluoroacetic acid

TPP	Totally porous particles
t_R	Retention time
t_M	Dead time
u	Linear velocity
UHMWPE	Ultrahigh molecular weight polyethylene
UHPLC	Ultrahigh pressure liquid chromatography
UV	Ultraviolet
v/v	Volume by volume
V_S	Volume of the stationary phase
V_M	Dead volume of a column
w	weight
w_h	Width of a peak at half height
w/w	Weight by weight
x	Charge on an anion
XPS	X-ray photoelectron spectroscopy
y	Charge on an eluent
μeq	Microequivalents
μm	Micrometers
α	Selectivity factor
λ	Packing factor
σ^2	Overall peak variance
σ_{obs}^2	Peak variance contribution due to the column
σ_{corr}^2	Peak variance after correcting extra-column effects

$\sigma^2_{extra\ col}$	Peak variance due to extra-column effects
ψ	Obstruction factor
φ	Volume fraction of the strong solvent

CHAPTER ONE: Introduction

1.1 Motivation and Thesis Overview

Hydrophilic Interaction Liquid Chromatography (HILIC) has gained interest among analytical chemists due to its ability to separate and retain hydrophilic polar analytes which cannot be separated by conventional reversed phase liquid chromatographic (RPLC) techniques [1-4]. HILIC usually utilizes a hydrophilic polar stationary phase in contrast to RPLC (Sec. 1.2.2.1) and a relatively less polar mobile phase. Under HILIC conditions (Sec. 1.2.2.3), a water rich layer is formed on the surface of the HILIC packing into which the hydrophilic analytes partition. This partitioning leads to retention and separation. Stationary phases for HILIC can be classified into bare silica and non-silica based columns [5]. Silica-based HILIC phases can be further classified according to their net surface charge into neutral, positively and negatively charged phases. This thesis discusses the development and characterization of new silica and carbon-based stationary phases for HILIC. Chapter 2 gives an overview of the commercially available HILIC stationary phases with respect to their chemistry and applications. Additionally, it compares the efficiency and selectivity of these different HILIC stationary phases. In reviewing the commercial stationary phases (Chapter 2), some of the deficiencies that I observed were the lack of understanding of columns selectivity, control of stationary phase selectivity, speed of analysis, and stability of the stationary phases. In this thesis, I have worked to address these column issues.

One of the most important parameters in optimizing the resolution in chromatographic separation is the selectivity factor. Consequently, classification of HILIC stationary phases based on their selectivity has gained great attention in the last few years due to the high number of HILIC stationary phases [6-8]. Recently, Irgum and co-workers probed the different interactions taking place on the surface of HILIC stationary phases and used these interactions as a tool to classify the HILIC columns based on principal components analysis (PCA) [6]. Although PCA was successful at classifying the different HILIC phases, PCA is highly complicated and is not easy to understand. To improve understanding of the selectivity of various HPLC stationary phases, in Chapter 3 we re-casted the retention data of 22 columns previously characterized by Irgum and co-workers [6] plus an additional 12 columns measured by us into simpler and more understandable selectivity plots. The ion exchange vs. hydrophilicity selectivity plot is used to characterize all the developed HILIC phases in this thesis (Chapters 4, 5, 6 and 7).

Silica monoliths are characterized by the presence of large macropores which allow fast separations with minimal backpressures [9-12]. Unfortunately, silica monoliths show weak retention of hydrophilic analytes under HILIC conditions due to the small water-rich layer formed on their surfaces [6, 13]. With respect to the speed of analysis, Chapter 4 describes a convenient method to enhance the HILIC retention characteristics of a silica monolith (Chromolith™) through flushing with positively charged latex nanoparticles (Dionex AS9-SC). The monolithic structure of the stationary phase allowed fast HILIC separations

of hydrophilic analytes in less than 15 s with reasonable backpressure. Furthermore, the HILIC performance of this latex coated silica monolith was evaluated using different hydrophilic model analytes (*e.g.* carboxylic acids, amino acids and nucleotides). The introduced latex nanoparticles provide another source of interaction (anion exchange) due to their positive charge. Therefore, these latex-coated silica monoliths are expected to exhibit mixed (HILIC and anion exchange) mode retention characteristics. Chapter 5 describes the mixed mode retention of three different latex coated silica monoliths *e.g.* AS9-SC, AS12A and DNAPac, for the separation of a mixture of chaotropic and kosmotropic anions.

Despite the advantages of silica-based HILIC phases, they are unstable under extreme pH conditions. Porous graphitic carbon (PGC) is considered a pH stable stationary phase. However, due to its highly hydrophobic nature, PGC's use is restricted to RPLC separations [14-16]. To address the pH stability issues associated with commercial silica based stationary phases, Chapter 6 describes the first development of a carbon-based HILIC stationary phase as a new class of HILIC phases. In Chapter 6, the PGC surface is modified by covalently attaching carboxylate groups *via* diazonium chemistry. The potential of carboxylate-PGC as a HILIC phase is demonstrated by the separation of hydrophilic model analytes such as amino acids and nucleotides (Chapter 6). Although PGC material is pH stable, it yields a relatively poorer separation efficiency compared to silica-based phases due to the slow mass transfer kinetics of carbon substrates [17]. To address the poor efficiencies accompanied with PGC based stationary phases developed in Chapter 6, Chapter 7 describes the development of a hybrid phase comprised of

core-shell silica coated with a monolayer of carboxylate modified carbon nanoparticles. This hybrid phase demonstrated both the unique selectivity of carbon and the high efficiency of core-shell silica particles.

1.2 High Performance Liquid Chromatography (HPLC)

Chromatography was reported by Mikhail Tswett for the first time in 1903 [18] during separation of pigments. Tswett named the process “chromatography”, originating from the Greek *chroma* (color) and *graphein* (write) [19]. Chromatography is an analytical technique that separates a sample mixture into individual components. In chromatography, a “mobile phase” transfers a sample mixture through a column packed with tightly packed particles, called the “stationary phase”. Separation of individual analytes takes place according to the degree of interaction the analyte experiences in the mobile and stationary phases, *i.e.*, analytes with higher affinity for the mobile phase elute faster than those with higher affinity for the stationary phase. Physical movement of the analyte (*i.e.* mass transfer) is needed for this equilibration. If the mass transfer is slow, it leads to broad peaks. Use of stationary phases of small particles hastens the mass transfer process and improves the peak sharpness. However, this requires the use of pumping systems to force the mobile phase through these beds of small packed particles. Horvath and co-workers introduced “High Performance Liquid Chromatography (HPLC)” by developing such pumping systems in 1960’s [20, 21].

Figure 1.1 describes the individual components of a modern HPLC system. Briefly, an HPLC consists of a high pressure pump (to pump the mobile phase through the column); an injector (to inject a reproducible volume of sample mixture into running mobile phase); a column containing the stationary phase; a detector (to detect the separated analytes); and a computer for data collection and processing. HPLC is considered the most powerful separation technique in analytical chemistry. Based on the chemistry of the employed stationary and mobile phases, four modes of liquid chromatography exist: reversed phase (RPLC), normal phase; ion exchange; and hydrophilic interaction liquid chromatography (HILIC).

1.2.1 Chromatography Theory and Terms [22]

1.2.1.1 Retention

Chromatographic separation is based on the thermodynamic equilibrium of an analyte between a mobile phase (M) and a stationary phase (S) as expressed as follows:

$$i_M \rightleftharpoons i_S \quad (\text{Equation 1.1})$$

This equilibrium constant (Equation 1.2) can be described by a distribution constant (κ_i) which is the ratio of the concentration of the sample in the stationary phase ($C_{i,S}$) and the mobile phase ($C_{i,M}$) as follows:

$$\kappa_i = \frac{C_{i,S}}{C_{i,M}} \quad (\text{Equation 1.2})$$

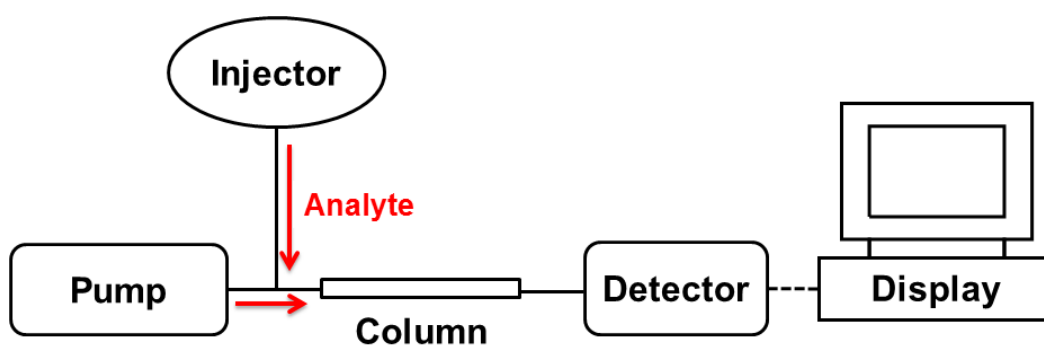


Figure 1.1 Schematic of the different parts of a modern HPLC system.

Retention can be quantified using the retention factor (k_i), formerly known as the capacity factor, which describes the ratio between the number of moles of an analyte in the stationary phase ($n_{i,S}$) and the number of the moles in the mobile phase ($n_{i,M}$) as shown in Equation 1.3.

$$k_i = \frac{n_{i,S}}{n_{i,M}} \quad (\text{Equation 1.3})$$

The relationship between the distribution coefficient (shown in Equation 1.2) and the retention factor (shown in Equation 1.3) can be described as follows:

$$k_i = \kappa_i \frac{V_S}{V_M} \quad (\text{Equation 1.4})$$

where V_S is the volume of the stationary phase and V_M is the volume of the mobile phase. Since the determination of V_S is not practical, retention factor is usually determined by using retention times (Equation 1.5).

$$k_i = \frac{t_R - t_M}{t_M} \quad (\text{Equation 1.5})$$

where t_R is the retention time of the analyte and t_M is the dead time of the column (the time required for unretained analyte to elute from the column).

1.2.1.2 Efficiency (N) and Plate Height (H)

As the band of an analyte propagates through a column, it broadens. Peak efficiency or the number of theoretical plates (Equation 1.6) and plate height (Equation 1.7) are terms used to express the sharpness of the peak, *i.e.*, the higher the N (the lower the H), the sharper the peak. Equation 1.6 describes the width-at-half-height method for calculating N of a Gaussian peak.

$$N = 5.54 \left(\frac{t_R}{w_h} \right)^2 \quad (\text{Equation 1.6})$$

where t_R is the retention time of the peak of interest and w_h is the peak width at 50% of the peak height. Equation 1.6 was used to estimate the peak efficiencies presented in Chapter 5 and Chapter 7. Expressing peak efficiency as H corrects for changes in column length.

$$H = \frac{L}{N} \quad (\text{Equation 1.7})$$

where L is the column length.

Since most peaks are non-Gaussian, calculating N based on the Gaussian assumption tends to overestimate the peak efficiency. Foley and Dorsey suggested the use of an equation (Equation 1.8) based on exponentially modified Gaussian peaks to give a more realistic measure of peak efficiency [23].

$$N_{sys} = \frac{41.7 \left(\frac{t_R}{w_{0.1}} \right)^2}{\left(\frac{B}{A} \right) + 1.25} \quad (\text{Equation 1.8})$$

where $w_{0.1}$ is the peak width at 10% peak height and B/A is the asymmetry factor. B/A is determined by drawing a vertical line through the peak maximum and calculating the ratio of the rear to the front portion of the peak width at 10% of the peak height as shown in Figure 1.2. Since most of the peaks presented in Chapter 4 are non-Gaussian, the Foley-Dorsey equation (Equation 1.8) was used to calculate the peak efficiency.

1.2.1.3 Selectivity Factor (α) and Resolution (R_S)

Equation 1.5 describes the absolute retention of a compound. In separation science we are more often interested in the separation of two compounds. Selectivity factor (α , also named separation factor) and resolution (R_S) quantify the retention difference or the separation distance between two analytes on a given stationary phase rather.

$$\alpha_{i,j} = \frac{k_j}{k_i} \quad (\text{Equation 1.9})$$

$$R_S = \frac{2 (t_j - t_i)}{w_j + w_i} \quad (\text{Equation 1.10})$$

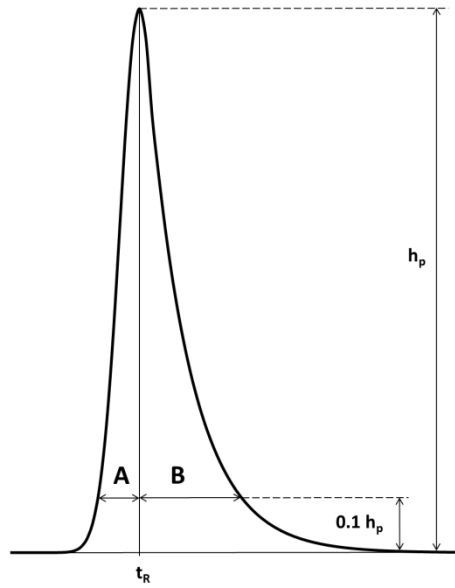


Figure 1.2 Graphical measurement of the asymmetry factor (B/A) of a non-Gaussian tailing peak. Adapted from Reference [24].

where w_j and w_i are the baseline width of analyte (j) and analyte (i). Alternatively, resolution can be described by the basic resolution equation (Equation 1.11) as follows:

$$R_s = \left(\frac{\sqrt{N}}{4} \right) \left(\frac{k}{1+k} \right) \left(\frac{\alpha - 1}{\alpha} \right) \quad (\text{Equation 1.11})$$

where N is the column efficiency (Equation 1.6), k is the retention factor (Equation 1.5) and α is the selectivity factor (Equation 1.9). This equation shows the direct dependence of the chromatographic resolution on the peak efficiency, retention and selectivity factor.

1.2.1.4 Band Broadening: van Deemter Equation and Parameters

Ideally, when an analyte elutes from a column, it is detected as a sharp peak. However, there are many factors that cause the analyte molecules to disperse as they travel along the column and result in the observed peak width. The van Deemter theory (Equation 1.12) identifies three effects that contribute to band broadening: eddy diffusion (A term); longitudinal molecular diffusion (B term); and resistance to mass transfer (C term) [25]. These parameters are related to the plate height (H) and to the linear velocity of the mobile phase (u) through the mathematical expression shown below.

$$H = A + \frac{B}{u} + Cu \quad (\text{Equation 1.12})$$

Eddy diffusion (known also as multipath band broadening) results from the non-uniformity of the packed particles in a particular column. Such non-uniform distribution of particle size leads to different flow paths and hence different linear velocity across the diameter of a given column. Analyte molecules flowing through wider pores travel faster compared to those flowing through narrower channels. Such differences in analyte speed through the column result in band broadening as shown in Figure 1.3. Eddy diffusion can also be described mathematically as shown in Equation 1.13.

$$A = 2\lambda d_p \quad (\text{Equation 1.13})$$

where λ is the packing factor of a given column and d_p is the particle size. Better packed columns with uniform (monodispersed) packing beds have small λ values and hence show minimal eddy diffusion. As a conclusion, the eddy diffusion should depend on the physical geometry of the packed particles and does not depend on the linear velocity of the mobile phase (Figure 1.4).

While an analyte travels along the separation column, random diffusion of the molecules forward and backward from the band center occurs along the longitudinal axis of the column. This random movement of analyte molecules is due to the concentration gradient along the column, and results in band broadening. The resultant B term can be described mathematically as:

$$B = 2\psi D_M \quad (\text{Equation 1.14})$$

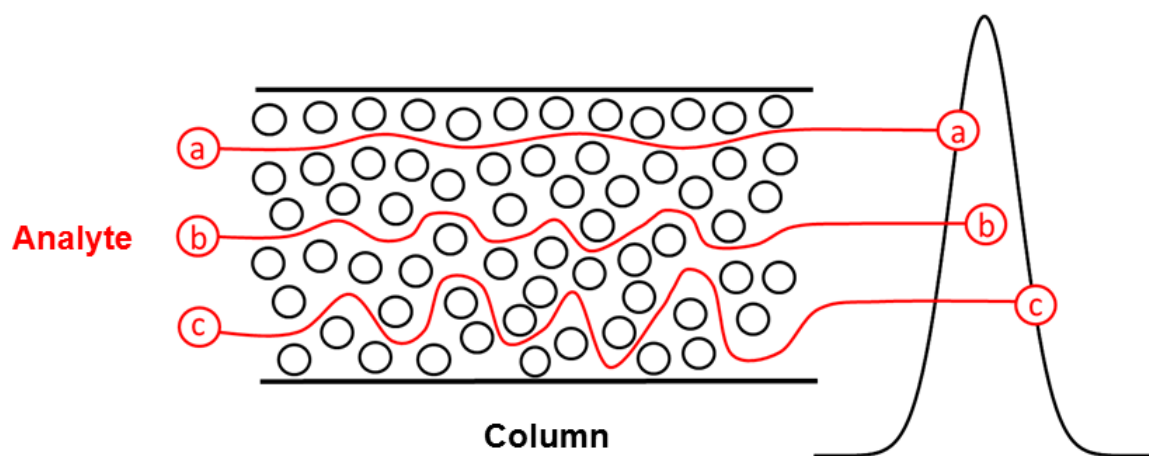


Figure 1.3 Schematic representation of the multipath band diffusion (A term). Adapted from Reference [26].

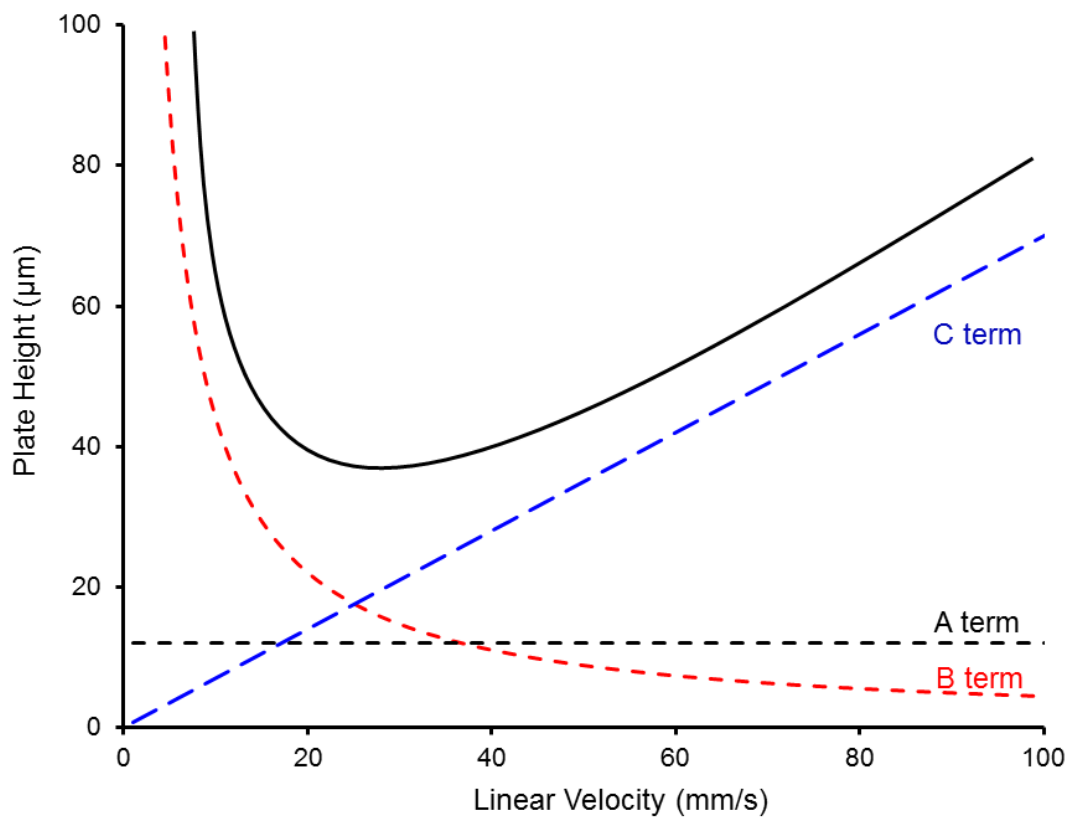


Figure 1.4 The van Deemter plot (solid line). The A, B and C terms are represented as dashed lines.

where ψ is the obstruction factor and D_M is the diffusion coefficient of the analyte in the mobile phase. The usage of higher linear velocities of the mobile phase allows less time for analyte molecules to diffuse, resulting in a smaller B term (Figure 1.4). Nevertheless B term is negligible for HPLC compared to gas chromatography owing to the much reduced diffusion coefficient of molecules in liquids relative to gases. However with the recent development of ultra high pressure liquid chromatography (UHPLC), the contribution of the B term to band broadening is higher relative to the very small C term. This requires the use of relatively higher linear velocities to minimize the B term.

The C term is the result of the resistance to mass transfer of the analyte molecules within the stationary (C_S) and mobile (C_M) phases. If an analyte diffuses slowly, it will be carried forward by the flow before achieving equilibrium between the mobile and stationary phase. This results in band broadening which gets worse when the flow rate of the mobile phase is increased. Mathematically, C_S and C_M are described in Equations 1.15 and 1.16.

$$C_S = \frac{8}{\pi^2} \frac{k}{(1+k)^2} \frac{d_f^2}{D_S} \quad (\text{Equation 1.15})$$

$$C_M = \frac{(1+6k+11k^2)d_c^2}{96(1+k)^2 D_M} \quad (\text{Equation 1.16})$$

where d_f is the thickness of the stationary phase; d_c is the diameter of the channels in the column packing occupied by the mobile phase; and D_S and D_M are the diffusion coefficients in the stationary and mobile phases, respectively.

A tightly and uniformly packed column would have smaller interstitial channels (d_c) resulting in faster equilibration and reduced band broadening. Contrary to its effect on the B term, greater diffusion coefficients (D_S and D_M) hasten analyte mass transfer and reduce band broadening due to the C terms as shown in Equations 1.15 and 1.16.

1.2.2 Modes of Chromatography

1.2.2.1 Reversed Phase Liquid Chromatography (RPLC)

Reversed phase liquid chromatography (RPLC) is the most widely used liquid chromatographic technique. RPLC utilize a hydrophobic stationary phase and a relatively polar mobile phase. The mobile phase in RPLC consists of a mixture of water (usually containing a buffer) and an organic solvent such as methanol or acetonitrile. Most RPLC stationary phases are based on alkyl-bonded silica (*e.g.* octyl or octadecyl), polymer or porous graphitic carbon (PGC) phases. Partitioning (absorption) of the analyte between the mobile phase and the stationary phase forms the basis of separation in RPLC. The retention is dependent on the solubility of an analyte in the mobile and stationary phases. Since the stationary phase employed for RPLC is hydrophobic, it is commonly used for separation of hydrophobic analytes.

The retention under RPLC conditions depends mainly on the polarity of the analytes and the strength of the mobile phase. The higher the polarity of an analyte, the stronger it interacts with the relatively polar mobile phase through polar interactions *e.g.* H-bonding and dipolar interactions which leads to lower retention. On the other hand, analytes with lower polarity interact very weakly with the mobile phase and spend greater time in the stationary phase leading to higher retention. Stronger eluents in RPLC are those containing higher contents of the organic solvent due to the increased solubility of an analyte in the mobile phase with the content of methanol or acetonitrile. Other factors affecting retention might include pH especially for charged analytes and temperature. Based on the Linear Solvent Strength model [27], Equation 1.17 describes the dependence of the retention on the volume fraction of organic solvent in the mobile phase.

$$\log k = \log k_w - S\varphi \quad (\text{Equation 1.17})$$

where φ is the volume fraction of the strong solvent, k_w is the retention factor when the mobile phase contains no strong solvent (*i.e.*, in pure water mobile phase), and S is the slope of the plot. Therefore a plot of $\log k$ vs. φ should yield a straight line for a partitioning mechanism (*e.g.* RPLC). Although RPLC constitutes the majority of LC separations, it cannot separate hydrophilic analytes due to their very weak solubility in the hydrophobic stationary phase. A special type of RPLC, named “Ion-pairing chromatography” is designed to enhance the

retention of the weakly retained charged analytes [28-31]. However, it suffers from the long equilibration times and incompatibility with mass spectrometers (MS) [32, 33].

With respect to the chemical nature of RPLC stationary phases, they can be classified into alkyl silica and porous graphitic carbon-based phases.

1.2.2.1.1 Alkyl-Silica RPLC Phases

Silica is covered with silanol groups (-Si-OH) with an approximate coverage of $8 \mu\text{mol}/\text{m}^2$ [34]. These silanols can be reacted with a chlorosilane to yield a modified silica with specific functional groups. Figure 1.5 represents the chemical synthesis of alkyl derivatized silica phases. The bonded group (R) is usually hydrophobic (*e.g.* C₈ for octyl and C₁₈ for octadecyl) for RPLC purposes. On the other hand, it can be a polar group (*e.g.* amino, diol) for normal phase liquid chromatography (NPLC) or HILIC purposes as discussed in Chapter 2 (Section 2.4.2).

Despite the advantages of silica substrates with regard to efficiency and ease of modification, they are unstable outside the pH range (2-8). Silica bonded phases undergo hydrolysis of the bonded groups at $\text{pH} < 2$ [34, 35]. Silica dissolves at $\text{pH} > 8$ [34, 36]. Porous graphitic carbon (PGC) can be used as a substitute to silica-based columns due to its superior pH stability [37].

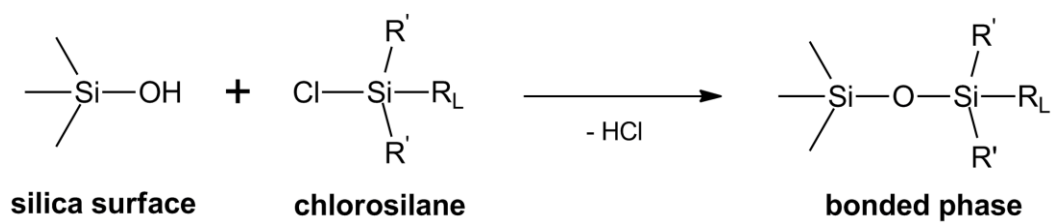


Figure 1.5 Chemical synthesis of derivatized silica phases.

1.2.2.1.2 Porous Graphitic Carbon (PGC)

Knox and co-workers introduced porous graphitic carbon (PGC) as a chemically robust RPLC substrate to overcome the pH stability problems associated with silica bonded phases [38]. PGC consists of continuous hexagonal arrays of graphite (carbon atoms) in the form of layers [38]. PGC is characterized by high chemical (pH 0-14) and thermal (up to 200 °C) stability. Due to its high hydrophobicity, PGC is mainly used for RPLC purposes. Interestingly, PGC can also retain polar analytes *via* dipole interactions in an effect called the polar retention effect on graphite (PREG) [39, 40]. Chapter 6 explores the development of a novel PGC-based stationary phase through diazonium chemistry. Chapter 7 utilizes carbon graphitic nanoparticles to modify the surface of core-shell silica particles.

1.2.2.2 Normal Phase Liquid Chromatography (NPLC)

Normal phase liquid chromatography (NPLC) is utilized for separation of polar analytes which is contrary to RPLC. NPLC uses a polar stationary phase (*e.g.* bare silica or alumina) and a relatively non-polar mobile phase containing non-aqueous solvents (*e.g.* hexane or dichloromethane). The strength of the mobile phase in NPLC is determined by its polarity. Strong solvents with high polarity (*e.g.* dichloromethane) can elute analytes faster than solvents with little polarity (*e.g.* hexane). The retention of analytes under NPLC conditions is also affected by their polarity and the polarity of the stationary phase. Highly polar analytes interact strongly with the polar stationary phase compared to the weakly

polar ones, *i.e.*, the order of retention in NPLC follows the order of polarity of analytes. Similarly, highly polar stationary phases retain polar analytes strongly. In regards to the retention mechanism, adsorption is the main mechanism of retention in NPLC as described in Equation 1.18 [27, 41].

$$\log k = \log k_B - \frac{A_S}{n_S} \log N_B \quad (\text{Equation 1.18})$$

where k_B is the retention factor when using 100% solvent B (strong solvent), A_S is the cross-sectional areas occupied by the solute, n_S is the cross sectional areas occupied by the mobile phase, and N_B is the mole fraction of the stronger solvent (B).

Although NPLC is a powerful separation technique for polar analytes, it suffers from the following problems: (1) the immiscibility of water soluble analytes with the employed non-aqueous eluents; (2) long equilibration times associated with NPLC phases; and (3) incompatibility with mass spectrometer-based detectors [3]. Moreover, NPLC requires special precautions to avoid water contamination in the mobile phase. The presence of even small amounts of water in the mobile phase might lead to drastic drifts of retention.

1.2.2.3 Hydrophilic Interaction Liquid Chromatography (HILIC)

In 1990, the term hydrophilic interaction liquid chromatography (HILIC) was coined by Alpert for the separation of peptides and carbohydrates [1]. HILIC is considered as an alternative to NPLC especially for hydrophilic water miscible

analytes. HILIC utilizes a hydrophilic stationary phase (much like NPLC) and a less polar organic rich mobile phase (usually a mixture of water and > 60% acetonitrile). Under HILIC conditions, a water rich layer forms on the surface of the hydrophilic stationary phase. Partitioning of hydrophilic analytes between this formed water layer and the running organic rich mobile phase was suggested to be the main mechanism of retention in HILIC [1, 3]. However, others sources of interactions that might be involved in HILIC are ion exchange, dipole-dipole and H-bonding [3, 6, 8]. Figure 1.6 represents the different types of interactions between the solute and the stationary phase in HILIC. Since HILIC uses an aqueous-based mobile phase, it overcomes the problems associated with NPLC with respect to miscibility between the aqueous sample and the mobile phase, and with moisture contamination of mobile phases. The higher organic content (> 60%) of the mobile phase eases the coupling of a MS detector due to the low interfacial tension of ACN [3]. Chapter 2 provides a general background about the history of HILIC, retention mechanisms of HILIC and the different classes of HILIC stationary phases.

1.2.2.4 Ion Exchange Chromatography

Ion exchange chromatography gained popularity among analytical chemists after the work of Small *et al.* in 1975 [42]. The two main types of ion exchange chromatography are anion- and cation exchange chromatography. Anion exchange chromatography uses a cationic stationary phase for the separation of anions, while cation exchange chromatography uses an anionic stationary phase

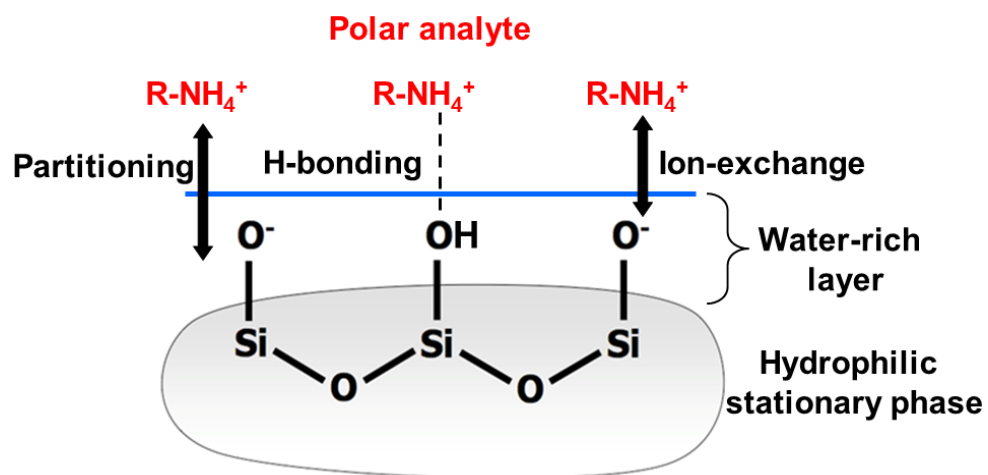
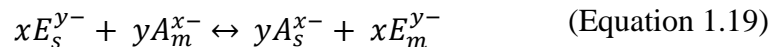


Figure 1.6 The different types of interactions between the analyte and the stationary phase in HILIC.

for separation of cations. Since anion exchange chromatography is the most widely used ion exchange chromatographic technique, further discussion will focus on it. The mobile phases used for anion exchange chromatography are commonly carbonate or hydroxide. Since such eluents are strongly alkaline, the stationary phase must have high pH stability which makes silica unsuitable for ion chromatography. Hence polymeric substrates are commonly used as stationary phases for ion exchange purposes. With respect to instrumentation, the HPLC used for ion chromatography may have an extra eluent generator and suppressor (to suppress the background signal of the eluent). Additionally, the whole path of the eluent should be metal free to avoid metal contamination which in turns affect the ion exchange process and hence the retention. Polyether ether ketone (PEEK) polymer is a commonly used material in ion chromatography instruments due to its chemical inertness, flexibility and pressure stability. Factors affecting retention under ion exchange conditions include the eluent strength, pH, temperature and solvents if present.

The process of ion exchange of analytes and eluent anions with a stationary phase is described by Equation 1.19.



where E and A are the eluent and the analyte, respectively. x and y refer to the stoichiometry coefficients of the eluent and analyte, respectively. The subscripts s

and m represent the stationary and mobile phase, respectively. The superscripts y^- and x^- denotes the charge carried by the eluent and the analyte, respectively.

The retention of a given anion by anion exchange chromatography can be explained by Equation 1.20 [43] as follows:

$$\log k = \text{const} - \frac{x}{y} \log [E_{(m)}^{y^-}] \quad (\text{Equation 1.20})$$

where x and y are the charges of the analyte and the eluent, respectively. Consequently, plotting $\log k$ of a given anion against $\log [\text{eluent}]$ should produce a straight line with a slope of $-x/y$ for a pure anion exchange model.

1.3 Summary

The ability of HILIC to retain polar analytes and its compatibility with MS detection systems has attracted the interest of many analytical chemists during the last decade. HILIC utilizes a hydrophilic stationary phase to retain polar analytes *via* partitioning. Chapter 2 discusses the different classes of HILIC phases in terms of chemistry, applications, efficiency and selectivity comparisons. Partitioning of the analytes between the water layer, held by the stationary phase and the mobile phase represents the basis of separation under HILIC conditions. However, other sources of interactions (*e.g.* ion exchange, H-bonding) play an important role in determining the selectivity differences between HILIC stationary phases. Developing new HILIC stationary phases with different selectivity was the goal of many scientists in the last two decades. Chapter 3 describes a very convenient way to characterize the different HILIC phases based

on probing the different interactions between model analytes and the stationary phase. These selectivity plots presented in Chapter 3 help to explore the behavior of the newly developed HILIC phases. Chapters 4 and 5 explain the HILIC characteristics of latex coated silica monoliths and their mixed mode retention under HILIC conditions. Chapter 6 describes the HILIC behavior of a covalently modified PGC column. Finally, Chapter 7 describes a non-covalent modification of silica core-shell particles with modified carbon nanoparticles to yield a highly efficient HILIC phase with unique selectivity.

1.4 References

- [1] A. Alpert, *J. Chromatogr.* **1990**, *499*, 177-196.
- [2] S. Di Palma, P.J. Boersema, A.J.R. Heck, S. Mohammed, *Anal. Chem.* **2011**, *83*, 3440-3447.
- [3] P. Hemstrom, K. Irgum, *J. Sep. Sci.* **2006**, *29*, 1784-1821.
- [4] R. Simon, Q. Enjalbert, J. Biarc, J. Lemoine, A. Salvador, *J. Chromatogr. A* **2012**, *1264*, 31-39.
- [5] M.E.A. Ibrahim, C.A. Lucy, In *Chapter 2: Stationary Phases for HILIC; Hydrophilic Interaction Chromatography: A Guide for Practitioners*, B.A. Olsen, B.W. Pack (Eds.), John Wiley & Sons Inc., 2013, pp. 43-85.
- [6] N. Dinh, T. Jonsson, K. Irgum, *J. Chromatogr. A* **2011**, *1218*, 5880-5891.
- [7] G. Schuster, W. Lindner, *J. Chromatogr. A* **2013**, *1273*, 73-94.
- [8] Y. Kawachi, T. Ikegami, H. Takubo, Y. Ikegami, M. Miyamoto, N. Tanaka, *J. Chromatogr. A* **2011**, *1218*, 5903-5919.
- [9] K. Cabrera, *J. Sep. Sci.* **2004**, *27*, 843-852.

- [10] K. Cabrera, D. Lubda, H.M. Eggenweiler, H. Minakuchi, K. Nakanishi, *J. High Resolut. Chromatogr.* **2000**, *23*, 93-99.
- [11] S. Pelletier, C.A. Lucy, *J. Chromatogr. A* **2006**, *1118*, 12-18.
- [12] K.M. Glenn, C.A. Lucy, P.R. Haddad, *J. Chromatogr. A* **2007**, *1155*, 8-14.
- [13] M.E.A. Ibrahim, C.A. Lucy, *Talanta* **2012**, *100*, 313-319.
- [14] M.J. Davies, E.F. Hounsell, *J. Chromatogr. A* **1996**, *720*, 227-233.
- [15] M.P.Y. Lam, E. Lau, S.O. Siu, D.C.M. Ng, R.P.W. Kong, P.C.N. Chiu, W.S.B. Yeung, C. Lo, I.K. Chu, *Electrophoresis* **2011**, *32*, 2930-2940.
- [16] B. Merelli, M. De Person, P. Favetta, M. Lafosse, *J. Chromatogr. A* **2007**, *1157*, 462-466.
- [17] Y. Cui, S.V. Olesik, *Anal. Chem.* **1991**, *63*, 1812-1819.
- [18] V.G. Berezkin, In *Chromatographic adsorption analysis: selected works of M.S. Tswett*, Ellis Horwood, New York, 1990.
- [19] L.S. Ettre, *LCGC North Am.* **2003**, *21*, 458-467.
- [20] C. Horvath, S.R. Lipsky, *J. Chromatogr. Sci.* **1969**, *7*, 109-116.
- [21] C.G. Horvath, B.A. Preiss, S.R. Lipsky, *Anal. Chem.* **1967**, *39*, 1422-1428.
- [22] T. Zhou, *Application of metal oxide columns in HPLC*, PhD Thesis, University of Alberta, Edmonton, **2009**.
- [23] J.P. Foley, J.G. Dorsey, *Anal. Chem.* **1983**, *55*, 730-737.
- [24] J.W. Dolan, *LCGC Eur.* **2012**, *25*, 370-383.
- [25] J.J. Van Deemter, F.J. Zuiderweg, A. Klinkenberg, *Chem. Eng. Sci.* **1956**, *5*, 271-289.

- [26] J.M. Miller, In *Chromatography: Concepts and Contrasts, 2nd Edition*, Wiley, New York, 2005.
- [27] L.R. Snyder, H. Poppe, *J. Chromatogr.* **1980**, *184*, 363-413.
- [28] S. Eksborg, P. Lagerstr, R. Modin, G. Schill, *J. Chromatogr.* **1973**, *83*, 99-110.
- [29] B.A. Bidlingmeyer, S.N. Deming, W.P. Price, B. Sachok, M. Petrusek, *J. Chromatogr.* **1979**, *186*, 419-434.
- [30] L.J. Felice, J.D. Felice, P.T. Kissinger, *J. Neurochem.* **1978**, *31*, 1461-1465.
- [31] C. Horvath, W. Melander, I. Molnar, P. Molnar, *Anal. Chem.* **1977**, *49*, 2295-2305.
- [32] T.M. Dillon, P.V. Bondarenko, M.S. Ricci, *J. Chromatogr. A* **2004**, *1053*, 299-305.
- [33] T. Franey, *LCGC North Am.* **2003**, *21*, 54-58.
- [34] J. Nawrocki, *J. Chromatogr. A* **1997**, *779*, 29-71.
- [35] J.L. Glajch, J.J. Kirkland, J. Kohler, *J. Chromatogr.* **1987**, *384*, 81-90.
- [36] J.J. Kirkland, M.A. Vanstraten, H.A. Claessens, *J. Chromatogr. A* **1995**, *691*, 3-19.
- [37] C.K. Lim, *Adv. Chromatogr.* **1992**, *32*, 1-19.
- [38] J.H. Knox, B. Kaur, G.R. Millward, *J. Chromatogr.* **1986**, *352*, 3-25.
- [39] T. Hanai, *J. Chromatogr. A* **2003**, *989*, 183-196.
- [40] C. West, C. Elfakir, M. Lafosse, *J. Chromatogr. A* **2010**, *1217*, 3201-3216.
- [41] P. Nikitas, A. Pappa-Louisi, P. Agrafiotou, *J. Chromatogr. A* **2002**, *946*, 33-45.

[42] H. Small, T.S. Stevens, W.C. Bauman, *Anal. Chem.* **1975**, *47*, 1801-1809.

[43] J.E. Madden, P.R. Haddad, *J. Chromatogr. A* **1998**, *829*, 65-80.

CHAPTER TWO: Stationary Phases for Hydrophilic Interaction Liquid Chromatography*

2.1 Hydrophilic Interaction Liquid Chromatography

Recently, literature and research on hydrophilic interaction liquid chromatography (HILIC) has increased dramatically. This has been accompanied by a correspondingly rapid increase in stationary phases developed for HILIC. The term "HILIC" was first coined by Alpert for the separation of polar analytes such as peptides and carbohydrates [1]. Usually a mixture of water and a high percentage of an organic modifier, in most cases acetonitrile (ACN), is employed with a polar stationary phase. This polar phase encourages the formation of a water layer on its surface. According to Alpert's theory [1], partitioning of analytes between the formed water layer and the mobile phase constitutes the major mechanism of retention in HILIC as shown in Figure 2.1. Thus, all HILIC stationary phases should be hydrophilic to encourage the formation of a stagnant water layer into which the analytes partition. In general the retentivity increases with the polarity of the stationary phase, *i.e.* the more hydrophilic the functional groups on the stationary phase, the longer the retention of polar analytes due to the formation of richer water layer. Numerous secondary interactions (*e.g.*, electrostatic attraction and repulsion) also affect retention and selectivity in HILIC.

*A version of this chapter has been published as "Chapter 2: Stationary Phases for HILIC, in *Hydrophilic Interaction Chromatography: A Guide for Practitioners*" by Mohammed E. A. Ibrahim, Charles A. Lucy, ed. B. A. Olsen, B. W. Pack. John Wiley & Sons Inc., 2013.

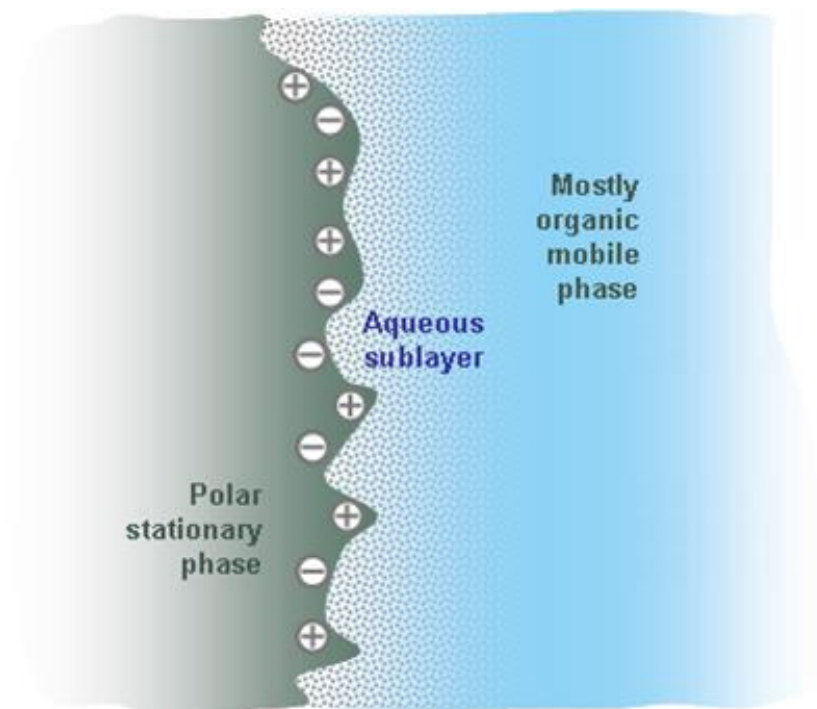


Figure 2.1 Formation of the water rich layer on the surface of stationary phase under HILIC conditions. Reprinted from Reference [2] with permission from Sielc Technologies.

2.2 Historical Aspects of HILIC Stationary Phases

Although HILIC was suggested by Alpert in 1990, this separation technique had been used since 1975 for separation of carbohydrates and oligosaccharides [3, 4]. Linden *et al.* separated a mixture of oligosaccharides using two different stationary phases using refractive index as a method of detection [3]. These phases are a strongly basic quaternary ammonium anion exchanger phase named Bondapak AX/Corasil and a weakly basic amine based anion exchanger named micro Bondapak. Moreover, Lampert *et al.* separated cocaine and its metabolites under HILIC conditions using cyanopropyl and silica columns [5] however, the authors claimed that the technique is RPLC. In 1951, it was suggested that ion exchange resins as hydrophilic stationary phases possessed a water enriched layer on their surfaces [6]. Sulfonated polystyrene cation exchange phases in different states (sodium, lithium, potassium and tetramethylammonium) were studied in the previously mentioned work [6]. The amount of water contained in the resin was increased in the following sequence: lithium > sodium > potassium > tetramethylammonium [6]. This stationary water layer was attributed to the uptake of non-electrolytes by ion exchange resins. This work was followed by separation of oligosaccharides on anion exchange resin in sulfate form and cation exchange resin in lithium form by Samuelson and co-workers in 1975 [7]. Fifteen years later, Alpert coined the term “HILIC” for separation of peptides, oligosaccharides and nucleic acids on various ion exchange resins including PolySulfoethyl Aspartamide and PolyHydroxyethyl Aspartamide [1]. HILIC has been steadily gaining interest along with emergence of new

hydrophilic stationary phases as an orthogonal alternative to RPLC. In the following section, HILIC stationary phases are classified into bare silica, silica based and non-silica based phases. Moreover, these phases are compared in terms of efficiency, retention and selectivity.

2.3 Modes of Retention of HILIC

According to Alpert theory, water is considered the strongest eluent in HILIC separations *i.e.*, the higher the water content in the mobile phase, the lesser is the retention of the analyte. That is why we observe increase in retention as % organic modifier (mainly ACN) is increased especially at high % ACN - the reverse of that in RPLC. As suggested by Alpert, the partitioning of hydrophilic analytes between the formed water layer on the surface of the stationary phase and the running organic rich mobile phase is the main retention mechanism in HILIC (Figure 2.1). However, there are other mechanisms of retention that contribute to retention under HILIC conditions including ion exchange, H-bonding, dipole-dipole and hydrophobic interactions [8-10]. Similarly to RPLC partitioning, Equation 2.1 represents the HILIC partitioning according to the linear solvent strength model [11].

$$\log k = \log k_w - S\varphi \quad (\text{Equation 2.1})$$

where k is the retention time of the hydrophilic analyte, k_w is the retention time of the analyte in the weakest eluent (*i.e.*, in absence of water), φ is the solvent

fraction of the strong eluent component *i.e.*, water and S is the slope when $\log k$ is plotted *vs.* ϕ . If the plot of $\log k$ *vs.* ϕ is linear ($R^2 \sim 1$), it indicates that partitioning is the dominant mechanism of retention. If non-linear relationship is obtained, it means that other mechanisms of retention is involved *e.g.* ion exchange. Chapter 5 discusses the ion exchange/HILIC mixed mode retention behavior of latex coated silica monoliths based on Equations 2.1 (partitioning) and 1.20 (Chapter 1, ion exchange).

2.4 HILIC Stationary Phases

This section discusses the chemistry of the different classes of HILIC stationary phases. Section 2.5 provides a comparison of various commercial HILIC columns.

2.4.1 Underivatized Silica

Although the term (HILIC) was coined by Alpert in 1990 using derivatized silica phases [1], the same approach had been applied by Jane in 1975 using an underivatized silica phase [12]. Bare silica columns (without any modifications) have been widely used in HILIC [13-22], particularly in LC-MS methods. In general HILIC is attractive for LC-MS as the high organic content in the mobile phase lessens the problem of ion suppression especially with electrospray ionization (ESI) [23]. Underivatized silica HILIC phases are further attractive due to the absence of ligands, that could otherwise leach from the column and appear as extra peaks in the mass spectrum [11].

Silanol groups ($-\text{SiOH}$) are the key chemical feature of hydrated silica surfaces [24]. Their surface concentration is $8 \mu\text{moles/m}^2$. These silanol groups can react with silanes to form the bonded phases discussed in Section 2.4.2. The silanol groups on the silica surface may be free, geminal or associated, as shown in Fig 2.2 (A-C) [25-29]. Treatment of the silica affects the distribution and type of the silanol groups. High temperature treatment of silica converts geminal and associated silanols into free silanols which are more acidic than geminal and associated silanols. The high acidity of free silanols contributes to the peak tailing and low efficiency (N) values for basic analytes. However, treatment at temperatures higher than $800 \text{ }^\circ\text{C}$ removes all active silanols and leaves hydrophobic siloxane bridges only, rendering the silica more hydrophobic [30].

The acidity of silanols is also affected by the purity of silica itself. The presence of contaminant metals such as Al^{3+} and Fe^{3+} increases the acidity of silica by withdrawing electrons from the oxygen atoms of the silanol groups. According to the degree of purity, silica can be classified into *type-A* or *type-B* silica. Type-A silica is less pure and more acidic than type-B silica and was widely used prior to 1990. Currently, type-A silica is reserved for primitive applications including sample preparation and preparative chromatography. On the other hand, type-B silica is prepared carefully in a metal free environment to prevent any contamination. Thus, type-B silica is less acidic and has lower tendency to generate tailed peaks with basic solutes as compared to silica type-A. The term type-C silica does not relate to the silica purity but rather indicates the phase is produced through hydrosilylation [31] where surface silanols (Si-OH) are

replaced by silicon hydride (Si-H). Cogent Silica-CTM from Microsolv (Eatontown, NJ, USA) is a good example of type-C silica column (Table 2.1). Separation of phenylalanine and phenylglycine has been achieved on a 4 μm Cogent Silica-CTM (100 Å) under HILIC conditions [32].

2.4.1.1 Totally Porous Silica Particles

Silica phases may be totally porous, superficially porous or monolithic. Generally, silica is characterized by high mechanical strength so silica can withstand high pressure values, as compared to polymeric phases, producing uniform peaks and higher N values. Totally porous silica particles (TPP) are widely used due to their greater column capacity which enables injection of larger sample masses and due to their availability in a wider variety of dimension options. The most common particle diameters are in the range of 1.5-5.0 μm. TPP are prepared either by sol-gel synthesis or aggregation (assembly) of smaller particles.

The sol-gel procedure involves the emulsification of a silica solution (*sol*) in an immiscible non-polar solvent. Droplets of this emulsified sol are converted into spherical beads of silica hydrogel. These beads are then dried and classified into a narrower particle size range. Controlling the pH, temperature and the concentration of the silica sol enables production of silica particles with the desired particle and pore sizes [24].

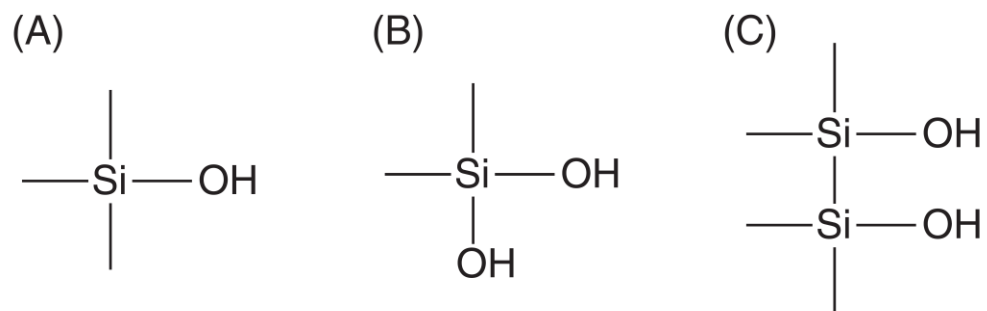


Figure 2.2 Different types of silanols on the surface of silica.

Table 2.1 Characteristics of commercial HILIC phases.

Column No. ^a	Brand name	Manufacturer	Support	Functionality	Particle size (µm)	Pore size (Å)	Surface area (m ² /g)	Column Length (mm)	Column Diameter (mm)
Underivatized silica phases									
14	Atlantis HILIC Si	Waters	Silica	Underivatized	3,5	100	330	30-250	1.0-4.6
	Betasil Silica	Thermo Electron Corporation	Silica	Underivatized	3,5	100	-	50-250	1.0-4.6
	Hypersil Silica	Thermo Electron Corporation	Silica	Underivatized	3-30	120	-	30-300	1.0-4.6
	Kromasil Si	Akzo Nobel	Silica	Underivatized	3.5-16	60-300	-	50-250	2.1-50
13	Chromolith Si	Merck	Silica	Underivatized	N/A	130	300	100	4.6
	Onyx Si	Phenomenex	Silica	Underivatized	N/A	130	300	100	4.6
15	Purospher STAR Si	Merck	Silica	Underivatized	5	120	330	125-250	4.0-4.6
16	LiChrospher Si 100	Merck	Silica	Underivatized	5	100	400	50-300	2.1-4.6
17	LiChrospher Si 60	Merck	Silica	Underivatized	5	60	700	50-300	2.1-4.6
	Spheri-5 Silica	PerkinElmer Brownlee	Silica	Underivatized	5	80	180	250	4.6
	Sphensorb Si	Waters	Silica	Underivatized	3-10	80	220	20-250	1.0-4.6
18	Cogent silica-C	Microsolv	Silica	Underivatized (Type C)	4	100	350	100	4.6

Continued

	HALO HILIC	Advanced materials technology	Silica	Underivatized (Type B)	2.7	90	150	50-150	2.1-4.6
BEH phases									
	Acquity UPLC BEH HILIC	Waters	Silica	BEH	1.7-10	130-300	185	50-150	1.0-3.0
Amide silica phases									
7-8 ^b	TSKgel Amide 80	Tosoh Bioscience	Silica	Amide	3-10	80	450	50-300	1.0-21.5
	GlycoSep N	ProZyme	Silica	Amide	5	-	-	250	4.6
Diol silica phases									
10	LiChrospher 100 Diol	Merck	Silica	2,3-dihydroxypropyl	5	100	350	50-300	2.1-4.6
	LiChrosorb 100 Diol	Merck	Silica	2,3-dihydroxypropyl	5,10	100	300	50-300	2.1-4.6
	Inertsil Diol	GL Sciences	Silica	2,3-dihydroxypropyl	3,5	100	450	33-250	1.0-4.0
	YMC-pack Diol NP	YMC	Silica	2,3-dihydroxypropyl	5	60-300	100-330	50-250	2.0-4.6
11	Luna HILIC	Phenomenex	Silica	Cross-linked diol	3,5	200	185	30-100	2.0-21.2
Cyanopropyl silica phases									
	LiChrospher 100 CN	Merck	Silica	3-cyanopropyl	5,10	100	350	125-250	4.0
	Altima HP Cyano	Grace Alltech	Silica	3-cyanopropyl	3,5	190	200	50-250	2.1-4.6

Continued

	Spherisorb CN	Waters	Silica	3-cyanopropyl	3,5,10	80	220	20-250	1.0-4.6
Cyclodextrin based silica phases									
	Nucleodex β-OH	Macherey- Nagel	Silica	B-cyclodextrin	5	100	-	200	4.0
	Cyclobond I 2000	ASTEC	Silica	B-cyclodextrin	5,10	100	-	50-250	2.1-10.0
Zwitterionic phases									
1-3°	ZIC-HILIC	Merck	Silica	Sulfoalkylbetaine	3,5,5	100,200	135,180	100-250	2.1-4.6
4	ZIC-pHILIC	Merck	Polymer	Sulfoalkylbetaine	5	-	-	50-150	2.1-4.6
5	Nucleodur HILIC	Macherey- Nagel	Silica	Sulfoalkylbetaine	1.8-5	110	340	30-250	2.0-4.6
	Obelisc N	SiELC	Silica	Unspecified	5,10	100	-	10-250	1.0-4.6
6	PC HILIC	Shiseido	Silica	Phosphoryl- choline	5	100	450	100-250	2.0-4.6
Aminopropyl silica phases									
19	LiChrospher 100 NH ₂	Merck	Silica	3-Aminopropyl	5	100	350	125-300	3.2-4.6
20	Purospher STAR NH ₂	Merck	Silica	3-Aminopropyl	5	120	330	125-250	4.0-4.6
	Luna NH ₂	Phenomenex	Silica	3-Aminopropyl	3-10	100	400	250	4.6
	Hypersil APS-2 (Amino)	Thermo scientific	Silica	3-Aminopropyl	3-10	120	170	30-250	2.1-4.6
	Spherisorb NH ₂	Waters	Silica	3-Aminopropyl	3-10	80	220	20-250	1.0-4.6
	Zorbax NH ₂	Agilent	Silica	3-Aminopropyl	5,7	70	300	50-250	4.6-21.2

Continued

21	TSKgel NH ₂ -100	Tosoh Bioscience	Silica	Aminoalkyl	3	100	450	50-150	2.0-4.6
Latex coated silica phases									
	AS9-SC silica	Home made	Silica monolith	Quaternary ammonium salts	N/A	130	300	100	4.6
Poly(succinimide) silica phases									
12	Poly(2-sulfoethyl A)	PolyLC	Silica	Poly(2-sulfoethyl aspartamide)	3-12	200	188	35-250	1.0-50.8
	PolyCAT A	PolyLC	Silica	Poly(aspartic acid)	3-12	200	188	35-250	1.0-50.8
9	Polyhydroxyethyl A	PolyLC	Silica	Poly(2-hydroxyethyl aspartamide)	3-12	200	188	35-250	1.0-50.8
Amino phases									
	Styros TM AminoHILIC	Orachrom Inc	Poly(styrene-divinyl benzene)	Amino	N/A	1000-2000	-	33-250	1.0-20
Sulfonated S-DVB phases									
	Agilent Hi-Plex H	Agilent	styrene-divinyl benzene	Sulfonic acid	8	-	-	300	6.5-7.7

a) Column numbers are represented in Figure 2.20

b) Column no. 7 for TSKgel Amide 80 (5 μm, 100 × 4.6 mm inner diameter (i.d.))

Column no. 8 for TSKgel Amide 80 (3 μm, 50 × 4.6 mm i.d.)

c) Column no.1 for ZIC-HILIC (5 μm, 100 × 4.6 mm i.d., 200 Å)

Column no.2 for ZIC-HILIC (3.5 μm, 150 × 4.6 mm i.d., 200 Å)

Column no.3 for ZIC-HILIC (3.5 μm, 150 × 4.6 mm i.d., 100 Å)

Aggregation of smaller particles (Figure 2.3) is an alternative approach for preparation of TPP. In this approach, a silica sol of a definite particle size is dispersed into a polar liquid followed by addition of a polymerizable material such as melamine. The polymerizable material initiates the coacervation of the silica particles to form spherical aggregates of uniform size. These aggregates are then sintered at high temperature to strengthen the network of the silica sol particles. Generally, the size of the silica-sol particle used to prepare the aggregate particle dictates the size of the resultant pores [24].

2.4.1.2 Superficially Porous (Core-Shell) Silica Particles

Superficially porous particles (SPP) consist of a solid core (2-5 μm) coated with a porous outer silica shell (0.25-0.5 μm). These phases are characterized by their high N values [33, 34]. The surface areas of SPP are about $\frac{3}{4}$ that of totally porous particles, but substantially greater than pellicular particles. The HALO HILIC phase (Table 2.1) is a representative example of the core shell silica particles [35]. This HALO HILIC phase consists of a 1.7 μm solid core particle with a 0.5 μm type-B porous silica layer fused to the surface. Gritti *et al.* recently demonstrated the Van Deemter behavior of a 150 \times 4.6 mm HILIC column packed with 2.7 μm HALO particles under HILIC conditions [36].

2.4.1.3 Monolithic Silica

A monolithic column consists of a single piece of porous material, rather

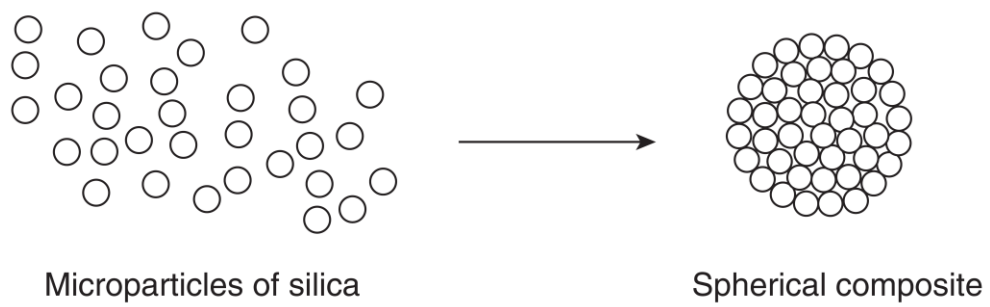


Figure 2.3 Assembly of small silica particles into spherical aggregates. Reprinted from Reference [24] with permission from Wiley.

than a column packed with discrete particles. Monolithic columns are characterized by the presence of large macropores (1-3 μm) for through-flow of mobile phase and relatively small mesopores (10-25 nm) to provide the surface area for retention [37-39]. Monoliths may be either polymeric or inorganic, with the latter being predominantly silica. Polymeric monoliths usually swell or shrink in the presence of organic solvents such as used in HILIC, leading to poor mass transfer and much lower efficiencies [40]. The highly porous structure of the monolith offers high permeability which allows fast separation of analytes at very high flow rates with minimal backpressures [41-44]. However, monoliths have a low phase ratio, *i.e.* lower sample capacity and hence lower retentivity compared to particulate columns [38, 41, 45, 46]. Although many research studies have been made on silica monoliths, HILIC applications using silica monoliths are limited. Some applications are separation of inorganic ions *e.g.* Li^+ , Na^+ , K^+ and Cl^- and some drugs including naproxen and warfarin on a Chromolith Si column (Table 2.1) [47].

2.4.1.4 Ethylene Bridged Hybrids (BEH)

Although silica-based packings are characterized by high chromatographic efficiency and excellent mechanical stability, bonded silica phases are chemically unstable at pH values lower than 2 (due to hydrolysis of the bonded phase) or higher than 8 (due to dissolution of the silica itself) [48-50]. This results in loss of column efficiency, an increase in column backpressure, and bed collapse of the

silica packing material [51]. Additionally, the high acidity of free silanols causes peak tailing especially with basic analytes.

One of the ways to overcome these problems was the invention of ethylene bridged hybrids (BEH). These hybrid phases (Figure 2.4) vary in particle size from 1.7 to 10 μm and have been derivatized to form a variety of bonded phases including C_8 , C_{18} , phenyl and HILIC. Reversed phase BEH columns are usually synthesized by the co-condensation of 1,2-bis(triethoxysilyl) ethane (BTEE) with tetraethoxysilane (TEOS) [52] as shown in Figure 2.4.

These hybrid materials are spherical and mechanically strong so they are frequently utilized in ultra high pressure LC (UHPLC) [52]. Column stability at extreme pH values (up to pH 10) can be attributed to the increased hydrolytic stability of the ethyl-bridged groups within the particle matrix. Additionally, the reduced acidity of the bridged silanols in these hybrid phases suppresses peak tailing for basic analytes. Neue and co-workers studied the HILIC behavior of a 1.7 μm underivatized BEH phase and compared it to other underivatized silica phases [53]. Neue concluded that the retention mechanism of the BEH phase includes partitioning, adsorption and secondary interactions which are quite similar to other underivatized silica. Factors affecting retention such as pH, organic modifier and % ACN were studied for the 1.7 μm BEH phase. Smaller particle size (3 μm) enhanced the efficiency and produced narrower peaks, hence, higher sensitivity for the BEH phase in ESI-MS mode was observed compared to other RP silica based phases [53]. Stable performance has been demonstrated for over 2000 injections [53].

2.4.2 Derivatized Silica

Chemical modification of the silica surface yields a variety of silica-based polar derivatized phases. These attached polar groups are able to induce formation of a water-enriched layer (due to their hydrophilic nature) into which polar analytes can partition [54]. For more simplification, in this chapter these silica modified polar phases are classified according to the net charge on their surfaces: *i.e.*, neutral, zwitterionic, positively charged and negatively charged derivatized silica phases.

2.4.2.1 Neutral Derivatized Silica

2.4.2.1.1 Amide Silica

The TSK gel Amide-80 (Tables 2.1 and 2.2) from Tosoh (King of Prussia, PA, USA) is a good example of amide silica-based columns and has been available since 1985. It is available in 3, 5, or 10 μm particles. The surface functionality consists of non-ionic carbamoyl groups bonded to the silica backbone through a short alkyl chain. Unlike amino phases, the amide group is not basic. Hence retention of unionized analytes should be unaffected by pH of the mobile phase. Moreover, the absence of amino groups prevents the formation of Schiff's bases with sugars and other carbonyl derivatives [11]. This phase was used for multidimensional mapping of oligosaccharides along with octadecyl silica (ODS) and diethylaminoethyl (DEAE) phases [55-57]. After this work, Yoshida used the same column for separation of peptides where the amide silica based column showed good recovery and stability after 500 injections [58, 59].

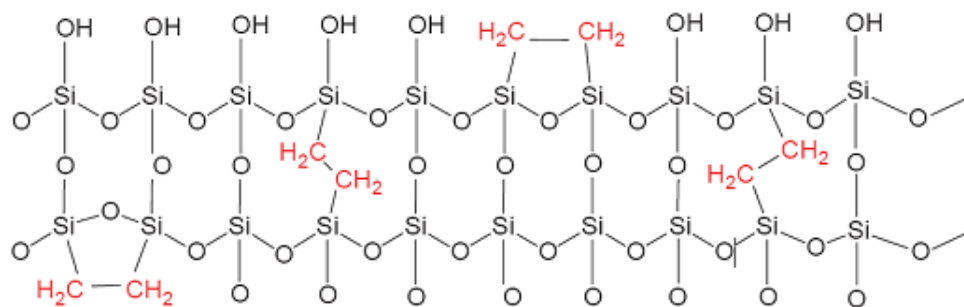


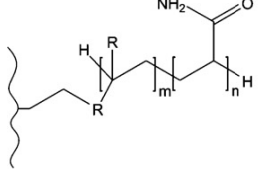
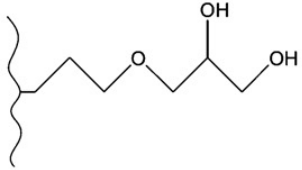
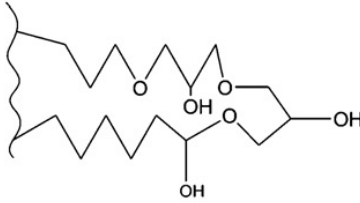
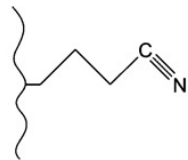
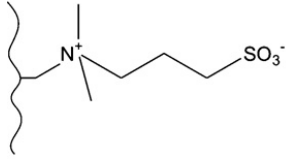
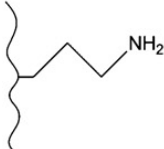
Figure 2.4 Schematic of Waters (Milford, MA, USA) BEH phase. Reprinted from Reference [53] with permission from Wiley.

During the last decade, HILIC applications of TSK gel Amide-80 have increased dramatically. Recently, a TSK gel Amide-80 column has been used for the simultaneous analysis of α -amanitin, β -amanitin, and phalloidin in toxic mushrooms by LC-time-of-flight MS [60]. Additionally, applications of the TSK gel Amide-80 column include the separation of melamine and cyanuric acid which have been used for adulteration of milk with excellent recovery and resolution [61], and the fast separation of both inactive and active ingredients in mannitol injections with a high degree of robustness and accuracy [62].

2.4.2.1.2 Diol Silica

Diol phases (Table 2.2) were some of the first bonded silica phases to be developed. The diol phase was developed primarily to overcome the problems of adsorption caused by the free silanols on bare silica phases [11]. It is prepared by reaction of silica with glycidoxypropyltrimethoxy silane, followed by acid-catalyzed ring-opening hydrolysis of the oxirane group to form the diol hydrophilic neutral phase. Diol silica phases contain hydrophilic hydroxyl groups and silanols can be blocked by a silylating reagent to overcome the adsorption of analytes on the surface. Hence, diol phases are considered as one of the best phases for HILIC due to the presence of the hydrophilic hydroxyl groups and absence of adsorptive properties of free silanols. The overall polarity of diol phases is quite similar to that of bare silica [63].

Table 2.2 Chemical structures of some selected silica-based HILIC phases

Phase type	Phase name	Chemical structure*
Neutral derivatized silica	Amide silica	
	Diol silica	
	Cross-linked diol	
	Cyanopropyl silica	
Zwitterionic derivatized silica	Sulfoalkylbetaine silica	
Positively charged silica	Aminopropyl silica	

* Chemical structures of the other HILIC phases are included in different figures.

Although the first HILIC applications of diol silica phases were for separations of proteins, nucleic acids and polysaccharides [64], diol phases are now commonly used for the separation of small sized polyols. Diol silica phases were evaluated against amino bonded silica phases [65]. Diol silica showed no irreversible retention of reducing sugars. Diol phases are the best for separation of carbohydrates due to the absence of amino groups and thus no Schiff's base formation [66]. Residual silanol activity can influence retention of some analytes on diol phases used for HILIC [67]. For instance, on an Inertsil Diol, 5 μm phase (Table 2.1), retention of glycine changed with the addition of trifluoroacetic acid (TFA), whereas urea and sucrose remained constant. More recently, different anomeric forms of monosaccharides have been resolved on a diol silica column which allows monitoring the rate of the mutarotation [68].

A HILIC/RPLC mixed mode phase, prepared by attaching an alkyl linker to a silica column, was released by Dionex (Sunnyvale, CA, USA) under the trade name Acclaim Mixed Mode HILIC-1. This linker consists of an alkyl chain to provide RP retention (hydrophobic interaction) and a glycol terminal group which contributes to diol type HILIC properties. This mixed mode phase was used for analysis of nonionic ethoxylated surfactants in ACN-rich eluents [69].

Diol columns may slowly release the bonded phase under acidic conditions. One of the approaches to increase its stability against hydrolysis is the synthesis of cross-linked diol phases (Table 2.2). Luna HILIC 200 is a good example of these cross-linked phases which shows high hydrolytic stability, stronger hydrophobic interactions and better peak shape compared to non-cross-

linked diol phases [70]. Furthermore, the Luna (cross-linked diol) column showed a dual HILIC/RPLC retention mode depending on the percentage of the organic modifier in the mobile phase [70].

2.4.2.1.3 Cyanopropyl Silica

Although cyanopropyl silica phases (Table 2.2) can be used in both normal phase and reversed phase (RP) chromatography, only a few HILIC applications have been reported [71, 72]. Due to its lower hydrogen bond donor capabilities compared to silanols, cyanopropyl silica phases are less retentive in normal phase chromatography than silica and other normal phase packings [30]. One of the major disadvantages of cyanopropyl silica phases is their mechanical instability, *i.e.* collapse of these particles in solvents of intermediate polarity. This instability is mechanical (not chemical) in nature [30]. In solvents of intermediate polarity, the adhesion of particles to each other decreases which leads to collapse of particle bed. On the other hand, the adhesion of these particles is strong in either non-polar or polar solvents, which prevents the collapse of bed. The limited number of applications of cyanopropyl phases in HILIC conditions can be attributed to the previously mentioned mechanical instability. Some hydrophilic analytes (*e.g.* uracil, cytosine and dihydroxyacetone) actually eluted *faster* than dead time markers on a LiChrospher CN, verifying the low potential of cyanopropyl silica as a HILIC stationary phase [10].

2.4.2.1.4 Cyclodextrin Based Silica

Cyclodextrins (CDs) are formed through enzymatic hydrolysis of starch. Chemically CD consists of sugar units bound together in the form of ring; hence they can be considered as cyclic oligosaccharides. Figure 2.5 shows the common types of cyclodextrins; α -CD, β -CD and γ -CD that consist of 6, 7 and 8 D-glucopyranoside units, respectively, which are 1-4 linked together. CD can be topologically represented as toroids, the rims of which are covered with the hydroxyl groups of the sugar units. This arrangement makes the interior of the CD hydrophobic and thus able to host other hydrophobic molecules. In contrast, the exterior is sufficiently hydrophilic to act as a HILIC stationary phase.

CD exhibit chiral recognition characteristics because they consist of optically active sugars. Cyclodextrins have been used as normal phase stationary phases for separations of sugars, sugar alcohols, flavones, and aromatic alcohols [73, 74]. Due to the hydrophilic nature of the hydroxyl groups of the sugars in cyclodextrins, they have been used for separation of plant extracts [75] and amino acids [76] under HILIC conditions. As the number of sugar units of the separated oligosaccharides increases, the retention increases due to stronger interactions with the sugar hydroxyl groups located on the exterior of CD rather than penetration inside the cavity of CD [77]. CD columns show greater retention for amino acids compared to the TSK gel Amide-80 phase and more reproducibility and stability than aminopropyl silica based phases [76].

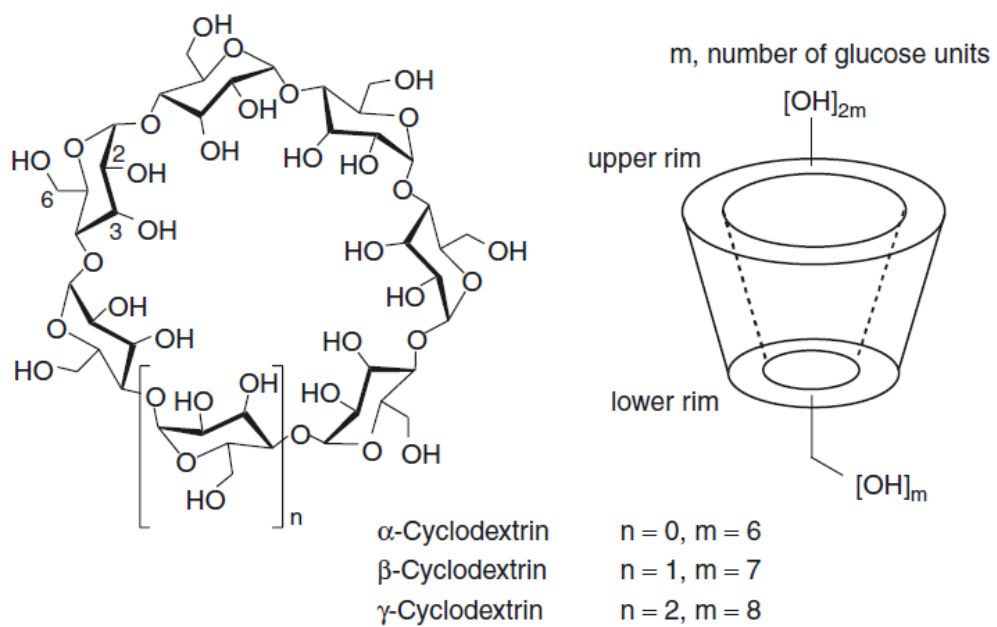


Figure 2.5 Chemical structure of different types of cyclodextrins. Reprinted from Reference [24] with permission from Wiley.

2.4.2.2 Zwitterionic Derivatized Silica

2.4.2.2.1 Sulfoalkylbetaine Silica

Irgum and co-workers introduced a group of zwitterionic silica-based stationary phases for HILIC [78, 79]. These zwitterionic phases are synthesized *via* grafting an active layer containing sulfoalkylbetaine groups (Table 2.2) onto wide pore silica (ZIC-HILIC) or a polymeric support (ZIC-pHILIC). Sulfoalkylbetaine phases are zwitterionic in nature due to the presence of basic quaternary groups and acidic sulfonic groups as shown in Table 2.2. While these phases contain both positive and negative charges, they have poor ion exchange characteristics. Their net charge is approximately zero since the oppositely charged groups exist in a molar ratio of 1:1. The poor ion exchange characteristics of these phases may be attributed to their low surface areas [11] and shielding of free silanols by the oppositely charged functionalities [80]. As zwitterions are strong osmolytes [81], *i.e.* encourage the binding of water to their surfaces, such phases are suitable for HILIC.

Sulfoalkylbetaine silica phases carry a very small negative charge, arising from the distal sulfonic acid groups [11]. This excessive negative charge is pH independent [82, 83]. Indeed, Guo *et al.* [80] found that the retention on sulfoalkylbetaine silica columns is the least affected by pH of the HILIC columns studied.

Although these phases were initially designed for the separation of inorganic anions and cations [78, 79], many HILIC applications have been reported including separations of nucleobases [84], peptides [85-87], metabolites

[88, 89], ions [90] and other polar analytes [91, 92]. Separation of inorganic ions and zwitterionic solutes was achieved on a zwitterionic micellar coated stationary phase using pure water as the mobile phase [93].

2.4.2.2.2 Obelisc R and Obelisc N Columns

Obelisc is a trade name of a group of zwitterionic stationary phases that are produced by SiELC (Prospect Heights, IL, USA). Figure 2.6 shows a schematic diagram of these phases. The manufacturer suggested that they are the first available columns with liquid separation cell technology, *i.e.*, a new chemical modification of silica pores into liquid separation cells with their own characteristics. These columns are distinguished by three main characteristics [94]: (1) the high density of cationic and anionic charges on the surface make Obelisc columns suitable for preparative chromatography; (2) the ionic strength inside the cells is higher than that of the mobile phase leading to higher mass transfer rates and hence higher efficiency and (3) both anionic and cationic charges are involved in electrostatic interactions with analytes.

Obelisc R has RP character while Obelisc N has normal phase character. As shown in Figure 2.6, Obelisc R and N phases differ in the position of the charged groups on surface. However, because Obelisc R has a RP character and hence cannot be used in HILIC mode, we will focus on the Obelisc N phase. Obelisc N has anionic groups close to the silica surface separated from cationic groups by a hydrophilic spacer. Packings are available as 5 and 10 μm with 100 \AA pore size as shown in Table 2.1. Unfortunately, the exact chemical structure of

these zwitterionic phases is not specified by the manufacturer. Obelisc N columns are characterized by high polarity due to the presence of charged groups and hydrophilic chains on their surfaces. Hence, Obelisc N can be utilized in ion exchange chromatography due to charged groups on the surface and in HILIC due to the water layer formed on its surface. The stability of Obelisc N is limited to a pH range of 2.5–4.5 and a temperature range of 20–45 °C [19].

A few HILIC applications have been reported on the Obelisc N phase. In 2011, the retention behavior of dexrazoxane (a model bisdioxopiperazine drug) and its three polar metabolites has been studied on Obelisc N and other HILIC phases [19]. Obelisc N showed a significantly lower hydrophobic selectivity compared to other mixed mode stationary phases and showed a comparable behavior to hydrophilic amino phases [9]

2.4.2.3 Positively Charged Derivatized Silica

2.4.2.3.1 Aminopropyl

Aminopropyl silica phases (Table 2.2) are among the oldest amine based phases. These phases have been introduced for either normal phase LC or HILIC purposes. Aminopropyl phases have been used extensively under HILIC conditions for separation of carbohydrates [3, 65, 95, 96], amino acids, proteins [97] and some antibiotics [98]. These phases have become more popular than bare silica in carbohydrate separations as they promote fast mutarotation which prevents formation of double peaks due to anomer resolution [11].

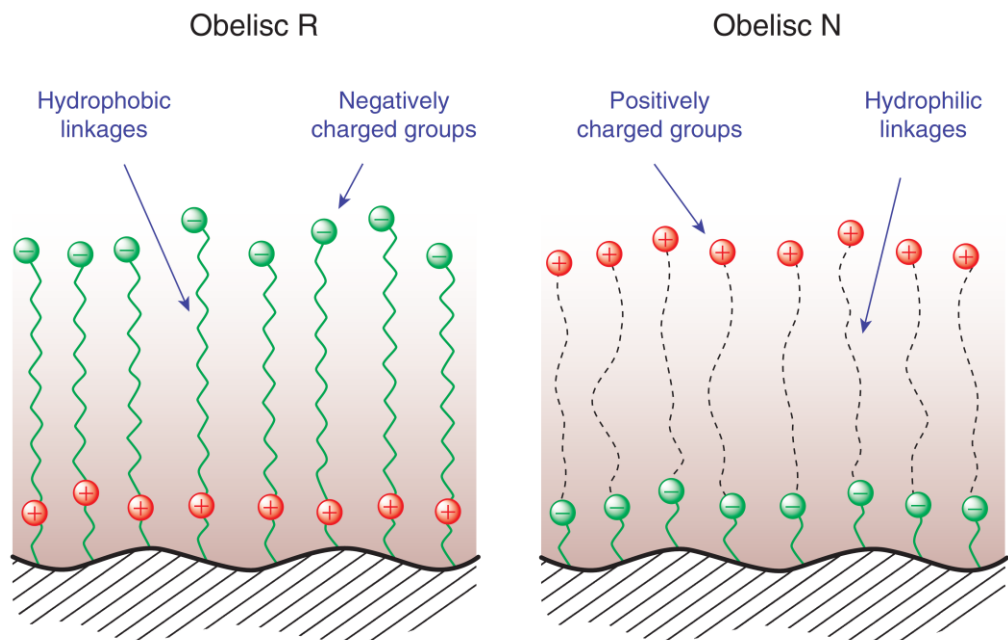


Figure 2.6 Schematic diagram of Obelisc R and Obelisc N. Reprinted from Reference [99] with permission from Sielc Technologies.

However there are a number of challenges with amino phases. Aminopropyl silica is more reactive than other HILIC phases. Amino phases suffer from irreversible adsorption problems, especially for acidic analytes [100]. Aminopropyl silica phases also exhibit significant bleed (*i.e.*, detachment of the ligand from the silica skeleton) compared to other hydrophilic bonded silica phases [101]. Slow pH equilibration can be observed [98]. Finally, Schiff's base formation with aldehydes leads to problems during separation of some sugars [45]. Stationary phases containing secondary or tertiary amine groups *e.g.* YMC Pack Polyamine II, cannot form Schiff bases with reducing sugars, resulting in improved column lifetime [102].

2.4.2.3.2 Latex Coated Silica

In 2010, we introduced an agglomerated silica monolithic column which was prepared by electrostatically attaching polycationic latex particles onto a silica monolith (Figure 2.7) by simply flushing a suspension of a latex possessing hydrophilic quaternary amines through a silica monolith [42, 44]. As per discussed in Chapter 4, this agglomerated phase was tested for separation of polar analytes *e.g.* benzoates, nucleotides and amino acids under HILIC conditions [44]. The high permeability offered by the monolith structure allowed fast (< 15 s) separation of naphthalene, uracil and cytosine with similar selectivity to other HILIC phases [44]. The positive charge on the agglomerated phase exhibited Electrostatic Repulsion Hydrophilic Liquid Interaction Chromatographic (ERLIC) for amino acids. Chromatographic details of this phase are given in Chapter 4.

2.4.2.4 Negatively Charged Derivatized Silica

Poly(succinimide) based silica represents the majority of stationary phases in this class. Figure 2.8 shows the synthesis of the poly(succinimide) based phases. Firstly, the aminopropyl silica skeleton reacts with poly(succinimide) where a fraction of the succinimide rings are opened and linked to the aminopropyl backbone through multiple amide linkages. Secondly, the unopened succinimide rings are reacted with different nucleophiles to form the various poly(succinimide) based phases shown in Figure 2.8.

Alpert proposed the synthesis of poly(aspartic acid) silica through hydrolysis of the succinimide rings to yield a weak cation exchanger [103]. These columns were stable and durable for the separation of proteins. Poly(aspartic acid) silica was used for separation of anions and/or cations due to its zwitterionic nature which is attributed to the presence of both protonated aminopropyl and dissociated carboxylic groups [104].

These poly(succinimide) silica based phases are manufactured by PolyLC (Columbia, MD, USA) and are available under the brand names of PolyCAT ATM for poly(aspartic acid) silica, PolySulfoethyl ATM for poly (2-sulfoethyl) aspartamide silica and PolyHydroxyethyl ATM for poly (2-hydroxyethyl) aspartamide silica (Table 2.1). PolyHydroxyethyl ATM has been used for separations of carbohydrates, phosphorylated and non-phosphorylated amino acids, peptides, glycopeptides, oligonucleotides, glycosides, metabolites and small polar analytes [105-108]. However, poly(2-hydroxyethyl aspartamide)

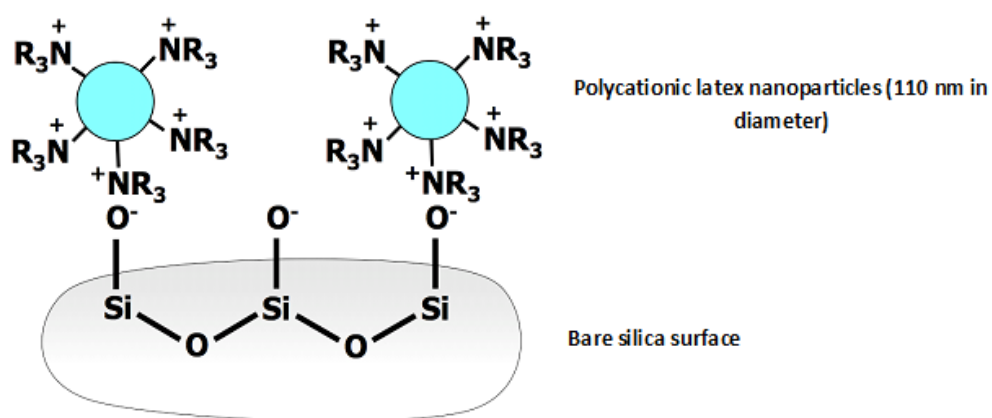


Figure 2.7 Structure of the agglomerated latex coated silica monolith. Reprinted from Reference [46] with permission from Wiley.

columns suffer from a lower efficiency relative to other HILIC phases [106], a limited stability [109], and column bleed [110].

PolySulfoethyl ATM has also exhibited bleeding troubles, resulting in several interfering peaks during a two dimensional LC-MS/MS study [110]. The level of interfering peaks was negligible for new columns, but became significant after 1 month of use [110].

2.4.3 Non Silica Based Stationary Phases

2.4.3.1 Amino Phases

The StyrosTM AminoHILIC phase manufactured by Orachrom Inc. (Woburn, MA, USA) is an amino phase on a monolithic polymer support [111]. Crosslinked poly(styrene-divinyl benzene) was functionalized with surface amino groups. The highly crosslinked nature of the matrix minimizes shrinking and/or swelling (< 0.2 %). The high permeability of the monolith structure and the 4000 psi maximum operating pressure enable fast separation of polar analytes. In contrast to silica based phases, the polymeric nature of the column support makes it compatible with buffers of extreme pH values. A mixture of nucleotides including adenosine monophosphate (AMP), adenosine diphosphate (ADP), adenosine triphosphate (ATP), and guanosine monophosphate (GMP) were separated in 2 minutes using a flow rate of 4 mL/min [111]. Separation of nucleobases like cytosine and uracil and benzoic acid derivatives were achieved on the same column under HILIC conditions. However, the efficiencies obtained

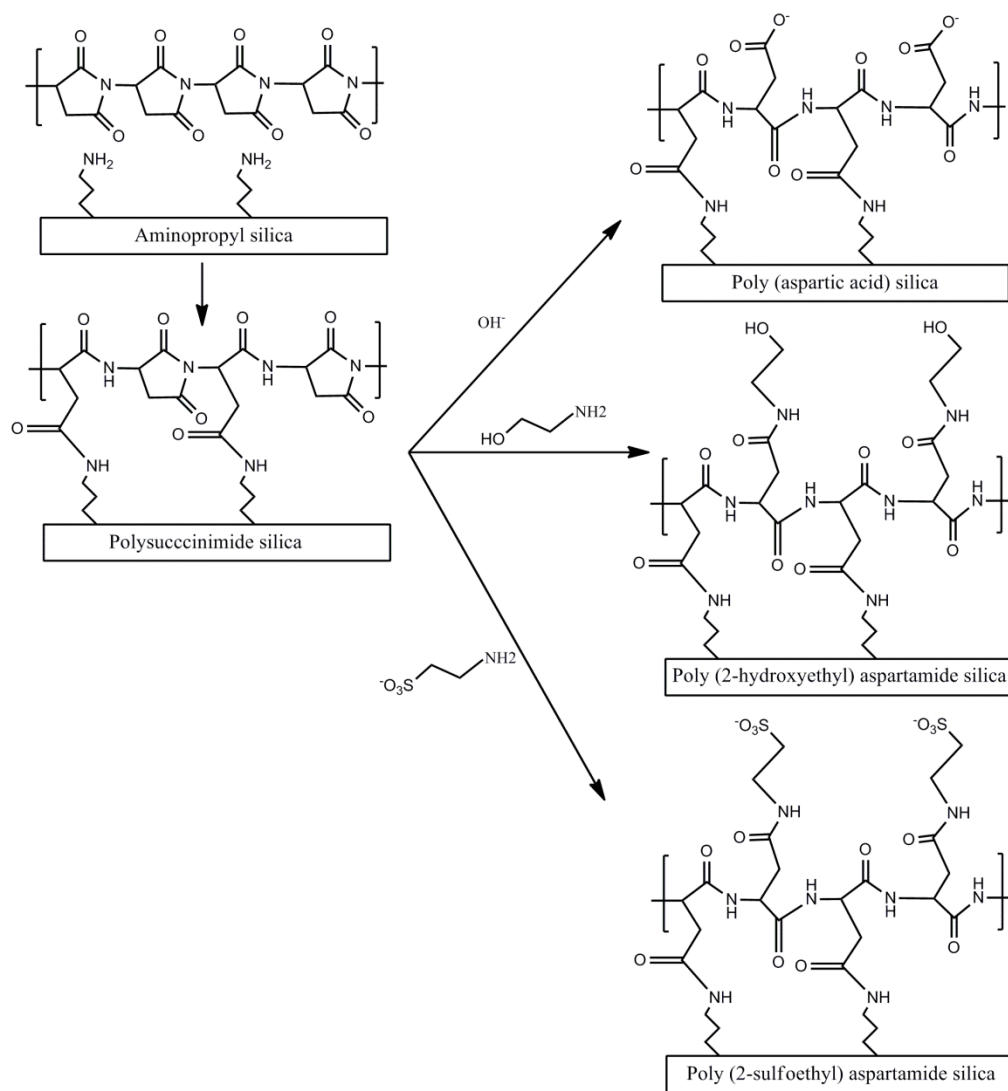


Figure 2.8 Synthesis of poly(succinimide) based silica stationary phases. Adapted from References [11, 103].

by the AminoHILIC were lower than the efficiencies obtained by a latex coated silica monolith discussed in Section 2.4.2.3.2 and Chapter 4 (*e.g.* H=250 μm vs. 59 μm for cytosine) [44]. The lower efficiency of the AminoHILIC column might be attributable to the poorer mass transfer characteristics of polymeric monoliths.

2.4.3.2 Sulfonated S-DVB Phases

These resins consist of styrene-divinyl benzene (S-DVB) functionalized with negatively charged sulfonates, and have been mainly used as cation exchangers [112, 113]. These phases have been used for aqueous normal phase chromatography [114, 115] for separation of oligosaccharides, and for the HILIC separations of propylene glycol, glycerol and dextrose [116]. HILIC retention increases with the sulfonation capacity, and with % ACN in the 70 to 95% range [116]. The Ca^{2+} form of S-DVB gave much more retention relative to the H^+ form [116].

2.5 Commercial HILIC Phases

Table 2.1 summarizes important characteristics of some selected commercial HILIC phases. The table classifies HILIC phases according to their chemical nature. The following sections compare these HILIC phases in terms of efficiency, retention and selectivity.

2.5.1 Efficiency Comparison

Two rich sources of information about the efficiency of commercial columns are the review of Ikegami *et al.* [45] and the recent study by Kawachi *et al.* [117]. Ikegami *et al.* provides an interesting and comprehensive review of efficiency of HILIC phases relative to the type of solute, type of stationary phase and format of stationary phase (particulate *vs.* monolithic) [45]. Many of the efficiencies and plate heights quoted in this section were measured from published chromatograms by Ikegami *et al.* Kawachi *et al.* compared retention, selectivity and efficiency of numerous model solutes on 14 commercial columns. Selected data from [117] are presented in Table 2.3.

In general, efficiency in HILIC follows similar broadening behavior to other forms of liquid chromatography. For instance, Figure 2.9 shows van Deemter curves for 3 and 5 μm . The Tosoh TSKgel amide-80 column packed with 5 μm yields an efficiency of 20,000 plates for mannitol on a 250 mm column [118]. Reducing the particle size enhances the mass transfer resulting in lower plate heights and thus higher efficiency (Figure 2.9). Similar improvements in efficiency with decreasing particle size were observed by Kawachi *et al.* [117] for amide and zwitterionic HILIC phases (Table 2.3).

Table 2.3 also shows that high efficiency can be achieved in HILIC using monolithic (Chromolith Si) and core-shell particles (HALO). However, the minimum reduced plate height ($H/d_p \sim 4$) achieved on Halo columns is greater than the theoretical minimum (1.5), possibly due to slow mass transfer of analyte from the water-rich adsorbed phase to the ACN-rich mobile phase [36]. HILIC

peaks are generally more symmetrical than those in *per* aqueous liquid chromatography (PALC), due to more homogeneous sorption energetics in HILIC [36]. Nonetheless, significant peak asymmetry (1.37-1.9) was observed for the HALO column under HILIC conditions [117]. Efficiencies are generally poorer if the retention mechanism is dominated by ion exchange (Figure 2.10) [117].

Decreasing separation efficiency with increasing HILIC retention has been observed [45], although more recently this has been attributed to the effect of increased ionic exchange retention [117]. Figure 2.10 shows that under conditions where ion exchange effects are reduced (*i.e.*, choosing analytes that are less ionized under experimental conditions), the plate height for a given column remains constant, independent of retention.

A number of studies compare the model analyte separations achieved on numerous HILIC columns [80, 117, 119, 120]. For example, Figure 2.11 allows comparison of the efficiency of the Atlantis HILIC silica and three other HILIC phases (all 5 μm , 250 x 4.6 mm i.d.) for nucleobases and nucleosides [80]. The Atlantis HILIC silica showed the lowest retention, but produced the highest efficiency ($N \sim 25,000$ plates, $H \sim 10 \mu\text{m}$). On the other hand, the YMC pack amino phase provided the lowest efficiency ($N = 5,000-17,000$ plates, $H = 15-50 \mu\text{m}$), while the TSKgel amide-80 and ZIC-HILIC phases showed intermediate efficiency ($N = 15,000-20,000$ plates, $H = 12-16 \mu\text{m}$ and $N = 12,000-22,000$, plates, $H = 11-21 \mu\text{m}$, respectively). Figure 2.12 shows similar behavior for model carboxylic acids analytes.

Table 2.3 Comparison of HILIC column efficiencies. ^a Reprinted from Reference [117] with permission from Elsevier.

Column	Uridine			Adenosine			Theophylline			Theobromine		
	k	H (μm)	Asym	k	H (μm)	Asym	k	H (μm)	Asym	k	H (μm)	Asym
Underivatized silica phases												
Chromolith Si ^b	0.31	12	1.00	0.73	13	2.02	0.26	14	1.09	0.31	13	1.14
HALO HILIC (2.7 μm)	0.64	8	1.47	1.59	6	1.37	0.50	8	1.36	0.64	7	1.3
Amide silica phases												
Amide-80 (5 μm)	3.30	26	1.37	3.80	28	1.38	0.76	36	1.41	1.06	32	1.37
Amide-80 (3 μm)	4.58	9	0.99	5.26	11	1.07	1.08	9	1.07	1.43	10	1.15
X-Bridge Amide (3.5 μm)	2.55	12	1.42	2.81	11	1.23	0.52	20	3.26	0.71	24	1.37
Diol silica phases												
LiChrospher Diol (5 μm)	1.50	17	0.98	2.50	17	0.97	0.55	12	1.14	0.57	15	1.28
Cyclodextrin based silica phases												
CYCLOBOND I (5 μm) ^c	0.70	18	1.73	1.36	25	1.84	0.43	12	1.14	0.44	11	1.1
Zwitterionic phases												
ZIC-HILIC (5 μm)	2.11	25	1.34	1.55	24	1.22	0.30	22	1.36	0.36	21	1.29
ZIC-HILIC (3.5 μm)	2.10	12	1.26	1.51	12	1.32	0.28	12	1.44	0.34	12	1.47
Nucleodur HILIC (3.5 μm)	2.20	14	0.88	2.33	14	0.97	0.52	16	1.00	0.52	16	1.00
Aminopropyl silica phases												
NH ₂ -MS (5 μm)	2.44	12	1.04	2.13	11	1.09	0.80	12	1.15	0.43	12	1.18
Poly(succinimide) silica phases												
PolySULFOETHYL (3 μm) ^d	1.58	62	1.11	1.15	44	2.56	0.23	114	1.91	0.23	138	2.17
PolyHYDROXYETHYL (3 μm) ^d	3.92	61	0.99	3.75	50	0.99	0.66	126	1.81	0.75	92	1.31

Continued

Column	Uridine			Adenosine			Theophylline			Theobromine		
	k	H (μm)	Asym	k	H (μm)	Asym	k	H (μm)	Asym	k	H (μm)	Asym
Underivatized silica phases												
Cosmosil HILIC (5 μm) ^a	1.60	12	1.11	2.20	12	1.16	0.55	16	1.37	0.49	16	1.7
Cosmosil Sugar-D (5 μm) ^f	1.58	17	1.12	1.88	15	0.98	0.59	22	1.11	0.31	15	1.44

- Conditions: dimensions, 150 mm x 4.6 mm i.d. unless otherwise noted; particle size, as noted in column 1; injection, 4 μL of 1 mg/mL analyte dissolved in mobile phase; dead time marker, 1 mg/mL toluene; flow rate, 0.5 mL/min for 4.6 mm i.d. columns and 0.1 mL/min for 2 mm columns; eluent, 90:10 v/v ACN-ammonium acetate buffer (pH 4.7, 20 mM in the aqueous portion); temperature, 30°C.
- Dimensions: 100 mm x 4.6 mm i.d.
- Dimensions: 250 mm x 4.6 mm i.d.
- Dimensions: 100 mm x 2.1 mm i.d.
- Triazole functionality.
- Secondary/tertiary amine functionality.

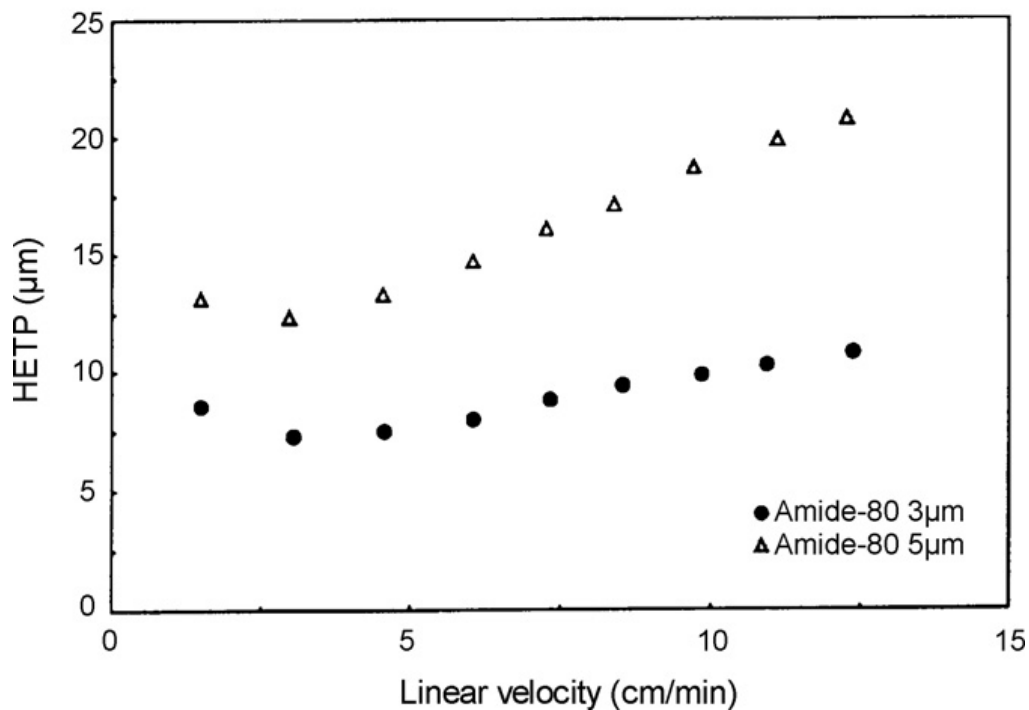


Figure 2.9 van Deemter plots of (●) TSKgel Amide-80, (150 mm × 4.6 mm i.d., 3 μm), (Δ) TSKgel Amide-80, (250 mm × 4.6 mm i.d., 5 μm); mobile phase, ACN/water = 75/25; temperature, 40 °C; detection, RI; injection volume: 10 μL; sample: mannitol. Reprinted from Reference [45] with permission from Elsevier.

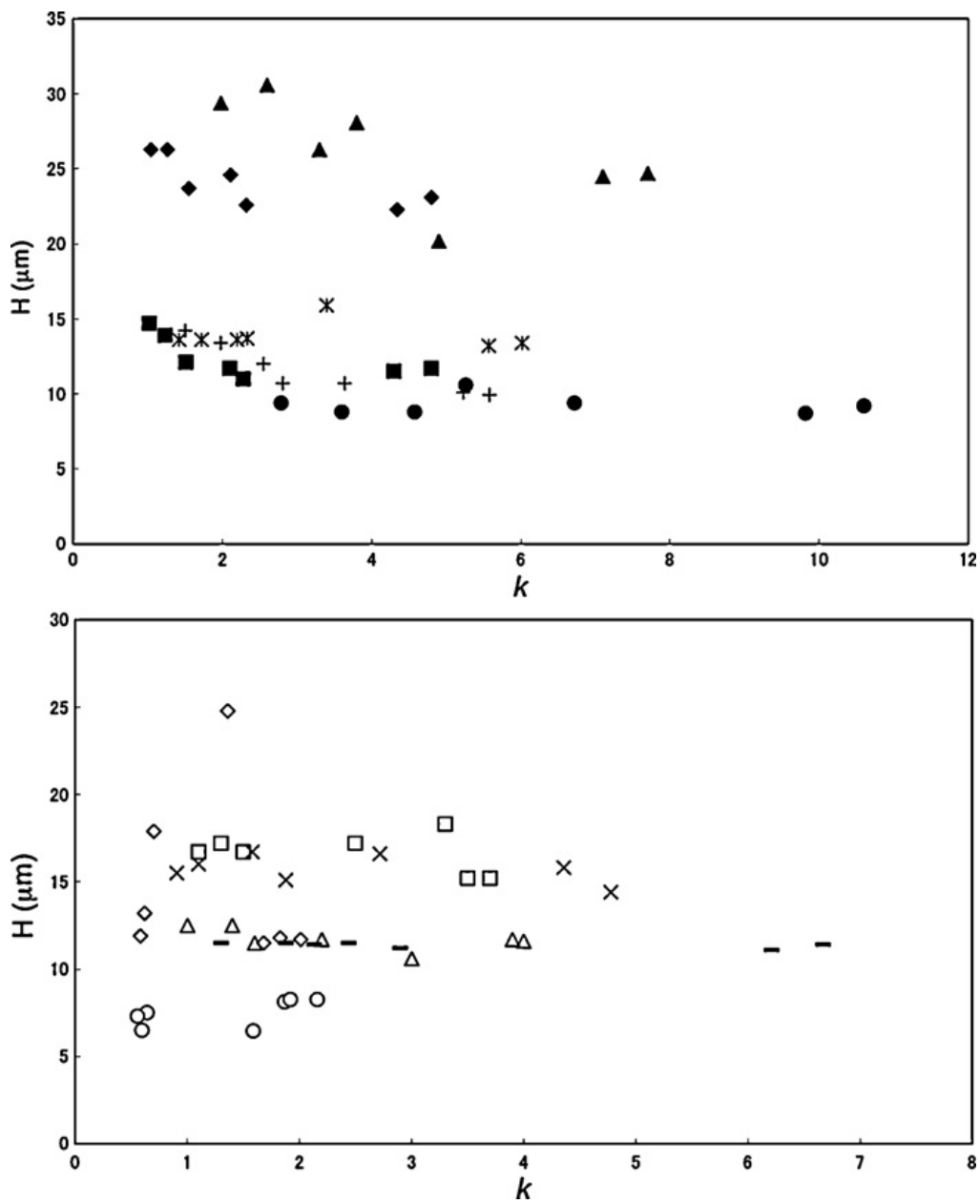


Figure 2.10 Relationship between retention and separation efficiency. Columns: ZIC-HILIC 5 μm (\blacklozenge), ZIC-HILIC 3.5 μm (\blacksquare), Amide-80 5 μm (\blacktriangle), Amide-80 3 μm (\bullet), Nucleodur ($*$), XBridge-Amide ($+$), CYCLOBOND I (\diamond), LiChrospher Diol (\square), COSMOSIL HILIC (Δ), Sugar-D (\times), MS-NH₂($-$), and HALO HILIC (\circ). Reprinted from Reference [117] with permission from Elsevier.

Peak tailing and low efficiencies are commonly observed for amines on silica based RPLC phases due to silanol activity. The degree of tailing depends on the nature and activity of the silanols [121, 122]. This effect has not been studied in as much detail for HILIC [45]. However, as shown in Fig 2.13, silica phases from different manufacturers provide different retention and efficiency [100]. Peak tailing and hence lower efficiency was observed for pyrimidines (upper trace) on Nucleosil and Zorbax SIL. However, no significant tailing was observed for purines on any of the silica columns (lower trace Figure 2.13).

Numerous studies report more limited comparisons of HILIC columns. Some interesting observations from these studies regarding efficiency are discussed below, in the order of column type discussed in Section 2.4 and Table 2.1.

The effect of retention on plate height has been studied on Betasil HILIC phase (5 μm , 50 x 4.6 mm i.d.) vs. two RP phases [23]. Betasil gave an intermediate efficiency between the two RP phases (optimum flow rate \sim 1-2 mL/min), yielding a plate height of 20 μm for fluconazole.

As shown in Table 2.3, amide columns generally provide good efficiency. Similarly, Figure 2.12 shows efficiencies of 15,000 to 20,000 plates an amide 80 phase (5 μm , 250 x 4.6 mm i.d., $H = 12\text{-}16 \mu\text{m}$) for k below 5 [45]. However, N-acetylneuraminic acid and glucuronic acid exhibited efficiencies of only 3,000 plates ($H = 83 \mu\text{m}$) and 2,400 plates ($H = 104 \mu\text{m}$), respectively [123] on a TSKgel amide-80 (5 μm , 250 x 4.6 mm i.d.). Similarly, strongly retained ($k = 7\text{-}$

17) tetramers and pentamers of proanthocyanidins exhibited significant broadening ($N \sim 1,000$) on the TSKgel amide-80 phase [45, 124].

Lichrosorb-DIOL (10 μm , 250 \times 4.6 mm i.d.) is a commercial diol phase manufactured by Merck (Darmstadt, Germany, Table 2.1). This diol phase provided N of 5,300 and 3,400 plates for sucrose ($H = 47 \mu\text{m}$) and lactose ($H = 74 \mu\text{m}$), respectively [65] which was comparable to an equivalent Lichrosorb NH_2 (amino silica phase). The galactose and lactose peaks were broad on the diol phase due to anomerization [65]. Thus aminopropyl phases are favored for carbohydrates. Addition of an amine to the mobile phase or separation at higher temperatures reduces the anomerization broadening on a diol phase. For example, addition of 0.1 % ethyldiisopropylamine increased the efficiency for lactose from 600 to 1,300 plates. Plate height on an Inertsil Diol (5 μm , 150 \times 4.6 mm i.d., Table 2.1) decreased with column temperature for glycine and sucrose, while urea displayed a U-shaped behavior [67].

A cyano silica column (5 μm , 150 \times 3.0 mm i.d.) yielded higher efficiency (N of 9,500-17,000 plates) and greater retention compared to bare silica and amino silica based phases for the analysis of denaturants in an alcohol formulation [125]. Separations of native oligosaccharides on a Cyclobond I 2000 (β -CD, 5 μm , 250 \times 4.6 mm i.d., Table 2.1) column yielded only 2,300-7,800 plates ($H \sim 60 \mu\text{m}$) [77], presumably due to use of a high mobile phase velocity [45]. The van Deemter plot for Cyclobond I shown in Figure 2.14 shows that a fast linear velocity (2 mm/s) was preferred for highly retained analytes such as sucrose and

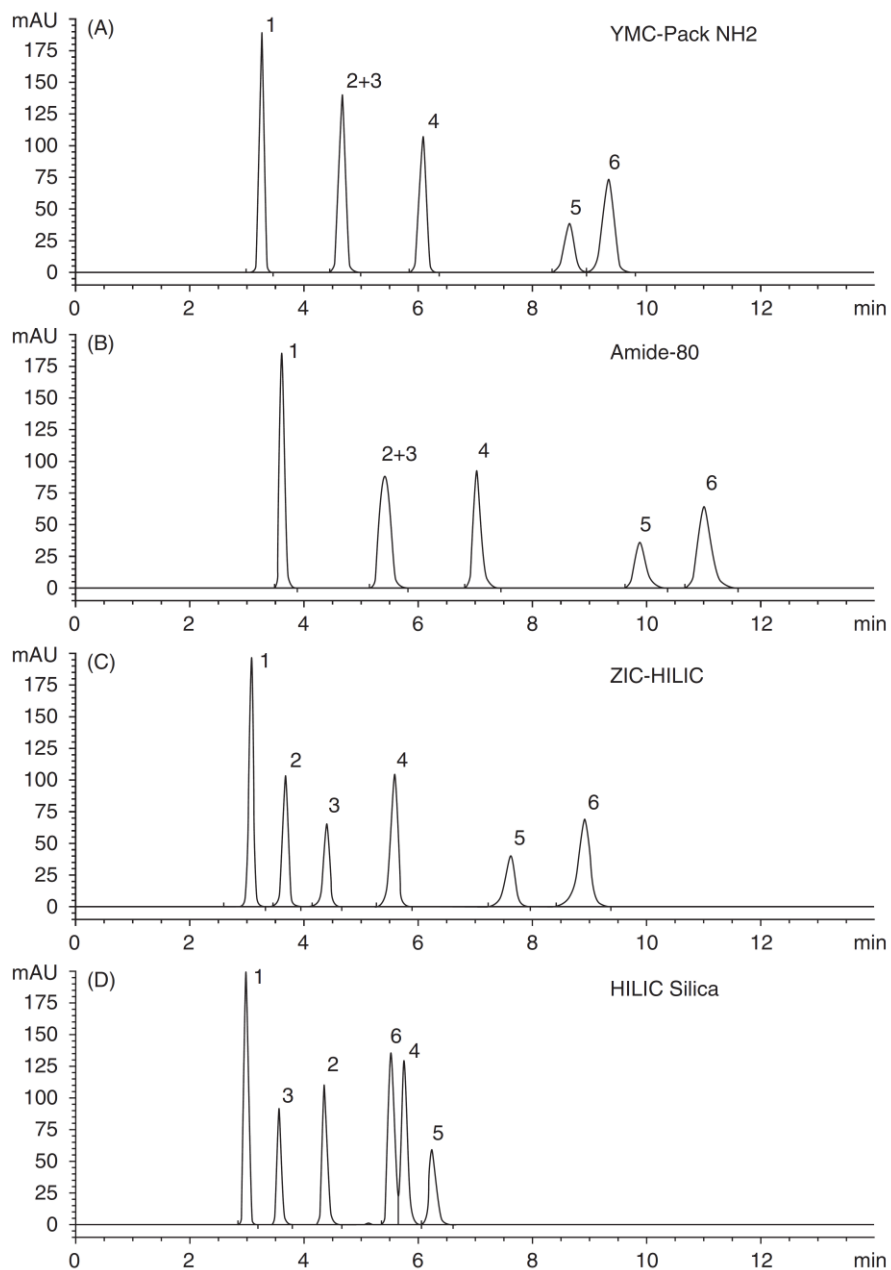


Figure 2.11 Separation of nucleic acid bases and nucleosides on: (A) YMC-Pack NH₂ (B) TSKgel Amide-80 (C) ZIC-HILIC and (D) Atlantis HILIC Silica columns. Dimensions: 5 μ m, 250 \times 4.6 mm i.d. Mobile phase: ACN/water (85/15, v/v) containing 10 mM ammonium acetate. Column temperature: 30 $^{\circ}$ C. Flow rate: 1.5 mL/min. UV detection at 248 nm. Compounds: (1) uracil, (2) adenosine, (3) uridine, (4) cytosine, (5) cytidine, and (6) guanosine. Reprinted from Reference [80] with permission from Elsevier.

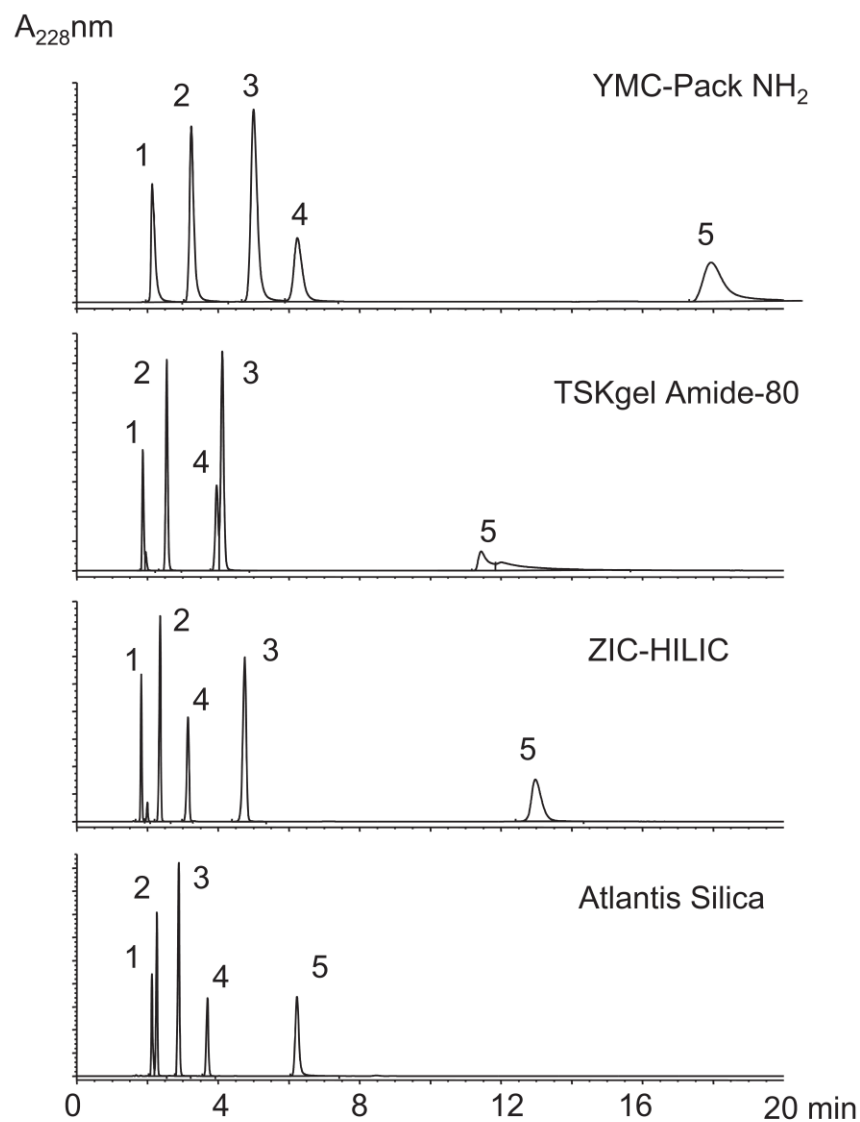


Figure 2.12 Separation of acidic compounds on 4 different columns (All columns 25 x 0.46 cm i.d. containing 5 μm particle size packing). Mobile phase: ACN:water (85:15, v/v) containing 20 mM ammonium acetate. Column temperature: 30° C. Flow rate: 1.5 mL/min. UV detection at 248 nm. Compounds: (1) salicylamide, (2) salicylic acid, (3) 4-amino salicylic acid, (4) acetylsalicylic acid, (5) 3,4-dihydroxyphenylacetic acid. Reprinted from reference [80] with permission from Elsevier.

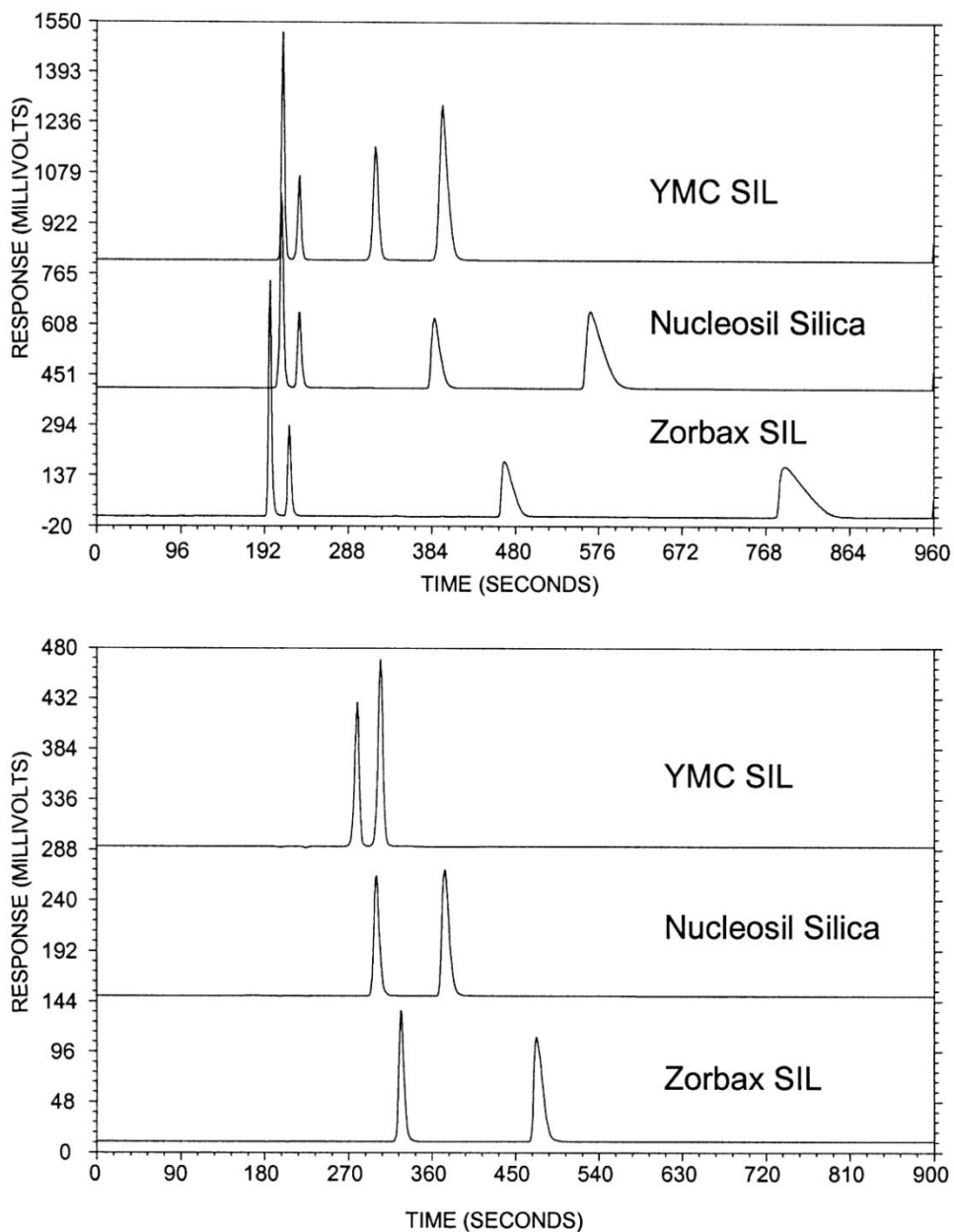


Figure 2.13 Separations of pyrimidines (upper) and purines (lower) on silica columns. Conditions: mobile phase 5 mM phosphoric acid in ACN:water (75:25) for pyrimidines, (70:30) for purines; 275 nm detection; pyrimidines, ~ 0.05 mg/ml (in order of elution): 5-fluorouracil, uracil, 5-fluorocytosine, cytosine; purines, ~ 0.02 mg/ml (in order of elution): acyclovir, guanine. Reprinted from Reference [100] with permission from Elsevier.

lactose, but a lower linear velocity (0.4 mm/s) was preferred for weakly retained analytes such as fructose ($k = 1.25$) [73].

As illustrated in Figures 2.11 and 2.12, Guo *et al.* compared four HILIC phases in terms of retention and efficiency [80]. The ZIC-HILIC (5 μm , 250 \times 4.6 mm i.d.) (Table 2.1) provided N of 12,000-22,000 plates ($H = 11\text{-}21$ μm) for carboxylic acids, nucleosides and nucleobases [45, 80]. Similarly 15 cm columns of 5 μm ZIC-HILIC yield 10,000-13,000 plates in both the 2.1 mm and 4.6 mm i.d. formats for well-behaved analytes (*e.g.*, ascorbic and dehydroascorbic acid) [45, 126], whereas lower efficiencies were observed for morphine and its glucuronide metabolite (1,400-3,500 plates) [45, 126] and oligopeptides including neurotensin, Gly-His-Lys and bradykinin (1,800-3,000 plates on a 100 mm column) [45, 126].

The efficiencies observed in Figure 2.11 on the YMC-Pack NH_2 column (5 μm , 250 \times 4.6 mm i.d.) were comparable to those obtained with other HILIC columns [45, 80]. However as noted above significantly lower efficiencies are observed in HILIC when ion exchange contributes significantly to retention. For instance, separations of benzoic acid derivatives on these same columns (Figure 2.12) yield distinctly different efficiencies (N \sim 5,000 plates) on a YMC-Pack NH_2 column. Further, significant differences in efficiency may exist between amino columns of the same dimensions but different manufacturers even for basic analytes (Figure 2.15) [127]. Fronted peaks were observed on both YMC-Pack NH_2 and Nucleosil NH_2 phases, while higher efficiency (N = 4,600-7,300 plates, $H = 21\text{-}33$ μm) was observed with the Zorbax NH_2 phase [127].

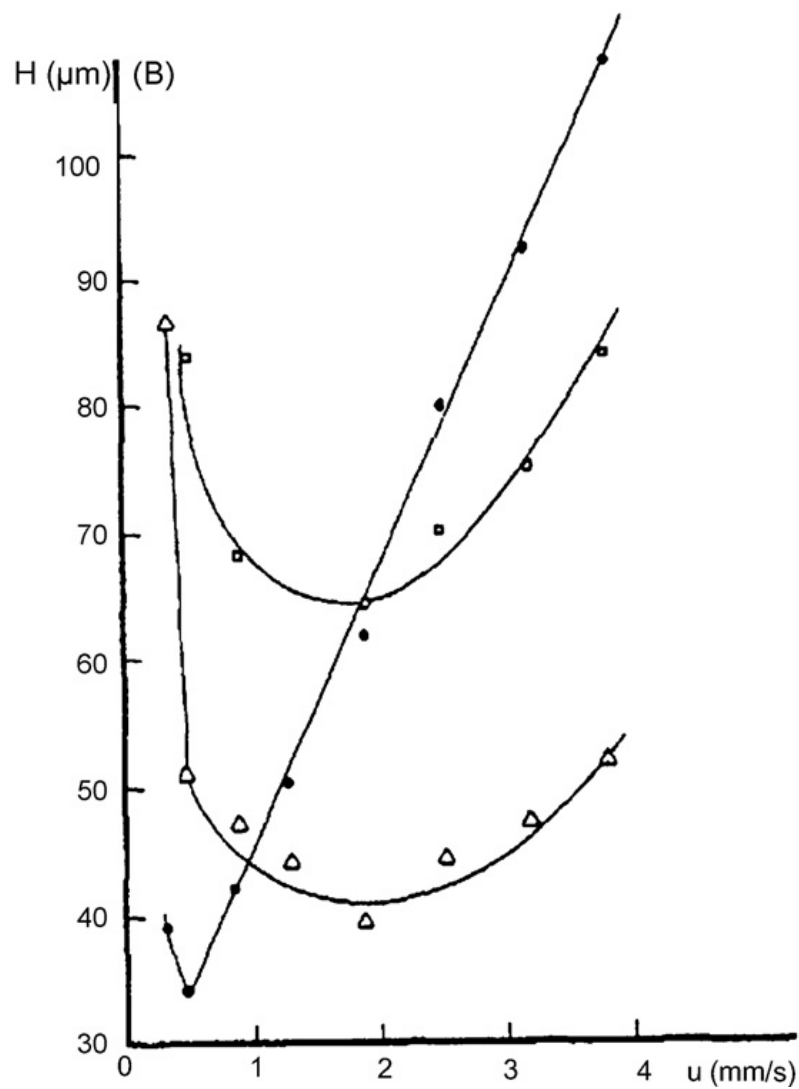


Figure 2.14 van Deemter plot for Cyclobond I HILIC Column (5 μm , 250 mm \times 4.6 mm i.d.); mobile phase of ACN:water (85:15, v/v); compounds: (●) fructose; (Δ) sucrose; (\square) lactose. Reprinted from References [45, 73] with permission from Elsevier.

Hypersil ASP-2 (Amino) (3 μm , 50 \times 4.6 mm i.d.) was used for separation of tetracycline antibiotics with efficiencies of 3,800 plates ($H = 13 \mu\text{m}$) for oxytetracycline [45, 98].

Separation of amino acids on PolySulfoethyl A (5 μm , 200 \times 4.6 mm i.d.) 2.0 mL/min [1] yielded N of 4,000 plates ($H = 50 \mu\text{m}$) [45]. The flow rate (2.0 mL/min) may have been too fast to achieve optimal efficiency. The efficiency of cyclopeptides on the same PolySulfoethyl A phase strongly depended on the mobile phase: 60% ACN displaying very poor efficiencies while 90% ACN yielded 9,000 plates as estimated by Ikegami *et al.* [1, 45]. Increasing % ACN further to 95% decreased efficiency to 5,000 plates and increased the retention factor [1]. Alpert suggested that this kind of phases should be used for analytes of small retention factor to provide high separation efficiency [1].

Contrary to Table 2.3, Tolstikov *et al.* observed that the PolyHydroxyethyl A (5 μm , 150 \times 1.0 mm i.d., $H = 15.8 \mu\text{m}$ for peak 12, maltoheptaose) is more efficient compared to the TSKgel Amide-80 phase (5 μm , 250 \times 2.0 mm i.d., $H = 23.8 \mu\text{m}$ for peak 12, maltoheptaose) for amino acids and carbohydrates [106]. The two columns provided different elution order of analytes, as well. The PolyHydroxyethyl A column (3 μm , 200 \times 4.6 mm i.d.) yielded 2,300-2,900 plates ($H = 69-87 \mu\text{m}$) for dipeptide standards [1]. Increasing buffer concentration or pH resulted in lower efficiency and lower retention. Separation of atosiban diastereomers on PolyHydroxyethyl A column (5 μm , 200 \times 4.6 mm i.d.) gave N of 5,000-6,000 plates ($H = 33-40 \mu\text{m}$) with lower resolution compared to an amino-silica phase [107].

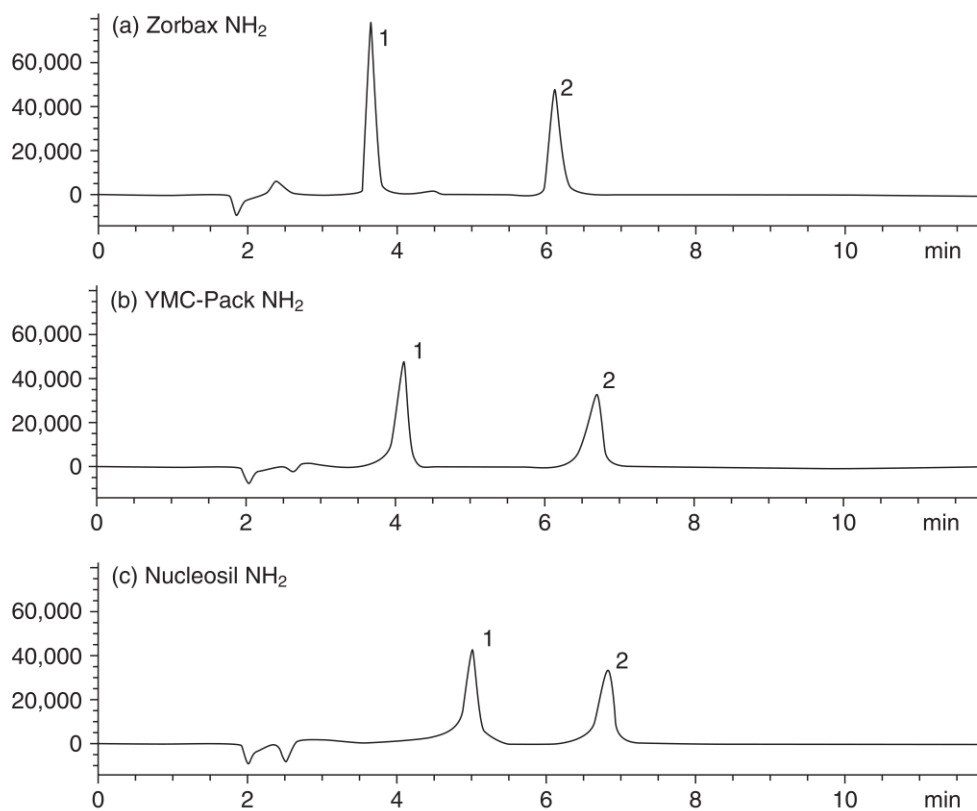


Figure 2.15 Separation of 2-amino-2-ethyl-1,3-propanediol (AEPD, peak 1) and tromethamine (peak 2) on: (A) Zorbax NH₂; (B) YMC-Pack NH₂; and (C) Nucleosil NH₂ columns (All, 5 μm , 150 \times 4.6 mm i.d.); mobile phase: ACN/water (80/20, v/v): 25 $^{\circ}\text{C}$; flow rate: 1 mL/min; Injection 50 μL . Reprinted from References [45, 127] with permission from Elsevier.

Separation of inorganic ions *e.g.* Li⁺, Na⁺, Cl⁻ and K⁺ and drugs *e.g.* naproxen and warfarin on Chromolith Si (100 × 4.6 mm i.d.) provided N of 1,000-4,800 plates (H = 21-100 μm) as estimated by Ikegami *et al.* [45, 47]. These efficiencies were much lower than observed on RP silica based monoliths. Monolithic silica capillaries (85 mm × 75 μm i.d.) yielded 9,300-17,500 plates under HILIC conditions for separations of alkaloids [128]. An AS9-SC coated Chromolith silica monolith (100 × 4.6 mm i.d., Figure 2.7) was used for separation of variety of polar analytes under HILIC conditions as discussed in Chapter 4 [44] and provided H of 59-67 μm for model nucleobases, 71-110 μm (N = 900-1,400 plates) for nucleotides, and 30-45 μm (N = 2,200-3,300 plates) for carboxylates [44]. The high column permeability enabled separations to be performed in less than 15 seconds. The StyrosTM polymeric AminoHILIC phase (50 × 4.6 mm i.d.) yielded lower efficiencies (H = 154-400 μm and 67-167 μm, for nucleotides and benzoates respectively) [44], possibly attributable to the poor mass transfer properties of its polymeric support.

2.5.2 Retention and Selectivity Comparisons

Several factors affect retention and selectivity in HILIC including the type of organic modifier, % organic modifier, buffer strength, pH of the mobile phase and stationary phase chemistry. In this section, we will focus on the effect of stationary phase chemistry on the selectivity in HILIC mode. Selectivity and retention of the HILIC phases have been studied and reviewed extensively during the last ten years [8, 10, 80, 119]. In 2005, Guo *et al.* demonstrated that different

stationary phases showed different degrees of retention and selectivity for polar analytes [80]. Four stationary phases including silica, amino, amide and zwitterionic columns (all are of the same dimensions of 250×4.6 mm, $5 \mu\text{m}$) were compared in terms of retention and selectivity using salicylic acid derivatives, nucleobases and nucleosides as model analytes [80]. As shown in Figure 2.12, the acids are strongly retained on YMC-Pack NH_2 phase due to the strong ion exchange interaction between the negatively charged acids and the amino groups of the stationary phase. However, the TSKgel Amide-80 showed weaker retention, resulting in aspirin and 4-aminosalicylic acid being only partially resolved. This resolution was improved for the rest of the studied phases. HILIC silica showed the least retention of the acids. On the other hand, TSKgel Amide-80 provided the strongest retention for nucleobases and nucleosides but did not baseline resolve adenosine and uridine (Figure 2.11). ZIC-HILIC and HILIC silica columns showed good resolution of adenosine and uridine. HILIC silica phase showed the least retention of the examined nucleosides as well, but also completely different retention order compared to the other columns (Figure 2.11) [80]. Thus, it is clear that the different elution patterns indicate that the chemistry of the stationary phases has a significant effect on retention and selectivity.

In 2010, McCalley investigated the retention and selectivity of strongly acidic and basic analytes on different HILIC stationary phases [8]. Five HILIC phases including ZIC-HILIC, Onyx Silica, Luna HILIC (diol), TSKgel Amide-80 and Acclaim mixed mode HILIC (all, $5 \mu\text{m}$, 250×4.6 mm i.d.) were compared in

terms of retention and selectivity. Figures 2.16a and 2.16b show the different elution patterns observed on the various HILIC columns. The silica phase showed the greatest retention of basic analytes which might be attributed to: 1) the high surface area of the silica phase ($400 \text{ m}^2/\text{g}$) compared to the other phases; 2) strong ionic interaction between the protonated bases and ionized silanols; and 3) the hydrophilic nature of the silica surface [8]. On the other hand, the silica phase showed weak retention of the acidic analytes due to the repulsive forces between the negatively charged analytes and the ionized silanols [8]. The zwitterionic, amide and especially the diol phase provided reasonable retention of the acids which could be explained by the use of low acidity silica in its manufacture and/or screening of ionized silanols by the bonded phase [8]. Finally, McCalley concluded that the difference in selectivity between different stationary phases, even when using the same eluent, suggests that the stationary phase is not working simply as an inert support for the adsorbed water layer, but rather it has a considerable and characteristic contribution to retention [8].

Guo *et al.* compared the selectivity and retention of hydroxyl stationary phases including diol, cross-linked diol, polyhydroxy and polyvinyl alcohol phases using nucleobases and nucleosides [129]. Figure 2.17 shows these phases have similar selectivity, with the cross-linked diol and polyhydroxy phases resolving cytidine and guanosine [119, 129]. The selectivity of the silica phase (Figure 2.11) is somewhat different to the HILIC phases included in Figure 2.17, attributable to specific interactions of the analyte with the silica surface [119, 129]. Figure 2.18 compares the selectivity of three cationic phases (amino,

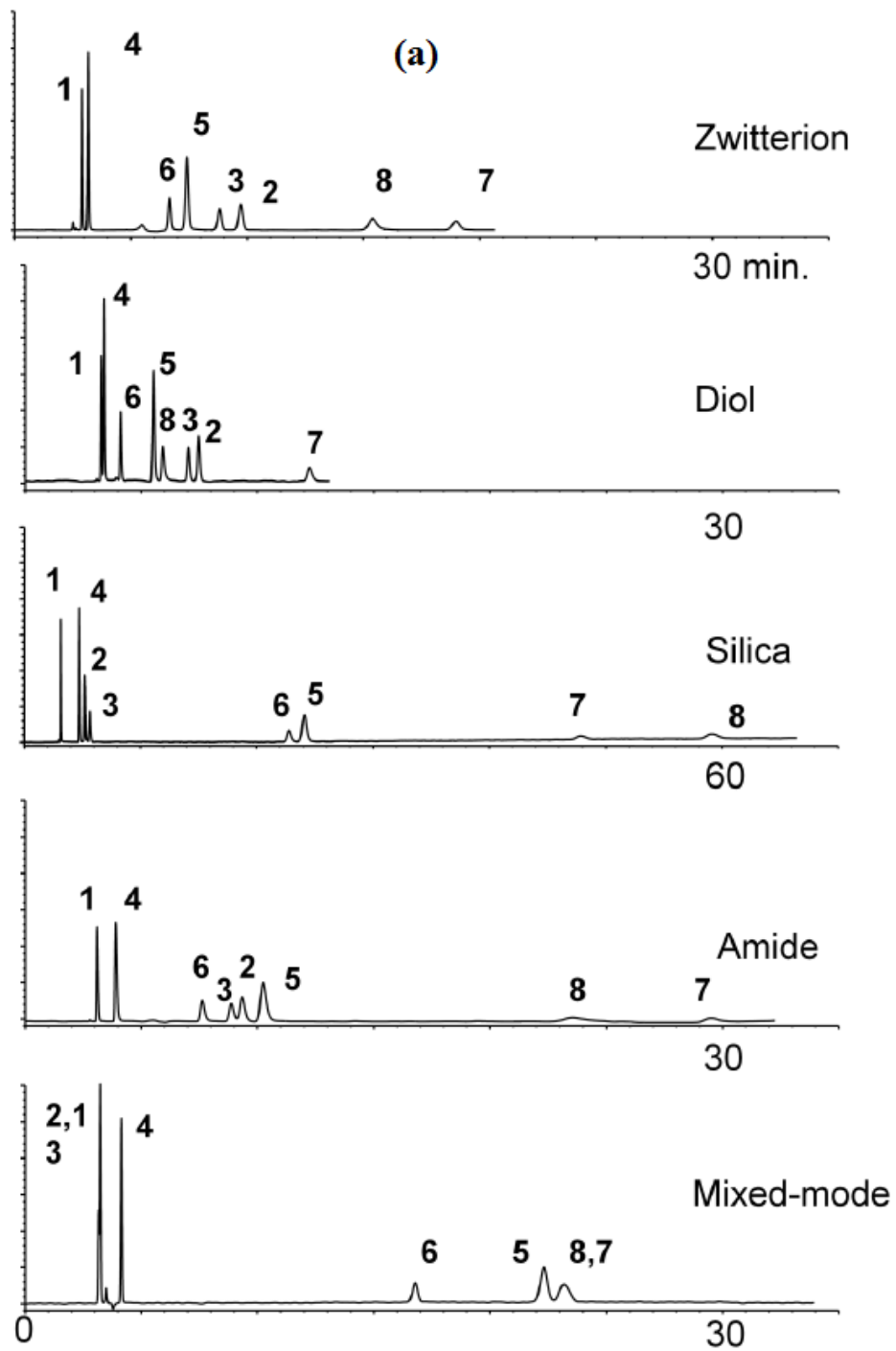
imidazole and triazole) using the same previously mentioned analytes [119, 129]. The imidazole and triazole phases display different selectivity. Although the amino phase did not resolve adenosine and uridine, the imidazole and triazole phases resolve them from each other but in a different elution order (Figure 2.18).

Lammerhofer *et al.* compared the selectivity of six different HILIC phases as shown in Figure 2.19. The amide phase shows similar selectivity to the amino and sulfobetaine phases, however, the silica phase provided a different elution order relative to the other phases [9].

Recently, Irgum and his co-workers probed the interactions taking place on 22 different HILIC stationary phases [10]. Using carefully selected pairs of analytes, interactions including hydrophilic, hydrophobic, electrostatic, hydrogen bonding, dipole-dipole and π - π interaction were characterized. By using principal component analysis, 22 different HILIC columns were classified in terms of selectivity, as shown in Figure 2.20 [10]. The first two principal components explained more than 70% of the total variance. In Figure 2.20, the gray loading vectors are defined by the analyte pairs (triangles) whose relative retention characterizes a single type of interaction. For instance, the relative retention of benzoate *vs.* cytosine (BA/CYT) reflects selectivity based on anion exchange. Moving clockwise from the anion exchange loading vector are the loading vectors reflecting adsorption, cation exchange, dipole-dipole and partitioning. Specific columns (as identified in Table 2.1) are plotted as squares in Figure 2.20. The higher the score of a column (*i.e.*, the further out from the center along a loading vector), the more a column possesses that particular character. For example,

Purosphere STAR NH₂ (square 20) has more anion exchange character than the TSKgel NH₂-100 (21). The numbers in parentheses indicate the phase number in Table 2.1.

In Figure 2.20, the HILIC columns cluster into four main groups: neutral columns such as amide (7, 8) and diol (10, 11) phases; amino columns (19-21); silica columns (14-17) including monolithic silica (13) and type-C silica (18); and zwitterionic phases (1-4). A few columns show selectivity that is surprising based on the manufacturer's stated functionality. For instance both the Nucleodur HILIC (5) and Shiseido PC HILIC (6) columns are purported to be zwitterionic phases, but both behaved as neutral columns. Also the sulfoethyl functionality of PolySulfoethyl A (12) would be expected to yield a column with strong cation exchange character, whereas it groups with the zwitterionic columns in Figure 2.20. Irgum and co-workers [10] speculate that this zwitterionic character may result from underivatized aminopropyl groups within the synthesis of this phase (Figure 2.8). Chapter 3 describes a simpler and easier to understand way to characterize different HILIC phases compared to the complicated principal component analysis. We re-casted the HILIC retention data of Irgum and his co-workers (21 HILIC phases) plus 12 additional phases (8 HILIC and 4 RPLC phases) [130]. Our selectivity plots are successful at categorizing different HILIC phases (silica, zwitterionic, amine, neutral) based on their hydrophilicity, ion exchange properties and H-bonding capability [130]. This selectivity plot is used as a key element in studying the selectivity of the newly developed silica and carbon based HILIC stationary phases shown in this thesis (Chapters 4-7).



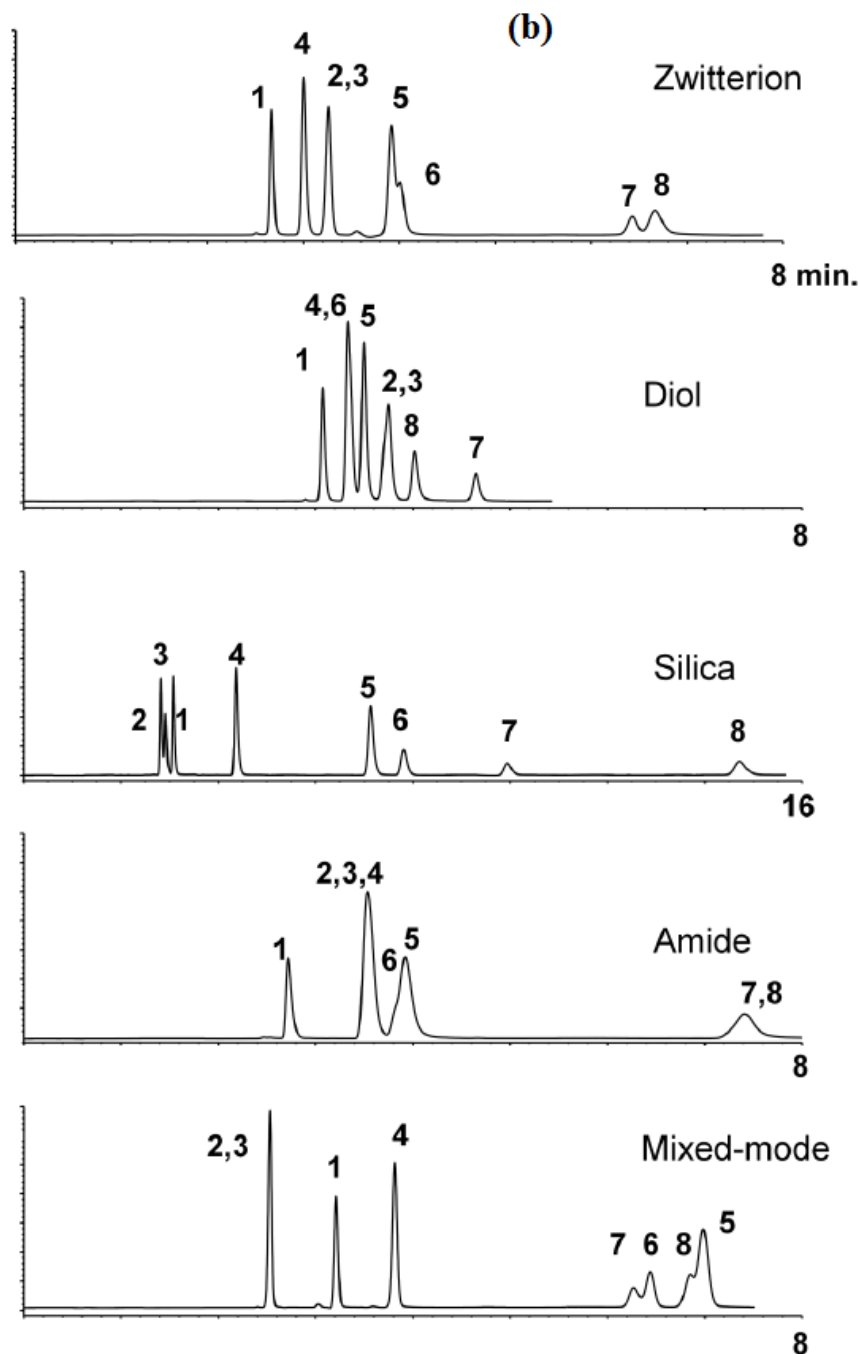


Figure 2.16 Chromatograms of 8 solutes on 5 different HILIC columns (all 25 x 0.46 cm i.d., 5 μ m particle size); (a) Mobile phase: ACN:water (95:5), v/v containing 5 mM ammonium formate pH 3.0, flow rate: 1 mL/min. Compounds: (1) phenol, (2) naphthalene-2-sulfonic acid, (3) p-xylenesulfonic acid, (4) caffeine, (5) nortriptyline, (6) diphenhydramine, (7) benzylamine, (8) procainamide; (b) Mobile phase ACN-water (85:15, v/v) containing 5 mM ammonium formate pH 3.0. Reprinted from Reference [8] with permission from Elsevier.

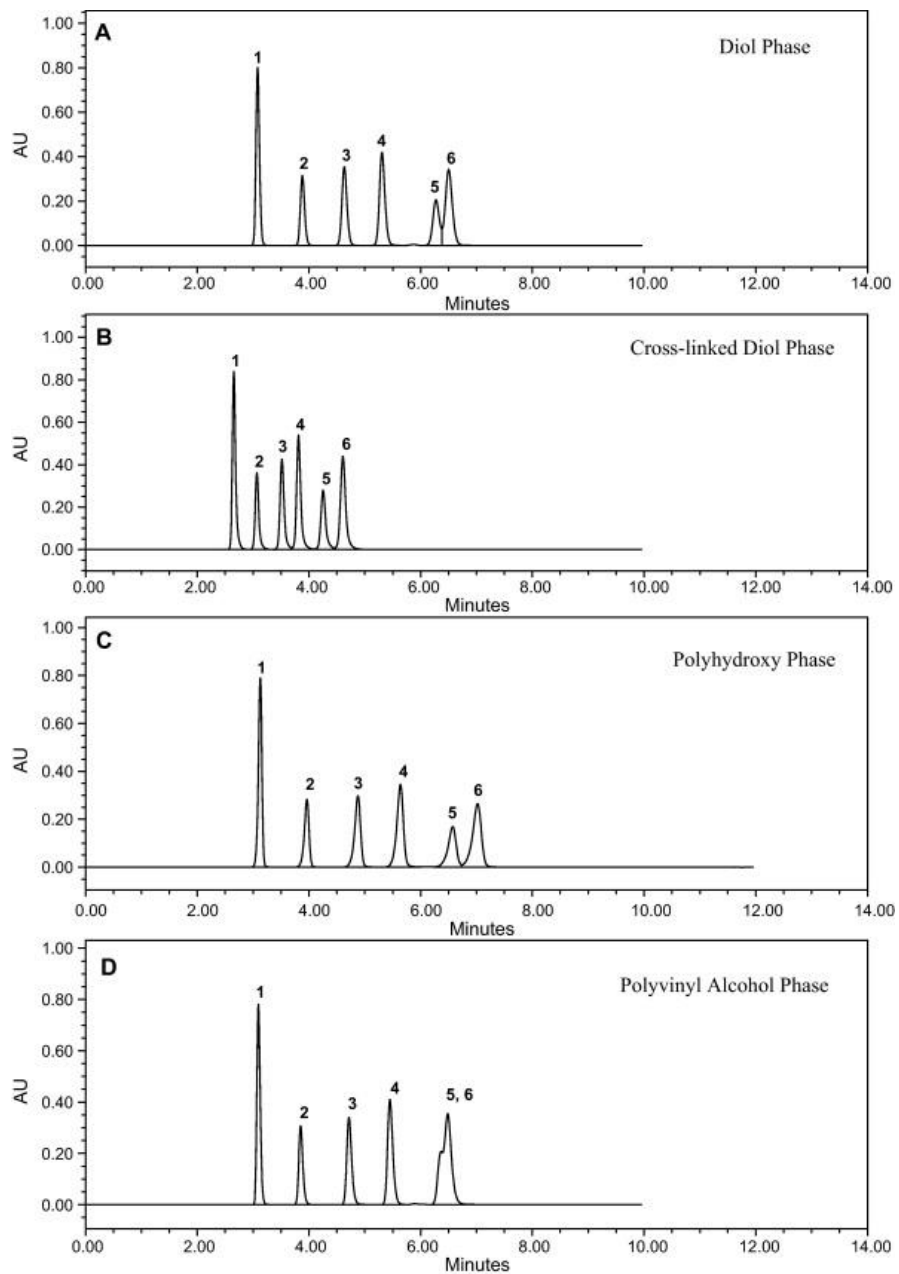


Figure 2.17 Separation of (1) uracil, (2) adenosine, (3) uridine, (4) cytosine, (5) cytidine and (6) guanosine on (a) diol, (b) cross-linked diol, (c) polyhydroxy and (d) polyvinyl alcohol phase. Column dimension: All, 5 μm , 250 \times 4.6 mm i.d. Mobile phase: ACN/water (85/15, v/v) containing 10 mM ammonium acetate. Column temperature 30 $^{\circ}\text{C}$. Flow rate: 1.5 mL/min. Reprinted from Reference [119] with permission from Elsevier.

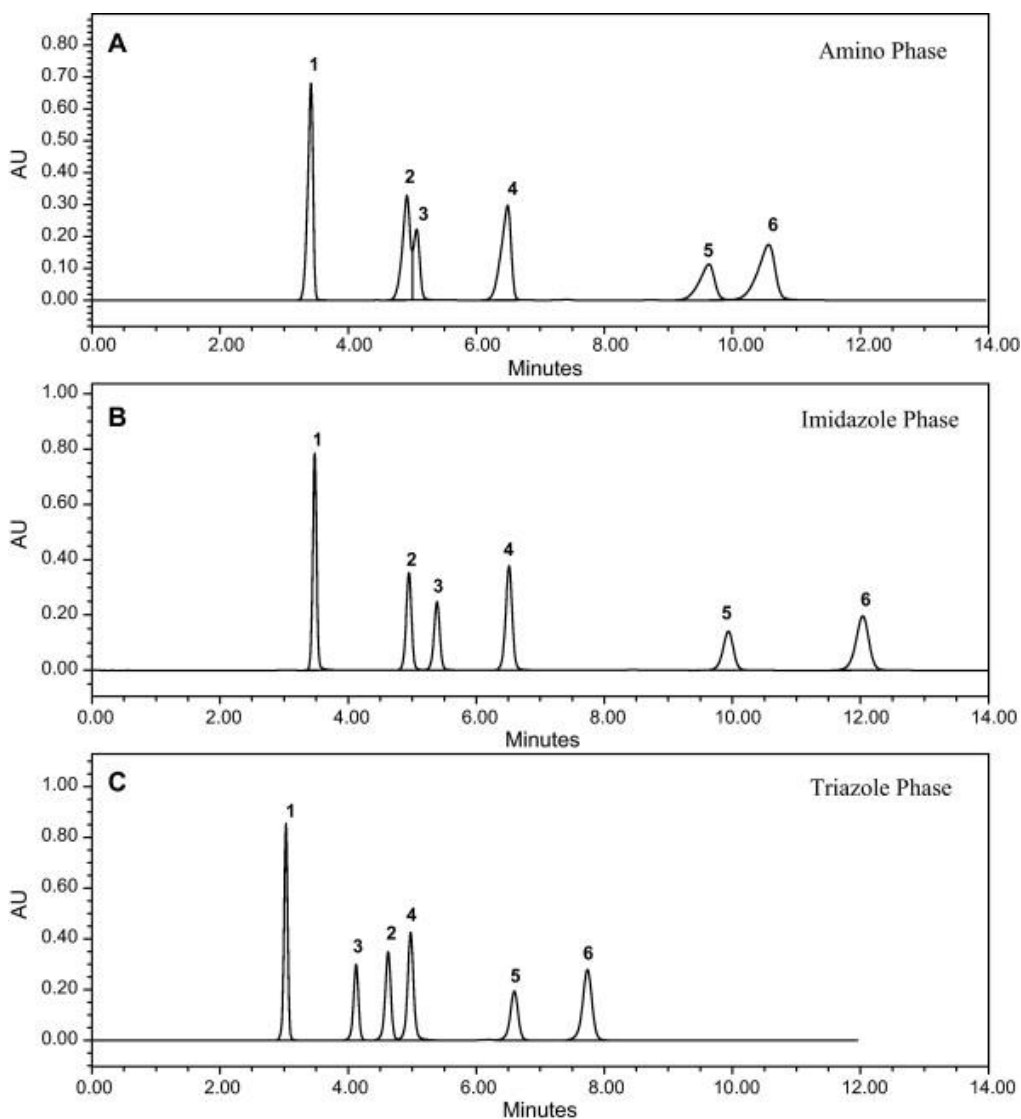


Figure 2.18 Separation of (1) uracil, (2) adenosine, (3) uridine, (4) cytosine, (5) cytidine and (6) guanosine on (a) amino, (b) imidazole and (c) triazole phase. Column dimension: All, 5 μ m, 250 \times 4.6 mm i.d. Mobile phase: ACN/water (85/15, v/v) containing 10 mM ammonium acetate. Column temperature: 30 $^{\circ}$ C. Flow rate: 1.5 mL/min. Reprinted from Reference [119] with permission.

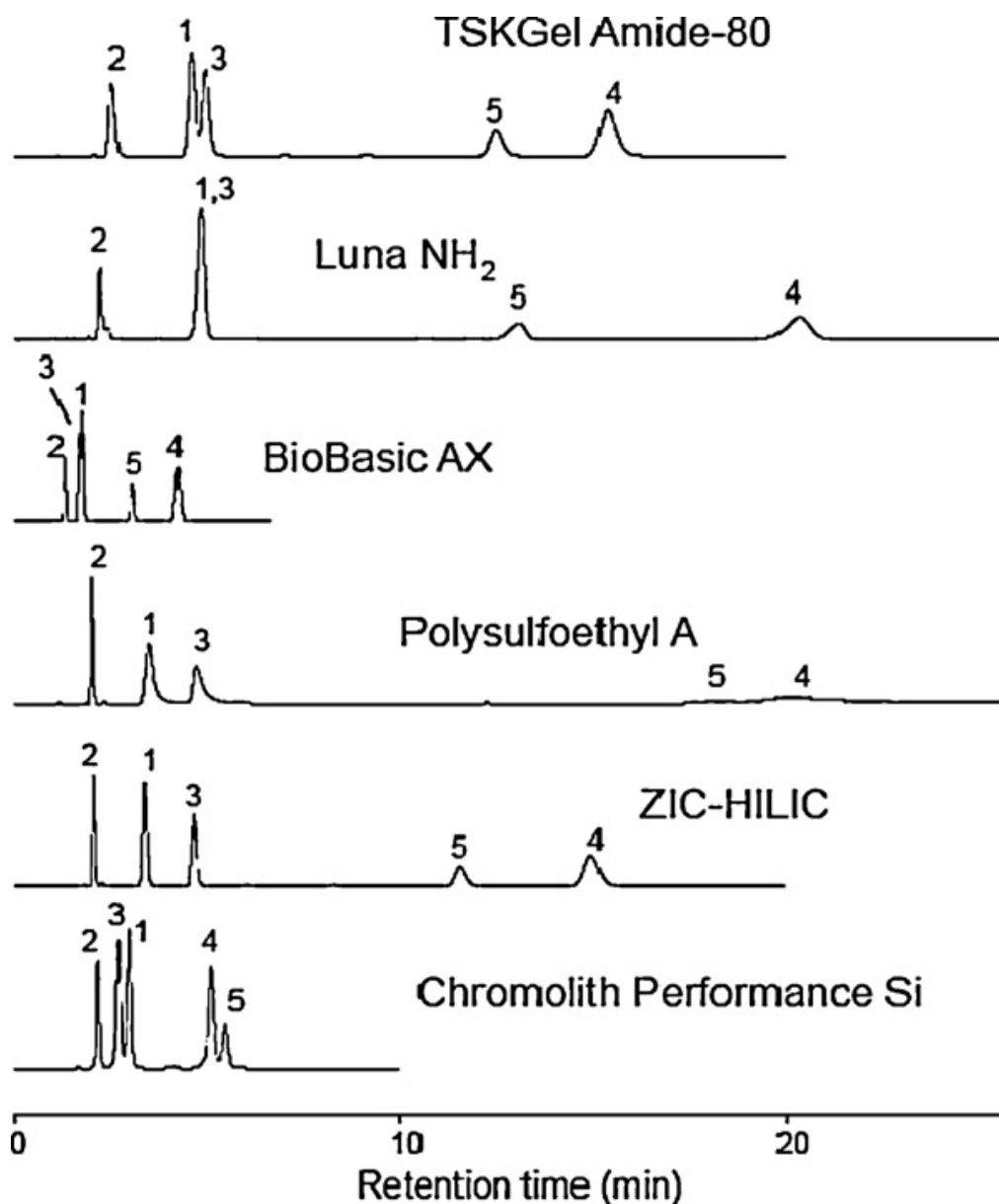


Figure 2.19 Separation of nucleosides on various HILIC phases. Column dimension: All, 5 μm , 100 mm \times 4 mm i.d. and 100 mm \times 4.6 mm i.d. for Chromolith Performance Si with a macropore diameter of 2 μm and a mesopore diameter of 13 nm. Column temperature 25 $^{\circ}\text{C}$. Mobile phase: ACN/5 mM ammonium acetate buffer (90/10, v/v), apparent pH \sim 8. The flow rate was adjusted to the same linear velocity (1.7 mm/s). Solutes: (1) adenosine, (2) thymidine, (3) uridine, (4) guanosine, and (5) cytidine. Reprinted from References [9, 119] with permission from Wiley and Elsevier.

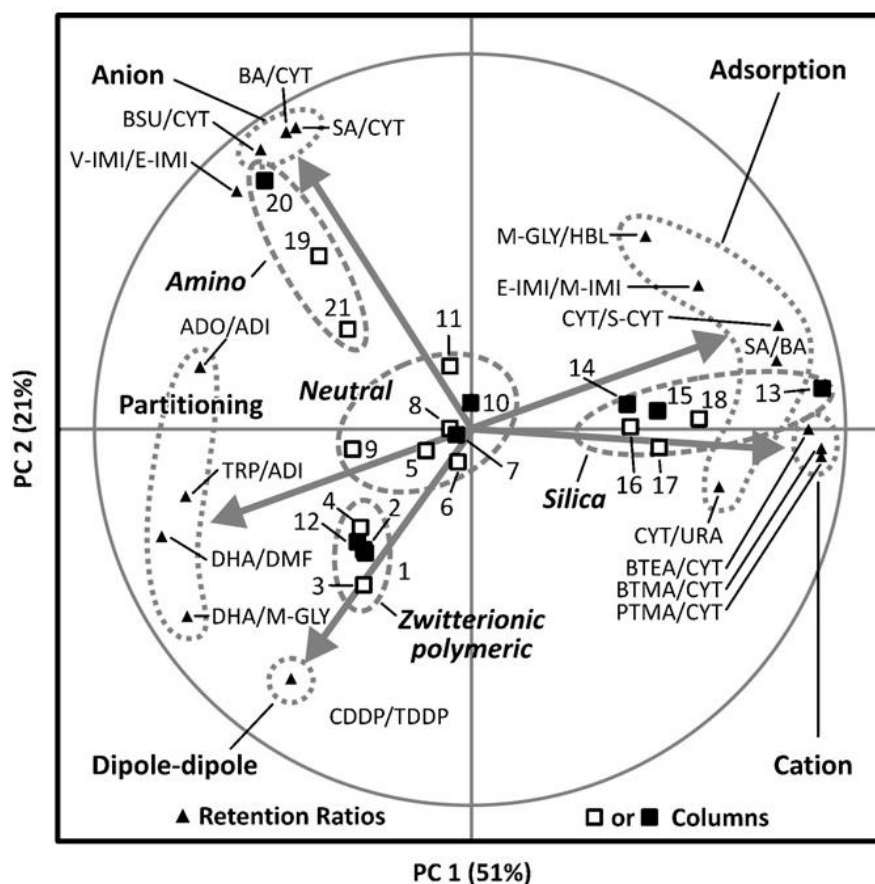


Figure 2.20 Score and loading biplot of the two first components of the model where the observations were the columns and the variables were the retention ratios of all 15 pairs of test analytes. For column numbering, see Table 2.1. Reprinted from Reference [10] with permission from Elsevier.

2.6 Summary

Recent years have seen a maturation of the field, such that insights into the broad properties of each class of columns are now available. This allows grouping of columns of similar character, and recognition of which columns will offer a different selectivity (and thus enable resolution of challenging samples). Nonetheless, it is anticipated that the field of HILIC will continue to see rapid growth in the number and types of columns commercially available. To keep abreast of these developments, Ron Majors' annual preview of the new chromatographic columns introduced at Pittcon is highly recommended [131].

2.7 References

- [1] A. Alpert, *J. Chromatogr.* **1990**, *499*, 177-196.
- [2] http://www.sielc.com/Technology_HILIC.html (accessed in November 2013).
- [3] J. Linden, C. Lawhead, *J. Chromatogr.* **1975**, *105*, 125-133.
- [4] J.K. Palmer, *Anal. Lett.* **1975**, *8*, 215-224.
- [5] B.M. Lampert, J.T. Stewart, *J. Chromatogr. B* **1989**, *495*, 153-165.
- [6] H.P. Gregor, F.C. Collins, M. Pope, *J. Colloid Sci.* **1951**, *6*, 304-322.
- [7] H. Ruckert, O. Samuelson, *Sven. Kem. Tidskr* **1975**, *66*, 337-344.
- [8] D.V. McCalley, *J. Chromatogr. A* **2010**, *1217*, 3408-3417.
- [9] M. Lammerhofer, M. Richter, J. Wu, R. Nogueira, W. Bicker, W. Lindner, *J. Sep. Sci.* **2008**, *31*, 2572-2588.
- [10] N. Dinh, T. Jonsson, K. Irgum, *J. Chromatogr. A* **2011**, *1218*, 5880-5891.
- [11] P. Hemstrom, K. Irgum, *J. Sep. Sci.* **2006**, *29*, 1784-1821.
- [12] I. Jane, *J. Chromatogr* **1975**, *111*, 227-233.

- [13] I. Paek, Y. Moon, H. Ji, H. Kim, *J. Chromatogr. B* **2004**, 809, 345-350.
- [14] W. Naidong, W. Shou, A. Eerkes, *J. Pharm. Biomed. Anal.* **2003**, 31, 917-928.
- [15] H. Koh, A. Lau, E. Chan, *Rapid Commun. Mass specrom.* **2005**, 19, 1237-1244.
- [16] S. Qi, H. Junga, T. Yong, A. Li, *J. Chromatogr. B* **2005**, 814, 105-114.
- [17] J. Su, R. Hirji, L. Zhang, C. He, a. et, *J. Exp. Bot.* **2006**, 57, 1129-1135.
- [18] S. Qi, W. Naidong, *J. Chromatogr. B* **2006**, 830, 135-142.
- [19] P. Kovarikova, J. Stariat, J. Klimes, K. Hruskova, K. Varova, *J. Chromatogr. A* **2011**, 1218, 416-426.
- [20] H. Mcroczeck, *J. Chromatogr. A* **2009**, 1216, 2519-2528.
- [21] T. Hayama, H. Yoshida, K. Todoriki, H. Nohta, M. Yamaguchi, *Rapid Commun. Mass specrom.* **2008**, 22, 2203-2210.
- [22] H. Ji, E. Park, K. Lee, H. Lee, *J. Sep. Sci.* **2008**, 31, 1628-1633.
- [23] W. Naidong, *J. Chromatogr. B* **2003**, 796, 209-224.
- [24] L. Snyder, J. Kirkland, J. Dolan, In *Introduction to modern liquid chromatography, 3rd Edition*, John Wiley & sons, Hoboken, NJ, 2010.
- [25] J. Kohler, D. Chase, R. Farlee, A. Vega, J. Kirkland, *J. Chromatogr. A* **1986**, 352, 275-305.
- [26] J. Nawrocki, *Chromatographia* **1991**, 31, 177-192.
- [27] H. Engelhardt, H. Low, W. Gotzinger, *J. Chromatogr.* **1991**, 544, 371-379.
- [28] D. Sindorf, G. Maciel, *J. Am. Chem. Soc.* **1983**, 105, 1487-1493.
- [29] J. Nawrocki, *Chromatographia* **1991**, 31, 193-205.

- [30] U. Neue, In *HPLC Columns theory, technology and practice*. New York: Wiley-VCH; 1997.
- [31] J. Sandoval, J. Pesek, *Anal. Chem.* **1989**, *61*, 2067-2075.
- [32] http://www.microsolvttech.com/hplc/app_aromatic.asp (accessed in February 2012).
- [33] J. Kirkland, F. Truszkowski, C. Dilks, G. Engel, *Journal of Chromatography A* **2000**, *890*, 3-13.
- [34] J. Kirkland, T. Langlois, J. DeStefano, *Amer. Lab.* **2007**, *39*, 18.
- [35] <http://www.advanced-materials-tech.com/products.html> (accessed in February 2012).
- [36] F. Gritti, A. Pereira, P. Sandra, G. Guiochon, *J. Chromatogr. A* **2010**, *1217*, 683-688.
- [37] N. Tanaka, H. Kobayashi, K. Nakanishi, H. Minakuchi, N. Ishizuka, *Anal. Chem.* **2001**, *73*, 420A-429A.
- [38] T. Ikegami, N. Tanaka, *Curr. Opin. Chem. Biol.* **2004**, *8*, 527-533.
- [39] K. Miyabe, G. Guiochon, *J. Sep. Sci.* **2004**, *27*, 853-873.
- [40] J. Dawkins, L. Lloyd, *J. Chromatogr.* **1986**, *352*, 157-167.
- [41] K. Cabrera, *J. Sep. Sci.* **2004**, *27*, 843-852.
- [42] K.M. Glenn, C.A. Lucy, P.R. Haddad, *J. Chromatogr. A* **2007**, *1155*, 8-14.
- [43] S. Pelletier, C.A. Lucy, *J. Chromatogr. A* **2006**, *1118*, 12-18.
- [44] M.E.A. Ibrahim, T. Zhou, C.A. Lucy, *J. Sep. Sci.* **2010**, *33*, 773-778.
- [45] T. Ikegami, K. Tomomatsu, H. Takubo, K. Horie, N. Tanaka, *J. Chromatogr. A* **2008**, *1184*, 474-503.

- [46] S.D. Chambers, K.M. Glenn, C.A. Lucy, *J. Sep. Sci.* **2007**, *30*, 1628-1645.
- [47] B. Pack, D. Risley, *J. Chromatogr. A* **2005**, *1073*, 269-275.
- [48] J. Nawrocki, *J. Chromatogr. A* **1997**, *779*, 29-71.
- [49] D.V. McCalley, *J. Chromatogr.* **1997**, *769*, 169-178.
- [50] D.V. McCalley, *LCGC North Am.* **1999**, *17*, 440-455.
- [51] J. Kirkland, J. Henderson, J.D. Stefano, M.v. Straten, H. Claessens, *J. Chromatogr. A* **1997**, *762*, 97-112.
- [52] K. Wyndham, J. O'Gara, T. Walter, K. Glose, N. Lawrence, B. Alden, G. Izzo, C. Hudalla, P. Iraneta, *Anal. Chem.* **2003**, *75*, 6781-6788.
- [53] E. Grumbach, D. Diehl, U. Neue, *J. Sep. Sci.* **2008**, *31*, 1511-1518.
- [54] P. Orth, H. Engelhardt, *Chromatographia* **1982**, *15*, 91-96.
- [55] N. Tomiya, J. Awaya, M. Kurono, S. Endo, Y. Arata, N. Takahashi, *Anal. Biochem.* **1988**, *171*, 73-90.
- [56] H. Higashi, M. Ito, N. Fukaya, S. Yamagata, T. Yamagata, *Anal. Biochem.* **1990**, *186*, 355-362.
- [57] N. Takahashi, H. Nakagawa, K. Fujikawa, Y. Kawamura, N. Tomita, *Anal. Biochem.* **1995**, *226*, 139-146.
- [58] T. Yoshida, *J. Chromatogr. A* **1998**, *811*, 61-67.
- [59] T. Yoshida, *Anal. Chem.* **1997**, *69*, 3038-3043.
- [60] W. Ahmed, K. Gonmori, M. Suzuki, K. Watanabe, O. Suzuki, *Forensic Toxicol* **2010**, *28*, 69-76.
- [61] C. Tomasek, *LCGC North Am.* **2009**, *27*, 44-45.
- [62] D. Risley, W. Yang, J. Peterson, *J. Sep. Sci.* **2006**, *29*, 256-264.

- [63] C. West, E. Lesellier, *J. Chromatogr. A* **2006**, *1110*, 200-213.
- [64] F. Regnier, R. Noel, *J. Chromatogr. Sci.* **1976**, *14*, 316-320.
- [65] C. Brons, C. Olieman, *J. Chromatogr* **1983**, *259*, 79-86.
- [66] B. Herbreteau, M. Lafosse, L. Morinallory, M. Dreux, *Chromatographia* **1992**, *33*, 325-330.
- [67] H. Tanaka, X. Zhou, M. Ohira, *J. Chromatogr. A* **2003**, *987*, 119-125.
- [68] J. Pazourek, *J. Sep. Sci.* **2010**, *33*, 974-981.
- [69] X. Liu, C. Pohl, *J. Chromatogr. A* **2006**, *1191*, 83-89.
- [70] P. Jandera, T. Hájek, V. Skeríková, J. Soukup, *J. Sep. Sci.* **2010**, *33*, 841-852.
- [71] C. McClintic, D. Remick, J. Peterson, D. Risley, *J. Liq. Chromatogr. Relat. Technol.* **2003**, *26*, 3093-3104.
- [72] N. Al-Tannak, S. Bawazeer, T. Siddiqui, D. Watson, *J. Chromatogr. A* **2011**, *1218*, 1486-1491.
- [73] D. Armstrong, H. Jin, *J. Chromatogr.* **1989**, *462*, 219-232.
- [74] X. Lai, W. Tang, S. Ng, *J. Chromatogr. A* **2011**, *1218*, 3496-3501.
- [75] J. Feng, Z. Guo, H. Shi, J. Gu, Y. Jin, X. Liang, *Talanta* **2010**, *81*, 1870-1876.
- [76] D. Risley, M. Strege, *Anal. Chem.* **2000**, *72*, 1736-1739.
- [77] A. Berthod, S. Chang, J. Kullman, D. Armstrong, *Talanta* **1998**, *47*, 1001-1012.
- [78] W. Jiang, K. Irgum, *Anal. Chem.* **2001**, *73*, 1993-2003.
- [79] W. Jiang, K. Irgum, *Anal. Chem.* **1999**, *71*, 333-344.
- [80] Y. Guo, S. Gaiki, *J. Chromatogr. A* **2005**, *1074*, 71-80.

- [81] R. Kane, P. Deschatelets, G. Whitesides, *Langmiur* **2003**, *19*, 2388-2391.
- [82] C. Viklund, K. Irgum, *Macromolecules* **2000**, *33*, 2539-2544.
- [83] W. Jiang, J. Awasum, K. Irgum, *Anal. Chem.* **2003**, *75*, 2768-2774.
- [84] E. Rodriguez-Gonzalo, D. Garcia-Gomez, R. Carabias-Martinez, *J. Chromatogr. A* **2011**, *1218*, 3994-4001.
- [85] M. Kato, H. Kato, S. Eyama, A. Takatsu, *J. Chromatogr. B* **2009**, *877*, 3059-3064.
- [86] S. Di-Palma, P. Boersema, A. Heck, S. Mohammed, *Anal. Chem.* **2011**, *83*, 3440-3447.
- [87] S. Van-Dorpe, V. Vergote, A. Pezeshki, C. Burvenich, K. Peremans, B.D. Spiegeleer, *J. Sep. Sci.* **2010**, *33*, 728-739.
- [88] I. Pasakova, M. Gladziszova, J. Charvatova, J. Stariat, J. Klimes, P. Kovarikova, *J. Sep. Sci.* **2011**, *34*, 1357-1365.
- [89] J. Bengtsson, B. Jansson, M. Hammarlund-Udenaes, *Rapid Commun. Mass specrom.* **2005**, *19*, 2116-2122.
- [90] D. Risley, B. Pack, *LCGC North Am.* **2006**, *24*, 776-785.
- [91] F. Dorr, V. Rodriguez, R. Molica, P. Henriksen, B. Krock, E. Pinto, *Toxicon* **2010**, *55*, 92-99.
- [92] N. Lindegardh, W. Hanpithakpong, A. Phakdeeraj, R. Singhasivanon, J. Farrar, T. Hien, N. White, N. Day, *J. Chromatogr. A* **2008**, *1215*, 145-151.
- [93] W. Hu, T. Takeuchi, H. Haraguchi, *Anal. Chem.* **1993**, *65*, 2204-2208.
- [94] http://www.sielc.com/upload/file/pdf/SIELC_Obelisc_Intro.pdf (accessed in November 2013).

- [95] B. Beilmann, P. Langguth, H. Hausler, P. Grass, *J. Chromatogr. A* **2006**, *1107*, 204-207.
- [96] A. Que, M. Novotny, *Anal. Chem.* **2002**, *74*, 5184-5194.
- [97] Z. Aturki, G. D'Orazio, A. Rocco, K. Si-Ahmed, S. Fanali, *Anal. Chim. Acta* **2011**, *685*, 103-110.
- [98] J. Valette, C. Demesmay, J. Rocca, E. Verdon, *Chromatographia* **2004**, *59*, 55-60.
- [99] http://www.sielc.com/Products_Obelisc.html (accessed in November 2013).
- [100] B. Olsen, *J. Chromatogr. A* **2001**, *913*, 113-122.
- [101] M. Lafosse, B. Herbreteau, M. Dreux, L. Morinallorym, *J. Chromatogr.* **1989**, *472*, 209-218.
- [102] P. Jandera, *Anal. Chim. Acta* **2011**, *692*, 1-25.
- [103] A. Alpert, *J. Chromatogr.* **1983**, *266*, 23-37.
- [104] M. Kiseleva, P. Kebets, P. Nesterenko, *Analyst* **2001**, *126*, 2119-2123.
- [105] B. Zhu, C. Colin, R. Hodges, *J. Chromatogr.* **1991**, *548*, 13-24.
- [106] V. Tolstikov, O. Fiehn, *Anal. Biochem.* **2002**, *301*, 298-307.
- [107] A. Oyler, B. Armstrong, J. Cha, M. Zhou, Q. Yang, R. Robinson, R. Dunphy, D. Burinsky, *J. Chromatogr. A* **1996**, *724*, 378-383.
- [108] M. Curren, J. King, *J. Chromatogr. A* **2002**, *954*, 41.
- [109] B. Zywicki, G. Catchpole, J. Draper, O. Fiehn, *Anal. Biochem.* **2005**, *336*, 178-186.
- [110] A. Mihailova, E. Lundanes, T. Greibrokk, *J. Sep. Sci.* **2006**, *29*, 576-581.

- [111] http://www.orachrom.com/Product_Folder/Amino_HILIC.html (accessed in February 2012).
- [112] A. Klingenberg, A. Seubert, *J. Chromatogr.* **1993**, *640*, 167-178.
- [113] T. Hargitai, P. Reinholdsson, B. Toernell, R. Isaksson, *J. Chromatogr.* **1992**, *630*, 79-83.
- [114] O. Samuelson, E. Sjoström, *Sven. Kem. Tidskr* **1952**, *64*, 305-314.
- [115] J. Havlicek, O. Samuelson, *Anal. Chem.* **1975**, *47*, 1854-1857.
- [116] T. Chambers, J. Fritz, *J. Chromatogr. A* **1998**, *797*, 139-147.
- [117] Y. Kawachi, T. Ikegami, H. Takubo, Y. Ikegami, M. Miyamoto, N. Tanaka, *J. Chromatogr. A* **2011**, *1218*, 5903-5919.
- [118] <http://www.separations.us.tosohbioscience.com> (accessed in February 2012).
- [119] Y. Guo, S. Gaiki, *J. Chromatogr. A* **2011**, *1218*, 5920-5938.
- [120] K. Fountain, J. Xu, D. Diehl, D. Morrison, *J. Sep. Sci.* **2010**, *33*, 740-751.
- [121] K. Kimata, K. Iwaguchi, S. Onishi, K. Jinno, R. Eksteen, K. Hosoya, M. Araki, N. Tanaka, *J. Chromatogr. Sci.* **1989**, *27*, 721-728.
- [122] U. Neue, *J. Sep. Sci.* **2007**, *30*, 1611-1627.
- [123] G. Karlsson, S. Winge, H. Sandberg, *J. Chromatogr. A* **2005**, *1092*, 246-249.
- [124] A. Yanagida, H. Murao, M. Ohnishi-Kameyama, Y. Yamakawa, A. Shoji, M. Tagashira, T. Kanda, H. Shindo, Y. Shibusawa, *J. Chromatogr. A* **2007**, *1143*, 153-161.

- [125] Z. Daunoravicius, I. Juknaite, E. Naujalis, A. Padaruskas, *Chromatographia* **2006**, *63*, 373-377.
- [126] <http://www.dichrom.com> (accessed in February 2012).
- [127] Y. Guo, A. Huang, *J. Pharm. Biomed. Anal.* **2003**, *31*, 1191-1201.
- [128] G. Puy, C. Demesmay, J. Rocca, J. Iapichella, A. Galarneau, D. Brunel, *Electrophoresis* **2006**, *27*, 3971-3980.
- [129] Y. Guo, In *Chapter 17: Retention and Selectivity of Polar Stationary Phases for Hydrophilic Interaction Chromatography; Hydrophilic Interaction Liquid Chromatography (HILIC) and Advanced Applications*, P.G. Wang, W. He (Eds.), CRC Press, 2011, pp. 401-426.
- [130] M.E.A. Ibrahim, Y. Liu, C.A. Lucy, *J. Chromatogr. A.* **2012**, *1260*, 126-131.
- [131] R. Majors, *LCGC North Am.* **2011**, *29*, 218-235.

CHAPTER THREE: A Simple Graphical Representation of Selectivity in Hydrophilic Interaction Liquid Chromatography*

3.1 Introduction

Recently, there has been a rapid growth in applications of hydrophilic interaction liquid chromatography (HILIC) for samples ranging from small polar analytes such as nucleosides [1, 2], food contaminants [3] and pharmaceuticals [4, 5] to macromolecules such as glycosylated proteins [6]. Recent publications illustrate the maturation of our understanding of the retention mechanism(s) of HILIC. As coined by Alpert in 1990 [7], HILIC referred to retention due to partitioning of analytes into a water rich layer formed on a polar stationary phase when an acetonitrile (ACN) rich mobile phase was used. Since 1990, numerous types of HILIC stationary phases have been commercialized, including bare silica, amide, zwitterionic, amine, and diol phases [8]. Based on solely partitioning into a water rich layer, all HILIC phases should yield similar selectivity. However, substantial variations in retention and selectivity have been observed on the various classes of commercial HILIC columns [8-11]. These differences in retention characteristics have been attributed to the hydrophilic, hydrophobic, dipole-dipole and ion exchange characteristics of the stationary phases [8]. Recently, Dinh *et al.* [12] and Kawachi *et al.* [10] used principal component

* A version of this chapter has been published as Mohammed E. A. Ibrahim¹, Yang Liu², Charles A. Lucy, *J. Chromatogr. A.* **2012**, *1260*, 126-131.

¹I mentored Y. Liu and wrote the manuscript.

²Y. Liu (chemistry undergraduate) performed the experiments under my supervision.

analysis to characterize these interactions for 22 and 14 commercial HILIC stationary phases, respectively. Both approaches were highly successful at categorizing the various types of HILIC phases. However both approaches are necessarily complex in order to characterize the numerous attributes of these columns. This chapter offers a simpler, albeit much more limited, representation of column selectivity in HILIC.

The simplified representation offered herein is inspired by the approaches to characterize stationary phases in RPLC [13]. The *Tanaka method* [13, 14] has been used to characterize over 200 RPLC stationary phases. The retentivity of the packing was quantified using the retention factor of n-pentylbenzene. The various contributing forces to this retention were then characterized using the relative retention (α) of selected paired solutes. Similarly, Snyder and co-workers have characterized over 300 RPLC stationary phases using the Hydrophobic Subtraction Model [15-18]. In this model, selectivity is related to the hydrophobicity, cation exchange character, hydrogen bond acidity, hydrogen bond basicity and steric effects of the stationary phase. Despite the rigor and power of these approaches, the simple *Neue plot* [13, 19, 20] remains highly popular, primarily due to its simplicity. In the Neue plot, the silanophilic character of a column (measured as the relative retention of amitriptyline vs. acenaphthene) is plotted vs. the hydrophobicity of the column (measured by the retention factor of acenaphthene). Even though the Neue plot considers only two of the interactions involved in RPLC and reflects the silanol activity at only a single pH, it has been found to be very useful for characterization and classification of RPLC

columns. Indeed, Waters provides an on-line interactive version of the Neue plot containing over 80 commercial RPLC phases [21].

This paper re-plots the HILIC selectivity data of Dinh *et al.* [12] for 21 commercial columns plus our own data for an additional 8 HILIC and 4 RPLC columns in the spirit of the Neue plot. That is, our objective is to depict the selectivity of HILIC columns in a simple, albeit limited, representation that we term the *HILIC-Phase Selectivity Chart*.

3.2 Experimental

3.2.1 Apparatus

The HPLC system used to collect retention data for the additional 12 columns (8 HILIC and 4 RPLC columns) studied herein consisted of: a Prostar 210 pump (Varian Australia PTY LTD, Australia); a 6-port Rheodyne model 7125 (Rheodyne, Berkeley, CA, USA) injection valve with a 20 μ L loop; and a Varian Pro Star 325 variable wavelength UV/VIS detector (Varian).

3.2.2 Reagents and Materials

All solutions were prepared in nanopure water (Barnstead, Dubuque, IA, USA). HPLC-grade ACN was from Fisher Scientific (Fair Lawn, NJ, USA). Cytosine, uracil and adenine were from Sigma-Aldrich (St. Louis, MO, USA). Adenosine was from Nutritional Biochemical Corporation (Cleveland, OH, USA), ammonium acetate was from Anachemia (Montreal, QC, Canada), and

benzyltrimethylammonium chloride (BTMA) was from Acros Organics (NJ, USA).

3.2.3 Chromatographic Conditions

All chromatographic tests have been performed under the same conditions as used in ref. [12]. The Chromolith Si column (column no. 13) previously characterized in ref. [12] was used to validate our measurements. The mobile phase consists of a mixture of ACN and buffer containing (80:20; v/v), whereby the water phase contained 25 mM ammonium acetate adjusted to pH 6.8 with HCl. Analytes were separated under isocratic conditions at 0.5 mL/min and detected at 254 nm. The buffer strength quoted in this work is that present after ACN addition. The % ACN quoted in this work represents the volume of the ACN relative to the total volume of the solvents including buffer and ACN. Retention factors (k) were calculated as the average of three injections. Toluene was used as the unretained dead time marker (t_M) for all HILIC phases, and the baseline deflection was used as the dead time marker for the RPLC phases. Retention factors and retention ratios were unaffected by a two-fold change in flow rate.

3.2.4 Tested Columns and Test Probes

Table 3.1 shows the characteristics of the tested HILIC columns. Irgum and his co-workers suggested numerous pairs of analytes as test probes for the interactions involved in HILIC [12]. A subset of the probe pairs identified by

Dinh *et al.* [12] have been used in our work. Specifically: cytosine/uracil is used to probe the hydrophobic/hydrophilic characteristics of the column; BTMA/cytosine to probe the column ion exchange character; and adenosine/adenine to probe the column's capability for hydrogen bonding (H-bonding). The chemical structures of these test probes are given in Appendix I. The standard deviations of the retention ratio measurements shown in Figures 3.1-3.3 are smaller than the size of the marker. Confidence ellipses for grouping the columns were constructed using a confidence level of 75% using: MATLAB, R2010a, windows 64-bit version; with PLS toolbox (Eigenvector Research Inc., Wenatchee, WA, USA) 5.8 (R5.8.3). Calculations were performed on a microcomputer (Intel Core i5, processor: 750 @ 2.67 GHz, RAM: 8 GB, GPU: NVIDIA GeForce. 210).

3.3 Results and Discussion

Table 3.1 shows the 21 previously studied HILIC phases [12] and an additional 12 stationary phases (8 HILIC and 4 RPLC columns) included in the study herein. Three plots (Figs. 3.1-3.3) were constructed based on the retention data of probe pairs selected to characterize the HILIC phases in terms of their hydrophilic nature, anion/cation exchange properties, and H-bonding capability. In the following discussion, the numbers within the parentheses indicate specific HILIC columns in Table 3.1. The columns previously studied by Irgum and co-workers include zwitterionic (1-6), neutral (7-11), cation exchange (12-18) and anion exchange (19-21) phases. Our additional columns include cation exchange

(22-24, 26), anion exchange (25, 27, 28), a neutral phase (29) and various RPLC phases (30-33). Since the pH of the eluent was 6.8, the underivatized silica phases are deprotonated and so possess cation exchange character. On the other hand, amino based columns may be protonated and thus have anion exchange character.

3.3.1 Selection of Test Pairs

Based on ref. [12], three pairs of analytes were chosen to probe the primary interactions taking place on the HILIC phases. First, cytosine and uracil are both highly hydrophilic (octanol/water partition coefficients of $10^{-1.24}$ and $10^{-0.86}$, respectively), and so both show strong retention in HILIC. Dinh *et al.* [12] used their relative retention (cytosine/uracil) as a generic measure of the “hydrophilic” character of the column. The higher the relative retention of cytosine *vs.* uracil, the more “hydrophilic” the stationary phase.

The value of using probe pairs becomes more apparent when probing specific types of hydrophilic interaction such as ion exchange. Irgum and co-workers used the benzyltrimethylammonium (BTMA)/cytosine pair to probe the cation exchange interactions of HILIC phases [12]. BTMA is a quaternary amine; consequently it is positively charged regardless of the eluent pH and will participate in cation exchange interactions. Cytosine is structurally similar to BTMA, but lacks the positive charge. Thus, cytosine does not engage in cation exchange but will experience all other types of hydrophilic interaction similarly to BTMA. Hence the retention ratio BTMA/cytosine reflects, as much as possible, a

Table 3.1 Characteristics of the tested stationary phases

#	Brand name	Manufacturer	Support	Functionality	Particle size (μm)	Pore size (\AA)	Surface area (m^2/g)	Column length (mm)	Column diameter (mm)
Irgum's tested phases									
1	ZIC-HILIC	Merck	Silica	Polymeric sulfoalkylbetaine zwitterionic	5	200	135	100	4.6
2	ZIC-HILIC	Merck	Silica	Polymeric sulfoalkylbetaine zwitterionic	3.5	200	135	150	4.6
3	ZIC-HILIC	Merck	Silica	Polymeric sulfoalkylbetaine zwitterionic	3.5	100	180	150	4.6
4	ZIC-pHILIC	Merck	Porous polymer	Polymeric sulfoalkylbetaine zwitterionic	5	-	-	50	4.6
5	Nucleodur HILIC	Macherey-Nagel	Silica	Sulfoalkylbetaine zwitterionic	5	110	340	100	4.6
6	PC HILIC	Shiseido	Silica	Phosphorylcholine zwitterionic	5	100	450	100	4.6
7	TSKgel Amide 80	Tosoh Bioscience	Silica	Amide (polymeric carbamoyl)	5	80	450	100	4.6
8	TSKgel Amide 80	Tosoh Bioscience	Silica	Amide (polymeric carbamoyl)	3	80	450	50	4.6
9	PolyHydroxyethyl A	PolyLC	Silica	Poly(2-hydroxyethyl aspartamide)	5	200	188	100	4.6
10	LiChrospher 100 Diol	Merck	Silica	2,3-Dihydroxypropyl	5	100	350	125	4.0
11	Luna HILIC	Phenomenex	Silica	Cross-linked diol	5	200	185	100	4.6

Continued

12	PolySulfoethyl A	PolyLC	Silica	Poly(2-sulfoethyl aspartamide)	5	200	188	100	4.6
13 ^a	Chromolith Si	Merck	Silica monolith	Underivatized	N/A	130	300	100	4.6
14	Atlantis HILIC Si	Waters	Silica	Underivatized	5	100	330	100	4.6
15	Purospher STAR Si	Merck	Silica	Underivatized	5	120	330	125	4.0
16	LiChrospher Si 100	Merck	Silica	Underivatized	5	100	400	125	4.0
17	LiChrospher Si 60	Merck	Silica	Underivatized	5	60	700	125	4.0
18	Cogent Type C Silica	Microsolv	Silica	Silica hydride ("Type C" silica)	4	100	350	100	4.6
19	LiChrospher 100 NH ₂	Merck	Silica	3-Aminopropyl	5	100	350	125	4.0
20	Purospher STAR NH ₂	Merck	Silica	3-Aminopropyl	5	120	330	125	4.0
21	TSKgel NH ₂ -100	Tosoh Bioscience	Silica	Aminoalkyl	3	100	450	50	4.6
Additional tested phases									
22	Atlantis HILIC	Waters	silica	Underivatized	3	100	330	50	1.0
23	Omyx silica monolith	Phenomenex	silica monolith	Underivatized	N/A	130	300	100	4.6
24	Zorbax HILIC plus	Agilent	silica	Underivatized	3.5	95	160	100	4.6
25	Silica monolith coated with AS9-SC	homemade	silica monolith	Silica – cationic nanoparticle	N/A	130	300	80	4.6

Continued

26	Zorbax RRHD HILIC plus	Agilent	Silica	Underivatized	1.8	95	160	100	3.0
27	Acclaim Trinity P1	Thermo Fisher Scientific	Silica	Silica-cationic nanoparticle	3	-	-	150	3.0
28	Cosmosil HILIC	Nacalai	silica	Triazole	5	120	300	150	4.6
29	Acclaim HILIC-10	Thermo Fisher Scientific	silica	Proprietary neutral polar functionality	3	120	300	150	4.6
30	Zorbax Eclipse XDB-C18	Agilent	silica	Octadecyl	5	80	180	150	4.6
31	XBridge C18	Waters	silica (BEH)	Octadecyl	5	130	185	150	4.6
32	YMC Pro C18	YMC	silica	Octadecyl	3	120	340	150	2.0
33	Zorbax SB-aq	Agilent	silica	Octadecyl	3.5	80	180	150	2.1
34 ^b	Hybercarb™	Thermo Fisher Scientific	carbon	Underivatized	5	250	120	100	4.6
35 ^b	Acclaim-WCX-1	Thermo Fisher Scientific	silica	Alkyl carboxylic acid	5	120	300	150	4.6
36 ^b	Carboxylate-PGC	homemade	carbon	Benzene carboxylic acid	5	120	nd	150	3.0

^a Measurements of the Chromolith Si column by Dinh *et al.* [12] and ourselves are indicated as 13a and 13b, respectively in Fig. 3.1.

^b Columns no 34-36 will be discussed in details in Chapter 6.

single type of interaction (cation exchange) as dictated by the structural difference between the two probes [12]. However BTMA is also highly hydrophilic, and so exhibits strong retention even on neutral HILIC phases. This strong retention enables this single probe molecule to be used herein to measure both the cation exchange character of the column and also its anion exchange nature (*via* electrostatic repulsion effects) [22]. Higher (BTMA/cytosine) retention ratios indicate stronger cation exchange behavior; while smaller (BTMA/cytosine) retention ratios indicate stronger anion exchange behavior.

Finally, the adenosine/adenine pair was used to measure the capability of the stationary phase to participate in H-bonding interactions, as suggested by Dinh *et al.* [12]. Adenosine has a higher ability to participate in H-bonding compared to adenine due to its additional ribose unit. See Appendix I for chemical structures. Ratioing the retention of adenosine to that of adenine minimizes the contribution of the common structural features and charge, such that the ratio predominantly reflects the ability of the column to engage in H-bonding. However it is important to recall that all chosen pairs are likely to probe other types of interaction to some extent [12].

3.3.2 Hydrophilicity vs. Ion Exchange Characteristics of HILIC Phases

Figure 3.1 represents a selectivity plot of different HILIC stationary phases (21 previously studied HILIC phases [12] and 12 additional phases). Figure 3.1 categorizes these different phases in terms of their “hydrophilicity” and ion exchange behavior whether cation or anion exchange. The retention ratio of

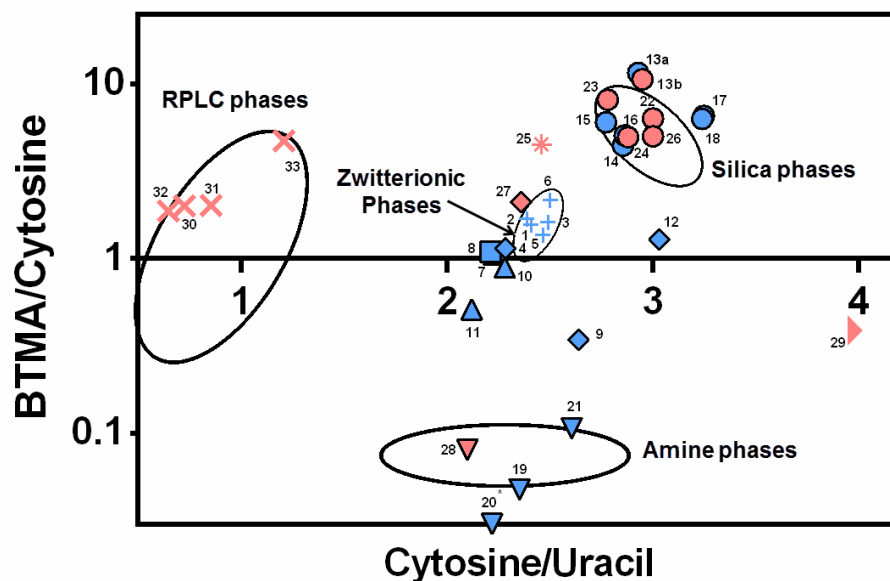


Figure 3.1 Hydrophilicity vs. ion exchange selectivity plot of HILIC phases; bare silica (●), amide (■), diol (▲), amine and/or triazole (▼), polymer substrate and/or polymer coated silica (◆), zwitterionic (+), RPLC (×), latex coated silica (*), proprietary polar phase (►). Blue markers are for Irgum's columns and red markers for our additional columns. Conditions: Columns; see column numbers in Table 3.1; flow rate, 0.5 mL/min; eluent, 5 mM ammonium acetate, pH 6.8, in 80 % ACN; test analytes (see Appendix I for chemical structures), 0.044-0.44 mM in 80 % ACN; UV detection at 254 nm with a 20 μ L loop injection.

* Column (20) gave (BTMA/Cytosine) ratio out of scale at -0.0026.

cytosine/uracil is plotted on the X-axis and categorizes the studied HILIC phases with respect to their generic “hydrophilicity”. Stationary phases to the left side of the plot are strongly hydrophobic, as exemplified by the four RPLC phases (30-33), and the phases on the right side are most “hydrophilic”. The Y-axis extends from strong cation exchange phases at the top (*e.g.*, silica) to strong anion exchange (*e.g.*, amine (19-21) and triazole (28) based columns) at the bottom.

Data from Dinh *et al.* [12] are indicated with blue symbols, while those collected herein are in pink. The consistency between the two sets of data was validated using the Chromolith Si (column 13) which was measured by both labs. Confidence ellipses (75% confidence level) were constructed using MATLAB to group the tested columns as: RPLC; bare silica; zwitterionic; or amine phases. RPLC phases (30-32) clustered close together, while Zorbax SB-aq (33) showed stronger cation exchange and hydrophilic character. The stronger cation exchange properties of Zorbax SB-aq (33) are consistent with its higher reported silanol activity ($C_{7.0} = 0.736$), based on the hydrophobic subtraction model [23] compared to other tested RP columns ($C_{7.0} = 0.006-0.138$). Also the higher hydrophilicity of the Zorbax SB-aq phase (33) (*i.e.*, to the right of the other RPLC columns in Figure 3.1) is consistent with the low hydrophobicity ($H = 0.593$) of the phase compared to the other RPLC columns ($H = 1.007-1.077$) [23].

Stationary phases appearing on the right hand side of Figure 3.1 are strongly hydrophilic as reflected by the stronger retention of the hydrophilic marker (cytosine). Acclaim HILIC-10 (29) exhibited the highest hydrophilicity

among the tested columns. The manufacturer indicates that this phase is made out of silica, but no information about its hydrophilic functionalities is given [24].

Underivatized silica phases, regardless of whether particulate or monolithic, exhibited high hydrophilicity and strong cation exchange character due its deprotonated silanols. Thus the silica phases cluster in the upper right of Figure 3.1. Silica phases studied by Dinh *et al.* [12] (blue) and herein (pink) display comparable characteristics. The ellipses in Figure 3.1 are the 75% confidence interval for behavior of a particular class of HILIC column, *e.g.* underivatized silica. The tightness of this cluster indicates the general uniformity of character for the various bare silica phases. Interestingly, the monolithic phases (13 and 23) exhibited higher cation exchange character than the particulate columns. However, even columns having the same nominal specifications but of different manufacturers displayed some differences. For example, the Chromolith silica monolith (13) produced by Merck is more hydrophilic and a stronger cation exchanger than the Onyx silica monolith (23) produced by Phenomenex. Finally, as observed by Dinh *et al.* [12], the Cogent Type C Silica (18) displayed the highest hydrophilicity - along with LiChrospher Si 60 (17) - amongst the silica phases in Figure 3.1, even though it is marketed as having some hydrophobic retention character due silicon hydride replacing the surface silanols.

Other phases, including zwitterionic (1-6), amide (7, 8), diol (10, 11), and amine (19-21) based phases, each exhibit clusters in Figure 3.1. All of these classes are less hydrophilic than the silica phases. The ZIC-HILIC columns (3-4) are synthesized by grafting a layer of sulfoalkylbetaine on either a silica (ZIC-

HILIC, 3) [25, 26] or a polymeric support (ZIC-pHILIC, 4) [8, 11]. These phases are zwitterionic due to the presence of both negative sulfonate groups and positive quaternary amine functionalities [8], but nonetheless do exhibit some ion exchange character. These sulfoalkylbetaine phases showed poor cation exchange properties despite the presence of distal acidic sulfonates [8, 11] as shown by the moderate BTMA/cytosine value of these columns in Figure 3.1. It should be noted that the dilute electrolyte buffer was used herein will emphasize the ion exchange characteristics of the columns. The ion exchange properties of sulfoalkylbetaine phases will decrease as the concentration of the buffer electrolyte increases [12, 27-30], increasingly behaving like a neutral column [12]. The ZIC-HILIC column (3) is more hydrophilic and a stronger cation exchanger compared to the ZIC-pHILIC phase (4) which might be attributed to the characteristics of the underlying silica support. Nucleodur HILIC (5) and PC HILIC (6) columns are made of silica modified with sulfobetaine and phosphorylcholine groups, respectively, and clustered with the other zwitterionic columns in Figure 3.1.

Amide (7, 8) and diol (10, 11) phases are expected to be neutral, so it is unsurprising that they have a BTMA/cytosine ratio close to 1. The cross-linked diol Luna HILIC phase (11) is an exception. Although the Luna HILIC (11) possesses hydrophilic cross-linked diol groups, it displayed weak anion exchange properties and overall was weakly hydrophilic compared to the other HILIC phases, consistent with the principal component characterization of Dinh *et al.* [12].

The polymer coated silica phases (9, 12) and the polymer substrate phase (4) show a wide range in hydrophilicity. The polySULFOETHYL A (12) displayed comparable hydrophilicity to bare silica phases. In addition, although the polySULFOETHYL A phase (12) possesses negative terminal sulfonates, it does not exhibit significant cation exchange character under the dilute electrolyte conditions used in Figure 3.1. Dinh *et al.* [12] suggest this may be due to protonation of residual aminopropyl groups within the polySULFOETHYL A phase. Increased buffer concentration has been observed to make the ion exchange properties of polySULFOETHYL A more similar to that of the diol phases [12].

Amine phases (19-21) are protonated at pH 6.8. Consequently these phases have strong anion exchange properties and hence a low BTMA/cytosine retention ratio, *i.e.*, they appear at the bottom of Figure 3.1. The anion exchange character of these phases follow the order: Purospher STAR NH₂ (20) > LiChrospher 100 NH₂ (19) > TSKgel NH₂-100 (21), consistent with the observations of Dinh *et al.* [12]. The Cosmosil column (28) has a triazole functionality which displays intermediate anion exchange character; between that of LiChrospher 100 NH₂ (19) and TSKgel NH₂-100 (21).

Recently, a new category of HILIC phases was prepared by electrostatically attaching polycationic latex particles onto a silica monolith simply by flushing a suspension of latex, possessing hydrophilic quaternary amines, *e.g.* AS9-SC, through a silica monolith [31, 32]. The AS9-SC coated silica monolith was utilized for separation of polar analytes such as benzoates,

nucleotides and amino acids under HILIC conditions (Refer to Chapter 4 for more details) [31]. The AS9-SC (25) coated silica monolith (Chapter 4) was expected to show strong anion exchange properties due to the attached quaternary amine functionalities. However, this coated monolith showed only marginally different selectivity to that of underivatized silica (Figure 3.1). This behaviour might be attributed to the size exclusion of the latex nanoparticles (105 nm in diameter) from the mesopores (25 nm) [33] of the monolith. This size exclusion of the latex nanoparticles leads to low coverage of the silica surface by the latex nanoparticles and hence the very similar cation exchange properties to other silica phases [33]. Nevertheless the AS9-SC coated column (25) did show unique selectivity, as its lower hydrophilicity moved it outside the 75% confidence ellipse that characterizes bare silica phases.

3.3.3 Ion Exchange vs. Participation in H-bonding

Figure 3.2 represents another simple selectivity plot classifying different HILIC columns. This figure plots the (BTMA/cytosine) retention ratio on the Y-axis vs. the (adenosine/adenine) retention ratio on the X-axis. As discussed in Sec. 3.3.1, the (adenosine/adenine) retention ratio predominantly reflects the ability of the column to participate in H-bonding [12]. Similar distributions of column classes and behavior were observed in Figure 3.2, as with Figure 3.1. As the Y-axis is the same in the two plots, bare silica columns (circles) are still distinct due to the cation exchange resulting from their deprotonated silanols, and the amine (19-21) and triazole (28) phases appear at the bottom of the plot due to their

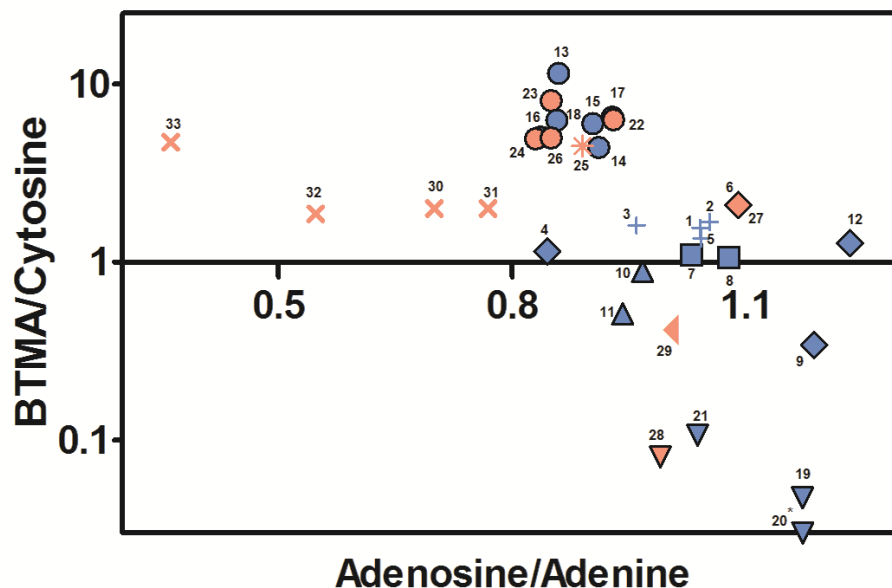


Figure 3.2 Ion exchange *vs.* H-bond formation capability selectivity plot of HILIC phases; bare silica (●), amide (■), diol (▲), amine and/or triazole (▼), polymer substrate and/or polymer coated silica (◆), zwitterionic (+), RPLC (×), latex coated silica (*), proprietary polar phase (◄). Blue markers are for Irgum's columns and red markers for our additional columns. Conditions: Columns; see column numbers in Table 3.1; flow rate, 0.5 mL/min; eluent, 5 mM ammonium acetate, pH 6.8, in 80 % ACN; test analytes (see Appendix I for chemical structures), 0.044-0.44 mM in 80 % ACN; UV detection at 254 nm with a 20 μ L loop injection.

* Column (20) gave (BTMA/Cytosine) ratio out of scale at -0.0026.

strong anion exchange properties. Other phases including diol (10, 11), zwitterionic (1-6), polymer substrate (4) and polymer coated silica (9) phases appear at the middle of vertical axis (BTMA/cytosine ratio close to 1) due to their weak ion exchange properties.

With respect to the X-axis in Figure 3.2 (*i.e.*, ability to participate in H-bonding), polySULFOETHYL A (12) and polyHYDROXYETHYL A (9) showed the highest capability to participate in H-bonding. On the other hand, underivatized silica phases displayed weak H-bonding compared to other HILIC phases. Amine (19-21), triazole (28), diol (10, 11) and the zwitterionic phases (1-6) with the exception of ZIC-pHILIC (4) have an intermediate capability to participate in H-bonding. RPLC columns (30-33) displayed weak ability to participate in H-bonding, as would be expected since the silanols are derivatized with octadecyl silane groups. While the information provided by Figures 3.1 and 3.2 are complementary, the column classes are more effectively clustered using the cytosine/uracil probe pair. Thus further discussion will focus on variants of Figure 3.1.

3.3.4 HILIC-Phase Selectivity Chart

Figure 3.3 represents another selectivity plot for HILIC phases in the spirit of the Neue plot that we term the *HILIC-Phase Selectivity Chart*. The appeal of the Neue plot is that it provides a simple representation of the retention behavior of RPLC columns [13, 19, 20]. In the Neue plot, the silanophilic character of a column is plotted *vs.* the hydrophobicity of the column. In the HILIC-Phase

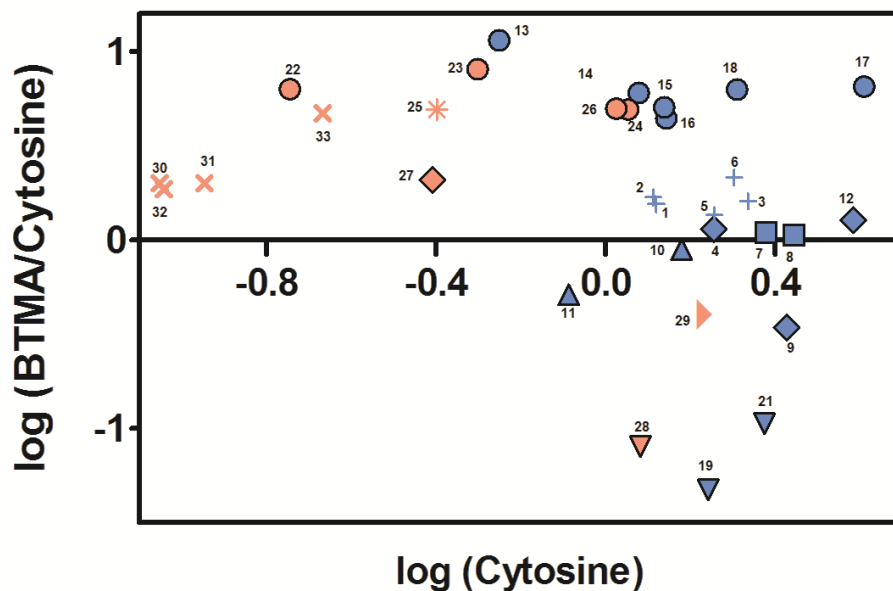


Figure 3.3: The HILIC-Phase Selectivity Chart. Columns; bare silica (●), amide (■), diol (▲), amine and/or triazole (▼), polymer substrate and/or polymer coated silica (◆), zwitterionic (+), latex coated silica (*), proprietary polar phase (◄). Blue markers are for Irgum's columns and red markers for our additional columns. Conditions: Columns; see column numbers in Table 3.1; flow rate, 0.5 mL/min; eluent, 5 mM ammonium acetate, pH 6.8, in 80 % ACN; test analytes (see Appendix I for chemical structures), 0.044-0.44 mM in 80 % ACN; UV detection at 254 nm with a 20 μ L loop injection.

Selectivity Chart (Figure 3.3), the ion exchange character of HILIC columns is reflected using the relative retention of BTMA *vs.* cytosine while the hydrophilic retentivity of the HILIC columns is measured by the retention of cytosine. This figure is similar to Figure 3.1 with respect to classifying columns with respect to their cation exchange characters and hydrophilicity. However, in Figure 3.3 plotting of $\log k_{\text{cytosine}}$ rather than the retention ratio (cytosine/uracil) reflects the effect of factors such as the pore size and surface area of the phase on the observed retention. For example, columns (2) and (3) are both ZIC-HILIC columns and so cluster together in Figure 3.1. However, in Figure 3.3 the greater retentivity of column no. 3 (pore size 100 Å, Surface area 180 m²/g) *vs.* column no. 2 (pore size = 200 Å, surface area = 135 m²/g) due to surface area is more evident. Likewise, the effect of surface area of LiChrospher 60 (17) *vs.* LiChrospher 100 (16) is also more evident.

In Figure 3.1 the monolithic silica phases (13, 23) displayed similar hydrophilic selectivity to other underivatized silica phases. However, attempts to use silica monoliths for HILIC have suffered from low retention [33]. This low retention is now apparent in Figure 3.3. Thus, Figure 3.3 better illustrates this important difference between monolithic and particulate silica phases. PolySULFOETHYL A (12) displayed higher retention than polyHYDROXYETHYL A (9), contrary to the observations of Alpert [7] but consistent with the results reported by Dinh *et al.* [12].

Finally, Figure 3.3 helps to demonstrate that factors such as particle size and column length do not influence the fundamental HILIC separation. This was

illustrated by columns packed with 3 μm (8) and 5 μm (7) TSKgel Amide 80; and by the columns packed with 3.5 μm (2) and 5 μm ZIC-HILIC (1). Thus, the purpose of Figure 3.1 is to aid in our understanding of the nature of the interactions within HILIC phases. Whereas Figure 3.3 better aids the selection of HILIC columns that will yield either comparable or different HILIC separations.

3.4 Conclusions

Two simple selectivity plots are constructed based on the retention data of Irgum and co-workers [12] plus an additional 8 HILIC phases studied herein. These plots are designed to be straightforward and easy to understand. These selectivity plots are capable of classifying different HILIC phases based on their hydrophilicity and ion exchange properties, and thereby enable understanding of the sometimes unexpected behavior of HILIC phases. In addition, in the spirit of the Neue plot, hydrophilic retention is plotted *vs.* ion exchange selectivity to yield a HILIC-Phase Selectivity Chart that provides a simple, easy to understand and handy tool for selection of HILIC phases of similar or different selectivity. However, the limited number of probes and single eluent condition used herein cannot capture the complete complexity of HILIC retention. Thus like the Neue plot for RPLC, the HILIC-Phase Selectivity Chart should be used for guidance in the selection of a phase, but should not be considered a definitive characterization of the phase.

3.5 References

- [1] J.W. Treadway, G.S. Philibert, S.V. Olesik, *J. Chromatogr. A* **2011**, *1218*, 5897-5902.
- [2] E. Johnsen, S.R. Wilson, I. Odsbu, A. Krapp, H. Malerod, K. Skarstad, E. Lundanes, *J. Chromatogr. A* **2011**, *1218*, 5981-5986.
- [3] A.L.N. van Nuijs, I. Tarcomnicu, A. Covaci, *J. Chromatogr. A* **2011**, *1218*, 5964-5974.
- [4] N. Fontanals, R.M. Marce, F. Borrull, *J. Chromatogr. A* **2011**, *1218*, 5975-5980.
- [5] N. Hatambeygi, G. Abedi, M. Talebi, *J. Chromatogr. A* **2011**, *1218*, 5995-6003.
- [6] T. Tetaz, S. Detzner, A. Friedlein, B. Molitor, J.L. Mary, *J. Chromatogr. A* **2011**, *1218*, 5892-5896.
- [7] A.J. Alpert, *J. Chromatogr.* **1990**, *499*, 177-196.
- [8] P. Hemstrom, K. Irgum, *J. Sep. Sci.* **2006**, *29*, 1784-1821.
- [9] Y. Guo, S. Gaiki, *J. Chromatogr. A* **2011**, *1218*, 5920-5938.
- [10] Y. Kawachi, T. Ikegami, H. Takubo, Y. Ikegami, M. Miyamoto, N. Tanaka, *J. Chromatogr. A* **2011**, *1218*, 5903-5919.
- [11] M.E.A. Ibrahim, C.A. Lucy, In *Chapter 2: Stationary Phases for HILIC; Hydrophilic Interaction Chromatography: A Guide for Practitioners*, B.A. Olsen, B.W. Pack (Eds.), John Wiley & Sons Inc., 2013, pp. 43-85.
- [12] N.P. Dinh, T. Jonsson, K. Irgum, *J. Chromatogr. A* **2011**, *1218*, 5880-5891.
- [13] U.D. Neue, *J. Sep. Sci.* **2007**, *30*, 1611-1627.

- [14] K. Kimata, K. Iwaguchi, S. Onishi, K. Jinno, R. Eksteen, K. Hosoya, M. Araki, N. Tanaka, *J. Chromatogr. Sci.* **1989**, *27*, 721-728.
- [15] N.S. Wilson, M.D. Nelson, J.W. Dolan, L.R. Snyder, R.G. Wolcott, P.W. Carr, *J. Chromatogr. A* **2002**, *961*, 171-193.
- [16] L.R. Snyder, J.W. Dolan, P.W. Carr, *J. Chromatogr. A* **2004**, *1060*, 77-116.
- [17] P.W. Carr, J.W. Dolan, U.D. Neue, L.R. Snyder, *J. Chromatogr. A* **2011**, *1218*, 1724-1742.
- [18] D.H. Marchand, P.W. Carr, D.V. McCalley, U.D. Neue, J.W. Dolan, L.R. Snyder, *J. Chromatogr. A* **2011**, *1218*, 7110-7129.
- [19] U.D. Neue, B.A. Alden, T.H. Walter, *J. Chromatogr. A* **1999**, *849*, 101-116.
- [20] U.D. Neue, K. VanTran, P.C. Iraneta, B.A. Alden, *J. Sep. Sci.* **2003**, *26*, 174-186.
- [21] http://www.waters.com/waters/promotionDetail.htm?id=10048475&icid=i1230&locale=en_US (accessed in July 2012).
- [22] A.J. Alpert, *Anal. Chem.* **2008**, *80*, 62-76.
- [23] <http://www.usp.org/app/USPNF/columnsDB.html> (accessed in July 2012).
- [24] <http://www.dionex.com/en-us/webdocs/86550-Man-065339-01-ACCLAIM-HILIC-10-Apr10.pdf> (accessed in July 2012).
- [25] W. Jiang, K. Irgum, *Anal. Chem.* **1999**, *71*, 333-344.
- [26] W. Jiang, K. Irgum, *Anal. Chem.* **2001**, *73*, 1993-2003.
- [27] Y. Guo, S. Gaiki, *J. Chromatogr. A* **2005**, *1074*, 71-80.
- [28] Y. Takegawa, K. Deguchi, H. Ito, T. Keira, H. Nakagawa, S. Nishimura, *J. Sep. Sci.* **2006**, *29*, 2533-2540.

- [29] Y. Guo, S. Srinivasan, S. Gaiki, *Chromatographia* **2007**, *66*, 223-229.
- [30] D.V. McCalley, *J. Chromatogr. A* **2010**, *1217*, 3408-3417.
- [31] M.E.A. Ibrahim, T. Zhou, C.A. Lucy, *J. Sep. Sci.* **2010**, *33*, 773-778.
- [32] K.M. Glenn, C.A. Lucy, P.R. Haddad, *J. Chromatogr. A* **2007**, *1155*, 8-14.
- [33] M.E.A. Ibrahim, C.A. Lucy, *Talanta* **2012**, *100*, 313-319.

CHAPTER FOUR: Agglomerated Silica Monolithic Column for Hydrophilic Interaction Liquid Chromatography*

4.1 Introduction

Hydrophilic interaction liquid chromatography (HILIC) has been used widely in recent years as it is very useful for the separation of polar compounds such as benzoates, nucleotides and amino acids which are weakly retained or even unretained by reversed phase liquid chromatography. HILIC can be regarded as an extension of normal phase chromatography into the realm of aqueous mobile phases. In HILIC, generally a high percentage of acetonitrile (%ACN) is added to an aqueous mobile phase. A water layer forms on the surface of the packing. It is the partitioning of analytes between this stationary water layer and the mobile phase that forms the basis for separation. In HILIC, retention increases with the polarity of the analyte and decreases with the polarity of the mobile phase. This is similar to normal phase chromatography and the opposite of reversed phase liquid chromatography.

As discussed in Chapter 2, most commercial HILIC phases are particle based. Decreasing the particle size of a particulate column increases the separation efficiency. However, columns packed with smaller particles result in higher backpressures [1]. In this chapter, I seek to improve the speed of analysis of HILIC by using monolithic stationary phases.

* A version of this chapter has been published as Mohammed E. A. Ibrahim¹, Ting Zhou, Charles A. Lucy, *J. Sep. Sci.*, **2010**, *33*, 773-778.

¹ I performed the experiments and prepared the manuscript under the supervision of Ting Zhou.

Monolithic stationary phases [2] can provide comparable efficiency but with much lower backpressure [3-7]. Monolithic columns have a different geometry compared to particle-based columns. They consist of a single piece of stationary phase, either silica or polymer with mesopores (typically around 10 to 25 nm) for retention and macropores (typically 1 to 3 μm) for through-flow [3, 8-10]. Silica based monoliths are generally prepared through the sol-gel process. This sol-gel process starts with the acid hydrolysis of tetramethoxysilane or tetraethoxysilane, followed by the formation and polymerization of monosilicic acid. Phase separation is induced by the addition of polymer or surfactant. The presence of a polymer in the sol-gel system promotes the formation of macropores, whereas exchanging the solvent for a different one helps to form the mesopores. Subsequent heat treatment and drying results in a single piece of silica. Finally, cladding *i.e.*, enclosure of the monolith into a column blank, is performed. Commercial silica monolithic columns supplied by Merck [11] and Phenomenex [12] are equivalent to 3 μm particulate columns in terms of efficiency and to 7-15 μm columns in terms of permeability [13-15]. Most monolithic columns used in HPLC for small molecular weight analytes are silica based [16-18].

Bare silica can be used for HILIC separations, but exhibits less retention than corresponding bonded phase materials [19]. Derivatized silica monoliths such as an on-column polymerization of acrylamide on a monolithic silica capillary column (weak cation exchange-HILIC) have been studied, but no commercial column has been manufactured yet [20-22]. The only commercially

available monolithic HILIC column is the fully pervious polymer monolith covalently coated with a hydrophilic monolayer, StyrosTM AminoHILIC [23]. Ordinary (less cross-linked) polymeric monolith has several disadvantages such as shrinking or swelling in the presence of organic solvents and yield much lower efficiency for small molecules due to the poor mass transfer properties of the stationary phase [24, 25]. For instance, efficiencies as low as 400 μm were observed for adenosine monophosphate (AMP) on the StyrosTM AminoHILIC column.

HILIC columns have been prepared by dynamically coating silica particles with polyamines such as spermidine, putrescine and triethylene tetramine [19]. Thus, a similar approach could be used with silica monoliths. However, it has also been observed that the retentive strength of a HILIC phase depends on the number of functional groups on the silica surface [19]. The greater the number of functional groups, the greater the amount of water bound to the surface [26]. In this work, agglomerated phases are prepared as a means of maximizing the number of functionalities on the surface of a silica monolith, while maintaining the efficiency and permeability of the native monolith.

Agglomerated phases are prepared by electrostatically attaching small polyionic latex particles onto an oppositely charged particle or phase [27]. For example, to create anion exchange phases for ion chromatography, non-porous highly cross-linked polymeric particles are used. The surface of this particle possesses a positive charge. Polycationic latexes (80-140 nm) electrostatically adsorb onto the surface to form a pellicular ion exchange layer. Agglomerated

phases, such as used by Dionex Corporation, are easy to prepare [5, 28] and provide high efficiency for ion exchange separations [29]. The electrostatic attachment is extremely rugged, able to withstand pH 0 to 14 and 1 to 100% (v/v) of common reversed-phase solvents in aqueous mixtures [27].

Previously, a homemade agglomerated silica monolithic column was prepared by flushing a suspension of Dionex AS9-SC latex through a silica monolith [5]. The agglomerated column yielded higher efficiency for anion exchange of inorganic anions and greater stability than a surfactant coated C₁₈ silica monolith [5]. Herein we describe the performance of this latex coated silica monolith under HILIC conditions. The HILIC performance is compared to the commercial StyrosTM Amino polymeric HILIC monolith, ZIC[®]-HILIC column [30] and PolyWAX LP column [31] in terms of selectivity and efficiency.

4.2 Experimental

4.2.1 Reagents and Materials

All solutions were prepared in nano-pure water (Barnstead, Dubuque, IA, USA). HPLC-grade acetonitrile (ACN), toluene, salicylic acid and naphthalene were purchased from Fisher Scientific (Fair Lawn, NJ, USA). Ammonium acetate was from Anachemia (Montreal, QC, Canada). Methylphosphonic acid, cytosine, benzoic acid, 4-hydroxybenzoic acid, 2,4-dihydroxybenzoic acid, phthalic acid, uracil, acetylsalicylic acid, proline, lysine, AMP, adenosine diphosphate (ADP) and guanosine monophosphate (GMP) were purchased from Sigma-Aldrich (St. Louis, MO, USA). 3,5-Dihydroxybenzoic acid was from Alfa Aesar (Ward Hill,

MA, USA). Aspartic acid was from Aldrich (Milwaukee, WI, USA). All solutions were filtered with 0.22 μm Magna nylon membrane filters (GE Osmonic, Trevose, PA, USA) prior to use. Ammonium acetate or methylphosphonic acid buffer with different percentage of acetonitrile was used as the mobile phase. Eluents were prepared from 2000 mM stock solutions. To prepare the 2000 mM stock solution, a small amount of sodium hydroxide or hydrochloric acid was added to adjust the buffer pH. The necessary volume of stock solution was firstly added to the volumetric flask, followed by the addition of ACN and then the right amount of water was added without adjusting the liquid level after mixing. The buffer concentrations quoted in this paper are that present after ACN addition. Eluent pH was adjusted by a Corning combination 3-in-1 electrode (Corning, Big Flats, NY, USA) before adding ACN.

4.2.2 Apparatus

Separations were performed on a HPLC system consisting of: a model 625 LC Waters HPLC pump (Milford, MA, USA) operating at either 1.0 (normally) or 10 mL/min (for the fast separation); a 6-port Rheodyne model 7125 (Berkeley, CA, USA) injection valve with either a 10 or 20 μL loop and a Lambda-Max Model 481 UV detector at either 200, 230 or 254 nm (Waters, Milford, MA, USA). Data was collected at 20 Hz using a Dionex Advanced Computer Interface with Dionex PeakNet 5.2 software. Preparation of the latex coated silica monolithic was reported previously [5]. Briefly, a Chromolith Performance silica monolith (100 x 4.6 mm i.d.) (Merck, Whitehouse Station, NJ, USA) was pre-

rinsed with 0.01 M HCl. A dialyzed 1:10 suspension of AS9-SC latex particles (Dionex) in 0.01 M HCl was rinsed through the column until breakthrough. The AS9-SC latex particles are 110 nm in diameter and consist of a polyacrylate backbone (20% cross-linked) and functionalized with alkyl quaternary ammonium groups. The column was then rinsed with nano-pure water to remove any unretained latex.

4.2.3 Calculations

Since the peaks were slightly tailed, the exponentially modified Gaussian (EMG) peak model (Equation 1.8, Chapter 1) [32] was used to accurately determine the separation efficiency (N). Since the comparison is established between columns of different dimensions, peak height (H, Equation 1.7, Chapter 1), is used in this paper to describe the efficiency.

4.3 Results and Discussion

4.3.1 Effect of %ACN in HILIC Mode

In HILIC mode, adding ACN above 60% will increase the retention of analytes and the peak efficiency. To investigate whether the retention and efficiency will change the same way on the latex coated silica monolith, different %ACN was added to the mobile phase. Figure 4.1 shows the effect of %ACN on retention on the AS9-SC latex coated silica monolith. The nonpolar naphthalene shows retention only at very low %ACN and is essentially unretained ($k < 0.1$)

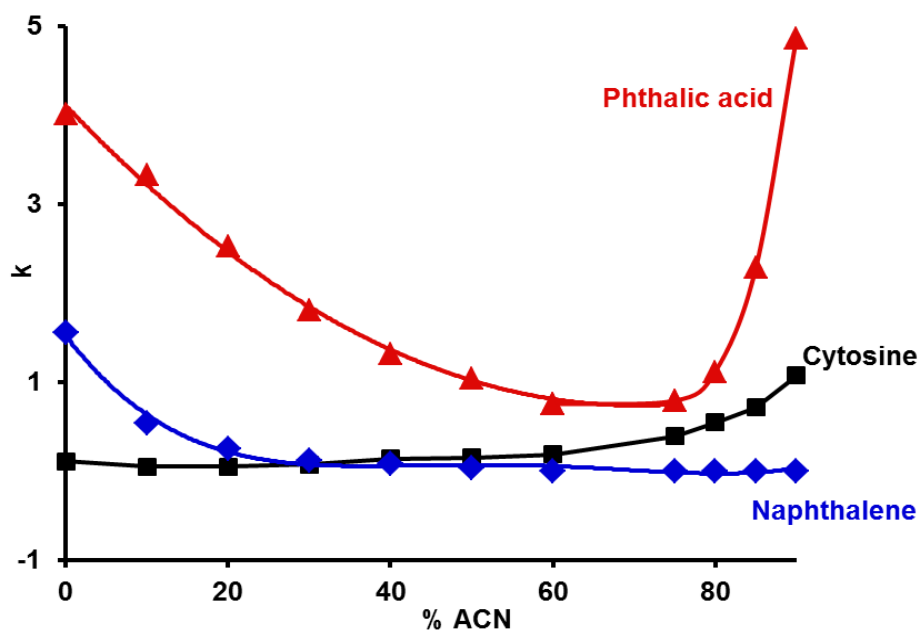


Figure 4.1 Effect of %ACN on the retention of naphthalene, cytosine and phthalic acid on the AS9-SC coated silica monolith. Conditions: flow rate, 1.0 mL/min; eluent, 25 mM ammonium acetate (pH 5.0) in 0 to 90% ACN; analyte, 0.1-0.4 mM naphthalene (◆), cytosine (■) and phthalic acid (▲) in the same % ACN as the mobile phase; UV detection at 254 nm with a 20 μ L loop injection. Lines are guides to the eye. The chemical structures of the analytes are shown in Appendix I.

above 30% ACN. For the polar cytosine and phthalic acid, a U-shaped retention behavior was observed in Figure 4.1. Retention decreases upon increasing % ACN from 0 to 60% for phthalic acid and from 0 to 20% for cytosine, followed by an increase in retention with higher % ACN.

The retention order (naphthalene, cytosine and phthalic acid at last) is similar to that observed on a Dionex Acclaim Mixed mode WCX-1 column (naphthalene, cytosine) [33] and on a StyrosTM Amino HILIC column (toluene, cytosine) [23]. Further, the effect of %ACN on retention on the AS9-SC coated silica monolith is very similar to that reported for toluene and benzoic acid on the Dionex Acclaim Mixed mode HILIC column. Similar to naphthalene in Figure 4.1, toluene retention on the Dionex Acclaim Mixed mode column showed decreasing retention with increasing %ACN [33]. The retention behavior of these compounds under low %ACN is due to hydrophobic (*i.e.*, reversed phase) interaction. Toluene is much more retained on the Dionex Acclaim Mixed mode column than naphthalene on the agglomerated phase (Figure 4.1) due to the strong reversed phase character (nonyl linker) of the mixed mode phase. The retention of naphthalene in Figure 4.1 is lower than that of toluene on a LiChrosorb[®] Diol phase. This indicates that the latex coated silica monolith possesses little reversed phase character, despite the AS9-SC latex being referred to as possessing “Medium” hydrophobicity in the Dionex literature [34].

Phthalic acid (Figure 4.1) shows U-shaped retention behavior which is very similar to that observed for HILIC separation of nucleotides on titania [35] and separation of benzoic acid on Lichrosorb[®] Diol column [33]. This similarity

indicates that the AS9-SC coated silica monolithic column shows similar retention behavior to the commercial HILIC columns.

For cytosine (AS9-SC coated silica monolith in Figure 4.1), the retention factor is low ($k = 0.1-0.18$) at %ACN from 0 to 60%, followed by a modest increase above 60 %ACN. This behavior may be attributed to the presence of ion exchange sites on the AS9-SC coated silica monolith. At the current eluent pH (5.0), cytosine is protonated and thus is electrostatically repelled from the positively charged surface, resulting in a low retention. With increasing %ACN in the mobile phase, HILIC starts to become the dominant mode, resulting in increasing retention. Thus the surface charge of the AS9-SC coated monolith results in mixed mode retention behavior.

4.3.2 Separation of Hydrophilic Analytes on AS9-SC Coated Silica Monolith

A number of separations of hydrophilic analytes were performed on the AS9-SC coated silica monolith to illustrate its selectivity and column performance.

4.3.2.1 Fast Separation of Naphthalene, Uracil and Cytosine

Monolithic columns have high permeability allowing separations to be performed at very high flow rates with minimal backpressures [3-7]. Figure 4.2 shows the fast separation of naphthalene, uracil and cytosine with 25 mM ammonium acetate (pH 5.0) in 85% ACN as the eluent. Baseline separation of these analytes was achieved in less than 15 s which is much lower than the 3 min

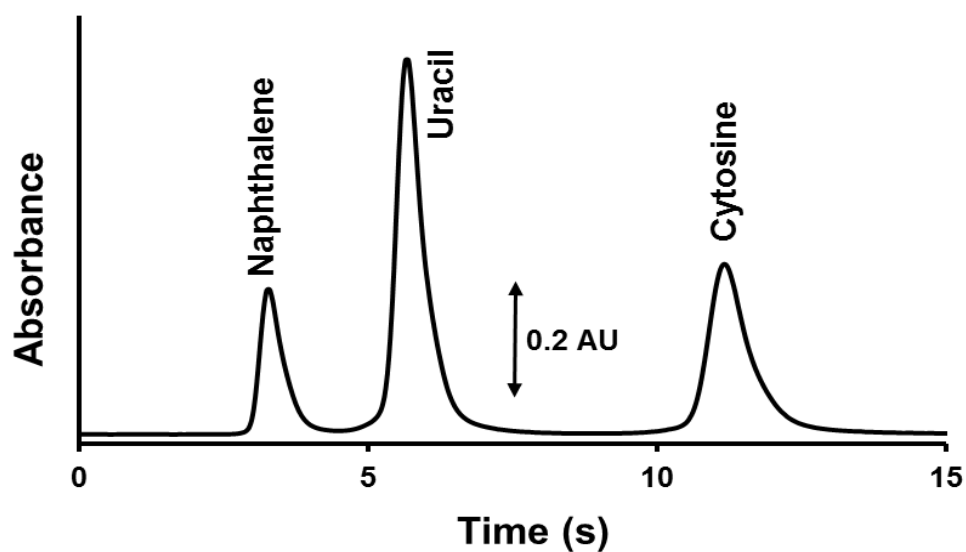


Figure 4.2 Fast HILIC separation of naphthalene, uracil and cytosine on the latex coated silica monolith. Conditions: column, Dionex AS9-SC latex coated silica monolith (100 x 4.6 mm i.d.); flow rate, 10.0 mL/min; pressure, 2106 psi; eluent, 25 mM ammonium acetate (pH 5.0) in 85% ACN; analyte, 0.1-0.4 mM naphthalene, uracil and cytosine in 85% ACN; UV detection at 254 nm with a 10 μ L loop injection. The chemical structures of the analytes are shown in Appendix I.

separation obtained by StyrosTM AminoHILIC column. It is also comparable to the separation obtained by Irgum and co-workers [30] in which separation of toluene, uracil and cytosine was achieved in less than 4 s using a ZIC-HILIC column (3.5 μm , 20 \times 2.1 mm) and 80% ACN/20% ammonium buffer (25 mM, pH 6.8) as the mobile phase. With the monolithic property of the latex coated column, it is possible to achieve an even faster separation with a reasonable backpressure.

As shown in Table 4.1, efficiencies of 25-110 μm were achieved on the latex coated column. These efficiencies are significantly higher than achieved with the commercial StyrosTM AminoHILIC (Table 4.1), particularly for the moderately retained cytosine. The efficiency of weakly retained components (*i.e.*, naphthalene) was strongly affected by extra-column band broadening. For example, increasing the sample loop volume from 10 to 20 μL reduced the efficiency of naphthalene from 50 to 140 μm . Therefore, for the remainder of this paper, efficiencies will only be quoted for retained species.

4.3.2.2 Separation of Benzoates

Figure 4.3 shows the separation of a series of benzoates on the AS9-SC coated silica monolith using a mobile phase of 25 mM ammonium acetate (pH 6.5) in 90% ACN. Increasing pH from 5.0 to 6.5 results in increased resolution ($R_s = 0.8$ for pH 5.0 and $R_s = 1.4$ for pH 6.5 between the critical pair) due to increases in both retention and selectivity. The efficiency achieved on the AS9-SC

Table 4.1 Comparison of efficiencies of model analytes on the AS9-SC coated silica monolith vs. commercial HILIC columns.

Analyte \ H (μm) ^a	Dionex AS9-SC coated silica monolith	Styros TM AminoHILIC polymeric monolith ^e	ZIC [®] - HILIC column ^f	PolyWAX LP column ^g
Dead time marker ^b	50 ^c	53	500	
Uracil	67	91	111	
cytosine	59	250	71	
AMP	110	400		
GMP	71	333		
ADP	71	154		
Salicylic acid	45	111		
Acetylsalicylic acid	30	67		
Benzoic acid	36	91		
2,4-dihydroxybenzoic acid	34	111		
3,5-dihydroxybenzoic acid	25	167		
Proline	40 ^{c,d}			50
Lysine	59 ^{c,d}			67
Aspartic acid	34 ^{c,d}			26

^a Columns: AS9-SC latex coated silica monolith with conditions as described in Figs. 4.2-4.5; StyrosTM AminoHILIC polymeric monolith; ZIC[®] -HILIC column [30]; PolyWAX LP column [31].

^b Naphthalene for Dionex AS9-SC coated silica monolith and toluene for the StyrosTM and ZIC[®] -HILIC columns.

^c 10 μL loop used.

^d Flow rate is 1.0 mL/min

^e Conditions: column, StyrosTM AminoHILIC polymeric monolith (50 x 4.6 mm i.d.); flow rate, 1.0 mL/min; eluent, 94% ACN / 6% 200 mM ammonium formate (pH 8.7); 50-300 $\mu\text{g}/\text{mL}$ analytes in 50% ACN; UV detection at 254 nm with a 5 μL loop injection.

^f Conditions: column, ZIC[®] -HILIC column (3.5 μm , 20 x 2.1 mm i.d.); flow rate, 2.5 mL/min; pressure, 3118 psi; eluent, 80% ACN / 20% 25 mM ammonium acetate (pH 6.8); UV detection at 254 nm with a 2 μL loop injection.

^g Conditions: column, polyWAX LP (5 μm , 200 x 4.6 mm i.d.); flow rate, 1.0 mL/min; eluent, 10mM triethylamine phosphate (pH 2.0) in 65% ACN; UV detection at 215 nm with a 10 μL loop injection.

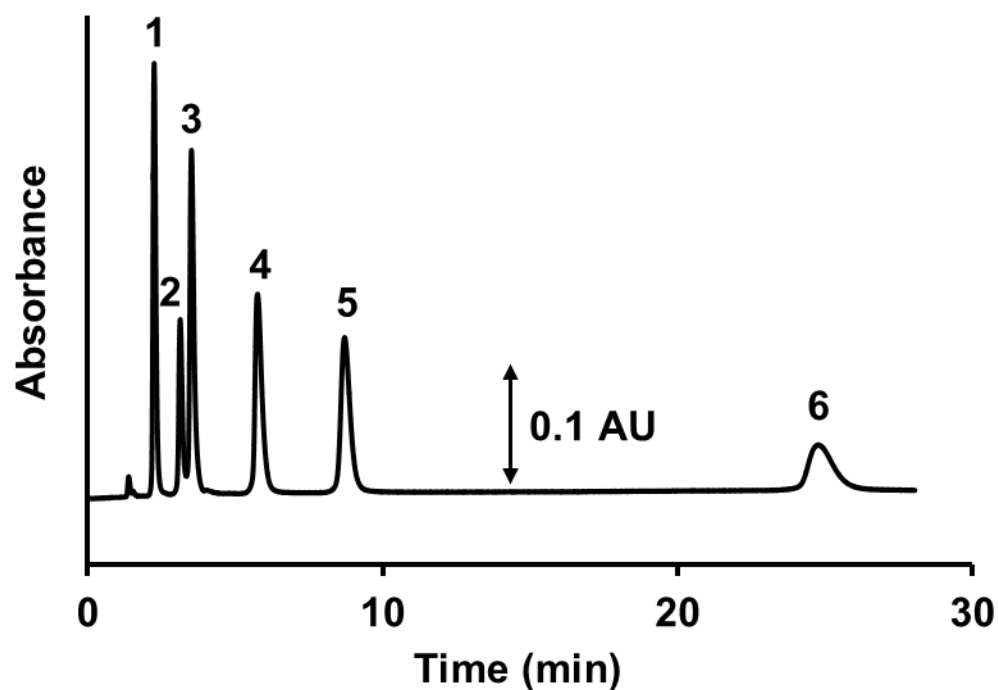


Figure 4.3 Separation of (1) salicylic acid, (2) acetylsalicylic acid, (3) benzoic acid, (4) 2,4-dihydroxybenzoic acid, (5) 4-hydroxybenzoic acid and (6) 3,5-dihydroxybenzoic acid on the latex coated silica monolith. Conditions: column, Dionex AS9-SC latex coated silica monolith (100 x 4.6 mm i.d.); flow rate, 1.0 mL/min; pressure, 180 psi; eluent, 25 mM ammonium acetate (pH 6.5) in 90% ACN; analyte, 0.14-0.20 mM carboxylic acids in 90% ACN; UV detection at 230 nm with a 20 μ L loop injection. The chemical structures of the analytes are shown in Appendix I.

coated silica monolith (25 to 45 μm) is also much higher than that on StyrosTM AminoHILIC polymeric monolith (67 to 167 μm in Table 4.1).

4.3.2.3 Separation of Nucleotides

Figure 4.4 shows the separation of three nucleotides on the AS9-SC latex coated silica monolith using a mobile phase of 25 mM ammonium acetate (pH 5.0) in 50 % ACN. Lower % ACN is used here to lower retention to get a faster separation. From Table 4.1, the efficiencies of the nucleotides on the silica monolith are higher than those on the StyrosTM AminoHILIC polymeric monolith. When comparing the selectivity, the retention order of nucleotides on the AS9-SC latex coated silica monolith (AMP, GMP, ADP) is the same as that on a bare titania column used under HILIC condition [35] and that on the StyrosTM AminoHILIC polymeric monolith [36].

4.3.2.4 Separation of Amino Acids

Figure 4.5 shows the separation of proline, lysine and aspartic acid on the AS9-SC latex coated silica monolith using 25 mM methylphosphonic acid (pH 4.0) in 60% ACN. Lower %ACN is used here to reduce retention to get a faster separation. The efficiencies achieved on the AS9-SC latex coated silica monolith are comparable to those achieved on a PolyWAX LP column [31] (Table 4.1).

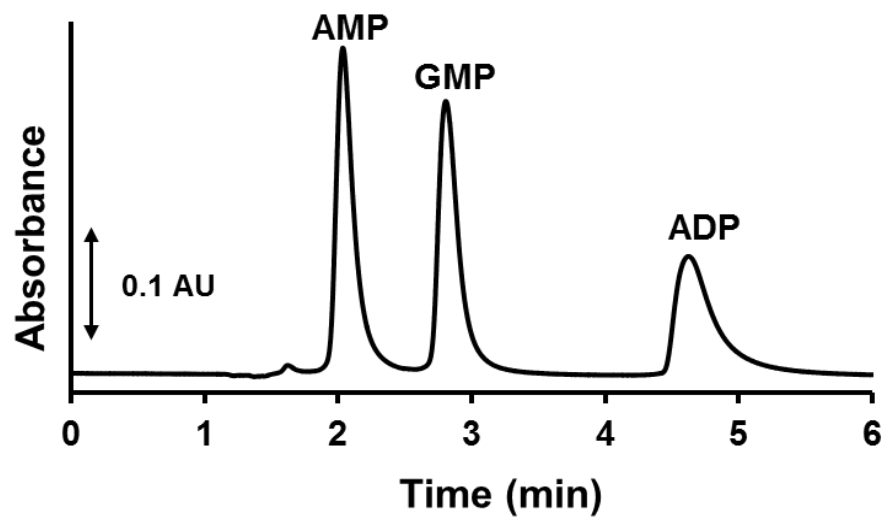


Figure 4.4 HILIC separation of nucleotides on the latex coated silica monolith. Conditions: column, Dionex AS9-SC latex coated silica monolith (100 x 4.6 mm i.d.); flow rate, 1.0 mL/min; pressure, 440 psi; eluent, 25 mM ammonium acetate (pH 5.0) in 50% ACN; analyte, 0.10-0.14 mM nucleotides in 50% ACN; UV detection at 254 nm with a 20 μ L loop injection. The chemical structures of the analytes are shown in Appendix I.

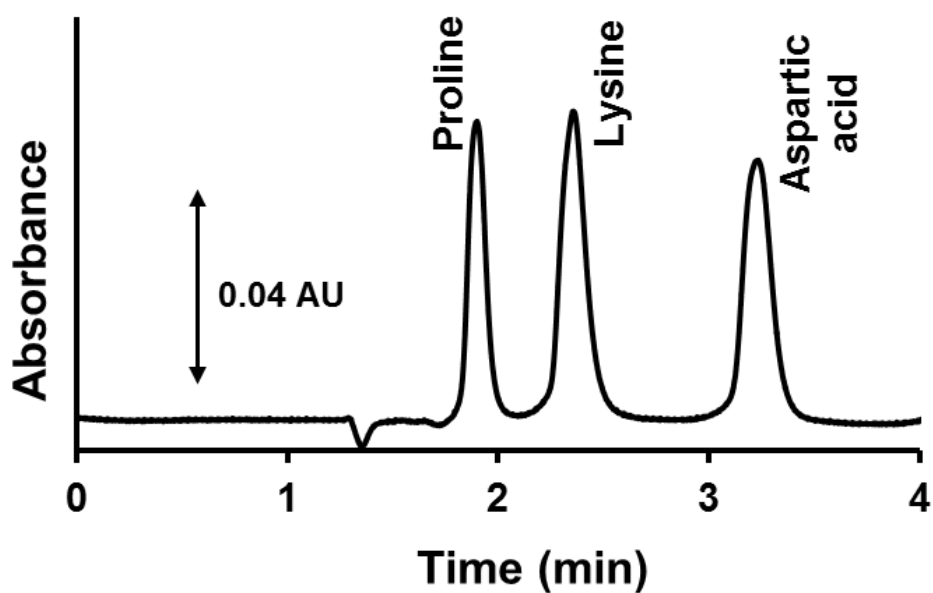


Figure 4.5 HILIC separation of amino acids on the latex coated silica monolith. Conditions: column, Dionex AS9-SC latex coated silica monolith (100 x 4.6 mm i.d.); flow rate, 1.0 mL/min; pressure, 288 psi; eluent, 25 mM ammonium acetate (pH 4.0) in 60% ACN; analyte, 2.2-5.5 mM amino acids in 60% ACN; UV detection at 200 nm with a 10 μ L loop injection. The chemical structures of the analytes are given in Appendix I.

4.3.3 Electrostatic Repulsion Hydrophilic Liquid Interaction Chromatographic (ERLIC) Behavior of the Dionex AS9-SC Coated Silica Monolith.

If an analyte possesses the same charge as the stationary phase, electrostatic repulsion (Donnan exclusion) occurs. However, when the mobile phase contains a high %ACN, then solutes may also be retained through hydrophilic interaction. This combination of electrostatic repulsion and hydrophilic interaction was termed ERLIC by Alpert [31] and offers different selectivities for charged polar analytes.

Herein the effect of salt concentration in the mobile phase on the retention of two amino acids is studied. Histidine is used as an example of a basic amino acid and aspartic acid as an example of an acidic amino acid. Figure 4.6 shows that increasing methylphosphonate concentration (from 10 to 50 mM) suppresses both electrostatic repulsion and attraction. Consistent with the results of Alpert [31], the model basic amino acid (Histidine) shows increased retention with increased electrolyte concentration in Figure 4.6 due to greater shielding of the electrostatic repulsion between the cationic amino acid and the cationic latexes on the monolith surface. Whereas, the model acidic amino acid (aspartic acid) shows decreased retention in Figure 4.6 when the methylphosphonate concentration in the eluent is increased due to shielding of the electrostatic attraction. Thus the behavior in Figure 4.6 is consistent with ERLIC behavior.

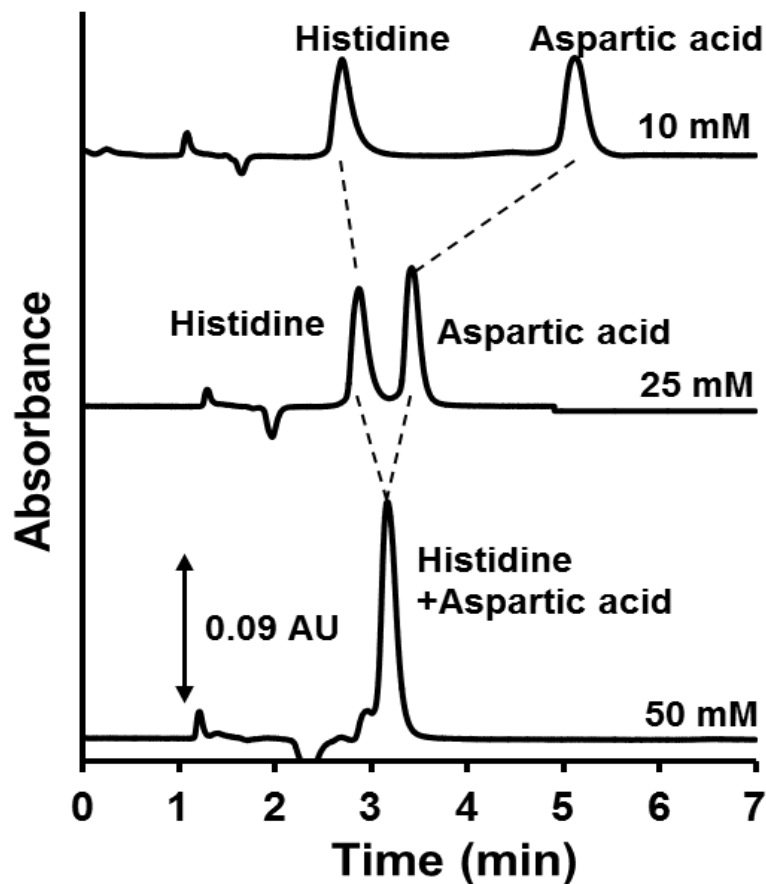


Figure 4.6 Effect of salt concentration on ERLIC separation of histidine and aspartic acid on the latex coated silica monolith. Conditions: column, Dionex AS9-SC latex coated silica monolith (100 x 4.6 mm i.d.); flow rate, 1.0 mL/min; pressure, 288 psi; eluent, 10-50 mM methylphosphonic acid (pH 4.0) in 60% ACN; analyte, 0.20 mM histidine and 3.75 mM aspartic acid in 60% ACN; UV detection at 200 nm with a 10 μ L loop injection. Dotted lines are to show the increase or decrease in retention. The chemical structures of the analytes are shown in Appendix I.

4.3.4 Stability of the AS9-SC Coated Silica Monolith

To test the stability of the agglomerated HILIC column, the column was continuously flushed with 2400 column volumes of 25 mM ammonium acetate in 85% ACN, pH 5.0. Repeated injections of naphthalene, uracil and cytosine yielded retention time RSD of 1.9, 1.5 and 1.8%, respectively as shown in Figure 4.7. This indicates that the electrostatically bound latex coating is stable at HILIC conditions *i.e.*, high concentrations of ACN do not impact the latex particles coated on the surface of the silica monolith. This stability is consistent with our previous work with latex-coated monoliths [5] and the general stability observed for agglomerated columns in ion chromatography.

4.4 Conclusions

The retention behavior of a latex coated silica monolith follows HILIC mode well. A series of hydrophilic compounds were separated on the coated silica monolithic column with a higher efficiency than that on other HILIC columns. The coated monolithic surface also has the potential for a fast separation. The ERLIC behavior of the column was studied using amino acids as model analytes. One thing needs to be noted is that the Dionex AS9-SC coated silica monolith cannot be used at high pH as it is silica based, which limits the use of the column in a wide pH range.

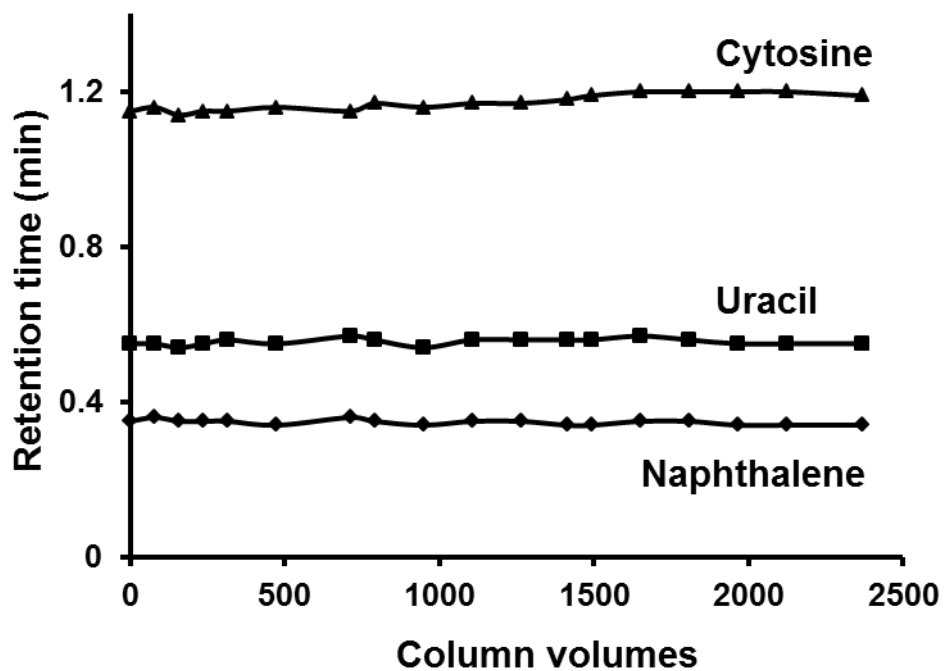


Figure 4.7 Stability of the latex coated AS9-SC coated silica monolith in HILIC mode. Conditions: column, Dionex AS-9 latex coated silica monolith (100 x 4.6 mm i.d.); flow rate, 3.0 mL/min; pressure, 540 psi; eluent, 25 mM ammonium acetate (pH 5.0) in 85% ACN; analyte, 0.1- 0.4 mM naphthalene (◆), uracil (■) and cytosine (▲) in 85% ACN; UV detection at 254 nm with a 10 µl loop injection. The chemical structures of the analytes are shown in Appendix I.

4.5 References

- [1] J.M. Miller, In *Chromatography: concepts and contrasts*, Wiley, Hoboken, N.J., 2005.
- [2] <http://www.merck.de/servlet/PB/MENU/1209750> (accessed in October 2009).
- [3] K. Cabrera, *J. Sep. Sci.* **2004**, 27, 843-852.
- [4] K. Cabrera, D. Lubda, H.M. Eggenweiler, H. Minakuchi, K. Nakanishi, *J. High Resolut. Chromatogr.* **2000**, 23, 93-99.
- [5] K.M. Glenn, C.A. Lucy, P.R. Haddad, *J. Chromatogr. A* **2007**, 1155, 8-14.
- [6] S. Pelletier, C.A. Lucy, *J. Chromatogr. A* **2006**, 1118, 12-18.
- [7] F. Rabel, K. Cabrera, D. Lubda, *Am. Lab.* **2000**, 32, 20-22.
- [8] T. Ikegami, N. Tanaka, *Curr. Opin. Chem. Biol.* **2004**, 8, 527-533.
- [9] K. Miyabe, G. Guiochon, *J. Sep. Sci.* **2004**, 27, 853-873.
- [10] N. Tanaka, H. Kobayashi, K. Nakanishi, H. Minakuchi, N. Ishizuka, *Anal. Chem.* **2001**, 73, 420A-429A.
- [11] <http://www.merck.de> (accessed in October 2009).
- [12] <http://www.phenomenex.com> (accessed in October 2009).
- [13] F.C. Leinweber, D. Lubda, K. Cabrera, U. Tallarek, *Anal. Chem.* **2002**, 74, 2470-2477.
- [14] F.C. Leinweber, U. Tallarek, *J. Chromatogr. A* **2003**, 1006, 207-228.
- [15] H. Kobayashi, T. Ikegami, H. Kimura, T. Hara, D. Tokuda, N. Tanaka, *Anal. Sci.* **2006**, 22, 491-501.
- [16] Y.M. Li, J.L. Liao, K. Nakazato, J. Mohammad, L. Terenius, S. Hjerten, *Anal. Biochem.* **1994**, 223, 153-158.

- [17] E.C. Peters, M. Petro, F. Svec, J.M.J. Frechet, *Anal. Chem.* **1998**, *70*, 2288-2295.
- [18] E.C. Peters, M. Petro, F. Svec, J.M.J. Frechet, *Anal. Chem.* **1998**, *70*, 2296-2302.
- [19] U.D. Neue, In *HPLC Columns theory, technology and practice*, Wiley-VCH, 1997.
- [20] T. Ikegami, K. Horie, J. Jaafar, K. Hosoya, N. Tanaka, *J. Biochem. Biophys. Methods* **2007**, *70*, 31-37.
- [21] T. Ikegami, H. Fujita, K. Horie, K. Hosoya, N. Tanaka, *Anal. Bioanal. Chem.* **2006**, *386*, 578-585.
- [22] K. Horie, T. Ikegami, K. Hosoya, N. Saad, O. Fiehn, N. Tanaka, *J. Chromatogr. A* **2007**, *1164*, 198-205.
- [23] http://www.orachrom.com/styros_AminoHILIC.htm (accessed in October 2009).
- [24] J. Weiss, In *Handbook of Ion Chromatography*, Wiley-VCH, Darmstadt, 2004.
- [25] J.V. Dawkins, L.L. Lloyd, F.P. Warner, *J. Chromatogr.* **1986**, *352*, 157-167.
- [26] P. Ortho, H. Engelhardt, *Chromatographia* **1982**, *15*, 91-96.
- [27] J.R. Stillian, C. Pohl, *J. Chromatogr.* **1990**, *499*, 249-266.
- [28] J.P. Hutchinson, E.F. Hilder, M. Macka, N. Avdalovic, P.R. Haddad, *J. Chromatogr. A* **2006**, *1109*, 10-18.
- [29] C.A. Lucy, P. Hatsis, E. Heftmann (Ed.) In *Chapter 4, Chromatography 6th edition*, Elsevier, 2004.

- [30] P. Appelblad, T. Jonsson, W. Jiang, K. Irgum, *J. Sep. Sci.* **2008**, *31*, 1529-1536.
- [31] A.J. Alpert, *Anal. Chem.* **2008**, *80*, 62-76.
- [32] J.P. Foley, J.G. Dorsey, *Anal. Chem.* **1983**, *55*, 730-737.
- [33] X.D. Liu, C. Pohl, *J. Chromatogr. A* **2008**, *1191*, 83-89.
- [34]http://www.thermoscientific.com/ecommerce/servlet/productsdetail_11152___14469150_-1 (accessed in October 2013).
- [35] T. Zhou, C.A. Lucy, *J. Chromatogr. A* **2008**, *1187*, 87-93.
- [36] <https://orachrom.com/wp-content/uploads/2012/10/57-AN040410.pdf> (accessed in October 2013).

CHAPTER FIVE: Mixed Mode HILIC/Anion exchange Separations on Latex Coated Silica Monoliths*

5.1 Introduction

Monoliths were introduced as HPLC columns in the late 1980s-mid 1990s [1-3]. A monolith is a single large rod of porous substance that fills the whole column volume without any gaps [4]. Monolithic columns can be prepared either through polymerization of organic monomers [5, 6] or through sol-gel technology for titania and silica based monoliths [3]. To date most monolithic columns have been prepared for reversed phase and ion exchange chromatography, and only limited research has been performed on monolithic columns for HILIC [7-10]. This chapter explores the use of agglomerated silica monolithic columns for mixed mode separations based on HILIC and anion exchange.

Silica based monolithic columns are characterized by the presence of relatively small mesopores (10-25 nm) for retention and large macropores (1-3 μm) for through-flow of mobile phase [6, 11, 12]. Silica based monoliths are usually used for small molecular weight analytes [13, 14]. The highly porous structure of the monolith offers high permeability which allows fast separation of analytes at very high flow rates with minimal backpressures [15-20]. For these reasons, silica based monolithic columns are used in this study. However, silica based monoliths have some disadvantages. They dissolve at $\text{pH} > 8$, are available in only limited column dimensions [21], and can exhibit tailing peaks even for

* A version of this chapter has been published as Mohammed E. A. Ibrahim, Charles A. Lucy, *Talanta* **2012**, *100*, 313-319.

neutral analytes [22]. The surface of bare silica possesses deprotonated silanols which act as cation exchange sites. Thus, silica excludes anions, rather than retains them. Several methods have been explored to convert silica columns into anion exchangers. A reversed phase silica particulate column was converted into an anion exchange column by adding a cationic surfactant to the eluent [23, 24]. Alternately, semi-permanent anion exchangers were produced by coating a reversed phase particulate column [25] or monolith [26] with a hydrophobic surfactant such as didodecyldimethylammonium bromide (DDAB). Separations of common inorganic anions on a surfactant coated monolithic columns have been performed in just 15-20 s [26]. However, the DDAB coating gradually leaches from the coated column requiring recoating of the column. Precipitation of DDAB in the column sometimes occurs upon recoating, leading to pressure and reproducibility issues [27].

Agglomerated particles are an alternate approach to producing high efficiency ion exchange columns [17]. In an agglomerated column for anion exchange, a stationary phase possessing a negative surface charge is coated with positively charged cationic nanometer sized latices. The alkyl quaternary ammonium functionalities on the latex irreversibly bind to the negatively charged surface. For simplification, AS9-SC, AS12A and DNAPac PA200 latex nanoparticles are assigned as latex A, B and C, respectively (Table 5.1). The Dionex IonPac AS9-SC (latex A), AS12A (latex B) and DNAPac PA200 (latex C) commercial columns are examples of latex coated particulate columns where 105 nm, 140 nm and 151 nm diameter latices coated cross-linked ethyl vinyl

benzene/divinyl benzene (EVB/DVB) microporous particles, respectively [28]. AS9-SC and AS12A Dionex commercial columns can separate common inorganic anions and oxyhalides in 10-12 min [28]. In addition, the IonPac AS9-SC column can separate polarizable anions such as iodide and thiocyanate in 8-15 min [28]. The DNAPac PA200 commercial column shows strong anion exchange properties and was developed for high-resolution analysis and purification of synthetic and modified oligonucleotides [29]. Recently, cationic latex A nanoparticles were used to convert a bare silica monolith into a stable anion exchange phase [17]. The resultant column was more stable and more efficient than a comparable surfactant coated monolith [17].

Such agglomerated phases can also be used for HILIC separations [20]. In HILIC, a mobile phase containing a large percentage of an organic modifier (usually ACN) equilibrates with a hydrophilic stationary phase. A water layer is formed on the surface of the packing. Analytes partition between this water layer and the mobile phase. In our previous work, the adsorbed hydrophilic latex facilitated the formation of a water layer enabling HILIC retention. A latex A coated silica monolith provided efficient ($H = 25\text{-}110\ \mu\text{m}$) separation of polar analytes (*e.g.* benzoates, nucleotides and amino acids) under HILIC conditions [20]. The high permeability of the monolith enabled separation of naphthalene, uracil and cytosine in less than 15 s. Selectivity of cationic analytes (*e.g.* amino acids) was governed by both hydrophilic partitioning and electrostatic repulsion.

Recently it has been recognized that many HILIC separations are in fact mixed mode in nature [30]. Lindner, Bicker and Lämmerhofer studied the

retention patterns on different stationary phases and concluded that partitioning alone cannot satisfactorily explain the chromatographic behavior of analytes under HILIC conditions [31-33]. Additionally, Dinh *et al.* studied the selectivity of different HILIC columns to widen the understanding of interactions taking place in HILIC [34]. Dinh *et al.* used principal component analysis to group different HILIC columns according to the predominant mechanism of retention involved using carefully selected test probes. For instance, Dinh *et al.* found that bare silica columns follow adsorption, in contrast to zwitterionic phases where partitioning is the main mechanism of retention [34]. Recently, Lucy and co-workers re-casted the retention data of Dinh *et al.* [34] mentioned above and an additional 12 columns into simple and easy to understand selectivity plots [35]. The current study builds on our past work to characterize the factors governing HILIC separations on latex coated monoliths. The ion exchange capacity and the amount of the water layer associated with these coated monoliths were measured and compared. Further, the recently reported selectivity plots [35] are used to demonstrate the contribution of partitioning and/or ion exchange to the retention of model anionic analytes on latex coated silica monoliths. Finally, the mixed mode retention is utilized to perform fast simultaneous separation of anions that are both weakly and strongly retained on traditional ion exchange columns.

Table 5.1 Characteristics of the studied latex nanoparticles*

Latex acronym	Corresponding Dionex column	Latex diameter (nm)	% cross-linking	Hydrophilicity
Latex A	AS9-SC	105	20	medium
Latex B	AS12A	140	0.2	medium
Latex C	DNApac	151	5	-

* Column characteristics are as reported by the manufacturer: <http://www.dionex.com/en-us/products/columns/ic-rfic/carbonate-eluent-packed/lp-73196.html>.

5.2 Experimental

5.2.1 Apparatus

The HPLC system was described previously [20]. Briefly, it consists of: a model 625 LC Waters pump (Waters, Milford, MA, USA); a 6-port Rheodyne model 7125 (Rheodyne, Berkeley, CA, USA) injection valve with a 10 μ L loop; and a Lambda-Max Model 481 UV detector (Waters). A model LC-600 Shimadzu LC pump (Shimadzu, Japan) was used for coating each silica monolith with the corresponding latex suspension.

5.2.2 Reagents and Materials

All solutions were prepared in nanopure water (Barnstead, Dubuque, IA, USA). HPLC-grade ACN, naphthalene, NaBrO₃ and KSCN were purchased from Fisher Scientific (Fair Lawn, NJ, USA). Methylphosphonic acid, adenine, cytosine and uracil were purchased from Sigma-Aldrich (St. Louis, MO, USA). NaNO₃ was from EMD Chemical Inc. (Darmstadt, Germany), NaI from BDH Inc. (Toronto, ON, Canada), sodium acetate from Caledon (Georgetown, ON, Canada) and sodium formate from BDH Inc. (Poole, England). Ammonium acetate was from Anachemia (Montreal, QC, Canada) and benzyltrimethylammonium chloride (BTMA) from Acros Organics (Morris Plains, NJ, USA). Three different latex nanoparticles (latices A-C) were provided by Dionex Corp. (Sunnyvale, CA, USA). Table 5.1 displays the characteristics of these latices A-C in terms of their particle size, % cross-linking and hydrophilicity. All latex nanoparticles are functionalized with alkyl quaternary ammonium groups. The % ACN quoted in

this work represent the volume of the ACN relative to the total volume of the solvents including water and ACN. Methylphosphonic acid and ammonium acetate concentrations are that present after addition of ACN. The aqueous phase pH was measured by a Corning combination 3 in 1 electrode (Corning, Big Flats, NY, USA). The pH was adjusted by addition of NaOH for all experiments except the ACN study where triethylamine (TEA) (Fair Lawn, NJ, USA) was used.

5.2.3 Tested Columns and Latex Coating

The latex coating procedure was as reported previously [17, 20]. Briefly, three Onyx (Phenomenex, Torrance, CA, USA) bare silica monoliths (100 mm × 4.6 mm i.d.) were pre-rinsed with 0.01 M HCl. A 1:10 suspension of the latex particles (Dionex) in 0.01 M HCl was prepared for each latex type (latexes A-C) and was rinsed through the column until breakthrough (approx. 5 mL). The column was then rinsed with nanopure water to remove any unretained latex. For comparison, the same procedure was applied to a Chromolith Performance (Merck, Whitehouse Station, NJ, USA) bare silica monolith (100 mm × 4.6 mm i.d.) using latex A nanoparticles. It is worth mentioning that Merck was the first company to commercialize silica monolithic rods under the brand name, Chromolith. They subsequently licensed Phenomenex to make and sell the same product under the brand name, Onyx [36, 37]. Both Onyx [38] and Chromolith [39] share the same characteristics of macropore size (2 μm), mesopore size (13 nm) and surface area (300 m²/g).

5.2.4 Measurement of the Ion Exchange Capacity

The ion exchange capacity of the coated silica monoliths was determined using the breakthrough method [40]. Briefly, the monoliths were flushed continuously with 20 mM NaCl for 30 min at 1 mL/min to saturate all the anion exchange sites with Cl⁻. The excess non-adsorbed Cl⁻ was removed by flushing with nanopure water. Thereafter, 1 mM NaNO₃ solution was pumped into the columns at 1 mL/min until breakthrough was observed at 210 nm. Subtraction of the dead time from the breakthrough time yielded the ion exchange capacity in $\mu\text{eq}/\text{column}$.

5.2.5 Measurement of the Water Layer Volume

Using the Bicker *et al.* method [31, 41], the volume of the water layer under HILIC conditions was determined by measuring the difference in the retention time of toluene (unretained) when the protic modifier was changed from water to methanol [31]. Other details of the method are given in Sec. 5.3.1.

5.3 Results and Discussion

As previously mentioned, a latex A coated silica monolith was used for separation of chloride, nitrite, bromide, nitrate, phosphate, iodide and sulfate ions under pure aqueous ion exchange conditions [17]. The latex A coated silica monolith was also utilized for separation of hydrophilic analytes under HILIC conditions [20]. In this study, latices A-C nanoparticles were used to coat three Onyx bare silica monoliths. The latex irreversibly binds to the silica surface

converting the bare silica monolith into an anion exchange phase as illustrated in Figure 2.7 (Chapter 2). The electrostatic binding of the polycationic latices to the surface is stable [20].

The mixed mode (HILIC vs. ion exchange) retention characteristics of these different latex coated silica monoliths were assessed with regards to the associated water layer volume, ion exchange capacity and selectivity. This study provided an overall comparison between the two different brands (Chromolith vs. Onyx) when coated with the same latex type in terms of selectivity, water layer thickness and ion exchange capacity. Finally the contribution of partitioning and/or ion exchange to retention of kosmotropic and chaotropic anions was studied.

5.3.1 Characterization of Latex Coated Monoliths

The formation of a water layer on the surface of HILIC stationary phases forms the basis of retention in HILIC [42]. Herein, the Bicker *et al.* method [31, 41] was used to determine the volume of the water layer associated with the surface of a three different latex (latices A-C) coated silica monoliths. The volume of the water layer was determined indirectly by measuring the difference in the retention time of an unretained compound (toluene) when the protic modifier was changed from water to methanol [31]. The retention time of toluene increases because the water layer is replaced by a methanol layer into which toluene partitions strongly. The difference in retention volume corresponds to the volume of the water layer associated with the packing material. Table 5.2

summarizes the water layer volumes associated with these latex coated monoliths and a bare silica Onyx column. The observed water layer on the monolithic bare silica (0.01 mL) is small compared to that measured for particulate columns (*e.g.* 0.19 mL for Atlantis HILIC silica [43]). This is consistent with observations that HILIC retention of polar analytes was much smaller on monolithic silica columns compared to particulate columns [44, 45]. Indeed silica monoliths showed the lowest retention of the recently studied 22 HILIC columns [34].

Some selected anions (acetate, formate, bromate, nitrate, thiocyanate and iodide) were used to test the performance of these latex coated monoliths under HILIC conditions. These anions represent a range of retention characteristics in traditional ion chromatography. In traditional ion chromatography, formate and acetate are weakly retained and thus difficult to discern from the water dip. Conversely, polarizable anions such as iodide, thiocyanate and thiosulfate are strongly retained on ion chromatography columns such as the Dionex IonPac AS9-SC column [28].

As shown in Figure 5.1, these anions are not retained on a bare silica monolith under HILIC conditions due to the very small adsorbed water layer (Table 5.2). Anionic analytes would experience further reductions in retention due to the repulsive forces between the negatively charged silanol groups of the bare silica and anion, as per the electrostatic repulsion-hydrophilic liquid interaction chromatography (ERLIC) mode [46]. Hence neither HILIC nor ERLIC separation of these anions can be achieved on a bare silica monolith.

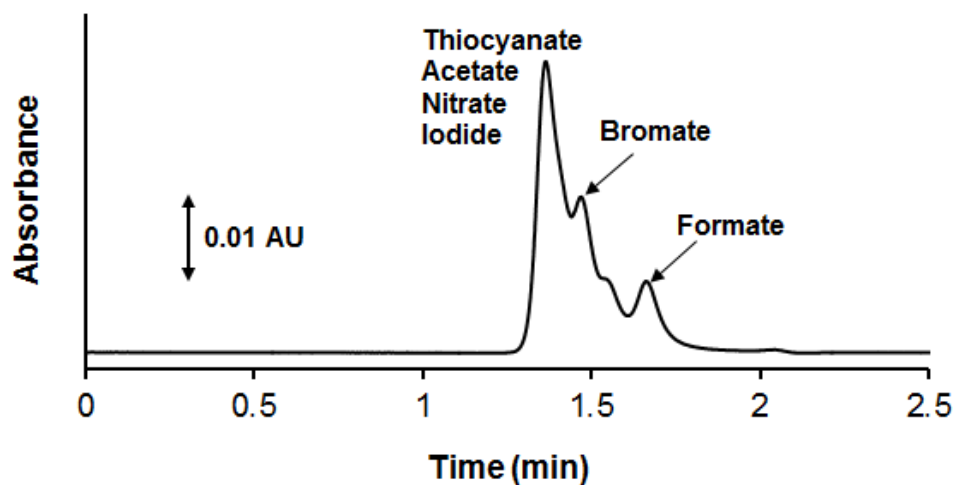


Figure 5.1 Separation of acetate, formate, bromate, nitrate, thiocyanate and iodide on Onyx bare silica monolith. Conditions: column, Onyx bare silica monolith (100 × 4.6 mm i.d.); flow rate, 1.0 mL/min; eluent, 15 mM methylphosphonic acid, pH 4.0, in 65% ACN; analytes, 0.02-14.7 mM in 65% ACN; UV detection at 210 nm with a 10 μ L loop injection.

Table 5.2 Water layer volume and ion exchange capacity of latex coated monoliths.^a

Column	Latex acronym	Water layer volume (mL/col ± SD)	Ion exchange capacity (µeq/col ± SD)
Bare silica Onyx	-	0.01 ± 0.010	-
Latex A coated Onyx	AS9-SC	0.10 ± 0.006	44.1 ± 0.2
Latex A coated Chromolith	AS9-SC	0.12 ± 0.003	43.8 ± 0.8
Latex B coated Onyx	AS12A	0.09 ± 0.012	4.4 ± 0.1
Latex C coated Onyx	DNAPac	0.08 ± 0.003	14.0 ± 0.7

a. Determined as per procedure in Sec. 5.2.4 and 5.2.5.

Adsorbing cationic latices onto the silica surface as depicted in Figure 2.7 (Chapter 2) resulted in a substantial increase in the adsorbed water layer (Table 5.2). The water layer volumes of the latex coated silica monoliths are 8-10 times larger than that of the bare silica monolith before coating. The greater water layer is believed to be due to the additional surface charge and the hydrophilic nature of the cationic sites of the latex. Adsorption of latex A stimulated the formation of a thicker water layer (0.10-0.12 mL) than latex B (0.09 mL) under HILIC conditions, possibly due to the greater hydrophilicity of latex A nanoparticles [47].

Obviously, coating the silica surface with cationic latex nanoparticles also introduces positively charged quaternary ammonium groups, enabling these coated phases to act as anion exchangers [17]. The ion exchange capacity was measured using the breakthrough method [40] as discussed in Sec. 5.2.4. The ion exchange capacity of the latex A coated Onyx silica monolith (44.1 ± 0.2 $\mu\text{eq}/\text{column}$, Table 5.2) is comparable to that of a Chromolith silica monolith coated with the same latex A (41 $\mu\text{eq}/\text{col.}$) [17] and is higher than that of the much longer commercial Dionex AS9-SC column (35 $\mu\text{eq}/\text{col.}$, 250 mm \times 4.0 mm i.d.) [47]. In contrast, the observed capacities of the latex B and C coated monoliths are substantially smaller than those of the corresponding commercial columns (52 and 40 $\mu\text{eq}/\text{col.}$, respectively). The higher capacity of the latex A coated monolith correlates with the higher degree of cross-linking (20 %) of latex A compared to the other latices *e.g.* latex B (0.5 % cross-linked) and latex C (5 % cross-linked) as shown in Table 5.1. The high degree of cross-linking of latex A

allows these nanoparticles to bind to the silica surface as distinct ion exchange sites, *i.e.*, the ion exchange sites are completely exposed and available for ion exchange interactions on the silica surface leading to higher ion exchange capacity. In contrast, latex nanoparticles with low degree of cross-linking *e.g.* latices B and C would spread out the ion exchange sites leading to reduction of the number of these sites per unit area. This is consistent with what has been reported previously that the use of latex nanoparticles with low degree of cross-linking yielded low ion exchange capacity of the coated resin [48].

5.3.2 Fast HILIC Separations on Latex Coated Monoliths

As noted earlier, in traditional ion chromatography formate and acetate are weakly retained and thus difficult to discern from the water dip. Conversely, polarizable anions such as iodide, thiocyanate and thiosulfate are strongly retained on ion chromatography columns such as the Dionex AS9-SC column [28]. Figure 5.2 shows that under HILIC conditions on the latex A coated monolith, both acetate and formate are retained sufficiently to separate them from the dead time marker, while still eluting iodide and thiocyanate in reasonable time.

Although all of the latex coated monoliths in Table 5.2 have similar water layers, only the latex A coated column was able to separate all fore mentioned anions (resolution between thiocyanate and iodide of 0.85). On the latices B and C coated monoliths (Figures 5.3 and 5.4), iodide and thiocyanate eluted together as a single peak and baseline resolution was not obtained between formate and bromate. This indicated that the retention of anions on the latex coated silica

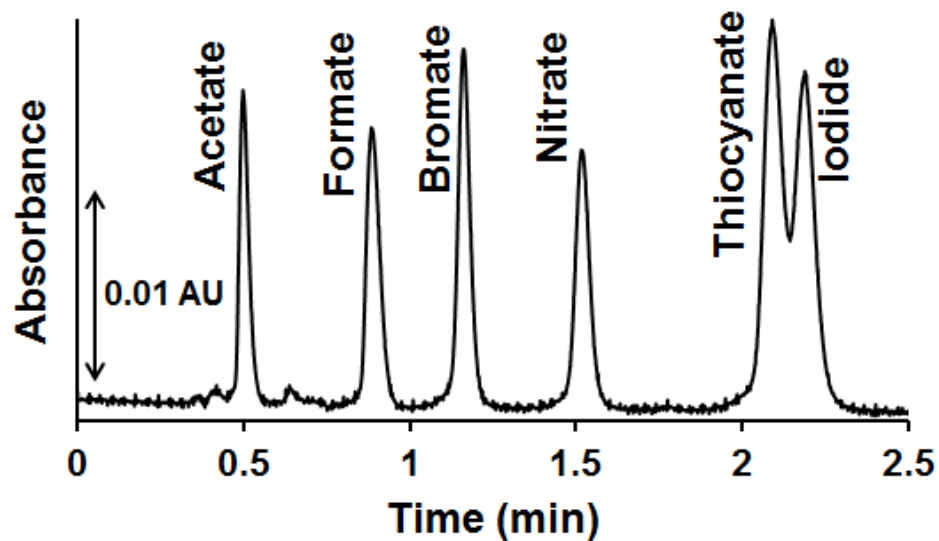


Figure 5.2 Fast separation of acetate, formate, bromate, nitrate, thiocyanate and iodide on the latex A coated Chromolith silica monolith. Conditions: column, latex A coated silica monolith (100 × 4.6 mm i.d.); flow rate, 3.0 mL/min; eluent, 25 mM methylphosphonic acid, pH 4.0, in 65% ACN; analytes, 0.025-7.352 mM in 65 %ACN; UV detection at 225 nm with a 10 μ L loop injection.

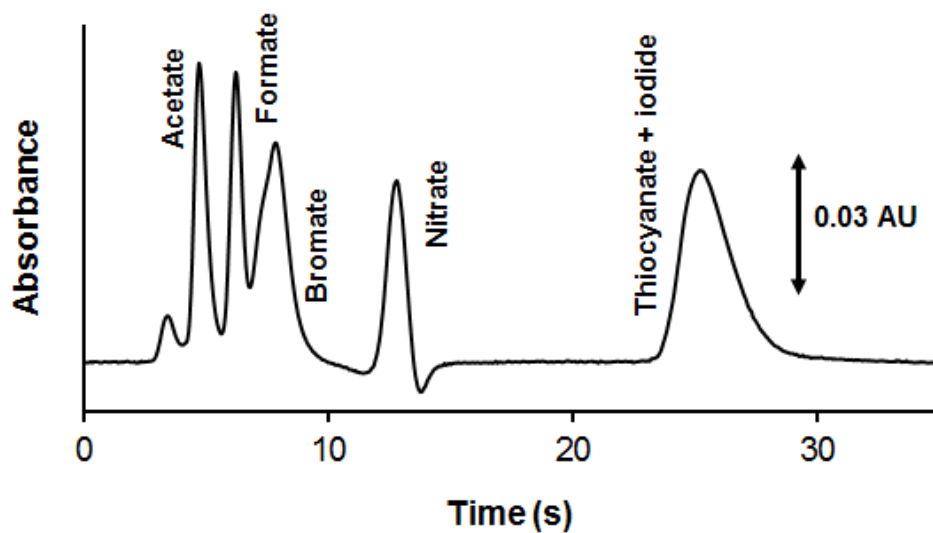


Figure 5.3 Fast separation of acetate, formate, bromate, nitrate, thiocyanate and iodide on the latex B coated Onyx silica monolith. Conditions: column, latex B coated silica monolith (100 × 4.6 mm i.d.); flow rate, 10.0 mL/min; eluent, 10 mM methylphosphonic acid, pH 4.0, in 60% ACN; analytes, 0.02-14.7 mM in 60 %ACN; UV detection at 210 nm with a 10 μ L loop injection.

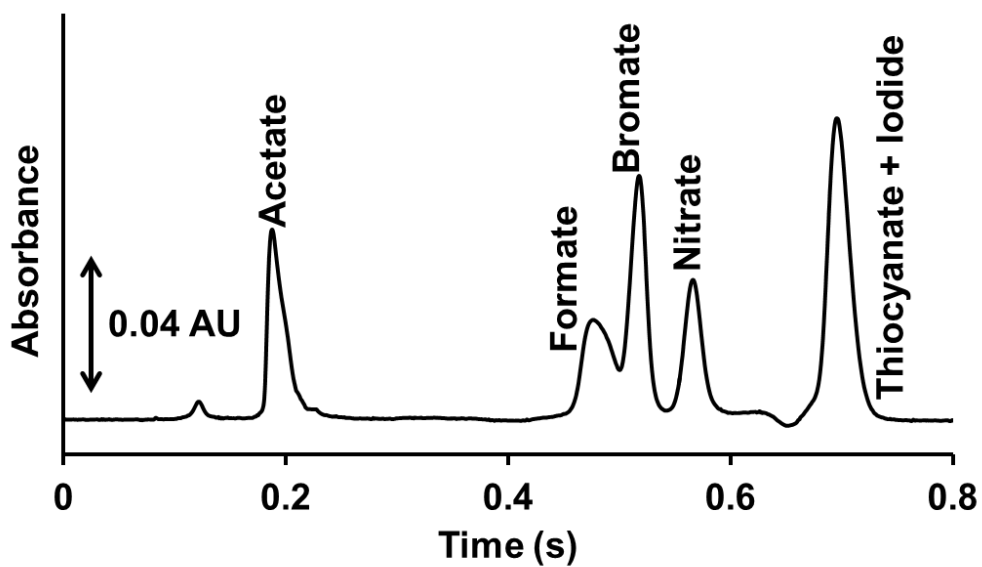


Figure 5.4 Fast separation of acetate, formate, bromate, nitrate, thiocyanate and iodide on the latex C coated Onyx silica monolith. Conditions: column, latex C coated Onyx silica monolith (100 × 4.6 mm i.d.); flow rate, 7.0 mL/min; eluent, 5 mM methylphosphonic acid, pH 4.0, in 65% ACN; analytes, 0.02-14.7 mM in 65 %ACN; UV detection at 210 nm with a 10 μ L loop injection.

monoliths does not solely follow the HILIC mechanism. Rather, the ion exchange nature of the column is also critical. The high ion exchange capacity of the latex A coated monolith may contribute to the superior separation performance of this column relative to the other latex coated columns (latices B and C).

The monolith silica support provides the latex coated column with high permeability allowing separation to be performed at very high flow rates with minimal backpressure [15-20]. Figure 5.2 shows a 2.5 min separation of some common UV absorbing anions on the latex A coated silica monolith under HILIC conditions at 3 mL/min. Higher flow rates resulted in decreased resolution between thiocyanate and iodide, such that by 8 mL/min only a single peak was observed. The separation in Figure 5.2 is comparable in speed to that achieved on a 10 cm long zwitterionic lysine bonded silica monolith (~1.8 min) [49] for anions ranging from NO_2^- to SCN^- . Figure 5.2 is slower than the 1.5 min ion exchange separation achieved on a 0.5 cm long DDAB coated silica based monolith [18] and the 30 s on a 5 cm DDAB coated RP monolith [26]. However the anions separated in this past work did not include neither kosmotropic anions such as acetate or formate nor chaotropic anions such as SCN^- or I^- .

5.3.3 Selectivity of Latex Coated Silica Monoliths

Since HILIC was coined by Alpert in 1990 [42], there has been a dramatic increase of the number of HILIC stationary phases including bare silica, amide, zwitterionic, amine, and diol phases [50, 51]. Substantial differences in selectivity have been observed between various types of HILIC phases [35, 50, 51]. These

differences in selectivity indicate that interactions including hydrophobic, hydrophilic, dipole-dipole, hydrogen bonding and/or ion exchange are important in HILIC [34, 50]. Recently, Dinh *et al.* [34] characterized these interactions in 22 commercial HILIC columns using principal component analysis (PCA). Dinh *et al.* were successful in classifying commercial HILIC phases into 4 main classes: zwitterionic, neutral, cationic and anionic phases [34]. More recently, Lucy and co-workers re-casted the retention results given by Dinh *et al.* into simpler selectivity plots [35]. Results displayed by Lucy and co-workers highly agreed with the column classifications of Dinh *et al.* The selectivity plot given by Lucy and workers [35] graphed the retention ratio of benzyltrimethylammonium (BTMA)/cytosine on the Y-axis vs. the retention ratio of cytosine/uracil on the X-axis. BTMA/cytosine pair was used to probe ion exchange interactions, *i.e.*, the higher the BTMA/cytosine retention ratio, the stronger the cation exchanger character [34, 35]. A BTMA/cytosine retention ratio of ~ 1 was indicative of a column without ion exchange character (*e.g.*, zwitterionic and diol columns). A low BTMA/cytosine retention ratio (< 1) indicates anion exchange character. The retention ratio of cytosine/uracil was used to probe hydrophilic interactions, *i.e.*, the higher cytosine/uracil ratio, the stronger the hydrophilic interactions [34, 35].

Herein the same probes were used to characterize the selectivity differences among the three latices (latices A-C) coated Onyx silica monoliths and a latex A coated Chromolith (Figure 5.5). For reference, the 75% confidence ellipses for the various classes of commercial HILIC columns are shown in the figure (*e.g.* bare silica, amine and zwitterionic phases).

Underivatized silica phases showed strong cation exchange properties as shown in Figure 5.5 due to the presence of free silanols. The bare Chromolith monolith displayed unusually strong cation exchange character as it is above the ellipse encompassing typical (75% confidence interval) silica character. This is consistent with the observations of Dinh *et al.* [34]. The bare Onyx monolith showed ion exchange and hydrophilic character that was typical of bare silica phases.

Coating the monolithic columns results in a decrease in the cation exchange character of the silica monolith (*i.e.*, lower BTMA/cytosine value). However the latex coated columns did not display anion exchange character (BTMA/cytosine < 1) such as observed for commercial amine based HILIC columns. With the exception of the latex B coated column, the latex columns displayed lower hydrophilicity than the bare silica (*i.e.*, are located to the left of the bare silica confidence ellipse in Figure 5.5). The result is that latices A and C coated monoliths display unique selectivity amongst HILIC columns.

Chromolith and Onyx bare silica monoliths displayed very similar cation exchange and hydrophilic character when coated with the same latex A (Figure 5.5). These columns also displayed similar water layers (Table 5.2). This is despite the bare Chromolith and Onyx silicas displaying different character. Thus the character of the latex coated monolith is determined by the nature of the latex rather than the underlying silica. Coating an Onyx silica monolith with latex B substantially decreased its cation exchange character. However the resultant retention characteristics were not statistically different from that of other HILIC

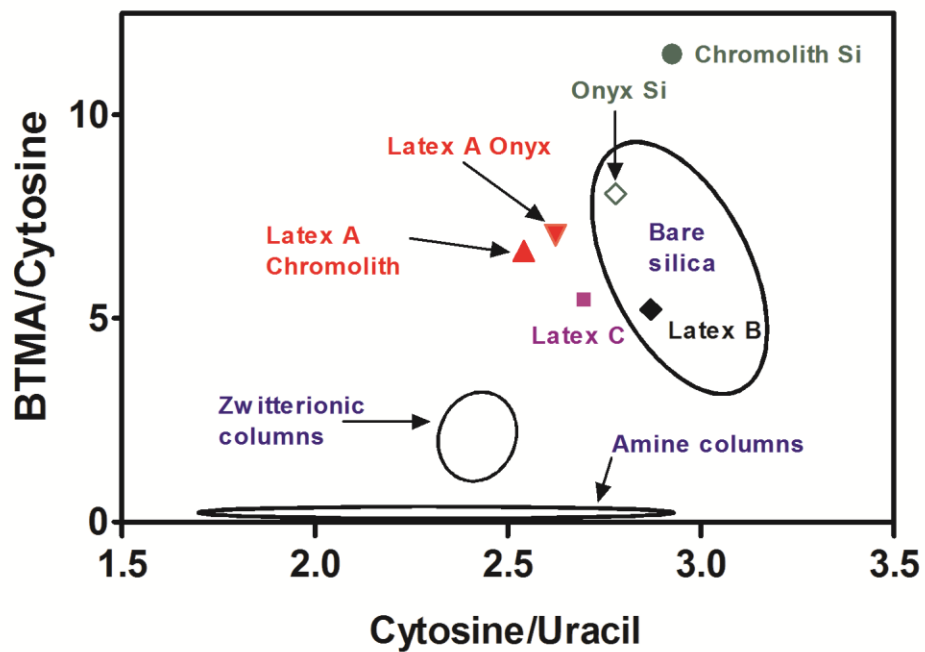


Figure 5.5 Selectivity plot of latex coated silica monoliths. Conditions: columns; Onyx bare silica (\diamond), Chromolith bare silica (\bullet), latex A coated Onyx (\blacktriangledown), latex A coated Chromolith (\blacktriangle), latex B coated Onyx (\blacklozenge) and latex C coated Onyx (\blacksquare); eluent, 5 mM ammonium acetate (pH 6.8) in 80 % ACN; test analytes, 0.044-0.44 mM in 80 % ACN; UV detection at 254 nm with a 10 μ L loop injection. The 75 % confidence ellipses around bare silica, amine and zwitterionic columns were adopted from Reference [35]. The chemical structures of the analytes are shown in Appendix I.

bare silica columns. This behavior might be attributed to the very low coverage of latex B nanoparticles on the silica surface, consistent with the low ion exchange capacity ($4.4 \pm 0.1 \mu\text{eq/col}$) given in Table 5.2. The behavior of latex C coated monolith was intermediate between latices A and B columns. The trend in behavior again correlates with the degree of cross-linking of the latex, rather than their size.

5.3.4 Influence of the Anion Nature on the Mixed Mode Retention Mode

Section 5.3.3 has demonstrated that retention on the latex monolith is mixed mode in nature. In this part, we explore the effect of buffer strength and % ACN of the mobile phase on the dominant retention mechanism (*i.e.*, partitioning or ion exchange) for anions of widely different character.

5.3.4.1 Effect of Buffer Strength

A partitioning retention mechanism, as originally postulated by Alpert for HILIC [42] would follow the relationship [51]:

$$\log k = \log k_w - S\varphi_B \quad (\text{Equation 5.1})$$

where φ_B is the volume fraction of the strong solvent, k_w is the retention factor when the mobile phase contains no strong solvent, and S is the slope of the plot. Thus a plot of $\log k$ vs. φ_B should yield a straight line for a partitioning mechanism. Increased retention with the increasing buffer concentration has also

been reported for a variety of HILIC stationary phases [31, 41, 52-54]. It has been hypothesized that increasing the buffer concentration results in a higher concentration of solvated ions in the water rich layer [31, 41, 52-54].

On the other hand, ion exchange chromatography is described by [55, 56]:

$$\log k_A = C_1 - \left(\frac{x}{y}\right) \log (\text{eluent strength}) \quad (\text{Equation 5.2})$$

where k_A is the retention factor of the analyte anion, C_1 is a constant, x is the charge of the analyte anion, and y is the charge of the eluent anion. Thus a plot of $\log k_A$ vs. $\log [\text{eluent strength}]$ should yield a straight line for an ion exchange mechanism.

In this study, the retention mechanism was investigated for a number of anions on the latices A-C coated silica monoliths. As shown in Figure 5.6, $\log k$ for kosmotropic (acetate and formate), intermediate (nitrate) and chaotropic anions (iodide) on the latex A coated monolith were plotted vs. $\log [\text{eluent strength}]$ resulted in linear relationships with a negative slope ($-x/y$ as described in Equation 5.2). Comparable linearity was observed for thiocyanate and bromate (Figure 5.7). According to Equation 5.2, the slope of $\log k$ vs. $\log [\text{eluent strength}]$ is equal to the negative ratio of the analyte and eluent charges [56]. Therefore, the slope of this linear relationship of monovalent anions should equal -1.0 under pure ion exchange conditions. Herein the slope of bromate (-0.92), nitrate (-0.86), thiocyanate (-0.87) and iodide (-0.87) are smaller than the theoretical slope (-1.0) expected for ion exchange of monovalent anions on the

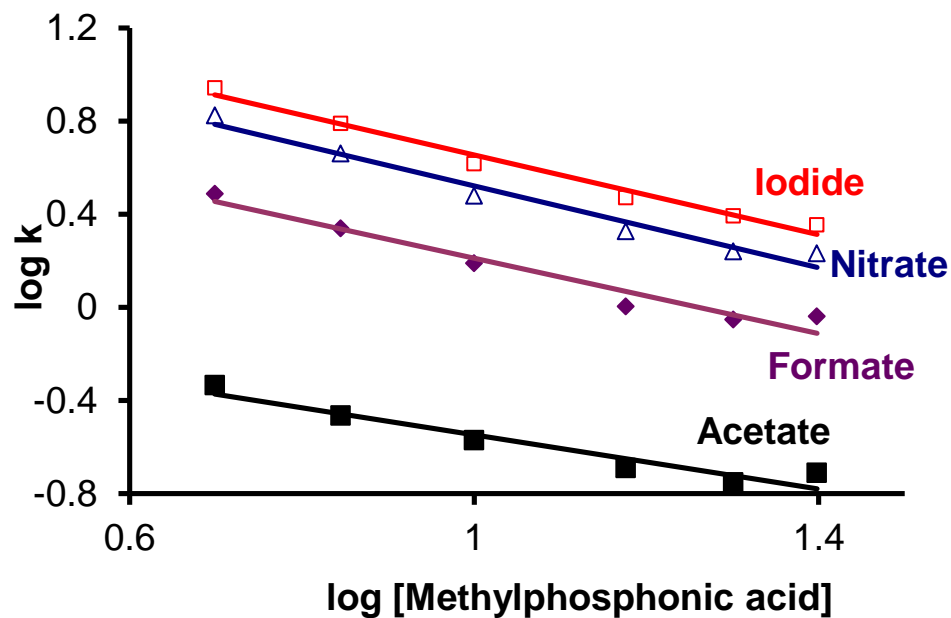


Figure 5.6 Effect of buffer strength on the retention of anions on the latex A coated Onyx silica monolith. Conditions: column, latex A coated silica monolith (100 × 4.6 mm i.d.); flow rate, 1.0 mL/min; eluent, 5-25 mM methylphosphonic acid, pH 4.0, in 65% ACN; analytes, 0.02–14.7 mM acetate, formate, nitrate and iodide in 65 %ACN; UV detection at 210 nm with a 10 μ L loop injection. Lines are fit to Equation 5.2. The size of the data points is equal or bigger than the Y error bar.

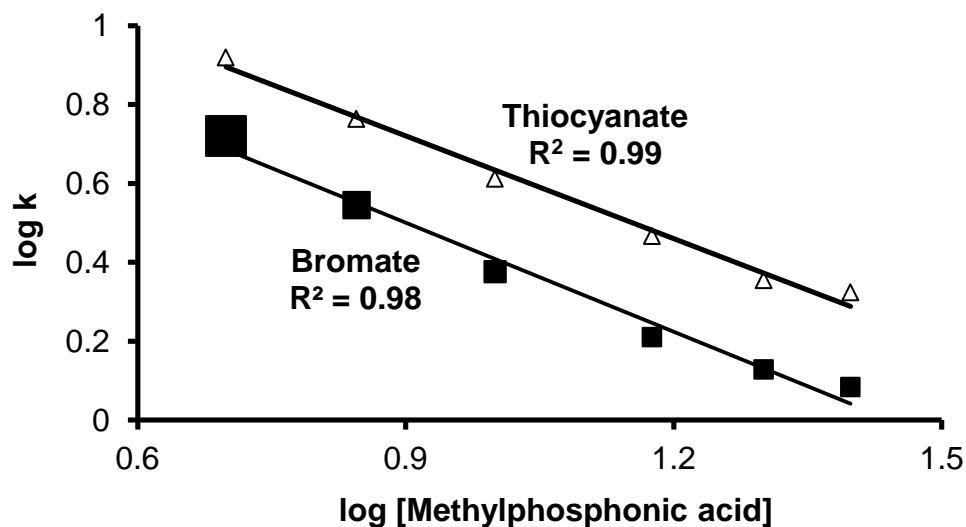


Figure 5.7 Effect of buffer strength on the retention of bromate and thiocyanate on the latex A coated silica monolith. Conditions: column, latex A coated Chromolith silica monolith (100 × 4.6 mm i.d.); flow rate, 1.0 mL/min; eluent, 5-25 mM methylphosphonic acid, pH 4.0, in 65% ACN; analyte, 0.65 mM bromate and 0.5 mM thiocyanate in 65% ACN; UV detection at 210 nm with a 10 μ L loop injection. Lines are fit to Equation 5.2. The size of data points is equal or bigger than the Y error bar.

latex A coated monolith. Thus the linearity and slopes in Figure 5.6 indicate that ion exchange is the dominant retention mechanism for many anions.

However, some positive curvature was observed in Figure 5.6, suggesting the presence of other competing retention mechanism such as partitioning. This is especially true for acetate and formate ($R^2 \sim 0.95$) on the latex A coated silica monolith. Moreover, acetate (-0.54) and formate (-0.79) exhibit much smaller slope values, again suggestive that partitioning is involved to a greater extent in the retention of kosmotropic anions. Comparable behavior was observed for other latex coated monoliths including latices B and C. This is not surprising as acetate and formate are weakly retained by typical ion exchangers, while thiocyanate is strongly retained by ion exchangers [28, 57].

Figure 5.8 compares the retention of iodide (A) and formate (B) vs. eluent strength on all three latex coated monoliths. Figure 5.8(A) shows a decreasing linear relationship for retention of iodide ($R^2 \sim 0.99$) indicating that ion exchange constitutes a major retention mechanism for all three latex coated silica monoliths. Moreover, the overlap of iodide retention on both latex B (Δ) and latex C (\times) coated monoliths (Figure 5.8) was highly consistent with their similarity in cation exchange selectivity in Figure 5.5. This consistency agrees with that ion exchange is the dominant retention mechanism of chaotropic anions *e.g.* iodide. Comparable linearity was observed for thiocyanate, nitrate and bromate, as shown in Figure 5.9. The slope of bromate (-0.66), nitrate (-0.72), thiocyanate (-0.73) and iodide (-0.76) are smaller than the theoretical slope (-1.0) expected for ion exchange of monovalent anions on the latex B coated monolith. On the other

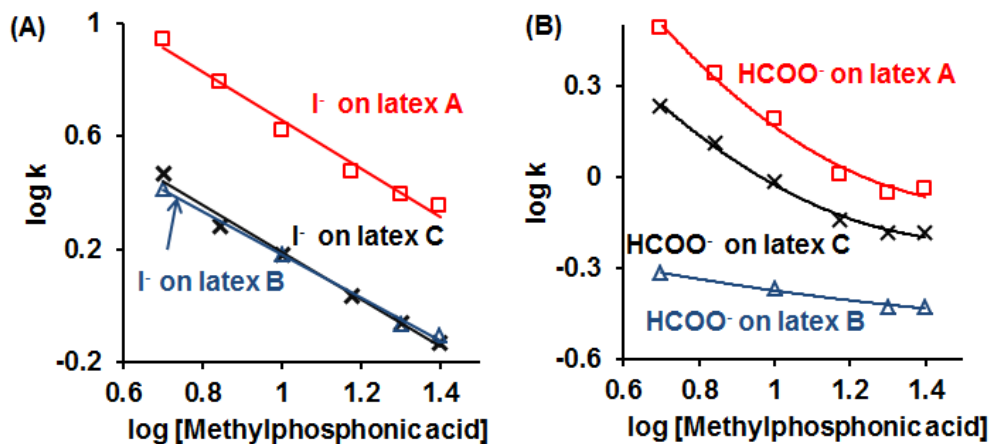


Figure 5.8 Effect of buffer strength on the retention of (A) iodide and (B) formate on latex coated Onyx silica monoliths. Conditions: columns, latex A (\square), latex B (Δ) and latex C (\times) latex coated Onyx silica monoliths (All, 100×4.6 mm i.d.); flow rate, 1.0 mL/min; eluent, 5-25 mM methylphosphonic acid, pH 4.0, in 65% ACN; analytes, 0.1–14.7 mM formate and iodide in 65 %ACN; UV detection at 210 nm with a 10 μL loop injection. Line of Figure 5.8(A) is fit to Equation 5.2. The size of the data points is bigger than the Y error bar.

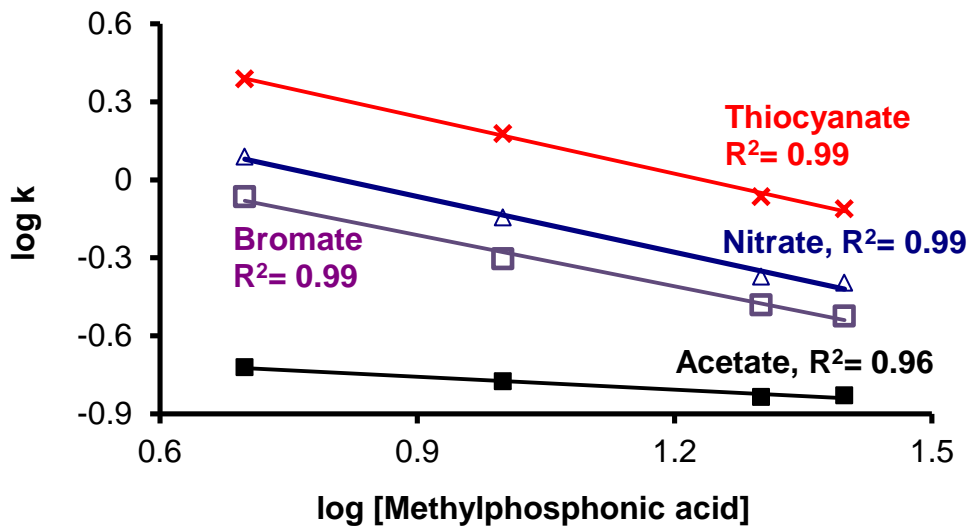


Figure 5.9 Effect of buffer strength on the retention of acetate, bromate, nitrate and thiocyanate on the latex B coated Onyx silica monolith. Conditions: column, latex B coated Onyx silica monolith (100 × 4.6 mm i.d.); flow rate, 1.0 mL/min; eluent, 5-25 mM methylphosphonic acid, pH 4.0, in 65% ACN; analyte, 0.05-12.19 mM acetate, bromate, nitrate and thiocyanate in 65% ACN; UV detection at 210 nm with a 10 μ L loop injection. Lines are fit to Equation 5.2. The size of the data points is bigger than the Y error bar.

hand, Figure 5.8(B) displayed positive curvature for formate on all latex coated monoliths indicating the presence of partitioning as a competing retention mechanism for kosmotropic anions. The lower slope for the latex C (-0.62) and latex B (-0.17) columns in Figure 5.8(B) are indicative that retention on these columns is dominated by partitioning. Comparable curvature was observed for acetate on the latex B coated monolith as shown in Figure 5.9.

5.3.4.2 Effect of % ACN

Figure 5.10 shows the effect of % ACN on retention of anions on the latex A coated silica monolith. In this study, TEA was used to adjust the pH of methylphosphonic acid due to its high solubility in ACN rich mobile phases [42]. Consistent with the results above, the retention behavior of acetate and formate differed from that of iodide and nitrate. The kosmotropic anions showed a moderate decrease in retention with % ACN up to 80-85 %, followed by an increase in retention. This U-shaped retention behavior is similar to that observed for other HILIC phases [20, 58] indicating that these kosmotropic anions follow HILIC partitioning at high %ACN. On the other hand, the chaotropic anions showed a dramatic decrease of retention with increasing % ACN, consistent with observations of ion exchangers in mixed aqueous/organic mobile phases [59]. As the amount of ACN in the mobile phase increases, the latex polymer swells. This leads to a decrease in the number of ion exchange sites per volume, and hence lower retention [59]. Latices B and C coated columns (Figures 5.11 and 5.12) showed comparable behavior to the latex A coated column.

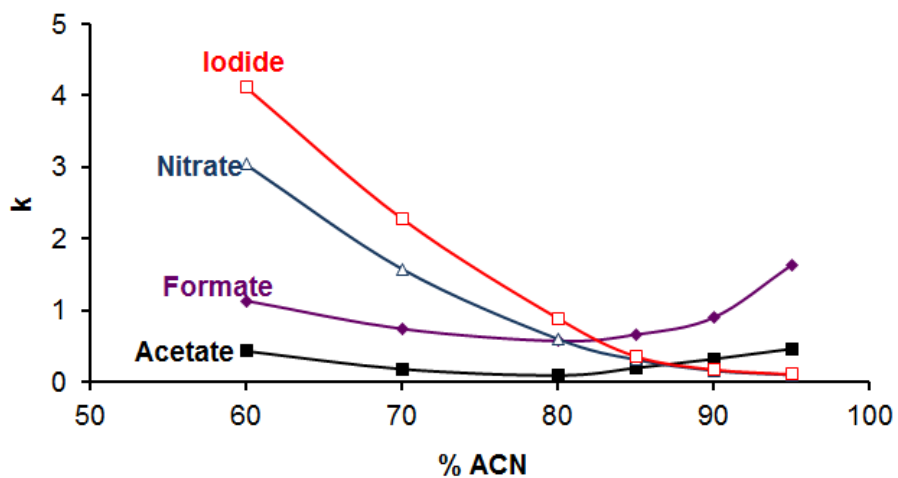


Figure 5.10 Effect of % ACN on the retention of anions on the latex A coated Chromolith silica monolith. Conditions: column, latex A coated silica monolith (100 × 4.6 mm i.d.); flow rate, 1.0 mL/min; eluent, 15 mM TEA-methylphosphonic acid, pH 4.0, in 60-95 %ACN; analytes, 0.02–14.7 mM acetate, formate, nitrate and iodide in 65% ACN; UV detection at 210 nm with a 10 μ L loop injection. Lines are guides to the eye.

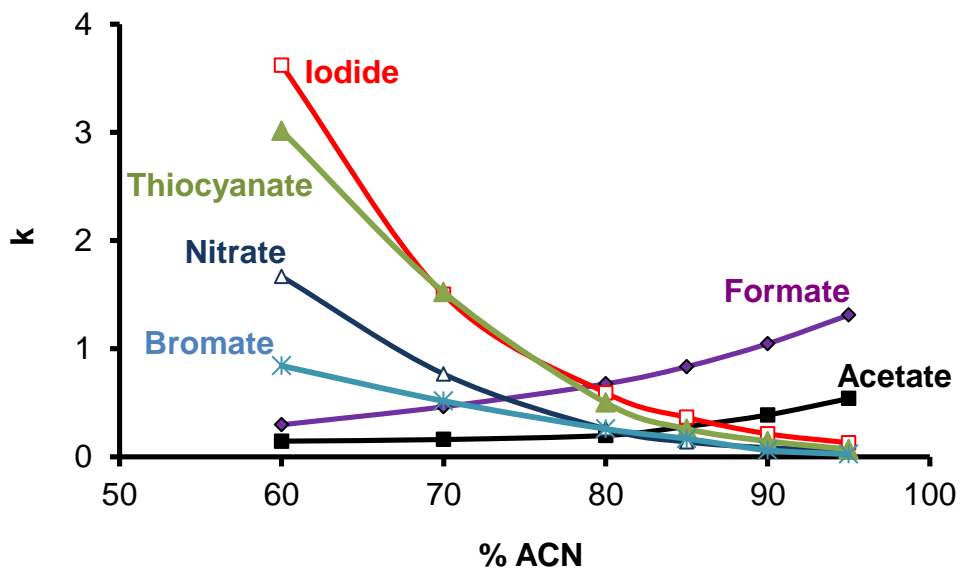


Figure 5.11 Effect of % ACN on the retention of anions on the latex B coated Onyx silica monolith. Conditions: column, latex B coated Onyx silica monolith (100 × 4.6 mm i.d.); flow rate, 1.0 mL/min; eluent, 15 mM TEA-methylphosphonic acid, pH 4.0, in 60-95% ACN; analyte, 0.02–14.7 acetate, formate, bromate, nitrate, thiocyanate and iodide in the same % ACN as the mobile phase; UV detection at 210 nm with a 10 μ L loop injection. Lines are guides to the eye.

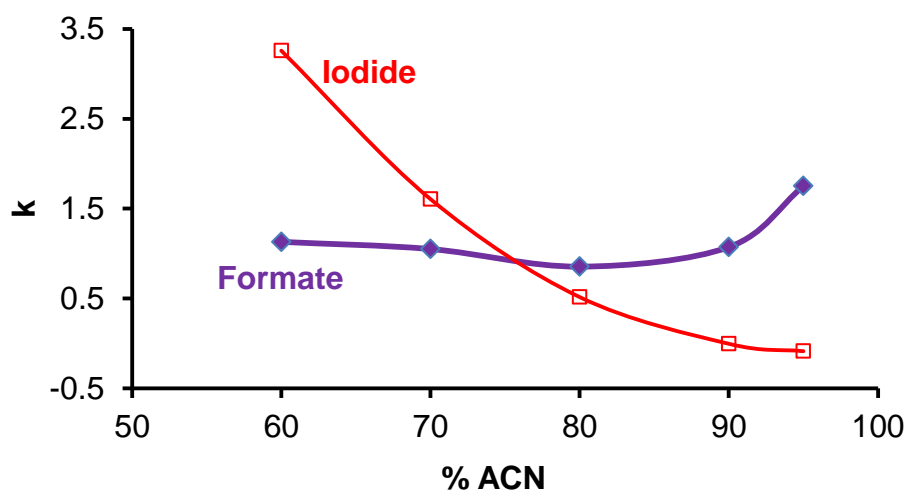


Figure 5.12 Effect of % ACN on the retention of formate and iodide on the latex C coated Onyx silica monolith. Conditions: column, latex C coated Onyx silica monolith (100 × 4.6 mm i.d.); flow rate, 1.0 mL/min; eluent, 5 mM TEA-methylphosphonic acid, pH 4.0, in 60-95% ACN; analytes, 0.1–14.7 mM formate and iodide in the same % ACN as the mobile phase; UV detection at 210 nm with a 10 μ L loop injection. Lines are guides to the eye.

5.4 Conclusions

The latex nanoparticles provided the silica surface with an 8-10 fold more rich water layer than bare silica phases, leading to greater retention. The AS9-SC (latex A) coated monolith provided the highest ion exchange capacity among the tested latex coated columns. The low degree of cross-linking of the AS12A (latex B) and DNAPac (latex C) may account for the lower capacity. Fast separation of kosmotropic and chaotropic anions was achieved on these latex coated monoliths due to the high permeability of the monolith and mixed mode retention mechanism. Latex coated monoliths provided weak cation exchange properties in contrast to the expected strong cation exchange properties. Chromolith and Onyx bare silica monoliths provided very similar selectivity when coated with the same AS9-SC (latex A) nanoparticles. The retention of anions on latex coated silica monoliths is mixed mode in nature. Chaotropic anions are predominantly retained *via* ion exchange; while kosmotropic anions are predominantly retained *via* HILIC partitioning.

5.5 References

- [1] S. Hjerten, J.L. Liao, R. Zhang, *J. Chromatogr. A* **1989**, 473, 273-275.
- [2] T.B. Tennikova, F. Svec, B.G. Belenkii, *J. Liq. Chromatogr.* **1990**, 13, 63-70.
- [3] H. Minakuchi, K. Nakanishi, N. Soga, N. Ishizuka, N. Tanaka, *Anal. Chem.* **1996**, 68, 3498-3501.
- [4] O. Nunez, K. Nakanishi, N. Tanaka, *J. Chromatogr. A* **2008**, 1191, 231-252.
- [5] H. Zou, X. Huang, M. Ye, Q. Luo, *J. Chromatogr. A* **2002**, 954, 5-32.

- [6] N. Tanaka, H. Kobayashi, K. Nakanishi, H. Minakuchi, N. Ishizuka, *Anal. Chem.* **2001**, 73, 420A-429A.
- [7] T. Ikegami, K. Horie, N. Saad, K. Hosoya, O. Fiehn, N. Tanaka, *Anal. Bioanal. Chem.* **2008**, 391, 2533-2542.
- [8] K. Hosoya, N. Hira, K. Yamamoto, M. Nishimura, N. Tanaka, *Anal. Chem.* **2006**, 78, 5729-5735.
- [9] Z.J. Jiang, N.W. Smith, P.D. Ferguson, M.R. Taylor, *Anal. Chem.* **2007**, 79, 1243-1250.
- [10] N.W. Smith, Z.J. Jiang, *J. Chromatogr. A* **2008**, 1184, 416-440.
- [11] T. Ikegami, N. Tanaka, *Curr. Opin. Chem. Biol.* **2004**, 8, 527-533.
- [12] K. Miyabe, G. Guiochon, *J. Sep. Sci.* **2004**, 27, 853-873.
- [13] Y.M. Li, J.L. Nakazato, K. Mohammad, *Anal. Biochem.* **1994**, 223, 153-158.
- [14] E.C. Peters, M. Petro, F. Svec, J.M.J. Frechet, *Anal. Chem.* **1998**, 70, 2288-2295.
- [15] K. Cabrera, *J. Sep. Sci.* **2004**, 27, 843-852.
- [16] K. Cabrera, D. Lubda, H.M. Eggenweiler, H. Minakuchi, K. Nakanishi, *J. High Resolut. Chromatogr.* **2000**, 23, 93-99.
- [17] K.M. Glenn, C.A. Lucy, P.R. Haddad, *J. Chromatogr. A* **2007**, 1155, 8-14.
- [18] S. Pelletier, C.A. Lucy, *J. Chromatogr. A* **2006**, 1118, 12-18.
- [19] F. Rabel, K. Cabrera, D. Lubda, *Am. Lab.* **2000**, 32, 20-22.
- [20] M.E.A. Ibrahim, T. Zhou, C.A. Lucy, *J. Sep. Sci.* **2010**, 33, 773-778.
- [21] L.R. Snyder, J.J. Kirkland, J.W. Dolan, In *Introduction to modern liquid chromatography 3rd Edition*, John Wiley & sons, Hoboken, New Jersey, 2010.

- [22] M. Kele, G. Guiochon, *J. Chromatogr. A* **2002**, *960*, 19-49.
- [23] D. Connolly, B. Paull, *Anal. Chim. Acta* **2001**, *441*, 53-62.
- [24] D. Connolly, B. Paull, *J. Chromatogr. A* **2001**, *917*, 353-359.
- [25] D. Connolly, B. Paull, *J. Chromatogr. A* **2002**, *953*, 299-303.
- [26] P. Hatsis, C.A. Lucy, *Anal. Chem.* **2003**, *75*, 995-1001.
- [27] B. Paull, D. Victory, International Ion Chromatography Symposium, Trier, Germany, 2004.
- [28] J. Weiss, In *Handbook of Ion Chromatography*, Wiley-VCH, Darmstadt, 2004.
- [29] <http://www.dionex.com/en-us/products/columns/bio/nucleic-acid/dnapac-pa200/lp-73371.html> (accessed in June 2012).
- [30] D.V. McCalley, *J. Chromatogr. A* **2010**, *1217*, 3408-3417.
- [31] W. Bicker, J. Wu, M. Lämmerhofer, W. Lindner, *J. Sep. Sci.* **2008**, *31*, 2971-2987.
- [32] M. Lämmerhofer, M. Richter, J. Wu, R. Nogueira, W. Bicker, *J. Sep. Sci.* **2008**, *31*, 2572-2588.
- [33] J. Wu, W. Bicker, W. Lindner, *J. Sep. Sci.* **2008**, *31*, 1492-1503.
- [34] N.P. Dinh, T. Jonsson, K. Irgum, *J. Chromatogr. A* **2011**, *1218*, 5880-5891.
- [35] M.E.A. Ibrahim, Y. Liu, C.A. Lucy, *J. Chromatogr. A* **2012**, *1260*, 126-131.
- [36] M. Waksmundzka-Hajnos, J. Sherma, In *High performance liquid chromatography in phytochemical analysis, Vol. 102*, CRC press, Boca Raton, Florida, 2011, pp. 155.

- [37] S. Pous-Torres, J.R. Torres-Lapasio, M.J. Ruiz-angel, M.C. Garcia-Alvarez-Coque, *J. Sep. Sci.* **2011**, *34*, 931-938.
- [38] F. Gritti, G. Guiochon, *J. Chromatogr. A* **2011**, *1218*, 5216-5227.
- [39] <http://www.hplc.sk/pdf/Merck/Chromolith.pdf> (accessed in June 2012).
- [40] D. Connolly, B. Paull, *J. Sep. Sci.* **2009**, *32*, 2653-2658.
- [41] T. Zhou, C.A. Lucy, *J. Chromatogr. A* **2010**, *1217*, 82-88.
- [42] A.J. Alpert, *J. Chromatogr.* **1990**, *499*, 177-196.
- [43] D.V. McCalley, U.D. Neue, *J. Chromatogr. A* **2008**, *1192*, 225-229.
- [44] T. Ikegami, H. Fujita, K. Horie, K. Hosoya, N. Tanaka, *Anal. Bioanal. Chem.* **2006**, *386*, 578-585.
- [45] Z. Jianga, N. Smithb, Z. Liua, *J. Chromatogr. A* **2011**, *1218*, 2350-2361.
- [46] A.J. Alpert, *Anal. Chem.* **2008**, *80*, 62-76.
- [47] <http://www.dionex.com/en-us/products/columns/ic-rfic/carbonate-eluent-packed/ionpac-as9sc/lp.73219.html> (accessed in June 2012).
- [48] J.S. Fritz, D.T. Gjerde, In *Ion Chromatography 4th Edition*, Wiley-VCH, Weinheim, 2009, pp. 56.
- [49] E. Sugrue, P.N. Nesterenko, B. Paull, *J. Chromatogr. A* **2005**, *1075*, 167-175.
- [50] M.E.A. Ibrahim, C.A. Lucy, In *Chapter Two: Stationary Phases for HILIC; Hydrophilic Interaction Chromatography-A guide for practitioners*, B.A. Olsen, B.W. Pack (Eds.), Wiley, 2013, pp. 43-85.
- [51] P. Hemstrom, K. Irgum, *J. Sep. Sci.* **2006**, *29*, 1784-1821.
- [52] Y. Guo, S. Gaiki, *J. Chromatogr. A* **2005**, *1074*, 71-80.

- [53] M. Liu, E.X. Chen, R. Ji, D. Semin, *J. Chromatogr. A* **2008**, *1188*, 255-263.
- [54] N.S. Quiming, N.L. Denola, Y. Saito, A.P. Catabay, K. Jinno, *Chromatographia* **2008**, *67*, 507-515.
- [55] L.R. Snyder, H. Poppe, *J. Chromatogr.* **1980**, *184*, 363-413.
- [56] J.E. Madden, N. Avdalovic, P.E. Jackson, P.R. Haddad, *J. Chromatogr. A* **1999**, *837*, 65-74.
- [57] <http://www.dionex.com/en-us/webdocs/110337-DS-IonPac-AS25-18Aug2011-LPN2790-01.pdf> (accessed in June 2012).
- [58] T. Zhou, C.A. Lucy, *J. Chromatogr. A* **2008**, *1187*, 87-93.
- [59] S. Rabin, J. Stillian, *J. Chromatogr. A* **1994**, *671*, 63-71.

CHAPTER SIX: Carboxylate Modified Porous Graphitic Carbon – A New Class of Hydrophilic Interaction Liquid Chromatography Phases*

6.1 Introduction

Hydrophilic interaction liquid chromatography (HILIC) can often retain and resolve hydrophilic analytes such as pharmaceuticals that are difficult to separate by reversed phase liquid chromatography (RPLC) [1, 2]. In HILIC, a hydrophilic stationary phase and an organic rich (*e.g.*, > 60 % ACN) aqueous eluent are used. Polar stationary phases (mainly ion exchangers) have been used with organic rich aqueous eluents for the separation of hydrophilic analytes since the early chromatographic literature [3, 4]. But it was not until 1990 that the term “HILIC” was coined by Alpert [1]. In HILIC, a stagnant water layer forms on the surface of the hydrophilic stationary phase. Analytes partition between the stagnant water rich layer and the moving organic rich eluent [1]. The primary mechanism of retention is postulated to be partitioning of the analyte into this water rich layer. However, adsorption, ion exchange, dipole-dipole interaction, hydrogen bonding [5-7], π - π , and n- π interactions [8] also contribute to retention on HILIC stationary phases. The majority of the stationary phases employed in HILIC are based on silica, polymer or pure inorganic oxides such as TiO₂ and ZrO₂. Surface modification can alter the selectivity of silica and polymer HILIC

*A version of this chapter has been published as M. Farooq Wahab¹, Mohammed E. A. Ibrahim², and Charles A. Lucy, *Anal. Chem.* **2013**, 85, 5684-91.

¹M. Farooq Wahab synthesized and physically characterized the stationary phase.

²I did the experiments needed for chromatographic characterization of the stationary phase.

phases. Neutral HILIC phases include diol, amide and cyanopropyl. Zwitterionic phases are mainly based on sulfoalkylbetaine chemistry. Positively charged phases include those containing aminoalkyl groups. Negatively charged HILIC phases may be underivatized silica or polysuccinimide derivatized silica [3, 7].

Hence, a variety of selectivities are available with silica and polymer based HILIC phases. However, silica has limited chemical and temperature stability, especially at high and low pH. This fragility is a liability for biological samples since highly acidic or alkaline washing steps (100 mM acid or base) are often required to elute any irreversibly bound matrix [9]. Polymeric particles overcame the pH stability issue associated with silica, but earlier polymer phases had limitations associated with swelling-deswelling in organic solvents [10]. More recent commercial polymeric HILIC phases such as ZIC-pHILIC[®], apHera-NH₂[®], and Frulic-N[®] are stable in common HILIC solvents [7].

Porous graphitic carbon (PGC) was introduced by Knox *et al.* [11] as a chemically robust reversed phase – an alternative to overcome the drawbacks of bonded silica phases. PGC is pH stable from 0-14, shows very low bleed in mass spectrometry, and can be used at temperatures up to 200 °C [12]. Some chromatographers refer to PGC as a “super reversed phase” [13] since 20-40% higher organic modifier is needed to yield the same retention as on a conventional reversed phase. Paradoxically, PGC also retains highly polar analytes, such as arsenic species [14], nucleosides, nucleotides, sugars [15], and lipid linked oligosaccharides [16]. This *polar retention effect on graphite* (PREG) [17] is due to induced dipole interactions between the analyte and the graphitic surface [18,

19]. In the presence of organic rich aqueous phases, the unmodified PGC shows only weak polar retention [20]. Thus PGC must be surface modified to behave as a HILIC phase.

The chemical inertness of PGC makes it very difficult to covalently modify the surface [21]. The hydrophilicity of carbon can be increased by using harsh oxidizing agents such as nitric acid [22], hypochlorite, and permanganate [12]. However this treatment forms multiple types of surface oxides on carbon [23] which lead to poor chromatographic performance. One of the most promising strategies for covalent modification of carbon is on-column electrochemical functionalization by aryldiazonium ions using a packed bed of particles as the electrode [24, 25]. However, the on-column electrografting apparatus is challenging to construct. Alternately, free radical chemistry of diazonium ions without electrochemical reduction can be applied [26-28]. Free radicals generated by peroxides, and alkyl or aromatic halides have also been employed for carbon surface modification [29]. Modified carbonaceous phases have been developed mainly for reversed phase applications [24, 30] and ion chromatography [27, 28].

In this work, we report the first description of HILIC on a covalently modified porous graphitic carbon phase. Benzene carboxylic acid moieties are covalently attached to the carbon surface *via* chemical reduction of diazonium ions pre-adsorbed onto the PGC. Detailed surface and chromatographic characterization of the phase is described. The selectivity and retention characteristics of the new carboxylate-PGC phase differs from that of 35

previously characterized stationary phases (representing different types of chemistries) [31].

6.2 Experimental

6.2.1 Reagents

Porous graphitic carbon (PGC, 5 μ m, Lot # PGC366C) was a gift from Thermo Fisher Scientific, UK. Deionized water was from a Barnstead E-pure system (Dubuque, IA, USA). Hydrochloric acid (37% wt/wt) and potassium hydroxide were from Caledon Laboratory Chemicals (Georgetown, ON, Canada). Sodium borohydride was purchased from EMD Chemicals (Gibbstown, NJ, USA). Sodium nitrite ReagentPlusTM, 4-aminobenzoic acid, and 50% sodium hydroxide Uracil, cytosine, benzylamine, 1-naphthoic acid, acetylsalicylic acid, gentisic acid, α -hydroxyhippuric acid, hippuric acid, salicylic acid, L-methionine, tryptophan, glycine, L-serine, L-threonine, cytidine monophosphoric acid (CMP), adenosine 5'-monophosphate (AMP) sodium salt, adenosine 5'-diphosphate (ADP) sodium salt, adenosine 5'-triphosphate (ATP) sodium salt, benzoic acid, 1,2,4-benzenetricarboxylic acid, 1,2,4,5-benzene tetracarboxylic acid, resorcinol (99%), isocytosine and aniline (99.5%) were from Sigma Aldrich (St. Louis, MO, USA). HPLC grade acetonitrile (ACN), salicylic acid and toluene were from Fisher Scientific (Fairlawn, NJ, USA). Ammonium acetate was from Anachemia (Lachine, QC, Canada) or Fisher Scientific (Fair Lawn, NJ, USA). Benzyltrimethylammonium chloride (BTMA) was from ACROS Organics (Fair Lawn, NJ, USA). Phenol (ACS reagent, 99%) was purchased from ACP

(Montreal, QC, Canada) and phloroglucinol (> 99 %) was from Fluka (Buchs, Switzerland).

6.2.2 Apparatus

The packing apparatus consisted of a Haskel pump (DSF-122-87153, Burbank, CA, USA) driven with N₂ gas (Praxair Inc., Edmonton, AB, Canada). The column packing process used the following supplies from Thermo Fisher, Dionex (Sunnyvale, CA, USA): an empty polyether ether ketone (PEEK) column (15 cm × 0.3 cm i.d.), PEEK screw caps, 2 μm Ti and stainless steel frit, Zitex membrane, and ultrahigh molecular weight polyethylene (UHMWPE) frits. A cylindrical (1.4 cm i.d.) 40 mL slurry reservoir from Lab Alliance (State College, PA, USA) was connected to a 5 cm × 0.4 cm i.d. stainless steel pre-column and then to the empty column. The other end of the column was capped with a PEEK screw cap by a 2 μm frit. The whole system was pressurized by the pneumatic Haskel pump.

Chromatographic studies were performed using a model 709 dual-piston pump (Metrohm, Herisau, Switzerland) operating at 0.8 or 1.0 mL/min. A 6-port Rheodyne 8125 injection valve (Cotati, CA, USA) with a 2 μL injection loop was used. A Lambda-Max Model 481 UV detector (Waters, Milford, MA, USA) was used at 215, 254 and 268 nm.

6.2.3 Method

6.2.3.1 Synthesis of the Stationary Phase (Carboxylate-PGC)

The synthetic approach using diazonium chemistry is based on reference [27]. 1.7 g of porous graphitic carbon (PGC) were mixed with 40 mmol of 4-aminobenzoic acid in 50 mL deionized water, and stirred over ice using a magnetic stir bar until the PGC particles were well dispersed (*unreacted PGC is highly hydrophobic and floats in water*). The stirring did not cause fracturing of the particles as confirmed by scanning electron microscopy (SEM). To the suspension, 40 mmol of NaNO₂ in 50 mL water was added quickly. The solution was allowed to stir very well before the addition of 33 mL conc. HCl. The mixture was stirred for 30 min to allow adsorption of the diazonium salt onto the PGC. Sodium borohydride (100 mmol in 50 mL water) was added in small portions over 30 min with vigorous stirring over ice. (CAUTION: *the reaction is vigorous due to evolution of both hydrogen and nitrogen. An open 1 L beaker was used for the reaction*). The suspension was filtered using a 0.22 μm nylon filter, and then successively washed with deionized water, 1% KOH, ACN, and then > 3 L of deionized water. The modified particles were de-fined by sedimentation (12-18 h) in deionized water. The grafting reaction was repeated a second time on the de-fined material. Repetition of the grafting reaction gave similar atomic O content by X-ray photoelectron spectroscopy (XPS) as a single grafting reaction. In contrast, surface loading improvements were observed in our previous study on repeated grafting reaction sulfonic acid moiety on carbon by the same borohydride reaction [27]. After the second modification, the particles were de-

fined once more, washed and vacuum dried in air for 90 min. Three different batches of carboxylate-PGC were synthesized from the same PGC lot to assess the chromatographic reproducibility of the surface modification.

6.2.3.2 Packing of the Stationary Phase (Carboxylate-PGC)

The modified PGC was slurried in deionized water and packed at constant pressure (5000 psi with a Haskel pneumatic pump) into a 150 x 3 mm i.d. PEEK column. Pressure was maintained for 1.5 h using deionized water as the driving solvent. The column was then detached from the packing assembly. Finally, PEEK screw caps with UHMWPE and Zitex membranes were installed on both ends after washing the column. The column was subjected to washing with mixtures of ACN-NaOH (0.1 to 0.2 M) till the baseline became stable at 254 nm. Before any separation, a final wash of 0.2 M aqueous NaOH at 40 °C (at least 60 mL) was used to ensure complete removal of any adsorbed species on the column. Further details of packing charged particles are detailed in reference [32].

6.2.3.3 Mobile Phase Preparation

The mobile phase consists of a mixture of ACN, ammonium acetate and water. The pH was adjusted with NaOH or HCl. The aqueous stock ammonium acetate solutions (2 M) at the desired pH were made and refrigerated. The reported buffer concentration is the final concentration in the eluent after mixing with ACN and the reported pH of the buffer is the final pH of aqueous diluted buffer of the same volume. The percentage of ACN in this work represents the

volume of the ACN relative to the total volume of the solvents including buffer and ACN.

6.2.4 Characterization of PGC Phases

X-ray Photoelectron Spectroscopy (XPS) was performed on an AXIS 165 spectrometer (Kratos Analytical, NY, USA). XPS spectra of the unmodified PGC were collected on the raw material as received. The modified particles were thoroughly soaked and washed with 1% KOH, deionized water and ACN, and then allowed to vacuum dry for 2 days prior to XPS analysis. The zeta potential was measured using a Malvern Zetasizer (Worcestershire, UK). Two 23 mg portions of the modified material were suspended in 15 mL of deionized water and 0.1 M NaOH, respectively, sonicated, and then transferred to the Zetasizer dip cell. The electrophoretic mobilities of the particles were converted into zeta potentials using the Smoluchowski equation within the Zetasizer software (version 6.2). Methods to determine the water layer thickness under HILIC conditions by Karl Fisher titration and Bicker *et al.* [33] were inappropriate for the carboxylate-PGC phase. Measurement of water adsorption is the most direct measure of relative hydrophilic character of a stationary phase. Direct method (Karl Fisher titration [34]) was attempted to measure the water adsorption on carboxylate-PGC and silica at various ACN-water compositions, however, both of these phases showed statistically negligible difference in water adsorption. The only exception to the method described in reference [34] is that we did not vacuum dry material in an oven for 3 days at 90 °C, since carbon spontaneously

forms surface oxides. Instead, the stationary phase was dried with acetone and kept in vacuum desiccator at room temperature for 24 hours. An indirect chromatographic measurement of the water layer, by Bicker's method [33] was not successful due to the lack of a suitable unretained marker on carboxylate-PGC.

6.3 Results and Discussion

Our aim is to design a hydrophilic graphitic carbon column for HILIC separations. To be useful as a HILIC phase, the carbon surface must be "wetable" by water in order to form a surface water layer. In this work, benzene carboxylate groups are attached onto porous graphitic carbon (PGC) to convert the hydrophobic PGC surface into a hydrophilic surface suitable for HILIC.

Numerous approaches have been reported in the literature to introduce bonded functionalities onto carbon for reversed phase and ion chromatography [24, 27, 30, 35]. Such bonded PGC phases have shown improved peak shape or decreased retention, but no selectivity changes. Figure 6.1 shows our synthetic route for introducing benzene carboxylate functionality onto PGC. This synthesis mimics the electrografting process in which the diazonium ions are reduced by a working electrode and the aryl radicals are formed adjacent to the carbon surface. Here, the *in-situ* formed diazonium salt of 4-aminobenzoic acid is pre-adsorbed directly onto the PGC surface (Figure 6.1). Due to the pre-adsorption, the aryl radicals generated by borohydride reduction are formed close to the surface [26, 36]. Borohydride does not attack the carboxylate group [37]. After modification,

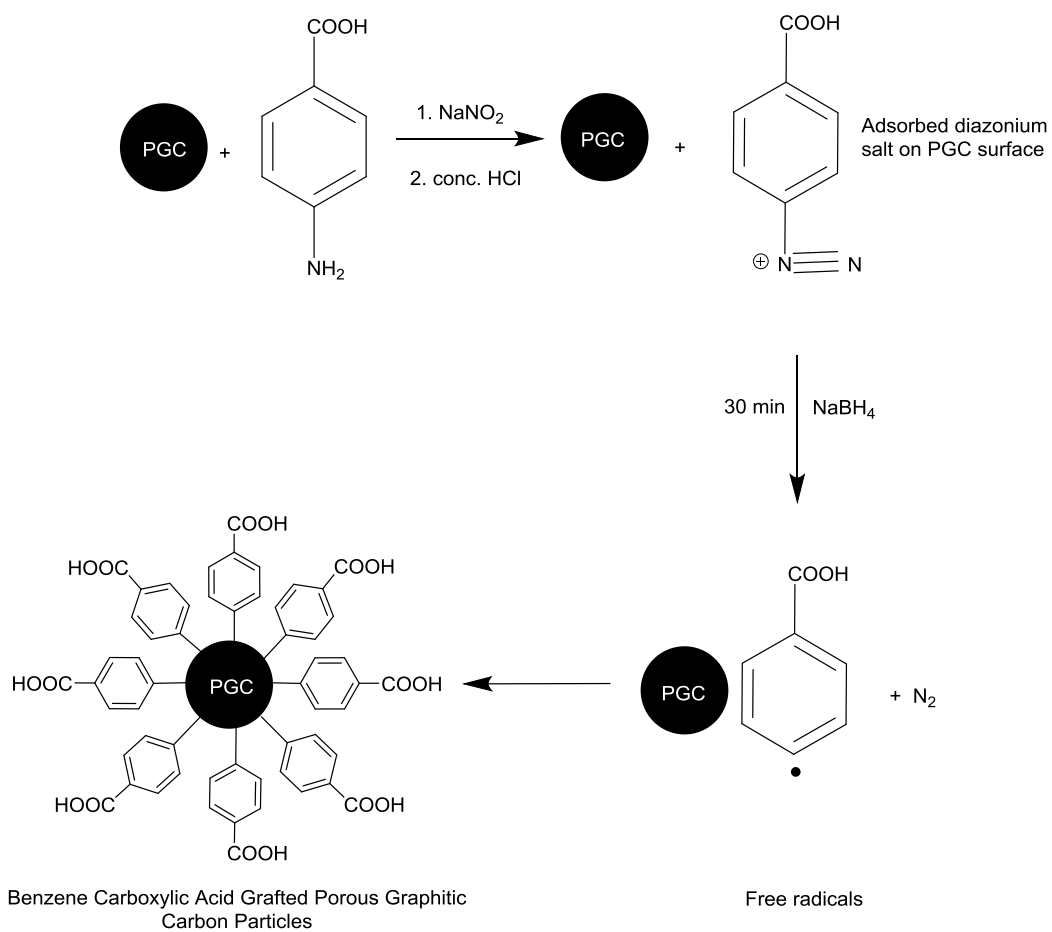


Figure 6.1 The scheme for creating carboxylate functionality on porous graphitic carbon (PGC) using *in situ* generated benzene carboxylic acid diazonium salt.

the particles become highly hydrophilic as shown in Figure 6.2. Additionally no physical damage to the particles was evident, in contrast to that observed when diazonium salts are reduced with sodium metal in non-aqueous medium [38].

The SEM of the modified and unmodified PGC particles (Figure 6.3) showed no changes in surface morphology or pore structure. The SEM also confirms the robustness and mechanical strength of the carboxylate-PGC particles, as no fragments were observed even after vigorous magnetic bar stirring, sonication, and exposure to 5000 psi for 1.5 h.

6.3.1 Characterization of the Carboxylate-PGC

Based on elemental analysis, the bulk unmodified porous graphitic carbon particles were 99.3% C with very low (0.2%) oxygen content. Synthesis as per Figure 6.1 decreased the carbon content to 97.7% and increased the bulk oxygen to 1.2%. Assuming all oxygen atoms exist in the carboxylate moiety, the bulk oxygen content is equivalent to 320 μeq $-\text{COOH}/\text{g}$ dry weight of the stationary phase (moisture free particles). Thermogravimetric analysis (under nitrogen) showed a negligible weight loss (0.3% decrease) up to 200 $^{\circ}\text{C}$, indicating an absence of moisture and other volatile matter. This also confirms the thermal stability of the carboxylate-PGC phase.

The zeta potential of carboxylate-PGC in water was -33.3 ± 2.6 mV, indicating the presence of anionic surface functional groups. The zeta potential

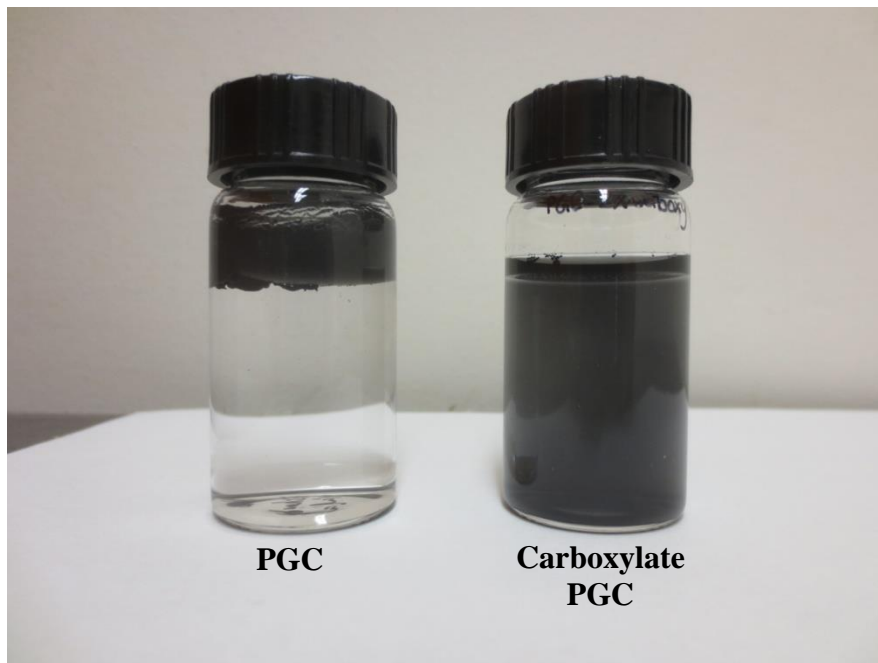


Figure 6.2 The difference in wettability between PGC and carboxylate-PGC in deionized water. The hydrophobic PGC particles do not disperse in water but hydrophilic carboxylate-PGC particles disperse uniformly.

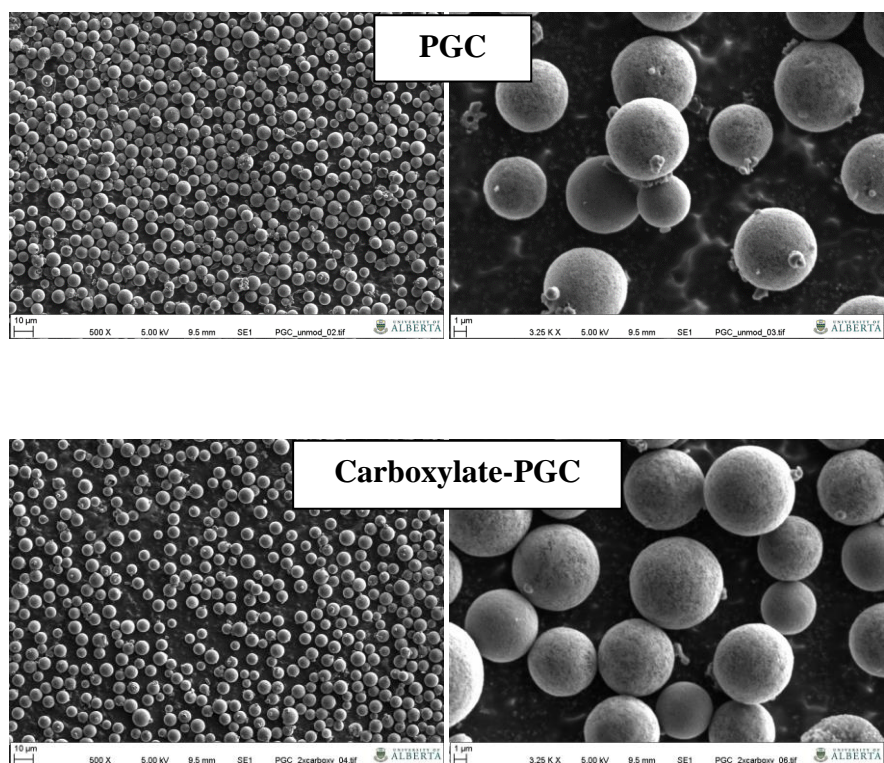


Figure 6.3 Scanning electron microscopy (SEM) images of both unmodified PGC (top) and carboxylate-PGC (bottom). The porous structure at higher magnification is clear (right) showing that the grafted layer does not clog the pores. The mechanical strength of the graphitic particles is also evident as the particles were subjected to stirring *via* magnetic bar, sonication, and 5000 psi. The modified particles were extruded from a slurry reservoir (1.5 hours) and they still remain intact without any breakage.

increased to -38.1 ± 2.9 mV in 0.1 M NaOH due to further ionization of the carboxylic acid groups. For comparison, a sulfonated divinylbenzene-ethylvinylbenzene resin has a zeta potential of -50 mV in deionized water and in 0.1M NaOH, a sulfobetaine type zwitterionic silica exhibited a zeta potential of -16 mV in 20 mM ammonium formate buffer (pH 7) [39] and methacrylate based particles have a zeta potential of -30 to -10 mV at $\text{pH} > 1.5$ [40]. Unmodified PGC particles do not disperse in water, and therefore their zeta potential could not be determined with accuracy. These results indicate that the carboxylate-PGC particles should behave as an anionic HILIC phase whose surface charge can be controlled by pH.

Surface composition analysis is also critical to rationalize the behavior of the stationary phases. The XPS survey scans (Figure 6.4) show that the PGC surface is composed predominantly of carbon, with 2 atom % oxygen. The surface oxygen content on bare PGC (Table 6.1) is comparable to the previously reported ~ 2.7 atom % oxygen [30]. "Surface oxides" form spontaneously along the edges of the graphene sheets on graphitic carbon when exposed to air [41]. However, these surface oxides are non-specific and are composed of carbonyls, phenols, lactones, carboxylates and quinones [23, 42]. Grafting benzene carboxylate groups on PGC results in a 167 % increase in atomic oxygen. The high resolution XPS of oxygen (Figure 6.5) shows the presence of both doubly bound (532.2 eV, C=O) and singly bound (533.8 eV, C-O) oxygen [42], supporting the presence of carboxylate groups on the modified PGC. Assuming that the population of carbon atoms is 7.3×10^{-9} mol/cm² (*i.e.*, equal to that of the flat surface of the basal plane

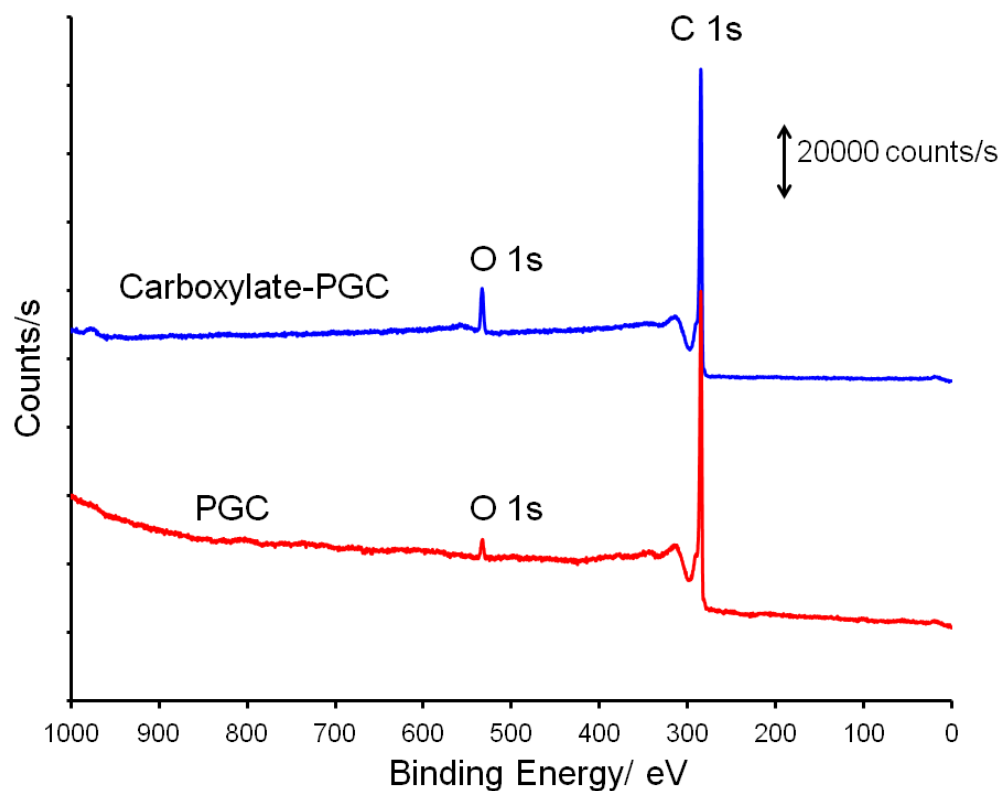


Figure 6.4 Survey XPS scans of PGC (as received) and carboxylate-PGC. XPS measurements were performed on an AXIS 165 spectrometer. The base pressure in the analytical chamber was lower than 3×10^{-8} Pa. Monochromatic Al $K\alpha$ source ($h\nu = 1486.6$ eV) was used at a power of 210 W. The analysis spot was 400×700 μm . Survey scans were collected for binding energy from 1100 eV to 0 with analyzer pass energy of 160 eV and a step of 0.35 eV.

Table 6.1 Surface composition from XPS survey scans of unmodified PGC and carboxylate-PGC

Element	Peak, eV	% Atomic concentration (PGC) ^a	% Atomic concentration (carboxylate-PGC) ^b	O/C Peak area ratio ^c
Carbon	1s, 285.0	98.0	94.6	0.053
Oxygen	1s, 531.8	2.00	5.35	0.147
Nitrogen ^d	1s, 393.7	0	0 ^d	

- ^{a.} The composition was calculated from the peak areas in the spectra using the CasaXPS (version 2.3) with Scofield values of relative sensitivity factors (RSF). A linear background was used.
- ^{b.} The second grafting reaction gave similar surface oxygen content as the first grafting reaction. The data reported in the table refers to two-times grafted reaction.
- ^{c.} The surface coverage of -COOH on carboxylate-PGC was estimated by subtracting the O_{1s}/C_{1s} ratios of both the modified and unmodified PGC, and then multiplying by the carbon atom density on basal plane graphite. This calculation assumes a flat sheet of basal plane carbon.
- ^{d.} Nitrogen was not found in high resolution scans indicating the absence of diazo linkages or other adsorbed reaction by-products.

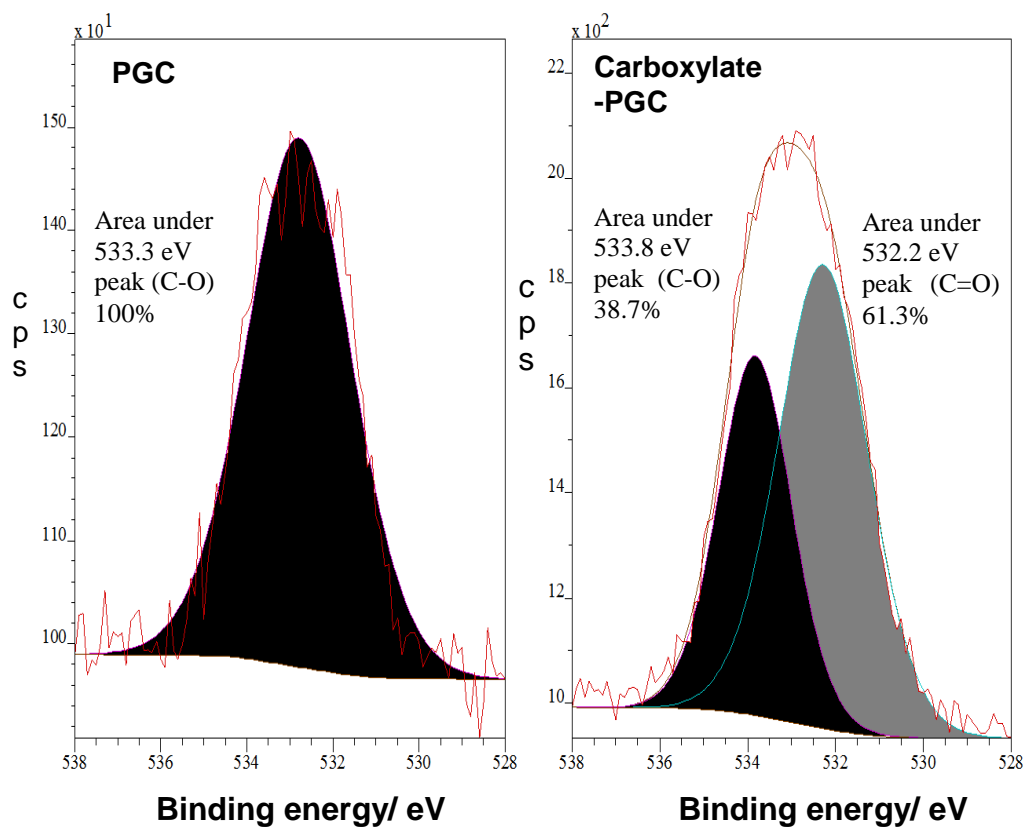


Figure 6.5 High resolution deconvoluted XPS spectrum of the oxygen 1s band. Fitting of the spectrum shows the presence of both doubly bound (532.2 eV, C=O) and singly bound (533.8 eV, C-O) oxygen on the carbon surface of carboxylate-PGC. Fits were generated by the CasaXPS software. Both one component and two component fits were attempted for each spectrum. The curves above are the optimized fits that yield the chemically most realistic results. The full widths half maximum of PGC and carboxylate-PGC are 3.351 eV and 3.366 eV respectively.

graphite) [43], we conservatively estimate the oxygen surface coverage of carboxylate-PGC to be 6.8×10^{-10} mol/cm². (However it should be noted that XPS cannot explore the level of grafting inside the pores of the particles). This oxygen coverage is near that expected for a complete monolayer coverage on the outer surface of the particles [43]. Moreover, this grafting makes the particles sufficiently hydrophilic to be dispersed in water [27], whereas unmodified PGC floats on water. No residual –N=N– signal is observed at 405 eV by XPS nitrogen signal, whereas residual diazonium has been observed on carbon electrochemically modified by diazonium chemistry [26, 44, 45]. On the other hand, nitric acid oxidized carbons show oxygen and as well as nitrogen species in XPS [42]. Thus the carboxylate-PGC particles are free of side products which might lead to undesired chromatographic interactions.

6.3.2 Approaches for Packing Carboxylate-PGC

Colloidal properties of charged particles are highly critical during the packing process. The aspects of chromatographic particles bearing charged functional groups have been examined in detail and involve non-Newtonian rheological properties as discussed in reference [32]. Mild shear thickening was observed on carboxylate-PGC. Water was chosen as slurry and driving solvent because the carboxylate-PGC gave a stable non-agglomerating suspension in water which should yield a tightly packed bed [32]. The early eluting peaks indicate the quality of the packed bed, whereas the late eluting peaks convolute the properties of the packed bed along with multiple interactions.

The water packed column with modified particles produced 5,000 plates/m for 2,5-dihydroxybenzoic acid (early eluting peak). This efficiency is better than the 3,400 plates/m efficiency for early eluting peaks on di-tert-amylperoxide modified PGC (packed by ThermoFisher) [30] but lower than that of 11,000 plates/m reported for unmodified PGC (HypercarbTM) capillaries with ACN [46]. Attempts to pack our carboxylate-PGC material using ACN as the slurry/driving solvent showed an agglomerated slurry, showing that ACN is not an optimum medium for packing. Thus, the carboxylate-PGC particles have a different packing behavior than HypercarbTM. Unfortunately, details and optimized conditions for packing for any carbon phase are not disclosed in the literature.

6.3.3 HILIC Behavior of Unmodified and Carboxylate-PGC

Unmodified PGC (HypercarbTM) shows a reversed phase behavior [18]. Figure 6.6 shows the effect of % ACN on the retention of uracil (neutral) and 1-naphthoic acid (anionic) on unmodified PGC and carboxylate-PGC. Uracil and 1-naphthoic acid are weakly retained on unmodified PGC ($k < 0.5$ and 4 respectively for 90% ACN). This minor increase in retention of uracil and 1-naphthoic acid on unmodified PGC is most likely due to small amounts of “hydrophilic” surface oxide functionalities, most likely phenolics (singly bonded oxygen) as supported by XPS (Figure 6.5). PGC can retain polar analytes by PREG, *i.e.*, by induced dipoles [17]. However PREG would decrease retention of polar analytes with increasing ACN. In Figure 6.6, retention increases with

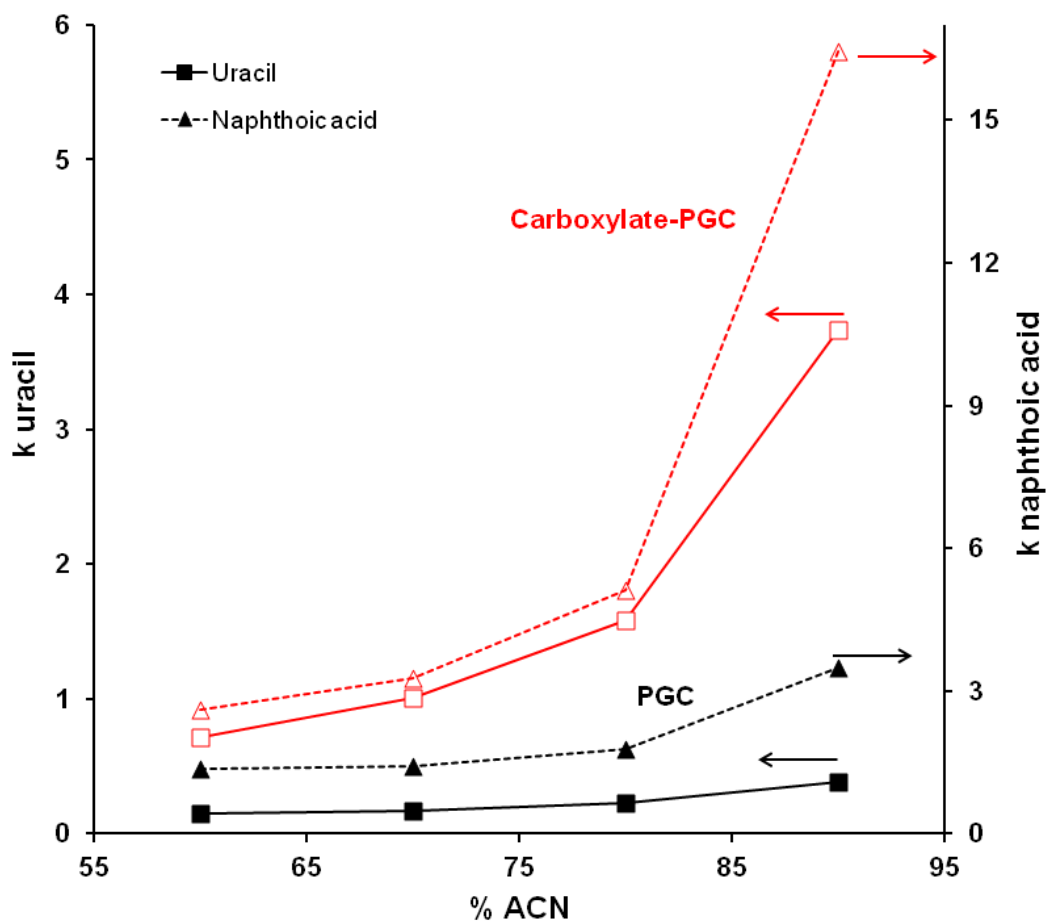


Figure 6.6 Retention behavior of uracil and 1-naphthoic acid on carboxylate-PGC (red) and Hypercarb (black) as a function of % ACN in the eluent. Experimental conditions: columns, carboxylate-PGC (150 mm \times 3 mm i.d.); Hypercarb (100 mm \times 4.6 mm i.d.); flow rate, 0.8 mL/min; eluent, 10 mM ammonium acetate (pH = 8.3) in 60–90% ACN; analytes, 0.2 mM uracil and 1-naphthoic acid in the same % ACN as the mobile phase; UV detection at 254 nm with a 2 μ L loop. The chemical structures of the analytes are shown in Appendix I.

%ACN supporting the speculation that the increased retention seen here reflects a low level of hydrophilic interaction [20]. In contrast, in Figure 6.6 carboxylate-PGC shows significantly greater retention for both polar analytes. Further retention increases significantly at high % ACN, consistent with HILIC behavior [1, 47]. 1-Naphthoic acid has a k of ~ 16 with 90% ACN despite being deprotonated at the mobile phase pH (8.3) – given that both carboxylate-PGC and the acid are negatively charged at this pH. Further, retention increases significantly at high % ACN, consistent with HILIC behavior [1, 47]. With 60% ACN, benzylamine ($pK_a = 9.35$) eluted with a k of 2.3, but did not elute within 40 min *i.e.* $k > 43$ with 70% ACN. This behavior parallels the strong retention of cationic benzyltrimethylammonium (BTMA as chloride) on bare silica columns under HILIC conditions [31].

6.3.4 HILIC Selectivity of Carboxylate-PGC

One of the most important parameters in optimizing separation resolution is the selectivity factor [48]. We devised a graphical visualization for the selectivity of HPLC columns to reflect the hydrophilic and electrostatic character of the column [31]. Figure 6.7 illustrates the selectivity of 35 different stationary phases in addition to the carboxylate-PGC phase. In the selectivity chart (Figure 6.7), the retention factor ratio $k_{\text{BTMA}}/k_{\text{uracil}}$ is plotted against the retention ratio $k_{\text{cytosine}}/k_{\text{uracil}}$. The use of relative retention eliminates the influence of factors such as surface area. For example in Figure 6.7, columns no. 2 and 3 are both 3.5 μm ZIC-HILIC phases with different surface areas (135 and 180 m^2/g , respectively).

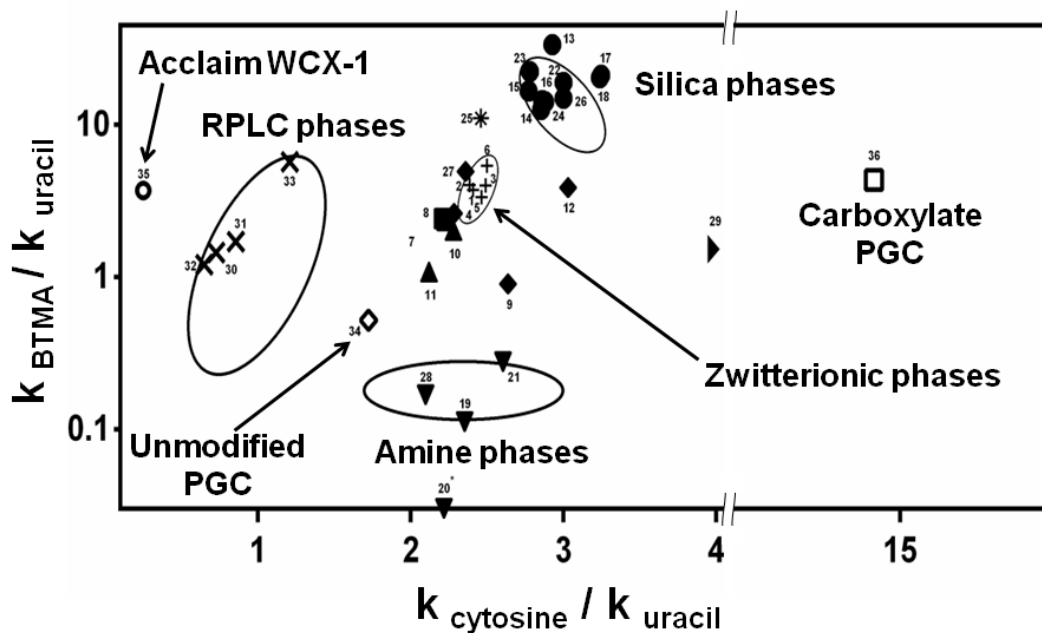


Figure 6.7 Selectivity plot of Carboxylate-PGC (no. 36) and PGC (HypercarbTM, no. 34) with respect to 35 commercial columns (see Table 3.1, Chapter 3 for commercial column data). Legend: bare silica (•), amide (■), diol (▲), amine and/or triazole (▼), polymer substrate and/or polymer coated silica (◆), zwitterionic (+), RPLC (×), latex coated silica (*), proprietary polar phase (▶), unmodified PGC (HypercarbTM) (◇, 34), carboxylate-PGC (□, 36), Acclaim WCX-1 (○, 35). Conditions: eluent, 5 mM ammonium acetate, pH 6.8, in 80% ACN; test analytes, 0.044–0.44 mM BTMA, cytosine, and uracil in 80% ACN; UV detection at 254 nm. 20 μ L loop injection for all columns except PGC, Acclaim-WCX-1, and carboxylate-PGC, where a 2 μ L loop was used. The chemical structures of the analytes are shown in Appendix I. Data adapted from Reference [31].

As the surface chemistry of these columns is the same, identical HILIC selectivity would be expected. Indeed, columns 2 and 3 are very closely clustered in Figure 6.7. Similarly LiChrospher Si 100 and LiChrospher Si 60 pair (columns no. 16 and 17) which differ only in surface area are adjacent in Figure 6.7 [31].

Irgum and co-workers [6] used the relative retention of cytosine/uracil as a generic measure of the “hydrophilic” character of HILIC columns. Cytosine and uracil are both highly hydrophilic (octanol/water partition coefficients at pH 7 of $10^{-1.97}$ and $10^{-1.05}$, respectively), and so both show strong HILIC retention. A higher $k_{\text{cytosine}}/k_{\text{uracil}}$ ratio indicates a more hydrophilic column. BTMA is a hydrophilic quaternary amine and it will undergo electrostatic interaction with the stationary phase regardless of the eluent pH. Therefore, the ratio $k_{\text{BTMA}}/k_{\text{uracil}}$ reflects the electrostatic character (attraction or repulsion) of the stationary phase. Also, on positively charged HILIC phases (*e.g.*, amine), BTMA still exhibits measurable retention, despite experiencing electrostatic repulsion. By using these two parameters, various classes of columns (silica, zwitterionic, diol, RPLC, and amine) can be classified [31].

Unmodified PGC (column no. 34) is a strong RP material [11, 24], and so appears to the left of Figure 6.7. It also exhibits weak anion exchange character, consistent with its ability to retain inorganic anions (data not shown). Attaching benzene carboxylate groups to PGC increases the water “wettability” of the phase, consistent with the behavior seen with aryl carboxylate modified glassy carbons [49]. The ratio of $k_{\text{BTMA}}/k_{\text{uracil}}$ for the carboxylate-PGC column (no. 36, $k_{\text{BTMA}}/k_{\text{uracil}} = 4.3$) is lower than that of silica, indicating a weaker electrostatic

character. The $k_{\text{BTMA}}/k_{\text{uracil}}$ of carboxylate-PGC is comparable to that of the Dionex Acclaim WCX-1 phase which consists of alkyl bonded silica phase with a carboxylate terminus. Cytosine shows much stronger retention on carboxylate-PGC ($k_{\text{cytosine}}/k_{\text{uracil}} \sim 14.9$) vs. silica ($k_{\text{cytosine}}/k_{\text{uracil}} \sim 3$). This may be due to hydrogen bonding interactions with the carboxylate moiety along with the hydrophilic character of this phase. Crystallographic studies of cytosine-carboxylic acid co-crystals show hydrogen bonds exist between the amino group, the pyrimidine backbone of cytosine and the carboxylate moiety [50].

To determine whether the high cytosine retention may also be influenced by the underlying graphitic carbon of PGC, the retention of isocytosine, an isomer of cytosine, was studied. If retention were purely hydrophilic in nature, isocytosine would be much less retained due to its higher octanol/water partition coefficient than cytosine ($10^{-0.59}$ vs. $10^{-1.97}$ at pH 7). In contrast, isocytosine is retained even more strongly on carboxylate-PGC phase than cytosine ($k > 70$ vs. $k = 19.3$, respectively). This indicates that the shape selective properties of the underlying graphitic planes of PGC [50] are still operative on the carboxylate-PGC phase.

To further examine the selectivity of carboxylate-PGC, Figure 6.8 compares the elution order of six carboxylic acids on the carboxylate-PGC phase to that on nine commercial chemistries [51, 52]. The elution order on carboxylate-PGC shows different selectivity than the other HILIC phases. Of the nine commercial phases, the elution order of carboxylate-PGC is most similar to that of the diol and polyvinyl alcohol phases. In addition, salicylic acid has an

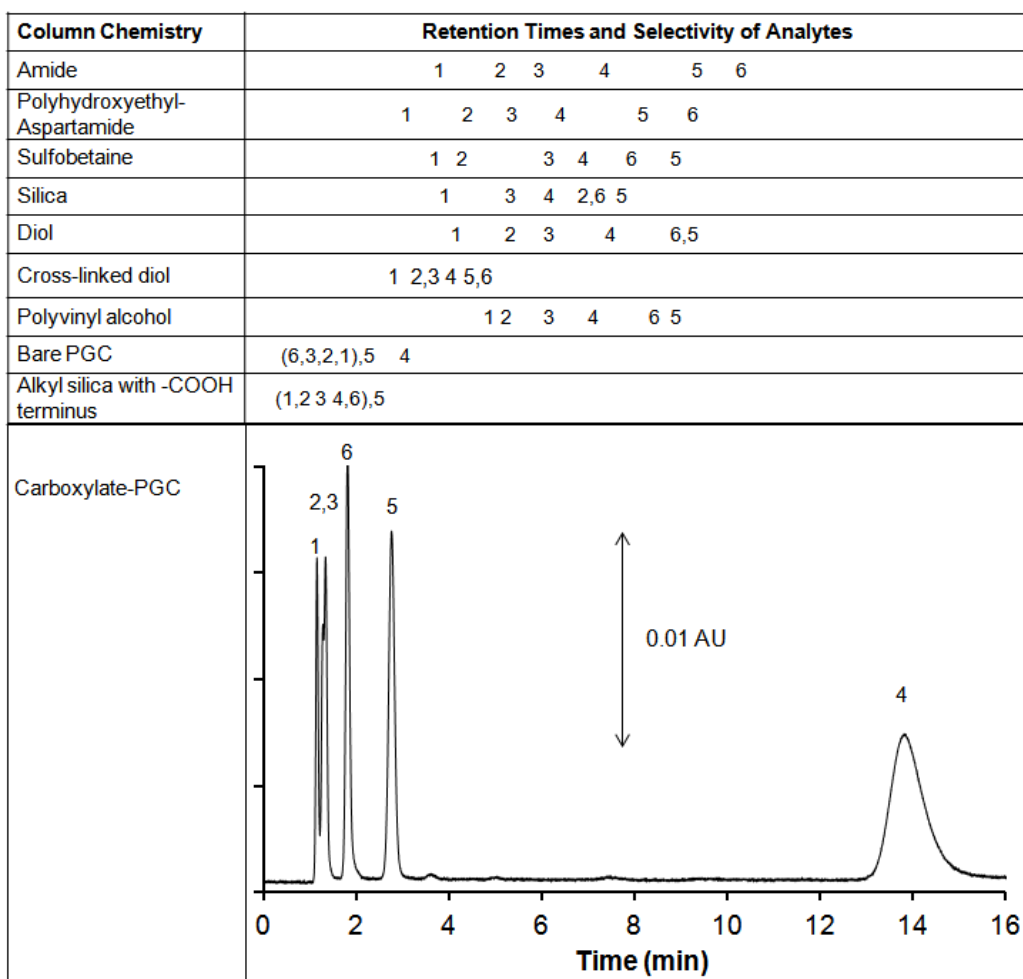


Figure 6.8 Comparison of the selectivity of six aromatic carboxylic acids on nine different column chemistries and carboxylate-PGC under HILIC mode. Analytes separated by commas coelute. The positions of the peak numbers reflect the actual retention time of the analytes. Experimental conditions: column, carboxylate-PGC (150 mm × 3 mm i.d., 5 μm); flow rate, 1.0 mL/min; eluent, 20 mM ammonium acetate (pH = 6.97) in 85% ACN; analytes, 0.12–0.35 mM of (1) salicylic acid, (2) gentisic acid, (3) acetylsalicylic acid, (4) salicyluric acid, (5) hippuric acid, and (6) α-hydroxyhippuric acid. UV detection at 254 nm with a 2 μL loop. The chemical structures of the analytes are shown in Appendix I. Retention data for the commercial columns is from Reference [52].

unusually strong retention ($k = 13.9$) on the carboxylate-PGC phase. On other HILIC phases including the Acclaim WCX-1 phase with terminal carboxylic acid groups - salicylic acid shows similar retention to its isomer α -hydroxyhippuric acid. These two acids differ in the -OH position from the rest of the acids; -OH is phenolic in salicylic acid whereas it is a secondary alcohol in α -hydroxyhippuric acid. The selectivity factor α of the two isomers on carboxylate-PGC is 14 with respect to each other, whereas the selectivity factors for the rest of the nine columns range from 0.70 to 0.92. As noted for cytosine above, this may indicate retention contributions from the shape selectivity properties of flat graphitic planes [53, 54]. Indeed, on unmodified PGC salicylic acid shows much stronger retention ($k = 1.1$) than all of the other acids ($k \sim 0.2$). Such a high isomeric selectivity on carboxylate-PGC is an appealing incentive for exploring covalently modified carbon based HILIC phases.

We note that all of the acids in Figure 6.8 are negatively charged ($pK_a \sim 2.9-3.7$) under the chromatographic conditions. Similarly the carboxylate-PGC is negatively charged (zeta potential ~ -33 mV in deionized water). Therefore all the negatively charged acids should undergo electrostatic repulsion and elute before the void volume. However in electrostatic repulsion hydrophilic interaction chromatography (ERLIC) when the organic content increases above 60%, hydrophilic interaction dominates the electrostatic effects.

6.3.5 Switching Retention Mode of Carboxylate-PGC with pH

The carboxylate functionality displays weak acid behavior ($pK_a \sim 2.8 - 3.1$) [55, 56]. At low pH, carboxylate modified glassy carbon was hydrophobic, as measured by contact angle [49]. Adjusting the pH above the pK_a increased the wettability of the modified glassy carbons [49]. A similar change in hydrophobic to hydrophilic character is illustrated in Figure 6.9 for the carboxylate-PGC phase. The hydrophobic toluene is retained due to interaction with the underlying carbon, and shows little change in retention with pH. At pH 9.7, benzoate is repelled by Donnan exclusion and elutes essentially unretained, while the deprotonated aniline shows weak hydrophobic retention. At low pH, benzoic acid retention increases due to protonation of the analyte and phase, while the protonated aniline shows lower reverse phase behavior. A silica column with alkyl carboxylate terminus (Acclaim WCX-1) shows very similar retention behavior with respect to pH [57].

6.3.6 Chromatographic Separations on Carboxylate-PGC at High pH

To illustrate the applicability of the carboxylate-PGC as a HILIC phase, we performed separations of carboxylates, nucleotides, phenols and amino acids (Figure 6.10). Many of these separations were facilitated by the use of alkaline mobile phases that would damage traditional silica based HILIC phases. Aromatic carboxylic acids can be retained on RPLC columns only by using low organic modifier content. However, the low organic modifier content can cause “phase collapse” leading to a drastic decrease in retention [58]. Similarly, ion

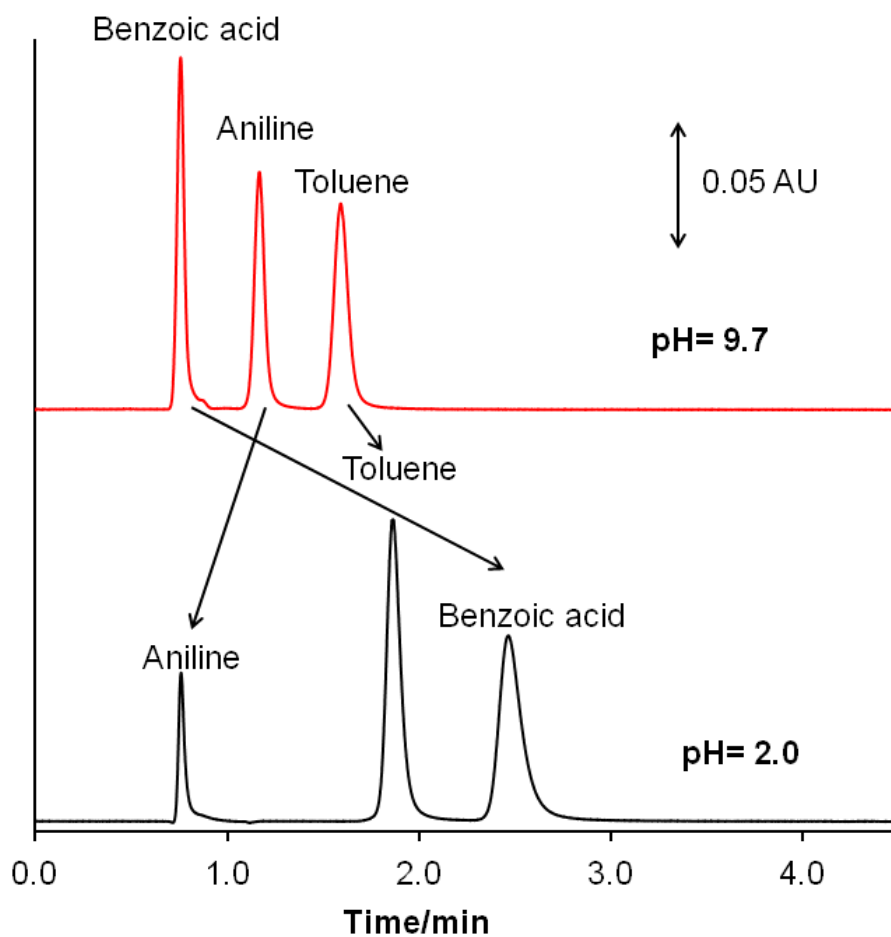


Figure 6.9 Selectivity changes with pH on carboxylate-PGC for aniline, benzoic acid and toluene. Conditions: Column, 150 x3 mm, carboxylate-PGC; eluent, 25 mM ammonium acetate in 65% ACN; desired pH adjusted with HCl or NaOH, 2 μ L loop injection, UV detection at 254 nm. The chemical structures of the analytes are shown in Appendix I.

chromatography cannot be used for organic acids due to their low conductivity especially in organic-rich mobile phases. Thus HILIC is an attractive alternative for carboxylic acids separations. Figure 6.10(A) shows the separation of five fully deprotonated aromatic carboxylic acids ($pK_a = 1.9 - 4.7$) [58]. Retention increased with the number of carboxylic acid groups, *i.e.* benzoic acid < phthalic acid < 1,2,4-benzenetricarboxylic acid < 1,2,4,5-benzenetetracarboxylic acid. 1-Naphthoic acid is more retained than phthalic acid based on its hydrophobic interaction with the underlying graphitic surface. Retention due to electrostatic attraction can be ruled out since the analytes and the stationary phase bear the same charge under alkaline conditions. All such anionic analytes should be expelled by Donnan exclusion from a negatively charged particle. The presence of a low dielectric medium solvent and high ionic strength ensures retention due to hydrophilic interaction despite the electrostatic repulsion. This parallels the ERLIC behavior of cationic analytes on cation exchangers in the presence of low dielectric medium solvent and high ionic strength buffers [47].

Analysis of nucleotides and nucleosides is challenging with RPLC [15, 59]. Several silica columns have been designed with polar embedded groups to increase the polarity of the stationary phase. Nonetheless very low retention factors ($k < 2$) are still observed for nucleotides [59]. Bare PGC can be used for nucleotides, but requires "electronic" modifiers such as diethylamine under gradient conditions to elute the otherwise strongly retained nucleotides [59]. ATP shows poor chromatographic performance on PGC compared to other nucleotides [15]. The nucleotides were irreversibly adsorbed when trifluoroacetic acid was

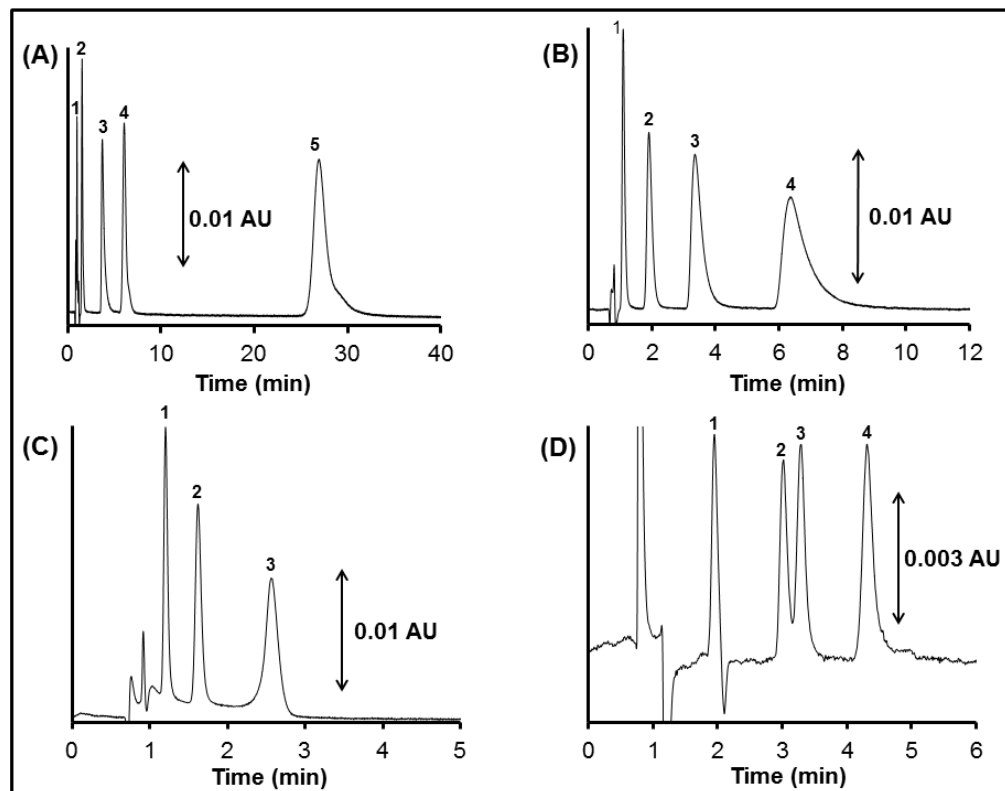


Figure 6.10 Separation of (A) aromatic carboxylic acids, (B) nucleotides, (C) phenols, and (D) amino acids on carboxylate-PGC. All chromatograms were processed by Savitzky-Golay smoothing. Experimental conditions: Column, carboxylate-PGC (150x3 mm i.d., 5 μ m), flow rate: 1.0 mL/min; eluent, (A), (D) 20 mM ammonium acetate (pH =7.6) in 80 %ACN, (B) 50 mM ammonium acetate (pH =9.8) in 60 %ACN, (C) 20 mM ammonium acetate (pH =9.7) in 70 %ACN; analytes: (A) 0.18-0.67 mM of (1) benzoic acid, (2) phthalic acid, (3) 1-naphthoic acid, (4) 1,2,4 benzene tricarboxylate, (5) 1,2,4,5 benzene tetracarboxylate; (B) 0.05-0.14 mM of (1) CMP, (2) AMP, (3) ADP, (4) ATP; (C) 0.2-0.75 mM of (1) phenol, (2) resorcinol, (3) phloroglucinol; (D) 0.17-5.31 mM of (1) L-methionine, (2) L-threonine, (3) glycine, (4) L-serine. UV detection at 254 nm for (A) and (B), 268 nm for (C) and 215 nm for (D) with a 2 μ L loop. The chemical structures of the analytes are shown in Appendix I.

used on PGC [15]. Thus, many challenges are still observed with the separation of nucleotides by RPLC on either silica bonded phases or bare PGC.

In recent years, HILIC has become a popular separation mode for these hydrophilic nucleotides [47]. Figure 6.10(B) shows the fast baseline resolution of four nucleotides (CMP, AMP, ADP, and ATP) on carboxylate-PGC under isocratic conditions. In line with the ERLIC behavior seen for the carboxylic acids in Figures 6.8 and 6.10(A), the negatively charged nucleotides show retention on carboxylate-PGC. The retention order is related to the number of phosphate groups in the nucleotides. ATP, being the most polar analyte is retained most strongly. This is different than the elution order seen on bare PGC [59].

Figure 6.10(C) shows the separation of phenol, resorcinol and phloroglucinol in 3 min at pH 9.7. As expected the most polar phloroglucinol (3 - OH) shows the highest retention, followed by resorcinol and phenol. On the other hand, bare PGC showed co-elution of the tested phenols under the same conditions (data not shown). The retention order on carboxylate-PGC follows the solubility order of the phenols at pH 9 (phenol 109 g/L, resorcinol 222 g/L and phloroglucinol 579 g/L) [58], consistent with the HILIC theory. Finally, Figure 6.10(D) shows the separation of four amino acids namely, methionine, threonine, glycine and serine on carboxylate-PGC and elute in the same order as listed. This elution order corresponds with the solubility: methionine has the lowest water solubility (16 g/L) as compared to the rest of the three amino acids (> 80 g/L) [58] at pH 7. Serine shows higher retention than glycine due to its additional hydroxyl

group. Amino acids with high pK_a (e.g. histidine and lysine) were strongly retained, similarly to benzylamine on carboxylate-PGC.

6.3.7 Column Stability and Retention Time Reproducibility

C_{18} silica columns begins to leach silica (10-30 $\mu\text{g/mL}$) when exposed to 10 mM NaOH : EtOH (50:50 v/v). Increasing the NaOH to 100 mM, increases the Si concentration in the effluent to 511 $\mu\text{g/mL}$ [60]. Simultaneously retention of the basic analyte amitriptyline increased by 20-31% due to the formation of new silanols and detachment of the bonded phase [60]. Thus, silica based columns are incompatible with high pH eluents.

In contrast, PGC is stable from pH 0-14 [11]. Flushing the carboxylate-PGC column with 100 mM NaOH : ACN (50:50 v/v) for 5 h (262 column volumes) had little impact on retention (t_R decreased by 0.7% for benzylamine and 0.9% for tryptophan, Figure 6.11). High pH eluents maximize the negative charge on the carboxylate PGC. The zeta potential of carboxylate-PGC in 0.1 M NaOH increases from -33 mV in deionized water to -38 mV at pH > 12. This increases the "wettability" of the carbonaceous stationary phase [49].

In order to assess the reproducibility of the synthesis, three batches were synthesized from the same lot. Figure 6.12 shows the overlaid chromatograms from the three columns. Retention time RSD for early and late eluting acid were 2.6% and 5.0%, respectively for three separate columns of carboxylate-PGC (Figure 6.12). The low relative standard deviations show that the batch to batch column performance is very good.

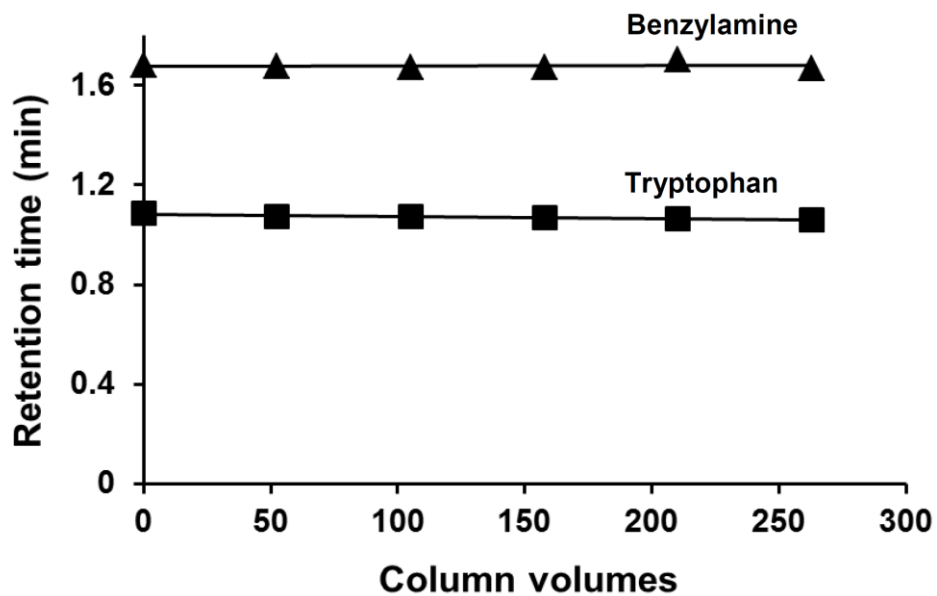


Figure 6.11 Stability of carboxylate-PGC column under strong alkaline conditions. Experimental conditions: Column, carboxylate-PGC (150x3 mm i.d., 5 μ m), flow rate: 0.8 mL/min (dead volume =0.91 mL); eluent, 100 mM sodium, hydroxide (pH =12.6) : ACN (50:50, v/v), analytes: 5 mM benzylamine and 0.5 mM tryptophan in the same % ACN as the mobile phase. UV detection at 254 nm with a 2 μ L loop. The y-axis error is less than the size of the markers.

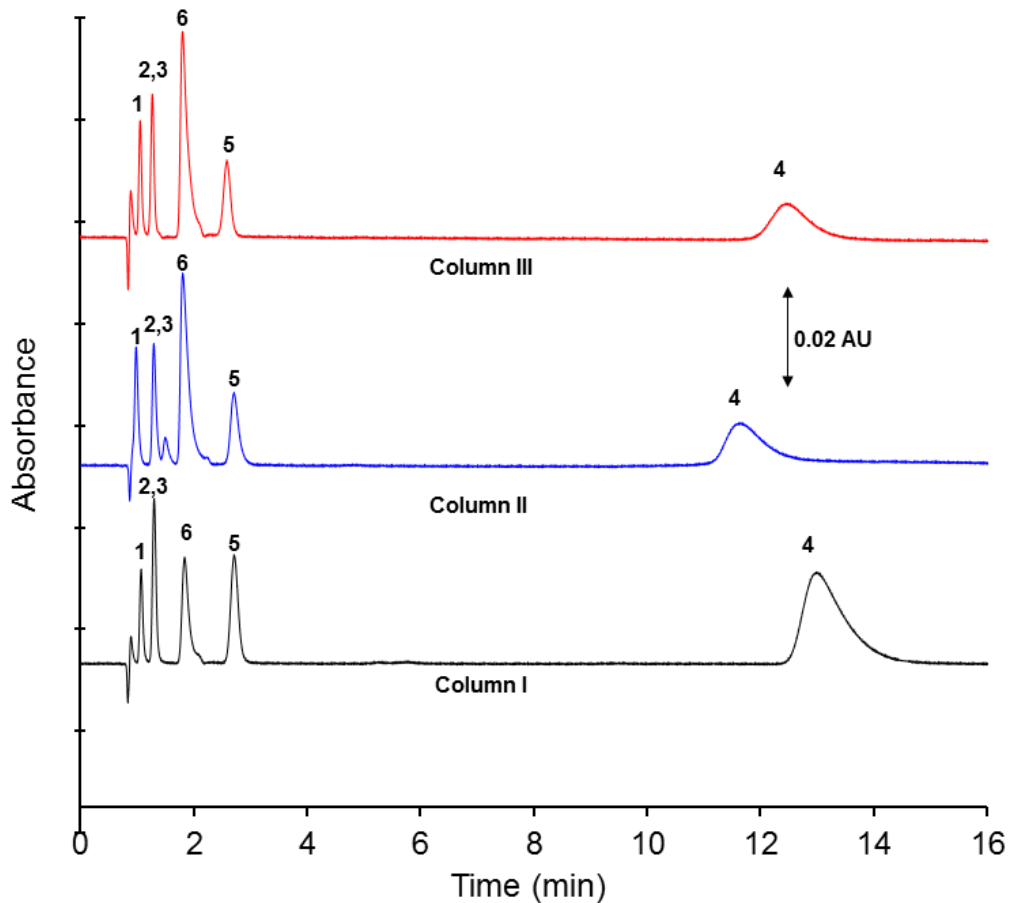


Figure 6.12 Reproducibility comparison of carboxylate-PGC under HILIC mode. The three columns were prepared separately from the same lot of PGC. Analytes separated by commas show refer to co-elution. Column II was even exposed to alcoholic KOH during pre-conditioning. Experimental conditions: Columns, flow rate: 1.0 mL/min; eluent, 20 mM ammonium acetate (pH =6.9) in 85 %ACN; analytes 1. salicylic acid, 2. gentisic acid, 3. acetylsalicylic acid, 4. salicyluric acid, 5. hippuric acid and 6. α -hydroxyhippuric acid. UV detection at 254 nm with a 2 μ L loop. The chemical structures of the analytes are shown in Appendix I.

6.4 Conclusions

Porous graphitic carbon is a highly attractive substrate for hydrophilic interaction liquid chromatography due to its appealing selectivity, high chemical compatibility, pH stability, temperature resistivity, and mechanical strength. The surface chemistry of highly hydrophobic carbon was modified with a benzene carboxylate moiety using diazonium chemistry. This modification converted the reversed phase PGC into a HILIC phase. The carboxylate-PGC demonstrated a selectivity that is different from that of 35 other columns with an additional advantage of retaining hydrophobic compounds. The effectiveness of the carboxylate-PGC column under high pH conditions was also demonstrated. The diazonium modification approach employing a hydrophilic functional group yielded the first example of HILIC on modified porous graphitic carbon, thus opening a new avenue of selectivity on robust stationary phases.

6.5 References

- [1] A.J. Alpert, *J. Chromatogr.* **1990**, *499*, 177-196.
- [2] S. Di Palma, P.J. Boersema, A.J.R. Heck, S. Mohammed, *Anal. Chem.* **2011**, *83*, 3440-3447.
- [3] M.E.A. Ibrahim, C.A. Lucy, In *Chapter 2: Stationary Phases for HILIC; Hydrophilic Interaction Chromatography: A Guide for Practitioners*, B.A. Olsen, B.W. Pack (Eds.), John Wiley & Sons Inc., 2013, pp. 43-85.
- [4] C. Wang, C. Jiang, D.W. Armstrong, *J. Sep. Sci.* **2008**, *31*, 1980-1990.
- [5] D.W. Armstrong, H.L. Jin, *J. Chromatogr. A* **1989**, *462*, 219-232.

- [6] N.P. Dinh, T. Jonsson, K. Irgum, *J. Chromatogr. A* **2011**, *1218*, 5880-5891.
- [7] P. Hemström, K. Irgum, *J. Sep. Sci.* **2006**, *29*, 1784-1821.
- [8] H. Qiu, E. Wanigasekara, Y. Zhang, T. Tran, D.W. Armstrong, *J. Chromatogr. A* **2011**, *1218*, 8075-8082.
- [9] D. Gétaz, M. Gencoglu, N. Forrer, M. Morbidelli, *J. Chromatogr. A* **2010**, *1217*, 3531-3537.
- [10] B. Ells, Y. Wang, F.F. Cantwell, *J. Chromatogr. A* **1999**, *835*, 3-18.
- [11] J.H. Knox, B. Kaur, G.R. Millward, *J. Chromatogr.* **1986**, *352*, 3-25.
- [12] A. Tornkvist, K.E. Markides, L. Nyholm, *Analyst* **2003**, *128*, 844-848.
- [13] E. Forgács, *J. Chromatogr. A* **2002**, *975*, 229-243.
- [14] S. Mazan, G. Crétier, N. Gilon, J.M. Mermet, J.L. Rocca, *Anal. Chem.* **2002**, *74*, 1281-1287.
- [15] M. Pabst, J. Grass, R. Fischl, R. Léonard, C. Jin, G. Hinterkorn, N. Borth, F. Altmann, *Anal. Chem.* **2010**, *82*, 9782-9788.
- [16] C.W. Reid, J. Stupak, C.M. Szymanski, J. Li, *Anal. Chem.* **2009**, *81*, 8472-8478.
- [17] J.H. Knox, P. Ross, *Carbon-based packing materials for liquid chromatography—Structure, performance, and retention mechanisms*, *Adv. Chromatogr.* (Boca Raton, FL, USA), Marcel Dekker Inc., New York, 1997.
- [18] M.C. Hennion, V. Coquart, S. Guenu, C. Sella, *J. Chromatogr. A* **1995**, *712*, 287-301.
- [19] C. West, C. Elfakir, M. Lafosse, *J. Chromatogr. A* **2010**, *1217*, 3201-3216.
- [20] L. Pereira, *LCGC North Am.* **2011**, *29*, 262-269.

- [21] J.H. Knox, Q.H. Wan, *Chromatographia* **1996**, *42*, 83-88.
- [22] N. Zhang, L.Y. Wang, H. Liu, Q.K. Cai, *Surf. Interface Anal.* **2008**, *40*, 1190-1194.
- [23] H.P. Boehm, W. Heck, R. Sappok, E. Diehl, *Angew. Chem., Int. Ed. Engl.* **1964**, *3*, 669-677.
- [24] J.A. Harnisch, D.B. Gazda, J.W. Anderegg, M.D. Porter, *Anal. Chem.* **2001**, *73*, 3954-3959.
- [25] J.L. Bahr, J.P. Yang, D.V. Kosynkin, M.J. Bronikowski, R.E. Smalley, J.M. Tour, *J. Am. Chem. Soc.* **2001**, *123*, 6536-6542.
- [26] M. Delamar, R. Hitmi, J. Pinson, J.M. Saveant, *J. Am. Chem. Soc.* **1992**, *114*, 5883-5884.
- [27] M.F. Wahab, C.A. Pohl, C.A. Lucy, *Analyst* **2011**, *136*, 3113-3120.
- [28] S.D. Chambers, M.T. McDermott, C.A. Lucy, *Analyst* **2009**, *134*, 2273-2280.
- [29] H. Ganegoda, D.S. Jensen, D. Olive, L. Cheng, C.U. Segre, M.R. Linford, J. Terry, *J. Appl. Phys.* **2012**, *111*, 053705.
- [30] D.S. Jensen, V. Gupta, R.E. Olsen, A.T. Miller, R.C. Davis, D.H. Ess, Z. Zhu, M.A. Vail, A.E. Dadson, M.R. Linford, *J. Chromatogr. A* **2011**, *1218*, 8362-8369.
- [31] M.E.A. Ibrahim, Y. Liu, C.A. Lucy, *J. Chromatogr. A* **2012**, *1260*, 126-131.
- [32] M.F. Wahab, C.A. Pohl, C.A. Lucy, *J. Chromatogr. A* **2012**, *1270*, 139-146.
- [33] W. Bicker, J.Y. Wu, M. Lammerhofer, W. Lindner, *J. Sep. Sci.* **2008**, *31*, 2971-2987.
- [34] N.P. Dinh, T. Jonsson, K. Irgum, *J. Chromatogr. A* **2013**, (in press).

- [35] M.R. Linford, D. Jensen, L. Yang, L. Wiest, *Functionalized graphitic stationary phase and methods for making and using same*, Brigham Young University, USA . USA Patent, 2010, pp. 40.
- [36] A. Rieker, *Industrie Chimique Belge-Belgische Chemische Industrie* **1971**, 36, 1078.
- [37] J.B. Hendrickson, *J. Am. Chem. Soc.* **1961**, 83, 1251-1251.
- [38] J.M. Englert, C. Dotzer, G.A. Yang, M. Schmid, C. Papp, J.M. Gottfried, H.P. Steinruck, E. Spiecker, F. Hauke, A. Hirsch, *Nature Chem.* **2011**, 3, 279-286.
- [39] W. Jiang, G. Fischer, Y. Girmay, K. Irgum, *J. Chromatogr. A* **2006**, 1127, 82-91.
- [40] A.P. Parker, P.A. Reynolds, A.L. Lewis, L. Kirkwood, L.G. Hughes, *Colloids and Surfaces B.* **2005**, 46, 204-217.
- [41] R.L. McCreery, *Chem. Rev.* **2008**, 108, 2646-2687.
- [42] S. Kundu, Y. Wang, W. Xia, M. Muhler, *J. Phys. Chem. C* **2008**, 112, 16869-16878.
- [43] Y.C. Liu, R.L. McCreery, *J. Am. Chem. Soc.* **1995**, 117, 11254-11259.
- [44] P.A. Brooksby, A.J. Downard, *Langmuir* **2004**, 20, 5038-5045.
- [45] S. Baranton, D. Belanger, *J. Phys. Chem. B* **2005**, 109, 24401-24410.
- [46] A. Tornkvist, *Aspects of Porous Graphitic Carbon as Packing Material in Capillary Liquid Chromatography*, PhD thesis, **2003**.
- [47] A.J. Alpert, *Anal. Chem.* **2008**, 80, 62-76.
- [48] J.L. Glajch, J.J. Kirkland, *Anal. Chem.* **1983**, 55, 319A-336A.

- [49] D.M. Packwood, P.A. Brooksby, A.D. Abell, A.J. Downard, *Aust. J. Chem.* **2011**, *64*, 122-126.
- [50] B. Sridhar, J.B. Nanubolu, K. Ravikumar, *CrystEngComm* **2012**, *14*, 7065-7074.
- [51] Y. Guo, S. Gaiki, *J. Chromatogr. A* **2005**, *1074*, 71-80.
- [52] Y. Guo, In *Chapter 17: Retention and Selectivity of Polar Stationary Phases for Hydrophilic Interaction Chromatography; Hydrophilic Interaction Liquid Chromatography (HILIC) and Advanced Applications*, CRC Press, 2011, pp. 401-426.
- [53] S. Bieri, E. Varesio, O. Munoz, J.L. Veuthey, P. Christen, *J. Pharm. Biomed. Anal.* **2006**, *40*, 545-551.
- [54] J.C. Reepmeyer, J.F. Brower, H.P. Ye, *J. Chromatogr. A* **2005**, *1083*, 42-51.
- [55] J.Y. Liu, L. Cheng, B.F. Li, S.J. Dong, *Langmuir* **2000**, *16*, 7471-7476.
- [56] C. Saby, B. Ortiz, G.Y. Champagne, D. Belanger, *Langmuir* **1997**, *13*, 6805-6813.
- [57] http://www.dionex.com/en-us/webdocs/65840-DS_Acclaim_Mixed_Mode_WCX-1_21Feb08_LPN2024.pdf (accessed in April 2013).
- [58] SciFinder Scholar, version 2006; Chemical Abstracts Service: Columbus, OH, 2006; RN 50-78-2.
- [59] J. Xing, A. Apedo, A. Tymiak, N. Zhao, *Rapid Commun. Mass Spectrom.* **2004**, *18*, 1599-1606.

[60] S.W. Pettersson, E. Collet, U. Andersson, *J. Chromatogr. A* **2007**, *1142*, 93-97.

CHAPTER SEVEN: Hybrid Carbon Nanoparticles Modified Core-Shell

Silica: A High Efficiency Carbon-Based Phase for Hydrophilic Interaction

Liquid Chromatography*

7.1 Introduction

Many biological compounds are hydrophilic molecules bearing amino, hydroxyl, or carboxylate functionalities. These polar analytes may be weakly retained in reversed phase liquid chromatography (RPLC). In recent years, the usage of hydrophilic interaction liquid chromatography (HILIC) has increased dramatically [1-3], as HILIC can retain highly polar compounds [1]. Polar stationary phases and organic rich mobile phases are employed in HILIC [1, 3] for the separation of hydrophilic analytes such as amino acids [4-6], nucleotides [4, 6, 7] and carbohydrates [8, 9]. An additional attractive feature is that the organic rich mobile phases are mass spectrometry friendly [10]. The low viscosity of the organic rich eluents also enhances solute diffusivity which improves the mass transfer kinetics, leading to faster high efficiency separations in HILIC mode [11].

Under HILIC conditions, a water rich layer is said to form on the surface of the HILIC packing into which the analyte partitions [3, 12]. The presence of this water layer has recently been confirmed by Dinh *et al.* using Karl Fisher titrations [13]. In addition to partitioning, other interactions have been shown to

*A version of this chapter has been submitted for publication in *Analytica Chimica Acta* by Mohammed E. A. Ibrahim¹, M. Farooq Wahab², and Charles A. Lucy.

¹Mohammed E. A. Ibrahim did the experiments needed for the chromatographic characterization of the stationary phase and wrote the manuscript.

²M. Farooq Wahab synthesized and physically characterized the stationary phase by elemental, XPS and TGA analyses.

be involved in HILIC retention, including H-bonding [14, 15], ion exchange [16, 17], adsorption [18] and dipole-dipole interactions [17].

Currently, the majority of commercial HILIC phases are silica based [19]. Silica-based HILIC stationary phases can be classified by their chemical nature as neutral (*e.g.* amide and diol), positively charged (*e.g.* amine and triazole) and negatively charged phases (*e.g.* polysuccinimide and bare silica) [19]. Alternately, silica phases may be classified morphologically as totally porous, superficially porous (often called core-shell) and monolithic silica. Core-shell silica particles consist of a solid core (2.2-5 μm) and an outer porous shell (0.2-0.6 μm) [20]. Until recently, fast and high efficiency separations in few minutes were offered by ultra-high performance liquid chromatography (UHPLC) employing high pressure pumps (>10,000 psi) and sub-2 micron particles. With their availability, core-shell silica particles offer the same high efficiency at much lower backpressures [11]. Thus, core-shell silica particles can be used on a conventional HPLC system to achieve the high efficiency of UHPLC. However, changing the particle morphology does not change the surface chemistry. Therefore the selectivity of core-shell silica particles remains similar to that of the totally porous silica particles [20].

Recently, we introduced a new class of carbon-based HILIC phases [4]. Porous graphitic carbon (PGC) is a very hydrophobic material, suitable for RPLC purposes [21, 22]. We showed that porous graphitic carbon modified with benzene carboxylate groups (carboxylate-PGC) exhibits strong HILIC character with a different selectivity from that of either silica or polymer stationary phases

[4]. The HILIC behavior of the carboxylate-PGC was illustrated by the separation of model hydrophilic analytes such as phenols, carboxylic acids, amino acids and nucleotides [4]. Unfortunately, PGC generally exhibits lower efficiencies than silica phases due to its slow mass transfer properties [23]. The attractive selectivity of carboxylate modified carbon gives an impetus to develop phases that carry the best properties of core-shell silica (high efficiency) and carbon (unique retention properties) phases.

Many hybrid stationary phases have been developed on inorganic oxides clad in monolayers of carbon such as carbon clad zirconia [24], carbon clad alumina [25] and carbon clad silica [26]. These hybrid phases were developed by a complex procedure of vapor deposition of carbon at high temperature. More recently, vapor deposition of carbon has been used to create a carbon clad core-shell silica (2.7 μm) phase [27].

In this work, we develop a hybrid HILIC phase consisting of core-shell silica particles onto which carbon nanoparticles have been anchored (Figure 7.1). First, the core-shell silica particles are modified *via* attaching cationic latex nanoparticles to impart a positive charge to the silica surface. Carbon nanoparticles are made negatively charged by introduction of benzene carboxylate groups to their surface through diazonium chemistry as reported previously [4]. The anionic carbon nanoparticles are electrostatically adsorbed onto the positively charged latexed silica particles. As will be demonstrated, such electrostatic interactions are very stable under HILIC conditions. The hybrid carbon-fused core

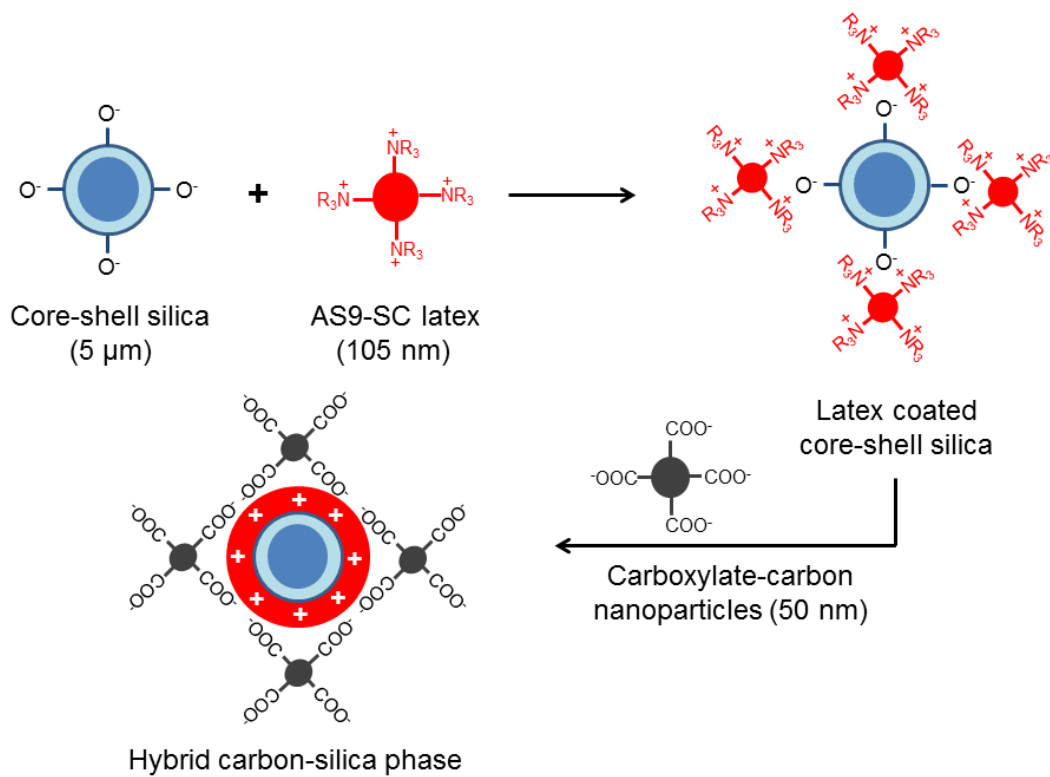


Figure 7.1 Schematic for the preparation of the hybrid carbon-silica phase.

silica phase exhibits high efficiency and distinct selectivities for the separation of carboxylates, phenols, and pharmaceuticals.

7.2 Experimental

7.2.1 Apparatus

The HPLC system consists of: a model 709 dual-piston pump (Metrohm, Herisau, Switzerland); a 6-port Rheodyne 8125 (Cotati, CA, USA) with a 2 μ L loop; and a Lambda-Max Model 481 UV detector (Waters, Milford, MA, USA) at 240 or 254 nm. Connecting tubes were made of polyether ether ketone (PEEK). Data was collected at 20 Hz using a Dionex advanced computer interface with Dionex PeakNet 5.2 software. The eluent consists of ammonium acetate buffer, ACN and water. The pH was adjusted with either NaOH or HCl. The eluents were degassed by sonication in a VWR[®] sonicator (Radnor, PA, USA) for 10 min. The reported buffer strength is the final concentration in the eluent after mixing with ACN. The reported %ACN stands for the volume of the ACN relative to the total volume of the eluent.

7.2.2 Materials

Carbon graphite nanopowder (99.5%, average particle size ~ 50 nm, Lot # 1173992379-249) was purchased from American Elements (Los Angeles, CA, USA). Core-shell bare silica particles were a gift of Phenomenex (5 μ m, Lot # Bulk_Beta_01, Torrance, CA, USA). AS9-SC latex nanoparticles with quaternary ammonium functionalities (105 nm in diameter, Lot # 025-07-042), ultra-high

molecular weight polyethylene (UHMWPE) frits, 2 μm Ti and stainless steel frits, Zitex membranes and empty PEEK columns (100 x 4 mm i.d.) were gifts of Thermo Fisher Scientific (Sunnyvale, CA, USA). Deionized water was obtained from a Barnstead E-pure system (Barnstead, Dubuque, IA, USA). Sodium nitrite ReagentPlusTM, 4-aminobenzoic acid, 50% sodium hydroxide, uracil, cytosine, 1-naphthoic acid, acetylsalicylic acid (ASA, Aspirin), gentisic acid, α -hydroxyhippuric acid, hippuric acid, salicylic acid, benzoic acid, resorcinol and acetaminophen were from Sigma Aldrich (St. Louis, MO, USA). Phthalic acid, isophthalic acid and 2-naphthoic acid were from Aldrich (Milwaukee, WI, USA). Hydrochloric acid (37% w/w) and potassium hydroxide were from Caledon Laboratory Chemicals (Georgetown, ON, Canada). Sodium borohydride was purchased from EMD Chemicals (Gibbstown, NJ, USA). HPLC grade acetonitrile (ACN), HPLC grade ammonium acetate, naphthalene, salicylic acid and methyl salicylate were from Fisher Scientific (Fairlawn, NJ, USA). Benzyltrimethylammonium (BTMA) chloride was from ACROS Organics (Fair Lawn, NJ, USA). Phenol (ACS reagent, 99%) was purchased from ACP (Montreal, QC, Canada) and phloroglucinol (> 99 %) was from Fluka (Buchs, Switzerland).

7.2.3 Preparation of the Hybrid Carbon-Silica Stationary Phase

7.2.3.1 Synthesis of Carboxylate Modified Carbon Nanoparticles

(Carboxylate-Carbon)

1.5 g of carbon nanopowder was mixed with 40 mmol (5.49 g) of 4-aminobenzoic acid in a 50 mL of deionized water and stirred over crushed ice for

20 min. Then, 40 mmol (2.77 g dissolved in 50 mL of deionized water) of NaNO₂ was quickly added and stirred for 10 min. After stirring, 33 mL conc. HCl were added and mixed by magnetic bar stirring for 30 min followed by the addition of 100 mmol (3.79 g dissolved in 50 mL of deionized water) of sodium borohydride over 15 min (*Caution: Significant foaming occurs while adding sodium borohydride. Slow addition is recommended*). The mixture was filtered using a 0.22 μm nylon filter, and then thoroughly washed with deionized water, 1% KOH, ACN, and then > 4 L of deionized water. The particles were dried and stored in a desiccator until used. Characterization of the modified carbon nanoparticles is discussed in Section 7.2.4.

7.2.3.2 Coating of Core-Shell Silica with Latex Nanoparticles (Latex Coated Core-Shell Silica)

As shown in Figure 7.1, to anchor the negatively charged carbon nanoparticles to the silica surface, the silica surface must bear a positive charge. This was accomplished by coating the core-shell silica with cationic AS9-SC latex nanoparticles (105 nm, Thermo Fisher Scientific) bearing quaternary ammonium groups. A 10% v/v solution of the latex was prepared in 200 mL of deionized water. Core-shell silica particles (4 g) were mixed with the latex solution and stirred for 30 min. After the latexing, the particles were washed thoroughly with deionized water and ACN. The material was vacuum dried on a filtration assembly for 24 min.

7.2.3.3 Modification of Latex Coated Core-Shell Silica with Carboxylate-Carbon (Hybrid Carbon-Silica Phase)

The damp latexed core-shell silica was mixed with 0.1 g of the carboxylate-carbon in 200 mL of deionized water and stirred for 30 min. Visually, particles with adsorbed carboxylate-carbon appear grey and settle from water. Uncoated silica remains white and suspended. After filtration, the procedure was repeated with an additional 0.1 g of the carboxylate-carbon, followed by washing with ACN and water. After two exposures, most particles were gray-black and settled from solution.

7.2.3.4 Column Packing Procedure

Bare core-shell silica, AS9-SC latex coated core-shell silica and hybrid carbon-silica phases were packed in the same way. A 3 g portion of the particles was slurried in 35 mL of deionized water and transferred into a 40 mL stainless steel slurry reservoir (Lab Alliance, State College, PA, USA). The remaining 5 mL of the final rinse from the container was added to the reservoir to remove any empty air space in the slurry reservoir. A 100 x 4.0 mm i.d. PEEK empty column with a Ti outlet frit was connected to the bottom of the slurry reservoir. The particles were packed at constant pressure (5000 psi) using a Haskel pneumatic pump (DSF-122-87153, Burbank, CA, USA) for 1.5 h in the downward direction. Water was used as the driving solvent. The column was then detached from the packing assembly. Finally, the PEEK screw caps with UHMWPE frits and Zitex membranes were installed on both ends.

7.2.4 Characterization of the Carbon-Silica Hybrid Phase

X-ray photoelectron spectroscopy (XPS) spectra were measured using an AXIS 165 spectrometer (Kratos Analytical, NY, USA). XPS spectra of the unmodified carbon nanoparticles and core-shell silica particles were collected on the raw materials as received without any treatment. The hybrid carbon-silica particles and the latexed core-shell particles were thoroughly washed with deionized water and ACN. The carboxylate modified carbon nanoparticles were washed with 1% KOH, deionized water and ACN. After washing, the particles were allowed to vacuum dry for 3 days prior to XPS analysis at room temperature. The CHN analysis was performed on a Carlo-Erba (EA1108, Milan, Italy) elemental analyzer. Thermogravimetric (TGA) studies were collected on a Perkin Elmer TGA analyzer (Norwalk, CT, USA) using oxygen atmosphere from ambient temperature to 900 °C at 10 °C/min.

7.2.5 Efficiency Calculations

Column efficiencies were calculated using the half-peak width method (Equation 1.6, Chapter 1) and corrected for extra-column band broadening [28]. Correction for the extra-column band broadening for the van Deemter plot (Figure 7.9) was performed as follows:

The efficiency of a Gaussian peak is defined as:

$$N_{obs} = \frac{t^2}{\sigma_{obs}^2} \quad (\text{Equation 7.1})$$

where N_{obs} is the observed efficiency, t is the retention time and σ_{obs}^2 is the observed peak variance. The observed peak variance includes the band

broadening contribution from the column and other components from the injector port to the detector cell. A van Deemter plot should have these extra-column effects removed from the system.

The extra-column band broadening was subtracted by removing the column and connecting the injection port directly to the detector by a zero dead volume connector. The peak widths at baseline ($4\sigma_{extra\ col}$) were determined by tangent method and converted into σ_{extra} (in min) by dividing by 4.

The corrected peak variance σ_{corr} was calculated as follows:

$$\sigma_{corr}^2 = \sigma_{obs}^2 - \sigma_{extra\ col}^2 \quad (\text{Equation 7.2})$$

Finally, N_{corr} was calculated using the σ_{corr}^2 in the efficiency equation as follows:

$$N_{corr} = \frac{t^2}{\sigma_{corr}^2} \quad (\text{Equation 7.3})$$

7.3 Results and Discussion

The aim of this work is to design a novel hybrid carbon-silica phase for high efficiency HILIC separations with a new selectivity. Typically, carbon phases show lower efficiencies than silica due to slow mass transfer kinetics [23]; however the unique selectivity of carbon makes it a powerful chromatographic phase for difficult separations. The newly developed hybrid phase combines the high efficiency of the core-shell silica support and the unique selectivity of carbon. Figure 7.1 schematically represents the preparation of the hybrid carbon-silica phase. In Figure 7.1, core-shell silica particles (5 μm in diameter) are

modified *via* electrostatic attachment of cationic latex particles (105 nm in diameter). This electrostatic attraction between the negatively charged silanols and the cationic latex nanoparticles is stable under HILIC eluent conditions [6]. Simultaneously, carbon nanoparticles (50 nm in diameter) are carboxylated *via* diazonium chemistry [4] to make the carbon surface anionic. The anionic carboxylate modified carbon nanoparticles electrostatically adsorb onto the cationic latex modified silica surface to yield the hybrid carbon-silica phase shown in Figure 7.1.

7.3.1 Physical Characterization of the Hybrid Carbon-Silica Phase

The various materials in Figure 7.1 including the hybrid carbon-silica phase were characterized by both bulk (CHN elemental analysis and TGA) and surface analysis (XPS) techniques (Tables 7.1 and 7.2 and Figures 7.2 and 7.3). Elemental analysis (Table 7.1) shows that the carboxylated carbon particles exhibit mostly the same carbon content as the unmodified carbon since the functionalization is restricted to the surface. XPS revealed that surface concentration of oxygen changes from 4.4 ± 0.2 to 5.0 ± 0.5 atomic % O. The O/C ratio changes from 0.0468 ± 0.002 to 0.0531 ± 0.006 after modification. The carboxylate-carbon nanoparticles are thermally stable up to 400 °C indicating the absence of adsorbed benzoic acid (boiling point ~ 250 °C [29]) and other adsorbed reaction side products (Figure 7.2).

The amount of carbon in the unmodified core-shell silica particles was below the detection limit of elemental analysis (<0.2% w/w). However, XPS of

Table 7.1 Bulk composition analysis of the materials employed in the synthesis of the hybrid carbon-silica phase

Sample Name^a	% w/w Carbon	% w/w Nitrogen^b	% w/w Hydrogen
Unmodified carbon	98.3	-	-
Carboxylate-carbon	98.7	-	-
Bare core-shell silica	< 0.2	-	0.194
AS9-SC coated core-shell silica	0.865	< 0.1	0.337
Hybrid carbon-silica (column material)	5.43	< 0.1	0.281

^a All analyses were performed in duplicate. The percent relative standard deviations (n=2) for the elemental analyses are 0.02-0.9 for carbon, 1.8-5.2 for nitrogen, and 1.6-6.2 for hydrogen.

^b Nitrogen peaks were detectable in the elemental analysis; however the quantity was below the calibration points.

Table 7.2 Average XPS surface composition of the materials employed in the synthesis of the hybrid carbon-silica phase in atomic percentages

Sample Name *	Si %	C %	N %	O %
Unmodified carbon (n=2)	0.53	94.8	-	4.44
Carboxylate-carbon (n=3)	0.18	94.4	-	5.01
Bare core-shell silica (n=1)	29.2	3.99	-	66.8
AS9-SC coated core-shell silica (n=1)	17.1	33.2	1.58	47.4
Hybrid carbon-silica (column material) (n=2)	16.6	35.5	1.33	45.7

* n is the number of replicates. The percent relative standard deviations by XPS analysis are 0.04-0.7 for carbon, 0.5-10.6 for oxygen and 0.5 for nitrogen.

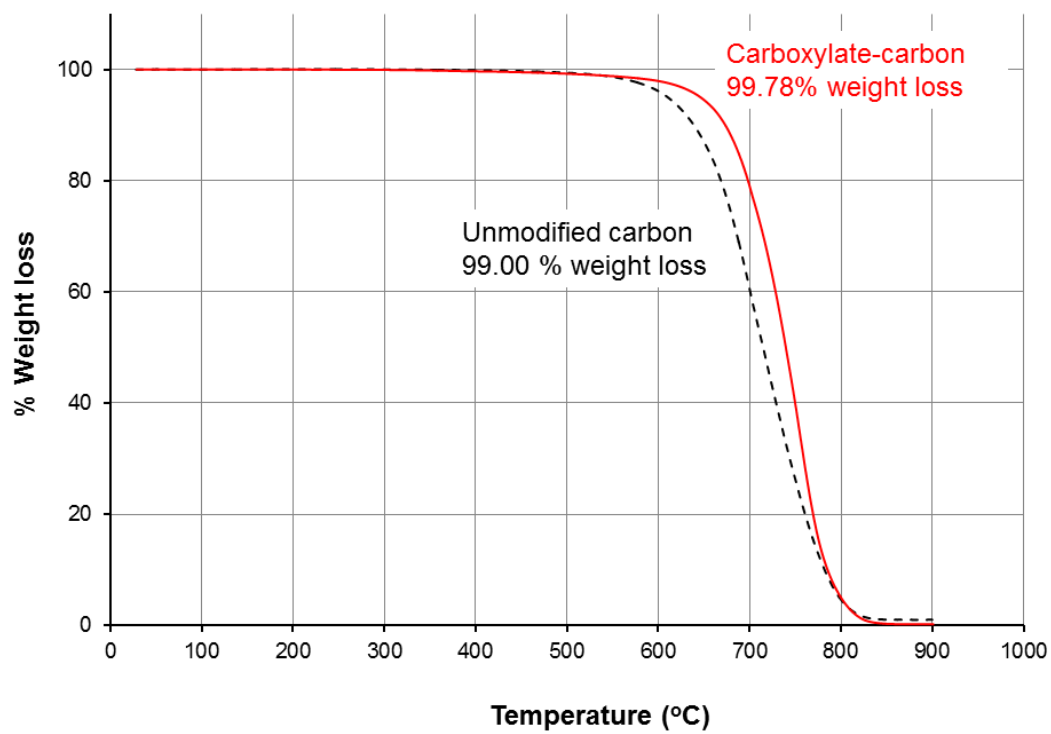


Figure 7.2 Thermogravimetry curves in oxygen atmosphere of the unmodified carbon (---) and carboxylate-carbon nanoparticles (—).

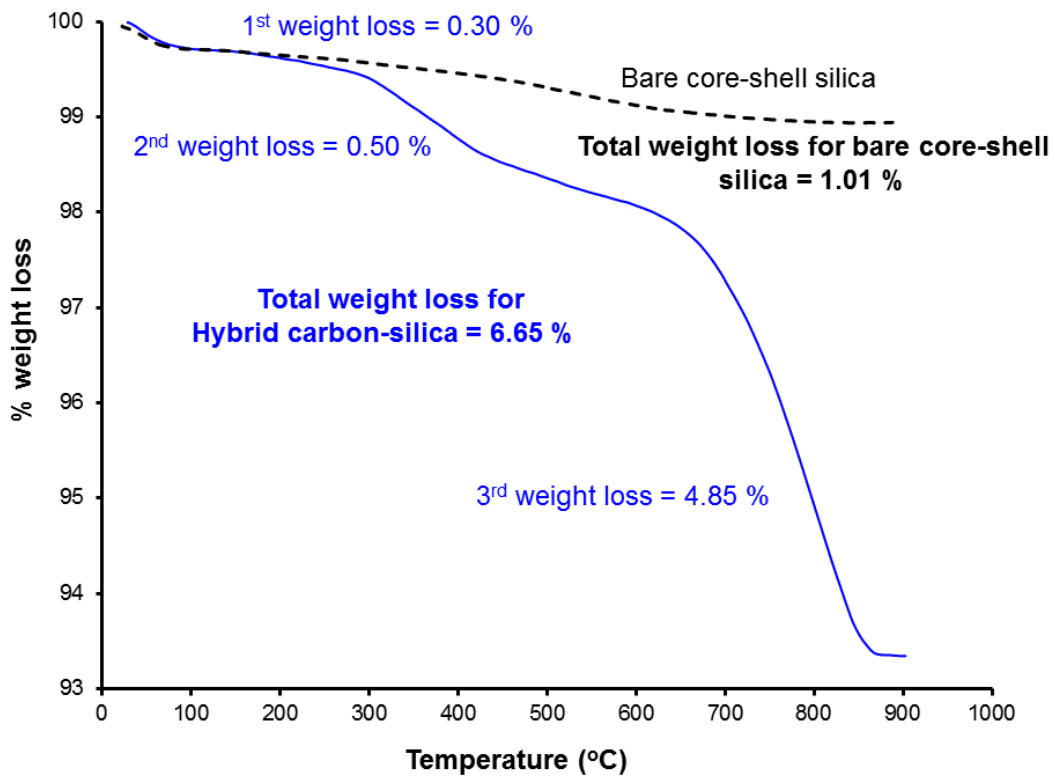


Figure 7.3 Thermogravimetry curves in oxygen atmosphere of the bare core-shell silica (---) and hybrid carbon-silica phase (—) material.

the unmodified core-shell silica showed traces of surface carbon (4.0%) and no nitrogen (Table 7.2). Adsorption of the cationic AS9-SC latex increased the carbon and nitrogen surface concentrations to 33.2 atomic % C and 1.58 atomic % N, respectively. These signals arise from the methacrylate backbone of the latex and their quaternary amine functionality, respectively. The Si measured by XPS decreases from 29.2 to 17.1 atomic %, indicating surface coverage of the silica by the AS9-SC latex nanoparticles. Elemental analysis of the AS9-SC latex coated core-shell silica particles showed similar trends (Table 7.1).

After mixing the AS9-SC latex coated core-shell silica with the modified carbon nanoparticles, the carbon load on the particles increased from 0.865 to 5.43 % w/w (Table 7.1). The carbon load on typical RPLC and HILIC Halo core-shell silica particles ranges from 3.5 to 8.2 % w/w [30]. Carbon clad core-shell silica phases, created by vapor deposition process, have up to 7 % w/w carbon load [27]. From the XPS data (Table 7.2), the surface concentration of carbon increased from 33.2 to 35.5 atomic % C. The surface % N decreased from 1.58 % to 1.33 %, indicating that the latex AS9-SC coated core-shell silica is covered by the carbon nanoparticles. Similarly the surface % Si decreased, supporting that a coating of carboxylate modified carbon nanoparticles exists on the surface. Finally, a simple test of the hydrophilicity of a phase is how well it disperses in water. The hybrid carbon-silica particles created in the manner depicted in Figure 7.1 were highly dispersible in water. This indicates that the phase is highly hydrophilic, and thus suitable as a HILIC phase [4].

7.3.2 HILIC Properties of the Hybrid Phase

Mobile phases in HILIC usually are mixtures of ACN and water. Water is considered the strongest eluent in HILIC mode [12]. As a consequence, HILIC stationary phases show increased retention for hydrophilic analytes as the %ACN in the mobile phase increases [3, 4]. Figure 7.4 shows the effect of %ACN on the retention of two hydrophilic markers (benzoate and uracil) under HILIC conditions. The attachment of carboxylate modified carbon to the silica surface has enhanced the HILIC properties of the stationary phase. At 90% ACN, the retention factors (k) of both benzoate and uracil on the hybrid phase have increased by 1.5 fold relative to the bare core-shell silica phase. This HILIC enhancement is consistent with the strong hydrophilic character of the recently developed carboxylate-PGC phase [4]. Even when using a strong HILIC eluent (65% ACN), benzoate is more retained on the hybrid HILIC phase ($k \sim 1.7$) than on the bare core-shell silica phase ($k \sim 0$). The weak retention of benzoate on the bare core-shell silica phase is due to the electrostatic repulsion between the deprotonated silanols (pK_a 4.5 [31]) and benzoate ($pK_a \sim 4.2$ [29]).

7.3.3 Selectivity of the Hybrid Carbon-Silica Phase

The selectivity factor (α) plays an important role in achieving optimum resolution (R_s) in chromatography. The development of new HILIC stationary phases with unique selectivity requires tools which can estimate and compare the selectivity of the new phase vs. other stationary phases. Recently, Ibrahim *et al.* constructed a simple and convenient selectivity plot to classify different HILIC

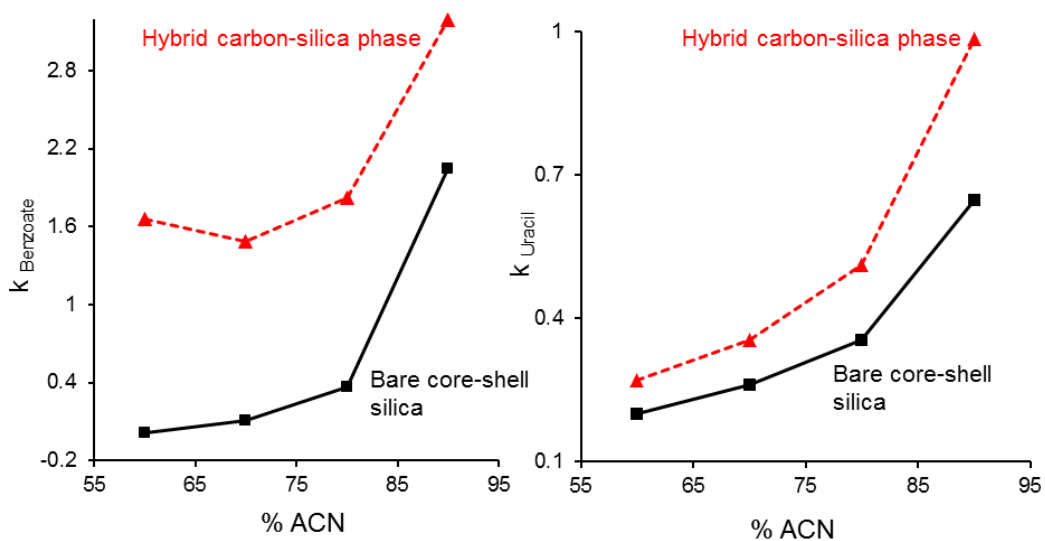


Figure 7.4. Effect of % ACN on the retention of benzoate and uracil on the hybrid carbon-silica phase under HILIC conditions. Conditions: columns, hybrid carbon-silica (▲) and bare core-shell silica (■) (100 × 4.0 mm i.d.); flow rate, 1.0 mL/min; eluent, 10 mM ammonium acetate, pH 6.1, in 60-90% ACN; analytes, 2 μ L injection of 0.2 mM benzoate and uracil in the same % ACN; UV detection at 254 nm. The chemical structures of the analytes are shown in Appendix I.

phases [15]. The HILIC selectivity plot (Figure 7.5) is a plot of the relative retention of BTMA and cytosine ($k_{\text{BTMA}}/k_{\text{cytosine}}$) vs. the relative retention of cytosine and uracil ($k_{\text{cytosine}}/k_{\text{uracil}}$). BTMA is cationic, and is moderately retained under HILIC conditions. It experiences electrostatic attraction with negatively charged columns (*e.g.* bare silica) which enhances its retention relative to a neutral hydrophilic compound such as cytosine. Similarly BTMA experiences repulsion from positively charged columns (*e.g.* amine columns) resulting in a decrease in its retention relative to cytosine. Consequently the relative retention of $k_{\text{BTMA}}/k_{\text{cytosine}}$ can be used as an indicator of the column's electrostatic character (whether attractive or repulsive). On the other hand, the ratio $k_{\text{cytosine}}/k_{\text{uracil}}$ has been suggested as a measure of the column hydrophilicity based on their difference in octanol/water partition coefficients [4, 17]. Using retention ratios rather than absolute retentions have the advantage of cancelling out other parameters affecting retention such as surface area and pore size [15].

Bare core-shell silica (column no. 34) clusters with other silica phases, since they share the same surface chemistry. Attaching AS9-SC latex nanoparticles on the core-shell silica does not significantly alter the selectivity, as the latex coated core-shell silica column (column no. 35) appears very close to the silica cluster in Figure 7.5. This is consistent with the selectivity observed for a silica monolith coated with the same type of latex (column no. 25) [15]. Coating the latexed core-shell silica with the carboxylate modified carbon nanoparticles results in an increase of the $k_{\text{cytosine}}/k_{\text{uracil}}$ ratio from 2.9 to 6.9 (*i.e.* > two-fold). This increased hydrophilicity for the hybrid carbon-silica phase correlates with

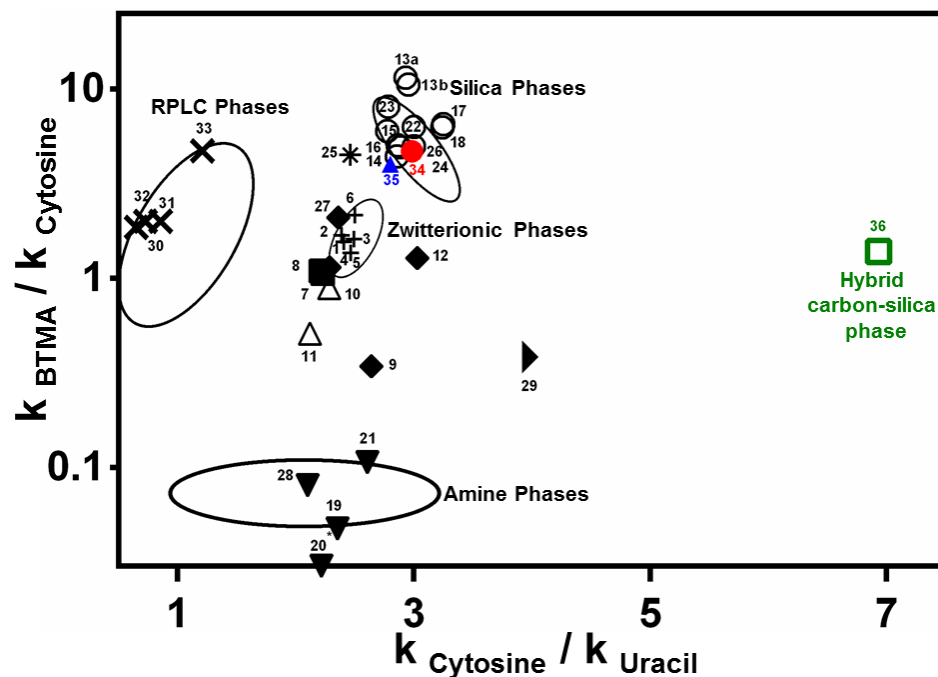


Figure 7.5 Selectivity plot of the hybrid carbon-silica phase vs. silica and polymer based- stationary phases (see Table 3.1, Chapter 3 for column names). Conditions: columns, Hybrid carbon-silica (\square), bare silica (\circ), bare core-shell silica (\bullet), amide (\blacksquare), diol (Δ), amine and/or triazole (\blacktriangledown), polymer substrate and/or polymer coated silica (\blacklozenge), zwitterionic ($+$), RPLC (\times), latex coated silica monolith ($*$), latex coated core-shell silica (\blacktriangle), proprietary polar phase (\blacktriangleright); eluent, 5 mM ammonium acetate, pH 6.8, in 80 % ACN; test analytes, 0.044-0.44 mM cytosine, uracil and BTMA in 80 % ACN; UV detection at 254 nm. The chemical structures of analytes are given in Appendix I. Figure is adapted from Reference [15].

the strong hydrophilic properties of the surface carboxylate-carbon nanoparticles [4]. As expected from a hybrid phase consisting of silica and modified carbon, the properties displayed by the hybrid stationary phase are intermediate between bare silica and carboxylated carbon phases. For instance, the relative retention $k_{\text{cytosine}}/k_{\text{uracil}}$ of bare core-shell silica and carboxylate modified carbon are 2.9 and 14.9 (data not shown) [4], respectively. The $k_{\text{cytosine}}/k_{\text{uracil}}$ of the hybrid phase is 6.9.

A key observation from Figure 7.5 is that the selectivity of the hybrid carbon-silica phase differs from 36 other stationary phases including bare core-shell silica (column no. 34) and carboxylate-PGC (not shown). Additionally since the hybrid carbon-silica phase contains both cationic latex and anionic carbon nanoparticles, its electrostatic character ($k_{\text{BTMA}}/k_{\text{cytosine}} \sim 1.4$) is similar to that of the zwitterionic phases ($k_{\text{BTMA}}/k_{\text{cytosine}} \sim 1.3-2.5$).

We also compared the selectivity of the hybrid carbon-silica phase with previously reported ten HILIC column chemistries for the separation of six aromatic carboxylic acids (salicylic acid, gentisic acid, acetylsalicylic acid, salicyluric acid, hippuric acid, and α -hydroxyhippuric acid) [32]. The elution order of the tested acids on the hybrid carbon-silica phase is completely different from all other column chemistries (Figure 7.6), including our pure carbon-based HILIC phase. The selectivity of the aromatic acids on the hybrid carbon-silica phase is similar to that of the AS9-SC latex coated core-shell silica column, except that the elution order of gentisic acid and salicyluric acid has interchanged. The strong retention of salicyluric acid on the hybrid phase is consistent with its

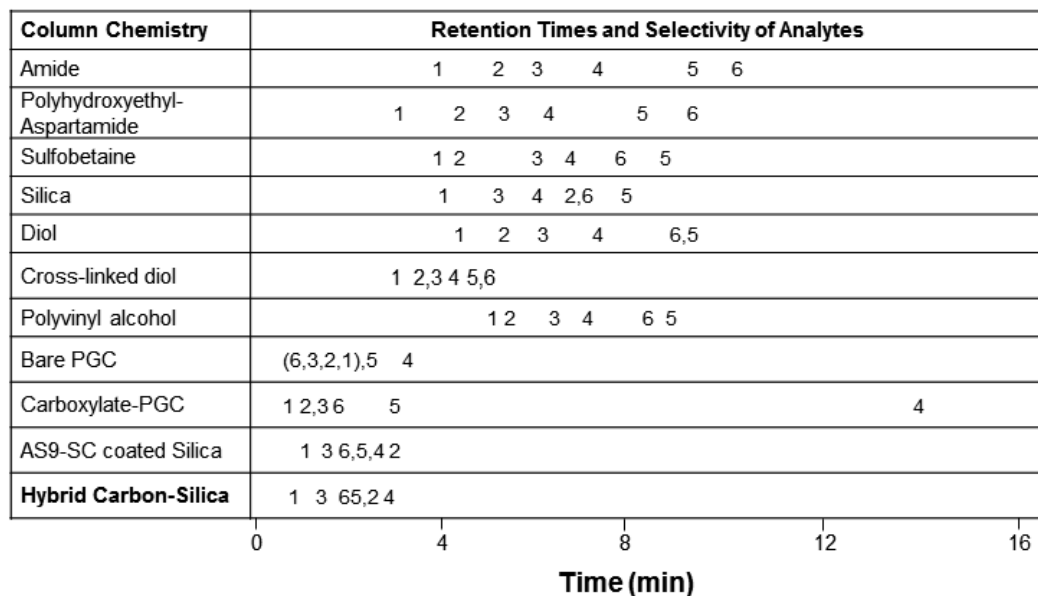


Figure 7.6 Selectivity of six aromatic acids on the hybrid carbon-silica phase vs. ten HILIC stationary phases. Analytes separated by commas co-elute. The positions of the peak numbers reflect the actual retention time of the analytes. Conditions: column, hybrid carbon-silica phase (100 × 4.0 mm i.d.); flow rate, 1.0 mL/min; eluent, 20 mM ammonium acetate (pH = 6.97) in 85% ACN; analytes, 2 µL injection of (1) salicylic acid, (2) gentisic acid, (3) acetylsalicylic acid, (4) salicylic acid, (5) hippuric acid, and (6) α-hydroxyhippuric acid. UV detection at 254 nm. The chemical structures of analytes are given in Appendix I. Figure is adapted from References [4, 32].

retention on the carboxylate-PGC phase [4]. This indicates that the carbon surface contributes to the unique selectivity offered by the hybrid carbon-silica phase.

7.3.4 Mixed Mode Behavior of the Hybrid Carbon-Silica Phase

A drawback of HILIC can be its weak retention of hydrophobic analytes [33] due to the very low hydrophobicity of most HILIC stationary phases. This makes the production of mixed mode HILIC/RPLC stationary phases very desirable [34-36]. The hybrid carbon-silica phase, with carbon attached to the highly hydrophilic latexed silica, is a suitable stationary phase for mixed mode HILIC/RPLC separations. Under HILIC mobile phase conditions (90% ACN in Figure 7.7(A)), the retention order of naphthalene and uracil correlates with the polarity of analytes, consistent with the HILIC theory. Retention of naphthalene and uracil is reversed when the % ACN is decreased to 50% (Figure 7.7(B)), indicating that the retention mode (HILIC vs. RPLC) can be manipulated, similar to other mixed mode stationary phases [34].

7.3.5 Isomeric Selectivity of the Hybrid Carbon-Silica Phase

The capability of carbon-based phases to separate isomers under typical RPLC conditions has been well known since the early days of chromatography [37-39]. Carbon stationary phases have been used to separate carbohydrate isomers [40], di-substituted benzene isomers [41] and alkylglycoside detergents [42] under RPLC conditions. Similarly, carboxylate-PGC was shown to have an

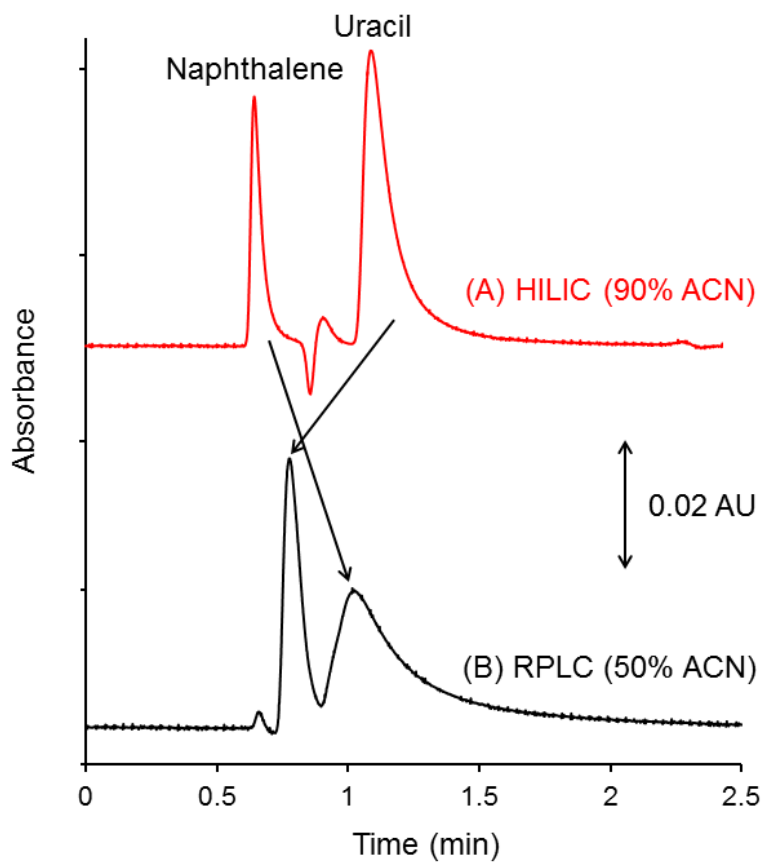


Figure 7.7 HILIC/RPLC mixed mode retention behavior of the hybrid carbon-silica phase. Conditions: column, hybrid carbon-silica (100 × 4.0 mm i.d.); flow rate, 1.0 mL/min; eluent, (A) HILIC mode: 10 mM ammonium acetate, pH 4.0, in 90% ACN, (B) RPLC mode: 10 mM ammonium acetate, pH 4.0, in 50% ACN; analytes, 2 μ L injection of 0.2 mM naphthalene and uracil in the same % ACN of the mobile phase; UV detection at 254 nm. The chemical structures of analytes are given in Appendix I.

isomeric selectivity (e.g. cytosine/ isocytosine and salicylic acid/ α -hydroxyhippuric acid pairs) [4].

In this work, acid isomers (e.g. phthalic/isophthalic acids and 1-naphthoic/2-naphthoic acids) co-eluted on bare core-shell silica under even the weakest HILIC conditions (e.g., 95% ACN, data not shown). Adsorption of latex nanoparticles converts the silica surface into an anion exchanger. Nonetheless, co-elution of the isomeric acids still occurs (Figure 7.8). This co-elution is attributed to weak ionization of these isomeric acids ($pK_a \sim 2.9-3.5$ [29]) at the working pH 2.3 which suppresses the ion exchange separations.

Attaching carbon nanoparticles onto latexed silica surface imparts an isomeric selectivity under HILIC conditions. Phthalic acid could be resolved from isophthalic acid ($R_s \sim 1.4$, Figure 7.8(A)), and 1-naphthoic and 2-naphthoic acids were partially resolved ($R_s \sim 0.8$, Figure 7.8(B)).

7.3.6 Efficiency of the Hybrid Carbon-Silica Phase

Core-shell silica particles show lower A and C terms as compared to totally porous particles of comparable diameter. The improved mass transfer (lower C term) is due to the smaller diffusion distance through the porous shell [11, 20]. The lower A term of core-shell particles results from their monodispersed particle size leading to a more uniform packing [43, 44]. Figure 7.9 compares the plate heights of the hybrid carbon-silica phase and a carbon-based HILIC phase. The hybrid carbon-silica phase yielded lower optimum

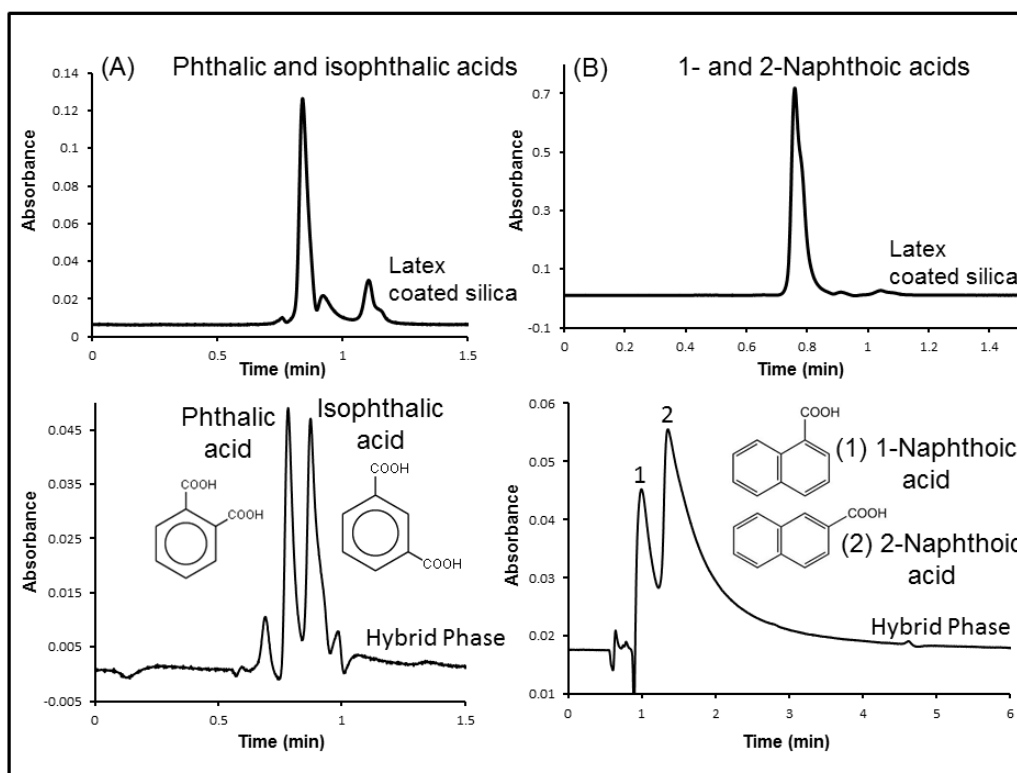


Figure 7.8 Isomeric separations on the hybrid carbon-silica phase. Conditions: column, hybrid carbon-silica (100 × 4.0 mm i.d.); flow rate, 1.0 mL/min; eluent, 5 mM ammonium acetate, pH 2.3, in 95% ACN; analytes, 2 μ L injection of 0.1 mM phthalic, isophthalic, 1-naphthoic and 2-naphthoic acids in 95 % ACN; UV detection at 240 nm.

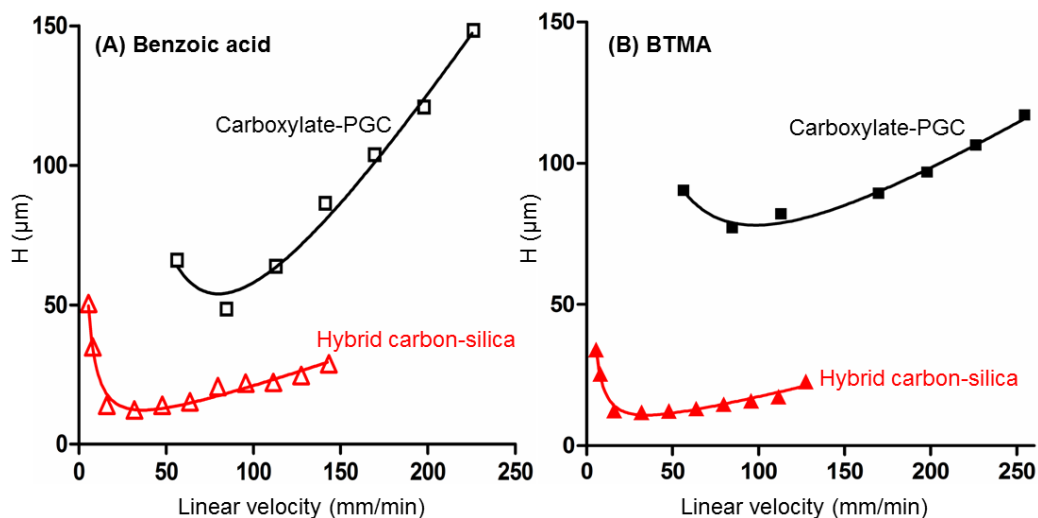


Figure 7.9 van Deemter plots for the hybrid carbon-silica and carboxylate-PGC columns. Conditions: column, hybrid carbon-silica (100 × 4.0 mm i.d.), carboxylate-PGC (150 × 3.0 mm i.d.); eluent, 25 mM ammonium acetate, pH 6.1, in 85% ACN; analytes, 2 μL injection of (A) 0.05 mM uracil and (B) 1 mM BTMA in 85% ACN; UV detection at 254 nm. A, B and C terms were calculated by fitting to van Deemter equation ($H = A + B/u + Cu$, where H is the plate height and u is the linear velocity of the eluent).

reduced plate heights (h) than the carboxylate-PGC column for both benzoic acid and BTMA. For instance, the hybrid HILIC phase achieved h of 1.9 which is about eight times lower than the carboxylate-PGC column ($h \sim 15.5$) for BTMA. This hybrid carbon-silica phase shows improved efficiency as compared to the recently developed carbon clad core-shell silica phase ($h \sim 2.5$) [27].

The hybrid carbon-silica phase shows faster mass transfer kinetics (C term ~ 0.025) vs. the carboxylate-PGC column (C term ~ 0.075). Improved eddy diffusion due to the narrow particle size distribution of core-shell particles [20] also contributes to the smaller h values (A term = 0.2 vs. 1.3 for the carboxylate-PGC).

7.3.7 HILIC Applications of the Hybrid Carbon-Silica Phase

Figure 7.10(A) shows the separation of a mixture of salicylic acid, acetylsalicylic acid, gentisic acid, α -hydroxyhippuric acid, salicyluric acid, and hippuric acid in less than 6 min on the hybrid carbon-silica phase. At pH 4.0, these acids (pK_a 3.01-3.71 [29]) are deprotonated and so would experience electrostatic repulsion from the anionic carbon surface (pK_a 2.8-3.1) [4]. This electrostatic repulsion hydrophilic interaction chromatography (ERLIC) behavior is similar to the retention behavior of carboxylic acids on a carboxylate-PGC column [4]. Peak efficiencies on the hybrid phase were 14,500-85,000 plates/m vs. 6,500 -13,000 plates/m [4] on a PGC-based HILIC phase.

Figure 7.10(B) shows a 2 min separation of phenol, resorcinol and phloroglucinol on the newly developed hybrid phase. The elution order is

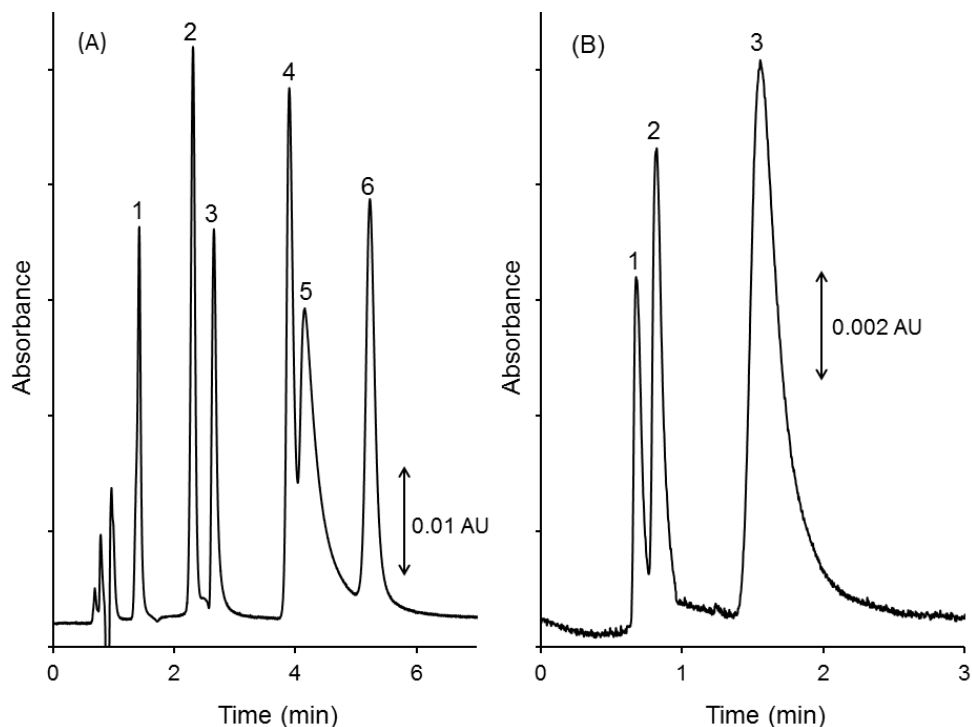


Figure 7.10 HILIC separations of (A) biological acids and (B) phenols on the hybrid carbon-silica phase. Conditions: column, hybrid carbon-silica (100 × 4.0 mm i.d.); flow rate, 1.0 mL/min; eluent, (A) 10 mM ammonium acetate, pH 4.0, in 90% ACN; (B) 5 mM ammonium acetate, pH 6.1, in 95% ACN; analytes, 2 μ L injection of (A) 0.2-1.0 mM of (1) salicylic acid, (2) acetylsalicylic acid (ASA), (3) gentisic acid, (4) α -hydroxyhippuric acid, (5) salicyluric acid, (6) hippuric acid in 90 % ACN; (B) 0.025-0.06 mM of (1) phenol, (2) resorcinol, (3) phloroglucinol; UV detection at (A) 254 nm, (B) 240 nm. The chemical structures of the analytes are shown in Appendix I.

consistent with the log (distribution coefficient) for the phenols at pH 6 (log $D_{\text{phenol}} = 1.54$, log $D_{\text{resorcinol}} = 0.82$ and log $D_{\text{phloroglucinol}} = 0.00$) [29]. This polarity dependent elution order is consistent with what is expected for HILIC mode [12], and is similar to that observed on a carboxylate-PGC column [4].

Core-shell silica particles enable high efficiency separations to be performed with larger particles which have inherently more permeable packed beds [11]. Additionally, backpressures are lower in HILIC due to the use of low viscosity organic rich mobile phases. The combination of core-shell packing and low viscosity eluents permits fast HILIC separations to be performed with low backpressure [11]. Figure 7.11 demonstrates a fast (<2 min) and highly efficient (13,400-80,500 plates/m) separation of four pain relief pharmaceuticals (methyl salicylate, acetaminophen, salicylic acid and aspirin) under HILIC conditions. The elution order of methyl salicylate, acetaminophen and salicylic acid follows the order predicted by the log D values (2.52, 0.48 and -1.06, respectively) [29]. The selectivity of acetaminophen, salicylic acid and aspirin offered by the hybrid carbon-silica phase is different from that achieved on the mixed mode Dionex Acclaim Wax-1 phase [45]. This different selectivity is attributed to the unique properties imparted by the surface carboxylate modified carbon nanoparticles.

7.3.8 Reproducibility and Stability of the Hybrid Carbon-Silica Phase

The separation of pain relief medicines was performed on two different columns packed with the hybrid carbon-silica material prepared from the same batch. Retention times differed by less than 2% (Figure 7.12) indicating the

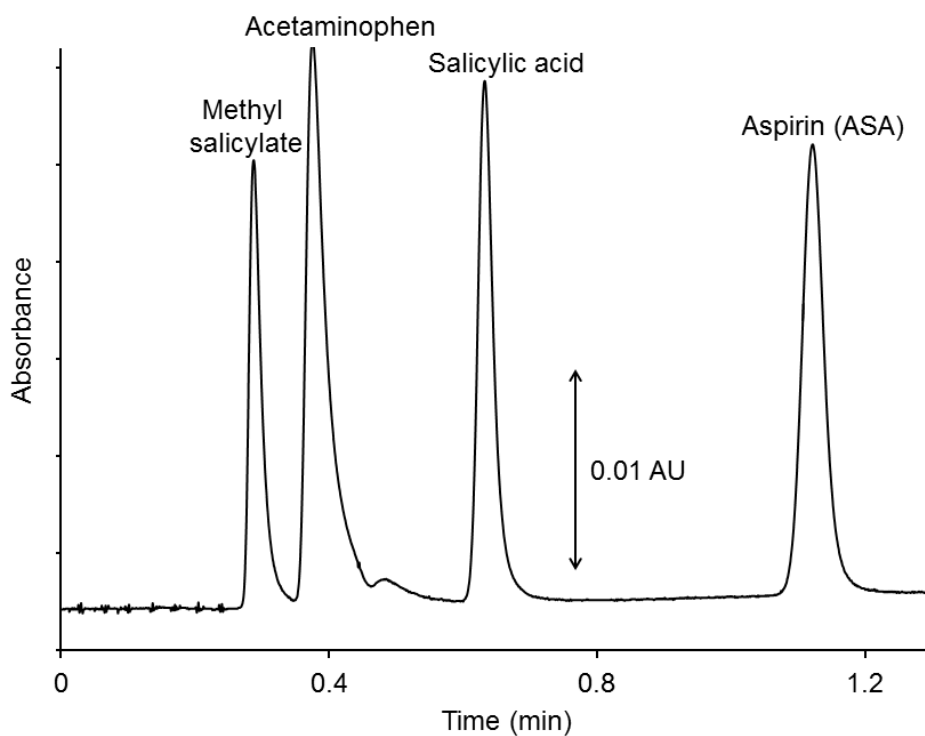


Figure 7.11 Fast HILIC separation of pain relief pharmaceuticals on the hybrid carbon-silica. Conditions: column, hybrid carbon-silica (100 × 4.0 mm i.d.); flow rate, 2.0 mL/min; eluent, 10 mM ammonium acetate, pH 6.1, in 90% ACN; analytes, 2 μ L injection of 0.04-0.12 mM methyl salicylate, acetaminophen, salicylic acid and aspirin (ASA); UV detection at 240 nm. The chemical structures of the analytes are shown in Appendix I.

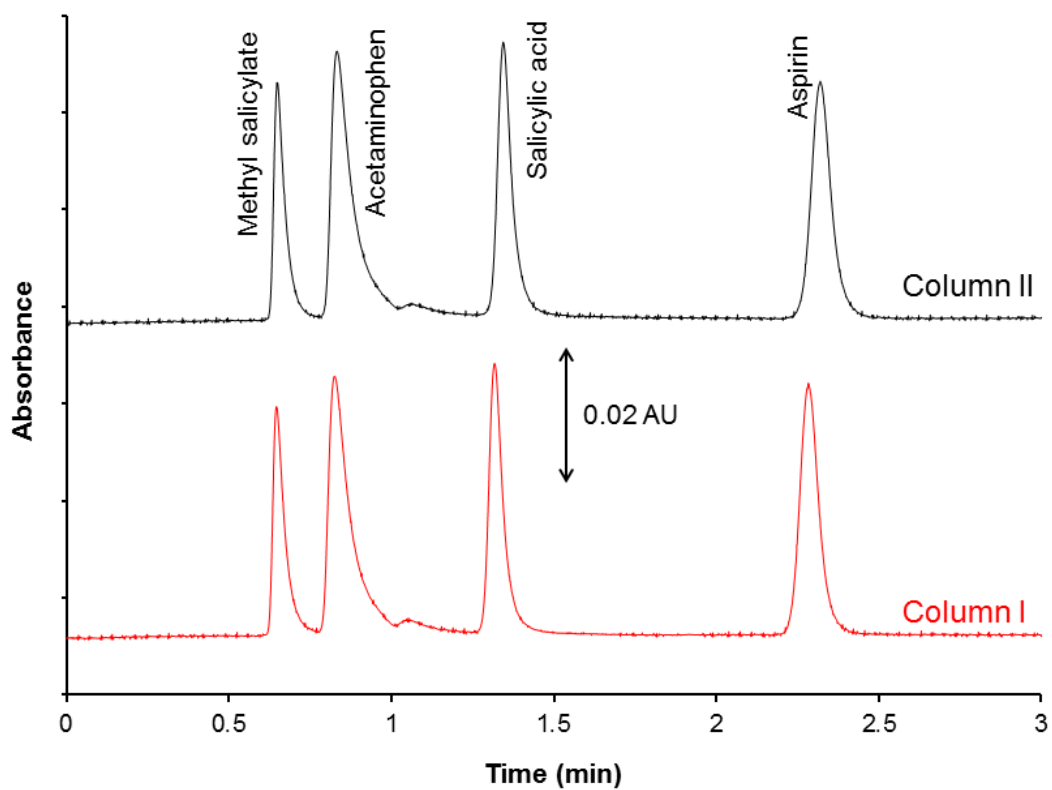


Figure 7.12 Reproducibility studies of the hybrid carbon-silica phase. Conditions: column, hybrid carbon-silica (100 × 4.0 mm i.d.); flow rate, 1.0 mL/min; eluent, 10 mM ammonium acetate, pH 6.1, in 90% ACN; analytes, 2 μ L injection of 0.04-0.12 mM methyl salicylate, acetaminophen, salicylic acid and aspirin (ASA); UV detection at 240 nm. The chemical structures of analytes are given in Appendix I.

packing reproducibility and the homogeneity of the hybrid material. We recommend that these columns should be washed with water and stored in 95% ACN/ 5% water mixtures.

The retention time of two hydrophilic markers were monitored over a three months period of intermittent usage and storage. The retention times of uracil and cytosine varied by 2.1 and 1.6%, respectively. In contrast, bare silica columns have shown up to 24% change in retention factor of cytosine when stored in typical HILIC eluents [33]. The reproducibility of the retention over this 3 month period demonstrates that the strong electrostatic attachment of carbon nanoparticles onto latex coated core-shell silica particles yields a stable hybrid carbon-silica column.

7.4 Conclusions

Core-shell silica particles are well-known for their high efficiency separations, and carbon is known for its unique chromatographic selectivity. Herein, we describe a procedure to synthesize a highly efficient carbon-based core-shell silica stationary phase that combines the advantages of core-shell silica and carbon in one chromatographic phase. The hybridization method is based on simple anchoring anionic carbon nanoparticles onto core-shell silica *via* electrostatic interactions. Such hybrid supports were shown to be stable and reproducible. The newly developed hybrid phase exhibits unique selectivity with respect to 36 silica, polymer and carbon-based stationary phases. The hybrid phase shows enhanced HILIC retention compared to bare core-shell silica. The

newly developed phase shows selectivity for isomeric separations. The hybrid phase yields peak efficiencies greater than that obtained on a pure carbon-based HILIC phase. Finally, the usage of such hybrid phase as a HILIC stationary phase was demonstrated by separation of carboxylates, phenols and pharmaceuticals.

7.5 References

- [1] D.V. McCalley, In *Chapter 1: Separation Mechanisms in HILIC; Hydrophilic Interaction Chromatography: A Guide for Practitioners*, B.A. Olsen, B.W. Pack (Eds.), John Wiley & Sons Inc, Hoboken, NJ, 2013, pp. 1-41.
- [2] A.L.N. van Nuijs, I. Tarcomnicu, A. Covaci, *J. Chromatogr. A* **2011**, *1218*, 5964-5974.
- [3] P. Hemstrom, K. Irgum, *J. Sep. Sci.* **2006**, *29*, 1784-1821.
- [4] M.F. Wahab, M.E.A. Ibrahim, C.A. Lucy, *Anal. Chem.* **2013**, *85*, 5684-5691.
- [5] S. Schiesel, M. Lammerhofer, A. Leitner, W. Lindner, *J. Chromatogr. A* **2012**, *1259*, 111-120.
- [6] M.E.A. Ibrahim, T. Zhou, C.A. Lucy, *J. Sep. Sci.* **2010**, *33*, 773-778.
- [7] S. Neubauer, A. Rugova, D.B. Chu, H. Drexler, A. Ganner, M. Sauer, D. Mattanovich, S. Hann, G. Koellensperger, *Anal. Bioanal. Chem.* **2012**, *404*, 799-808.
- [8] J.P. Hutchinson, T. Remenyi, P. Nesterenko, W. Farrell, E. Groeber, R. Szucs, G. Dicoski, P.R. Haddad, *Anal. Chim. Acta* **2012**, *750*, 199-206.
- [9] X. Wang, M.R. Emmett, A.G. Marshall, *Anal. Chem.* **2010**, *82*, 6542-6548.
- [10] S. Di Palma, P.J. Boersema, A.J.R. Heck, S. Mohammed, *Anal. Chem.* **2011**, *83*, 3440-3447.

- [11] D.V. McCalley, *J. Chromatogr. A* **2008**, *1193*, 85-91.
- [12] A.J. Alpert, *J. Chromatogr.* **1990**, *499*, 177-196.
- [13] N.P. Dinh, T. Jonsson, K. Irgum, *J. Chromatogr. A* **2013**, in press.
- [14] A. Yanagida, H. Murao, M. Ohnishi-Kameyama, Y. Yamakawa, A. Shoji, M. Tagashira, T. Kanda, H. Shindo, Y. Shibusawa, *J. Chromatogr. A* **2007**, *1143*, 153-161.
- [15] M.E.A. Ibrahim, Y. Liu, C.A. Lucy, *J. Chromatogr. A* **2012**, *1260*, 126-131.
- [16] M.E.A. Ibrahim, C.A. Lucy, *Talanta* **2012**, *100*, 313-319.
- [17] N.P. Dinh, T. Jonsson, K. Irgum, *J. Chromatogr. A* **2011**, *1218*, 5880-5891.
- [18] F. Gritti, G. Guiochon, *J. Chromatogr. A* **2013**, *1297*, 85-95.
- [19] M.E.A. Ibrahim, C.A. Lucy, In *Chapter 2: Stationary Phases for HILIC; Hydrophilic Interaction Chromatography: A Guide for Practitioners* Olsen, B. A., Pack, B. W. (Eds.), John Wiley & Sons Inc., Hoboken, NJ, 2013, pp. 43-85.
- [20] J.J. DeStefano, S.A. Schuster, J.M. Lawhorn, J.J. Kirkland, *J. Chromatogr. A* **2012**, *1258*, 76-83.
- [21] N. Tanaka, T. Tanigawa, K. Kimata, K. Hosoya, T. Araki, *J. Chromatogr.* **1991**, *549*, 29-41.
- [22] J.H. Knox, B. Kaur, G.R. Millward, *J. Chromatogr.* **1986**, *352*, 3-25.
- [23] Y. Cui, S.V. Olesik, *Anal. Chem.* **1991**, *63*, 1812-1819.
- [24] E.F. Funkenbusch, P.W. Carr, D.A. Hanggi, T.P. Weber, *Regents of the University of Minnesota, USA* 1992.
- [25] C. Paek, A.V. McCormick, P.W. Carr, *J. Chromatogr. A* **2010**, *1217*, 6475-6483.

- [26] C. Paek, A.V. McCormick, P.W. Carr, *J. Chromatogr. A* **2011**, *1218*, 1359-1366.
- [27] C. Paek, Y. Huang, M.R. Filgueira, A.V. McCormick, P.W. Carr, *J. Chromatogr. A* **2012**, *1229*, 129-139.
- [28] K.M. Usher, C.R. Simmons, J.G. Dorsey, *J. Chromatogr. A* **2008**, *1200*, 122-128.
- [29] SciFinder Scholar; Chemical Abstract Services: Columbus, OH, 2006
- [30] <http://www.advanced-materials-tech.com/products.html> (accessed in October 2013).
- [31] R.E. Majors, *LCGC North Am.* **2003**, *21*, 19-26.
- [32] Y. Guo, In *Chapter 17: Retention and Selectivity of Polar Stationary Phases for Hydrophilic Interaction Chromatography; Hydrophilic Interaction Liquid Chromatography (HILIC) and Advanced Applications*, CRC press, Boca Raton, FL, 2011, pp. 401-426.
- [33] L. Pereira, *LCGC North Am.* **2011**, *29*, 262-269.
- [34] X. Liu, C. Pohl, *J. Chromatogr. A* **2008**, *1191*, 83-89.
- [35] P. Jandera, *Anal. Chim. Acta* **2011**, *692*, 1-25.
- [36] Y.Y. Li, Z.G. Xu, Y.Y. Feng, X.Y. Liu, T. Chen, H.X. Zhang, *Chromatographia* **2011**, *74*, 523-530.
- [37] H. Colin, N. Ward, G. Guiochon, *J. Chromatogr. A* **1978**, *149*, 169-197.
- [38] D. Průšová, H. colin, G. Guiochon, *J. Chromatogr. A* **1982**, *234*, 1-11.
- [39] K.K. Unger, *Anal. Chem.* **1983**, *55*, 361A-375A.
- [40] K. Koizumi, *J. Chromatogr. A* **1996**, *720*, 119-126.

- [41] Q.H. Wan, P.N. Shaw, M.C. Davies, D.A. Barrett, *J. Chromatogr. A.* **1995**, 697, 219-227.
- [42] C. Elfakir, M. Lafosse, *J. Chromatogr. A.* **1997**, 782, 191-198.
- [43] F. Gritti, I. Leonardis, J. Abia, G. Guiochon, *J. Chromatogr. A.* **2010**, 1217, 3819-3843.
- [44] F. Gritti, G. Guiochon, *Anal. Chem.* **2013**, 85, 3017-3035.
- [45] <http://www.dionex.com/en-us/products/columns/lc/mixed-mode/acclaim-mixed-mode-wax-1/lp-71737.html> (accessed in September 2013).

CHAPTER EIGHT: Conclusions and Future Work

8.1 Conclusions

This thesis explored the development and characterization of new silica and carbon-based stationary phases for hydrophilic interaction liquid chromatography (HILIC). Firstly Chapter 2 provides a general discussion of the different HILIC stationary phases regarding their chemistry, development, efficiency and selectivity. This general background given in Chapter 2 is essential to better understand the HILIC behavior of the newly developed HILIC phases discussed later in the thesis. This thesis addressed some of the deficiencies associated with HILIC stationary phases, e.g. lack of understanding of column selectivity and thus a lack of control of the stationary phase's selectivity, speed of analysis, and stability of the stationary phases. Chapter 3 addressed the lack of understanding of HILIC columns selectivity. A simple and easy to understand method for categorization of HILIC stationary phases was generated. The proposed classification shown in Chapter 3 is based on probing the various interactions occurring on the surface of the HILIC stationary phases such as hydrophilic interaction, ion exchange and H-bonding. Based on this work, classification of HILIC stationary phases into silica, zwitterionic, amine and neutral (diol and amide) was performed.

To address the issue of analysis speed, the high permeability of monolithic structure was used to enable fast separations with minimal backpressures [4-7]. Bare silica monoliths show very weak retention of polar analytes under HILIC conditions [1-3]. Chapter 4 presents a convenient way to convert a silica monolith

into a HILIC phase through flushing with cationic latex nanoparticles. The latex coated silica monolith exhibits enhanced HILIC properties *vs.* the bare silica monolith. Separations of amino acids, carboxylic acids, and nucleotides were achieved on the latex coated monolith under HILIC conditions. Indeed separation of naphthalene, uracil and cytosine was achieved in less than 15 s. This latex coated HILIC phase had been used for ion chromatography purposes earlier because of the presence of the anion exchange sites introduced by the latex nanoparticles [8]. Chapter 5 studied the mixed mode retention (HILIC and ion exchange) on latex coated silica monoliths under HILIC mobile phase conditions. Fast separation of kosmotropic and chaotropic anions on the latex coated silica monolith was achieved under HILIC conditions. Retention of chaotropic anions on the latex coated silica monoliths followed ion exchange behavior, while retention of kosmotropic anions followed HILIC behavior.

To improve the pH stability of HILIC, Porous graphitic carbon (PGC) based stationary phases were explored. PGC are used mainly for RPLC purposes [9-11]. Chapter 6 explores the modification of PGC through attaching benzene carboxylate moieties *via* diazonium chemistry to yield a HILIC stationary phase. The newly developed phase (named carboxylate-PGC) exhibited strong HILIC properties and unique selectivity, different from 35 commercial stationary phases. As a HILIC phase, the carboxylate-PGC phase was applied to the separation of carboxylic acids, phenols, nucleotides and amino acids. This carboxylate-PGC phase showed high stability under extreme pH conditions and overcame the instability issues associated with commercial silica based stationary phases.

Generally, carbon based phases usually show low peak efficiencies because of their slow mass transfer properties [12]. Finally, Chapter 7 shows the improvement in peak efficiencies that can be obtained through the use of core-shell silica surface coated with modified carbon nanoparticles. The newly developed hybrid carbon-silica phase has yielded greater peak efficiencies compared to the carboxylate-PGC. In regard to chromatographic selectivity, the hybrid carbon-silica phase showed different selectivity relative to silica and carbon phases.

8.2 Future Work

8.2.1 Development of New Multimodal Stationary Phases

Multimodal chromatography is becoming a powerful way for separation of various analytes. Multimodal liquid chromatography refers to chromatographic separations utilizing at least two different kinds of interactions depending on the mobile phase composition [13]. Multimodal chromatography enables the retention and separation of more than one class of analytes in the same chromatogram. For instance, reversed phase liquid chromatography (RPLC) phases with anion exchange sites can retain both hydrophobic analytes as well as anionic analytes [14]. The major advantages of multimodal chromatography lie in its broader selectivity and economicity of the separation since one multimodal phase can replace two or more columns [14]. This interest in multimodal chromatography has drawn our attention to the importance of developing new multimodal stationary phases.

Since RPLC and HILIC modes of retention are orthogonal *i.e.*, RPLC retains hydrophobic analytes whereas HILIC retains hydrophilic ones, we are aiming to synthesize a stationary phase with such orthogonal selectivity. The proposed multimodal phase will be synthesized based on the protocol, described early in Chapter 4 [15]. Briefly, a suspension of latex AS9-SC latex nanoparticles are flushed through a RP column and the excess latex will be washed off (Figure 8.1) [15]. The latex nanoparticles are hydrophilic in nature which in turn allows the formation of a water rich layer on the surface of the stationary phase [16]. This formed water rich layer enables HILIC separation of hydrophilic analytes on the proposed stationary phase. On the other hand, RPLC separations still can be performed based on the hydrophobicity of the underlying alkyl chains. Interestingly, the positively charged latex nanoparticles can add ion exchange as another valuable source of interaction [16, 17], as previously discussed in Chapter 5. This ion-exchange characteristic of the proposed phase will enable separation of charged species whether hydrophilic or hydrophobic.

It is proposed that the multimodal column be prepared on a RP monolith, e.g., the Phenomenex Onyx C₈ RP column. The monolith can support the coating of more latex nanoparticles *via* physical entrapment of latex in the smaller mesopores of the monolith. The short alkyl chains (C₈ vs. C₁₈) may encourage the attachment of more latex nanoparticles due to their low steric hindrance and low hydrophobicity. Additionally, fast separation of analytes can be achieved due to the high permeability of the monolithic column.

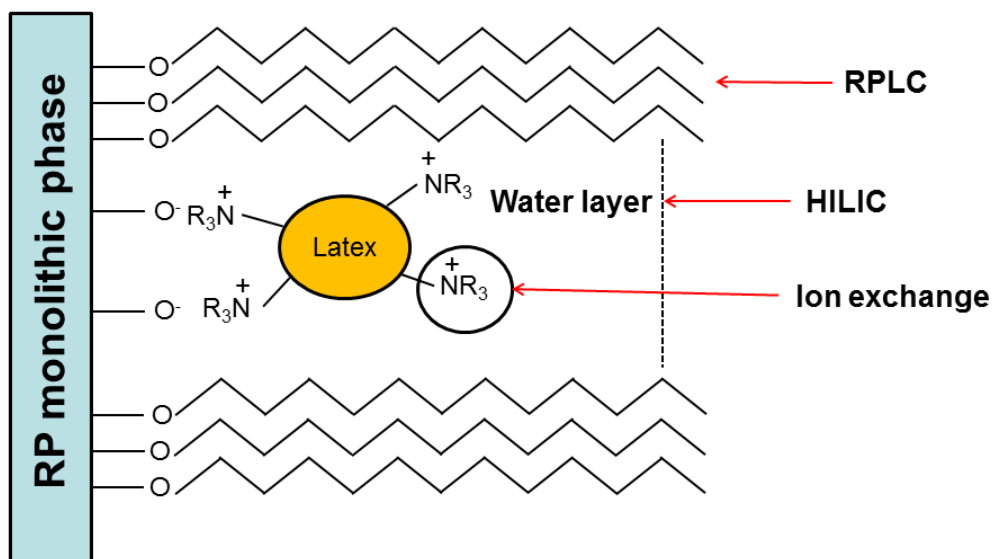


Figure 8.1 The design of the proposed multimodal stationary phase along with the expected retention modes (RPLC, HILIC and Ion exchange).

8.2.2 Sulfonated Porous Graphitic Carbon for HILIC

As previously discussed in Chapter 6, a carboxylate modified porous graphitic carbon (PGC) was developed *via* diazonium chemistry for HILIC. Similarly, we are planning to synthesize a sulfonated PGC phase [18] to be employed as a possible HILIC phase. Preliminary studies show the high wettability characters of the sulfonated PGC material which in turn suggests it as a probable HILIC phase. We are interested to use this sulfonated PGC phase for separation of carbohydrates under HILIC conditions. The challenge of carbohydrates separation is the use of strong alkaline eluents to overcome the peak splitting caused by anomerization [19]. Being highly stable under extreme pH conditions [18], sulfonated PGC is a potential stationary phase for such a separation. Since carbohydrates absorb very weakly in the wavelength range which can be used with acetonitrile containing eluents (UV cut off ~ 190 nm), electrochemical detection will be used for such an application [20].

8.2.3 Factors Affecting the Selectivity Plot of HILIC Stationary Phases

Although the selectivity plots represented in Chapter 3 are based on a single set of experimental conditions, they were able to classify different HILIC stationary phases. We found that changing pH of the eluent had a drastic effect on the selectivity of the stationary phase e.g. the amino derivatized PGC showed anion exchange selectivity when using acidic eluent conditions; however it showed a BTMA/cytosine ratio very close to 1 when the pH was increased to 6.8. Such observations have drawn our attention to the fact that eluent conditions

including pH, % ACN and buffer strength may have a drastic effect on the selectivity plots represented in Chapter 3. A research project conducted by Chad Iverson (PhD student) and a chemistry undergraduate student has been initiated to study the effect of such parameters on the selectivity plots. These studies are very important since they testify the robustness of the selectivity plots against minor changes in the eluent conditions *e.g.* pH, buffer strength and %ACN. Moreover, from these studies we could get a newer way to classify the different HILIC stationary phases. In turns this will help us to better understand the behavior of the HILIC stationary phases under different mobile phase conditions.

Another factor that may need further investigation is the choice of test probe analytes. In Chapter 3 based on ref. [21], three sets of test probes were selected; BTMA/cytosine to test the ion exchange (or electrostatic character) character, cytosine/uracil to test hydrophilic interactions and adenosine/adenine to test the capability to participate in H-bonding. As shown in Chapter 3, these test probes were successful at classifying the different HILIC phases to silica, neutral (amide and diol), zwitterionic and amine based HILIC groupings. We are more interested to use other test probes as per ref. [21] to construct additional selectivity plots which are able to classify the different HILIC stationary phases in new ways. For example: dimethylformamide/dihydroxyacetone or dihydroxyacetone/methylglycolate to test participation in hydrogen-bonding; and phenyltrimethylammonium/cytosine or benzyltriethylammonium/cytosine to test ion exchange (or electrostatic character). This will help us to know the effect of

choice of different test probes which testify the same character of a column on the structure of the selectivity plots.

Additionally, we are interested to construct new selectivity plots based on probing different type of interactions rather than using different test probes to test the same type of interaction. We are planning to construct a new selectivity plot based on probing the dipole-dipole interactions and molecular shape selectivity. Based on ref. [21], *cis*- and *trans*-diamminedichloroplatinum (II) was selected to probe dipole-dipole interactions due to their difference in the asymmetric orientation of the ammine- and chloro-ligands and hence their difference in dipole moment [21]. Molecular shape selectivity can be testified by two test probes: sorbic acid and benzoic acid which have different sizes and shapes of the hydrophobic part of the molecule; and methylglycolate and α -hydroxy- γ -butyrolactone which have different orientations and flexibilities of the hydrophilic part [21]. The 1-ethylimidazole/1-vinylimidazole test pair can be used to probe π - π interactions as discussed by Irgum and co-workers [21]. This last test pair can be used to explore the extent to which the unmodified PGC surface contributes to retention.

8.2.4 Covalently Modified Carbon Clad Silica Phase for HILIC

In Chapter 7, a new hybrid carbon-silica phase was developed by electrostatic attachment of anionic modified carbon on the cationic latex coated core-shell silica. As shown in Chapter 7, this hybrid carbon-silica stationary phase exhibited a different selectivity from 35 other stationary phases and 10 different

column chemistries. Since this hybrid phase behaved differently from other HILIC stationary phases, we are interested in investigating the HILIC behavior of carbon clad core-shell silica phase, recently developed by Carr and co-workers [22]. Firstly, the carbon surface of carbon clad core-shell silica will be covalently modified *via* diazonium chemistry as early stated in Chapter 6 [18] to yield either benzene carboxylate (as described in Chapter 6 [18]) or aniline moieties [23]. Secondly, we will check the selectivity of the modified carbon clad silica phase using the selectivity plots, represented in Chapter 3. Secondly, the covalently modified carbon clad silica phase is expected to demonstrate mixed mode retention (HILIC *vs.* RPLC) and isomeric selectivity due to the presence of surface carbon. We are planning to compare the efficiency of our previous hybrid HILIC phase (Chapter 7) against the covalently modified carbon clad core-shell silica phase under the same HILIC eluent conditions. Furthermore, the potential of the newly developed carbon clad silica phase as a HILIC stationary phase will be testified by separation of model hydrophilic analytes (e.g. nucleotides, amino acids and peptides). Finally, the stability of the covalently modified carbon clad silica phase will be assessed and compared to the stability offered by our previous hybrid HILIC phase (Chapter 7).

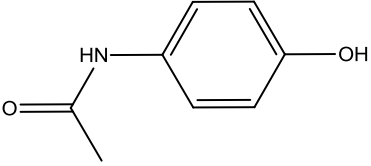
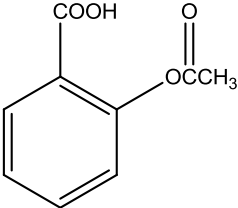
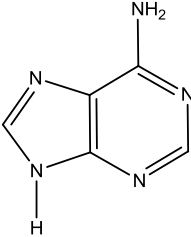
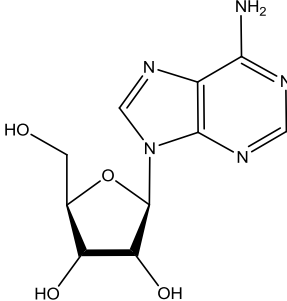
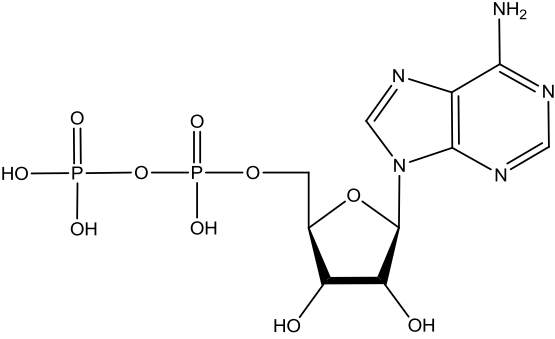
8.3 References

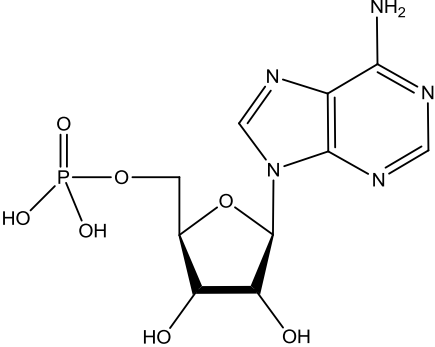
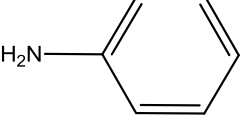
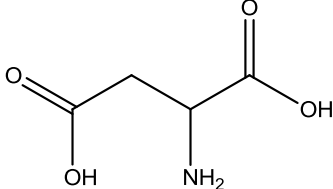
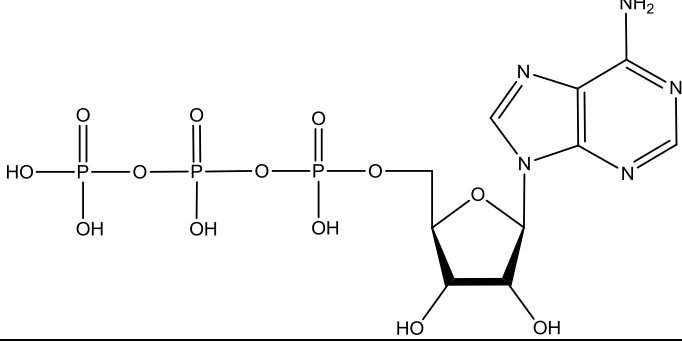
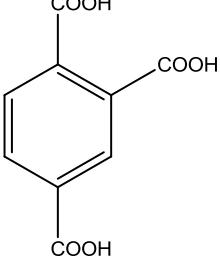
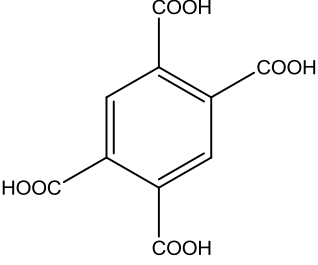
- [1] N.P. Dinh, T. Jonsson, K. Irgum, *J. Chromatogr. A* **2011**, *1218*, 5880-5891.
- [2] T. Ikegami, H. Fujita, K. Horie, K. Hosoya, N. Tanaka, *Anal. Bioanal. Chem.* **2006**, *386*, 578-585.

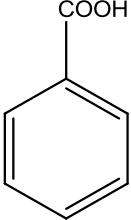
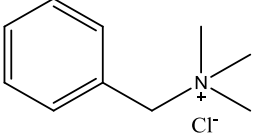
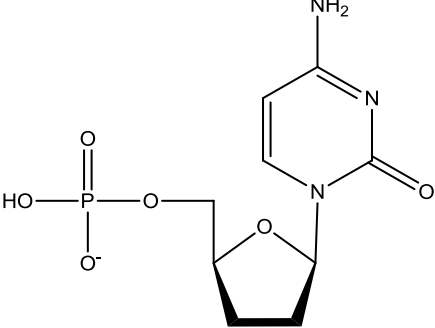
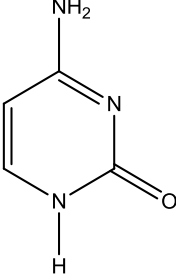
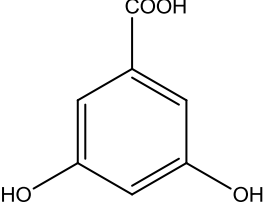
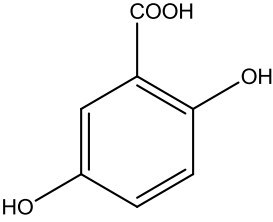
- [3] Z. Jianga, N. Smithb, Z. Liua, *J. Chromatogr. A* **2011**, *1218*, 2350-2361.
- [4] Z.J. Jiang, N.W. Smith, P.D. Ferguson, M.R. Taylor, *J. Sep. Sci.* **2009**, *32*, 2544-2555.
- [5] R. Wu, L.G. Hu, F.J. Wang, M.L. Ye, H. Zou, *J. Chromatogr. A.* **2008**, *1184*, 369-392.
- [6] T.A.E. Jakschitz, C.W. Huck, S. Lubbad, G.K. Bonn, *J. Chromatogr. A.* **2007**, *1147*, 53-58.
- [7] D. Schaller, E.F. Hilder, P.R. Haddad, *J. Sep. Sci.* **2006**, *29*, 1705-1719.
- [8] K.M. Glenn, C.A. Lucy, P.R. Haddad, *J. Chromatogr. A.* **2007**, *1155*, 8-14.
- [9] N. Tanaka, T. Tanigawa, K. Kimata, K. Hosoya, T. Araki, *J. Chromatogr.* **1991**, *549*, 29-41.
- [10] N. Tanaka, K. Kimata, K. Hosoya, H. Miyaniishi, T. Araki, *J. Chromatogr. A.* **1993**, *656*, 265-287.
- [11] C. Lepont, A.D. Gunatillaka, C.F. Poole, *Analyst* **2001**, *126*, 1318-1325.
- [12] Y. Cui, S.V. Olesik, *Anal. Chem.* **1991**, *63*, 1812-1819.
- [13] V.Orlovsky, Y. Zelechonok, *Chromatography Today, August/September* **2011**, 24-28.
- [14] F.R. Mansour, N.D. Danielson, *Anal. Methods* **2013**, *5*, 4955-4972.
- [15] M.E.A. Ibrahim, T. Zhou, C.A. Lucy, *J. Sep. Sci.* **2010**, *33*, 773-778.
- [16] M.E.A. Ibrahim, C.A. Lucy, *Talanta* **2012**, *100*, 313-319.
- [17] K.M. Glenn, C.A. Lucy, P.R. Haddad, *J. Chromatogr. A* **2007**, *1155*, 8-14.
- [18] M.F. Wahab, M.E.A. Ibrahim, C.A. Lucy, *Anal. Chem.* **2013**, *85*, 5684-5691.

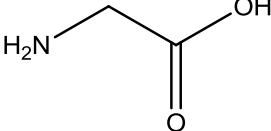
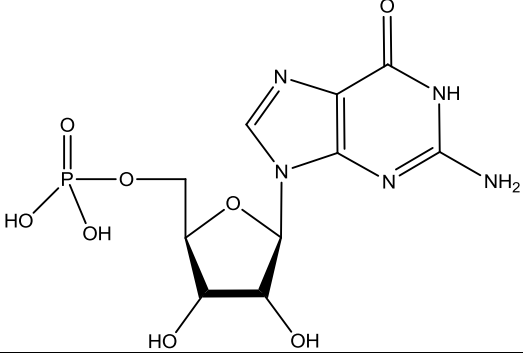
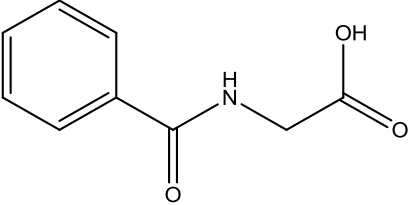
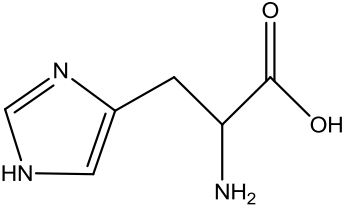
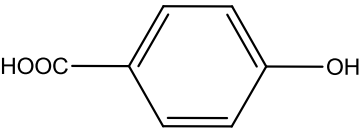
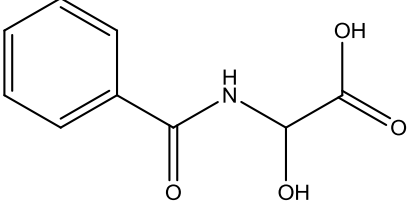
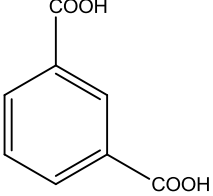
- [19] F. Rabel, B.A. Olsen, In *Chapter 6:Advances in Hydrophilic Interaction Chromatography (HILIC) for Biochemical Applications; Hydrophilic Interaction Chromatography: A Guide for Practitioners*, B.A. Olsen, B.W. Pack (Eds.), John Wiley & Sons, Inc., 2013, pp. 195-217.
- [20] F. D'Eramo, J.M. Marioli, A.A. Arévalo, L.E. Sereno, *Electroanalysis* **1999**, *11*, 481-486.
- [21] N.P. Dinh, T. Jonsson, K. Irgum, *J. Chromatogr. A* **2011**, *1218*, 5880-5891.
- [22] C. Paek, Y. Huang, M.R. Filgueira, A.V. McCormick, P.W. Carr, *J. Chromatogr. A* **2012**, *1229*, 129-139.
- [23] C. Iverson, C.A. Lucy, *J. Chromatogr. A*, in preparation.

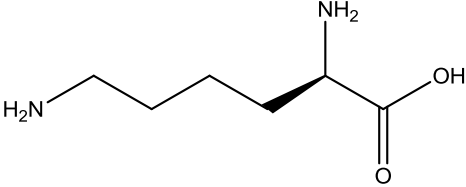
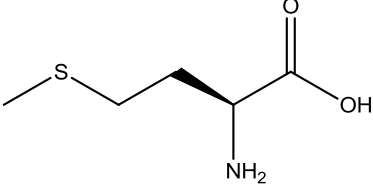
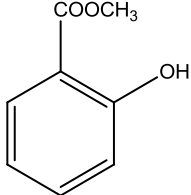
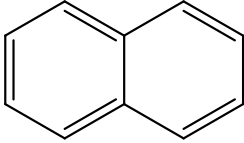
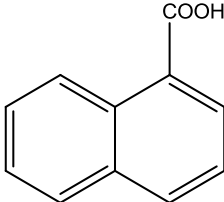
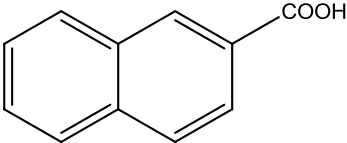
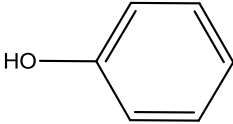
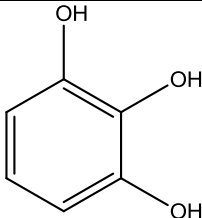
Appendix I. Chemical Structures

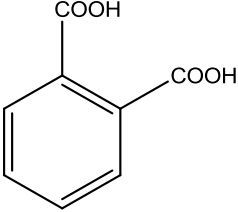
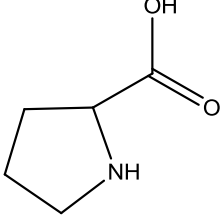
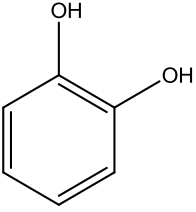
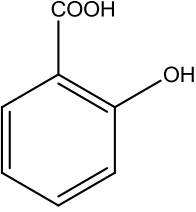
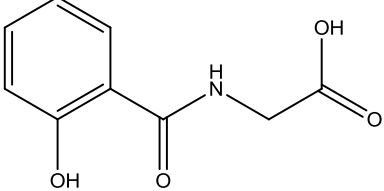
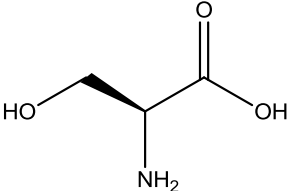
Analyte Name	Chemical Structure
Acetaminophen	
Acetylsalicylic acid	
Adenine	
Adenosine	
ADP	

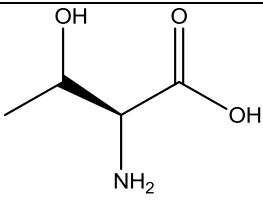
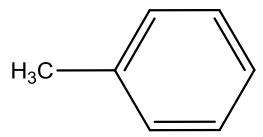
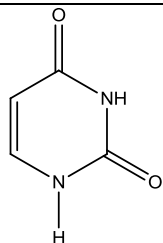
AMP	
Aniline	
Aspartic acid	
ATP	
1,2,4 Benzene tricarboxylate	
1,2,4,5 Benzene tetracarboxylate	

Benzoic acid	
BTMA	
CMP	
Cytosine	
3,5-Dihydroxybenzoic acid	
Gentisic acid	

Glycine	
GMP	
Hippuric acid	
Histidine	
4-Hydroxybenzoic acid	
α -Hydroxyhippuric acid	
Isophthalic acid	

Lysine	
Methionine	
Methyl salicylate	
Naphthalene	
1-Naphthoic acid	
2-Naphthoic acid	
Phenol	
Phloroglucinol	

Phthalic acid	
Proline	
Resorcinol	
Salicylic acid	
Salicyluric acid	
Serine	

Threonine	 <p>The structure shows Threonine, an amino acid. It consists of a central chiral carbon atom bonded to a methyl group (represented by a single line), a hydroxyl group (OH), an amino group (NH₂), and a carboxyl group (COOH). The hydroxyl group is shown with a wedge bond, indicating its stereochemistry.</p>
Toluene	 <p>The structure shows Toluene, which is a benzene ring with a methyl group (H₃C) attached to one of the carbons.</p>
Uracil	 <p>The structure shows Uracil, a pyrimidine nucleobase. It is a six-membered ring with two nitrogen atoms and two carbonyl groups (C=O). The nitrogen at the bottom position has a hydrogen atom (H) attached to it.</p>